# Regulation of fission yeast cohesin by the Cyclin Dependent Kinase PeF1

Adrien Birot

université de BORDEAUX

THÈSE PRÉSENTÉE par Adrien BIROT

POUR OBTENIR LE GRADE DE

# DOCTEUR DE

# L'UNIVERSITÉ DE BORDEAUX

ÉCOLE DOCTORALE Sciences et Vie de la Santé

SPÉCIALITÉ Génétique

Par Adrien BIROT

# Regulation of fission yeast cohesin by the Cyclin Dependent Kinase Pef1

Sous la direction de : Sabine VAUR
Co-directeur : Karl EKWALL

Soutenue le 9 décembre 2016

Membres du jury :

| | | |
|---|---|---|
| M. Martin TEICHMANN | Professeur de l'Université de Bordeaux | Président |
| Mme. Katja WASSMANN | Directeur de recherche, Paris | Rapporteur |
| M. Pascal BERNARD | Directeur de recherche, Lyon | Rapporteur |
| Mme. Sylvie TOURNIER | Directeur de recherche, Toulouse | Examinateur |
| Mme Sabine VAUR | Chargé de recherche, Bordeaux | Directrice de thèse |
| M. Karl EKWALL | Professeur, Université de Stockholm | Co-directeur de thèse |
| M. Jean-Paul JAVERZAT | Directeur de recherche, Bordeaux | Invité |

# Remerciements

A l'issue de cette thèse je tiens à remercier les membres de mon jury : Madame Katja Wassmann, Monsieur Pascal Bernard, Madame Sylvie Tournier et Monsieur Martin Teichmann pour avoir accepté de juger ce travail.

Un « merci général » à l'ensemble des personnes du 1er étage de l'IBGC. Un grand merci aux membres de l'équipe dans laquelle j'ai effectué ma thèse. Bien plus qu'une équipe, c'est une famille que j'ai trouvée. C'est dans une ambiance chaleureuse, amicale et studieuse que j'ai pu évoluer au cours de ces dernières années.

Je souhaite remercier ma directrice de thèse, Sabine Vaur : non seulement pour ton aide lors de la rédaction de ce manuscrit mais également pour tes encouragements tout au long de ma thèse. Tu m'as appris à relativiser et analyser sous un autre angle de nombreux résultats. Comme tu m'as souvent dit « La seule personne à ne jamais faire d'erreurs est celle qui ne fait rien ».

Je remercie Jean-paul Javerzat, pour m'avoir accueilli dans son laboratoire quand je n'étais qu'un « petit étudiant de master ». Tu as toujours été pour moi un exemple scientifique et intellectuel, auquel je porte mes plus grandes considérations et estime.

Merci à Stéphanie Vazquez pour sa bonne humeur et son énergie. Je retiens de ces années passées ta grande bienveillance à mon égard, ainsi que ton obstination notamment pour faire « marcher ces PCR » !! Ton « petit Adrien » te remercie !

A vous trois vous avez façonné le scientifique que je suis.

Mes remerciement vont également à l'équipe « podo » : Mathieu, Frédérique, Sven, Alexandra et des remerciements plus particuliers à Corinne et Martine.

Durant cette thèse, j'ai également eu la chance de passer quelques mois « frileux » en Suède dans le laboratoire du Dr Karl Ekwall, que je remercie pour son accueil. Un grand merci à son équipe et notamment à Olga, qui m'a permis une intégration rapide et facile dans le groupe.

Je remercie également l'ensemble des étudiants, doctorants, et post-doctorants de l'étage avec lesquels j'ai pu interagir, notamment Karen, Assen, Marina, Khalid et plus récemment Marta.

Je remercie toutes les personnes de l'IBGC qui ont croisé mon chemin.

Un merci à ma famille et belle-famille qui m'ont soutenu durant cette thèse. Merci à ma femme, Charline, pour son soutien dans mes moments de doute, et à notre petit Paul qui illumine notre quotidien.

*A ma mère,*

## Régulation des cohésines chez *Schizosaccharomyces pombe* par la Kinase Cycline Dépendante Pef1

Le complexe cohésine est un ensemble protéique en forme d'anneau conservé de la levure à l'Homme. Sa fonction la plus connue est d'assurer la cohésion des chromatides sœurs, un processus cellulaire essentiel, nécessaire à la ségrégation correcte des chromosomes durant la mitose et la méiose. Les cohésines établissent la cohésion en piégeant physiquement les chromatides sœurs à l'intérieur de leur structure en forme d'anneau. Outre la ségrégation des chromosomes, les cohésines sont nécessaires pour la réparation des cassures double brin de l'ADN et l'organisation spatiale de la chromatine dans le noyau avec des conséquences sur l'expression des gènes.

Le complexe cohésine est constitué de trois sous-unités qui forment l'anneau: Smc1, Smc3 et Scc1 (Psm1, Psm3 et Rad21 dans le modèle de la levure de fission *Schizosaccharomyces pombe*). Smc1 et Smc3 sont de longues protéines, flexibles qui se replient sur elles-mêmes le long du leur domaine *coiled-coil* amenant à proximité les domaines N et C terminaux constituant une extrémité ATPase (tête globulaire). L'autre extrémité est dite domaine "charnière". Les domaines charnière de Smc1 et Smc3 se dimérisent, tandis que les têtes ATPasiques des Smc sont reliées par la sous unité Scc1/Rad21. Ensemble, ces protéines forment une structure en forme d'anneau qui ont la capacité d'encercler les molécules d'ADN. La capture de l'ADN par les cohésines nécessite l'hydrolyse de l'ATP par les protéines Smc et l'ouverture transitoire de l'anneau. Une fois capturé, l'ADN peut s'échapper de l'anneau par l'ouverture de l'interface Smc3-Rad21, appelée "porte de sortie", ouverture médiée par la protéine Wpl1. En conséquence, l'association des cohésines avec l'ADN est dynamique et la quantité de cohésines liée à la chromatine résulte de l'équilibre entre les réactions de chargement et de dissociation.

La cohésion des chromatides sœurs est établie en fermant la porte de sortie des cohésines. Ce processus est normalement limité à la phase S. En conséquence, seule les cohesines chargées avant la réplication de l'ADN peuvent créer un lien physique entre les chromatides sœurs. L'association des cohésines avec les chromosomes (capture de l'ADN) dépend de l'action d'un complexe distinct, dit le «complexe de chargement» qui est constitué de deux protéines essentielles nommées Mis4 et Ssl3 chez *S. pombe*. Lorsque Ssl3 ou Mis4 sont altérées, les cohésines ne peuvent pas s'associer aux chromosomes et la cohésion entre les chromatides sœurs ne peut être établie. Les nombreuses fonctions des cohésines impliquent une régulation fine de leur capacité à capturer l'ADN. Ceci est réalisé

en partie en contrôlant le temps pendant lequel l'ADN est capturé, en modulant son entrée et sa sortie. Un autre niveau de régulation est obtenu en contrôlant où et quand le « dépôt » des cohésines doit avoir lieu sur les chromosomes. La façon dont le complexe de chargement régule la capture de l'ADN par l'anneau de cohésine dans l'espace et le temps reste mal compris et mon travail a visé à aborder cette question dans le système modèle *Schizosaccharomyces pombe*.

Un crible génétique a été réalisé pour identifier des suppresseurs d'un allèle thermosensible de *mis4* (*mis4-ts*) et a permis la découverte de Pef1 qui est l'une des deux CDK de type Cdc2 (*Cyclin Dependent Kinase*) chez *S.pombe*. La délétion du gène *pef1* (ainsi que la délétion de sa cycline partenaire *pas1*) est suffisante pour restaurer la viabilité et la cohésion des chromatides sœurs dans le mutant *mis4-ts* à température restrictive. En utilisant l'allèle *pef1* shokat (*pef1-as*), nous avons découvert que la kinase Pef1 doit être inactivée avant la phase S pour restaurer la cohésion dans une souche *mis4-ts* suggérant que la CDK régule négativement la cohésion.

La CDK Pef1 peut réguler la cohésion par la phosphorylation de substrats clés. De nombreuses protéines de cohésion telles que Mis4, Wpl1, Pds5, Eso1 et Rad21 contiennent des sites consensus CDK suggérant que Pef1 peut avoir un effet direct sur les cohesines en phosphorylant une ou plusieurs de ces cibles potentielles. Selon cette idée, nous avons montré que Pef1 co-immunoprécipite Mis4 et les sous-unités de l'anneau de cohésine, Psm3, Psm1 et Rad21. Nous avons comparé la mobilité électrophorétique de ces protéines par western-blot dans des cellules sauvage par rapport aux cellules *pef1Δ*. Aucune différence n'a été notée à l'exception de la protéine Rad21 qui apparaît hypo-phosphorylée lorsque le gène *pef1* est délété, ce qui suggère que la CDK Pef1 pourrait phosphoryler Rad21. Pour tester cette idée, nous avons développé un essai de phosphorylation *in vitro* basé sur l'aptitude de la kinase Pef1-as à utiliser un analogue de l'ATP-y-S (N6-ATP-y-S) pour catalyser la thiophosphorylation de ses substrats. L'alkylation des résidus sérine ou thréonine thiophosphorylés crée un épitope permettant la détection des cibles de Pef1 par des anticorps spécifiques anti thiophosphate-ester. Par western blot, nous avons observé des signaux spécifiques (c'est-à-dire supprimés lorsque la kinase Pef1 est inhibée). De façon intéressante, l'un de ces signaux est superposable avec Rad21. Pour augmenter la quantité de Rad21 disponible pour une analyse par spectrométrie de masse, nous avons développé un autre essai dans lequel Rad21 a été produit par transcription / traduction *in vitro* avec

l'extrait d'*Escherichia coli*. De nouveau, Rad21 est détectée thio-phosphorylée de manière dépendante de Pef1. Pour tenter d'identifier le ou les résidu(s) de Rad21 qui est (sont) thio-phosphorylé(s) *in vitro*, Rad21 a été analysé par spectrométrie de masse (MS / MS). La mauvaise couverture de Rad21 n'a pas permis la détection de résidus thio-phosphorylés. Pour pallier à ce problème, nous avons entrepris une approche candidate. Nous avons cartographié 15 sites de phosphorylation par analyse MS / MS de Rad21 purifiée à partir de cellules cyclantes de type sauvage. De façon intéressante, nous avons identifié une zone spécifique dans Rad21 contenant des sites consensus CDK et des résidus serine phosphorylés aux positions 163, 164 et 165. La pertinence fonctionnelle des sites phosphorylés a été évaluée en créant des phosphomutants de Rad21. Ces mutants ont été analysés pour leur capacité à supprimer des défauts de cohésion (non phosphorylables) ou exacerbés (phospho-mimiques). En effet, le mutant *rad21-163A164A* donne un niveau de suppression semblable à *pef1Δ* et aucun effet additif n'a été observé pour le double mutant, ce qui est compatible avec l'hypothèse selon laquelle la kinase Pef1 agit à travers ces deux résidus de Rad21. Cependant, *rad21-163E164E* est neutre vis-à-vis du phénotype thermosensible de *mis4-367* et n'empêche pas l'effet suppresseur de *pef1Δ* suggérant que Pef1 pourrait phosphoryler d'autres résidus au sein de Rad21.

Nos données indiquent jusqu'à présent que l'inhibition de la kinase Pef1 supprime le défaut de cohésion du mutant *mis4-367* en contrôlant vraisemblablement la phosphorylation de la sous-unité Rad21 de l'anneau de cohésine. Il a été démontré que lorsque la machine de chargement des cohésines est inactivée dans les cellules arrêtées en phase G1, la dissociation des cohésines liées aux chromosomes est totale. Ainsi, l'inhibition de la kinase Pef1 pourrait stimuler l'activité résiduelle de chargement de Mis4-ts. Pour tester cette hypothèse, nous avons développé un essai de chargement des cohésines *in vivo*. Le gène *rad21* a été inséré à un locus ectopique dans le génome. La protéine Rad21 ectopique est étiquetée avec un épitope FLAG et son expression peut être induite par addition de tétracycline. En utilisant ce système, nous avons montré que dans les cellules *mis4-ts* arrêtées en phase G1 à température restrictive, Rad21-FLAG induit ne s'associe jamais à la chromatine lorsque Pef1 est active. En revanche, l'inhibition de la kinase Pef1 est suffisante pour permettre l'association de Rad21-FLAG aux chromosomes. Ces résultats ont été obtenus par trois méthodes complémentaires: d'abord en analysant les protéines liées à la fraction chromatinienne par western blot après fractionnement cellulaire, par détection immunofluorescence de Rad21-FLAG sur étalement de chromatine et par

immunoprécipitation de la protéine Rad21-FLAG et analyse par PCR quantitative de l'ADN ainsi immuniprécipité (ChIP qPCR). Cet ensemble d'expériences indique que l'inhibition de Pef1 pourrait stimuler le chargement des cohésines dans le mutant *mis4-ts*. De même, l'association de Rad21-FLAG est également stimulée dans les cellules *mis4*$^{+}$, suggérant que Pef1 pourrait être un régulateur négatif du chargement des cohésines chez *S. pombe*.

Un autre aspect de mon travail a été de comprendre si l'inhibition de Pef1 peut favoriser le chargement des cohésines de façon globale à travers le génome ou si le chargement est stimulé à des sites spécifiques. Des expériences de ChIP-seq ont été effectuées pour répondre à cette question dans un projet collaboratif avec le groupe du Dr Karl Ekwall au Karolinska Institutet à Stockholm. J'ai pu réaliser ces expériences dans son laboratoire lors d'un déplacement de trois mois à Stockholm. Dans un premier temps, une cartographie de référence a été établit pour apprécier la répartition des cohésines dans le génome avant de la comparer avec les données publiées. Ensuite, j'ai concentré mes premières analyses dans les cellules déficientes pour le chargement des cohésines (*mis4-ts*), afin d'apprécier l'effet de l'inhibition de la kinase Pef1 sur la distribution *genome-wide* de Rad21-FLAG exprimé de façon ectopique. Ces analyses révèlent deux aspects. Tout d'abord, l'inhibition de la kinase n'entraîne pas une stimulation globale et uniforme de l'association de Rad21-FLAG ectopique aux sites connus d'association des cohésines à la chromatine. Seulement un sous-ensemble de ceux-ci est influencé pour l'inhibition de la kinase. Deuxièmement, nous avons étudié la possibilité que l'inhibition de Pef1 puisse provoquer la génération de nouveaux sites d'association de Rad21-FLAG à la chromatine. Nous avons ainsi détecté 94 pics Rad21 à des loci non conventionnels dans le génome. Ces «néo-pics» sont préférentiellement situés dans des unités de transcription divergentes contrairement à l'emplacement « classique » des cohésines préférentiellement situé dans des régions intergéniques avec un fort biais vers des unités de transcription convergentes. Ces données suggèrent que Pef1 pourrait être un régulateur local de l'association des cohésines à la chromatine.

L'ensemble des données suggère que la CDK Pef1 peut réguler de façon négative l'association des cohésines à des loci précis dans le génome probablement par la phosphorylation de la sous-unité Rad21 de l'anneau de cohésine sur les résidus sérine 163 et 164.

# Table of contents

# Introduction

Cohesin is a ring-shaped protein complex conserved from yeast to Human that was named for its ability to mediate sister chromatid cohesion (Gruber, Haering, and Nasmyth 2003). Cohesin establishes cohesion by physically trapping sister chromatids together within its ring-shaped structure (Haering and al. 2002; Haering and al. 2008). This function is essential for faithful chromosome segregation in both mitosis and meiosis and also for DNA double-strand break repair (Remeseiro and Losada 2013). During the past few years, new cohesin functions have emerged. Indeed, cohesin has been shown to promote intra-molecular DNA-looping with consequences on spatial organization of chromatin and gene transcription (for review (Mehta and al. 2013)). Cohesin now appears as a global organizer of chromatin architecture that influences many biological processes in the cell.

By its pivotal role in a wide range of biological processes it is expected that cohesin must be tightly regulated in space and time. This may be achieved in part by controlling cohesin binding to chromatin. Cohesin recruitment to chromatin requires the action of a "loading complex" composed of two conserved and essential proteins named Mis4 and Ssl3. How this complex regulates where and when cohesin deposition must occur remains poorly understood and our work aims at addressing this question in the model system *Schizosaccharomyces pombe.*

We have made a genetic screen for suppressors of a *mis4* thermosensitive allele (*mis4-367*) and uncovered the Cyclin Dependent Kinase Pef1. The aim of my thesis has been to address the function of Pef1 in the regulation of cohesin binding to chromatin and more generally in sister chromatid cohesion. Cohesin function in cohesion is intimately linked to the cell cycle progression. Hence, in the following introduction I will briefly describe the cell cycle and its regulation before presenting cohesin features and functions. Finally, I will present the data I obtained during my thesis about Pef1 function in sister chromatid cohesion in *S. pombe*.

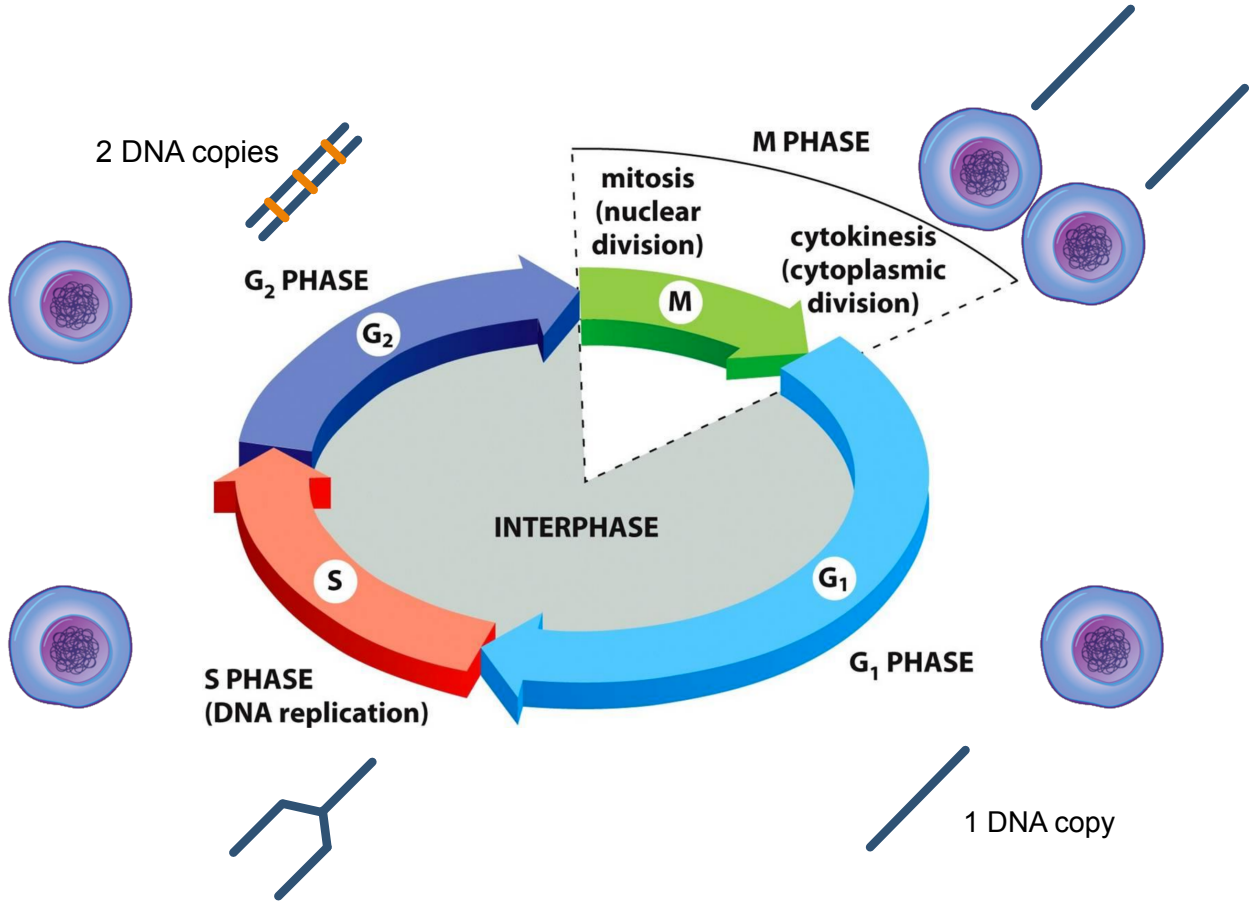


**Figure 1 : The cell cycle**. G1 phase: The cell contains a single copy of each chromosome. S phase: The cell undergoes DNA replication. G2 phase: Each chromosome consists of two DNA copies (sister chromatids) physically linked by cohesin. M phase: As nuclear division operates sister chromatids segregate equally in the two daughter cells. Cytokinesis allows cell membrane separation.
Adapted from www.studyblue.com/notes/note/n/11-cell-cycle

# *I. The cell cycle*

## A. An overview of the cell cycle

The cell cycle can be defined as the regulated sequence of events that leads to cell division. It is classically divided into four phases: G1, S, G2 and M (Figure 1). Together, the G1, S, and G2 phases make up the period known as interphase by opposition to mitosis (M). G1 and G2 are two Gap phases that allow cell growth and maturation. S phase is characterized by DNA replication that generates two identical copies of each chromosome, called sister chromatids. During mitosis, sister chromatids are separated and partitioned evenly to the two daughter cells. The memory of which one is whose sister, from the time when the chromatids are generated until they separate, is provided by cohesin, the molecular glue that keeps the sister chromatids together. Duplication of the genetic materials and its accurate transmission into daughter cells are two critical aspects of the cell cycle that must be coordinated and executed with precision to avoid aneuploidy that is often associated with developmental defects and cancers.

## B. Cell cycle regulation by CDKs

Central to cell cycle are the Cyclin Dependent Kinases (CDKs) and the cyclin proteins that regulate the cell progression through the G1, S, G2 and M phases. CDK is a highly conserved class of proteins and constitute a family of heterodimeric serine/threonine kinases. CDK protein structure is characterized by a conserved catalytic core made up of an ATP-binding pocket, a PSTAIRE-like cyclin-binding domain and an activating T-loop motif (Figure 2A). T-loop closes ATP pocket on monomeric CDK. Cyclin recognizes PSTAIRE motif on CDK and its binding induces conformational changes by pushing PSTAIRE motif on ATP binding pocket, and allows T-loop displacement. In *Saccharomyces cerevisiae* and *Schizosaccharomyces pombe*, only one CDK (Cdc28 and Cdc2 respectively) is sufficient to drive the cell cycle (Hartwell, Culotti, and Reid 1970; Simchen 1978) contrary to mammals in which different CDKs are involved.

CDKs are regulated by several mechanisms, one of which is the phosphorylation of some specific threonine and tyrosine residues (Figure 2A-B). Indeed, CAK (CDK activating Kinase) induces an activating phosphorylation on a conserved threonine within the T-loop

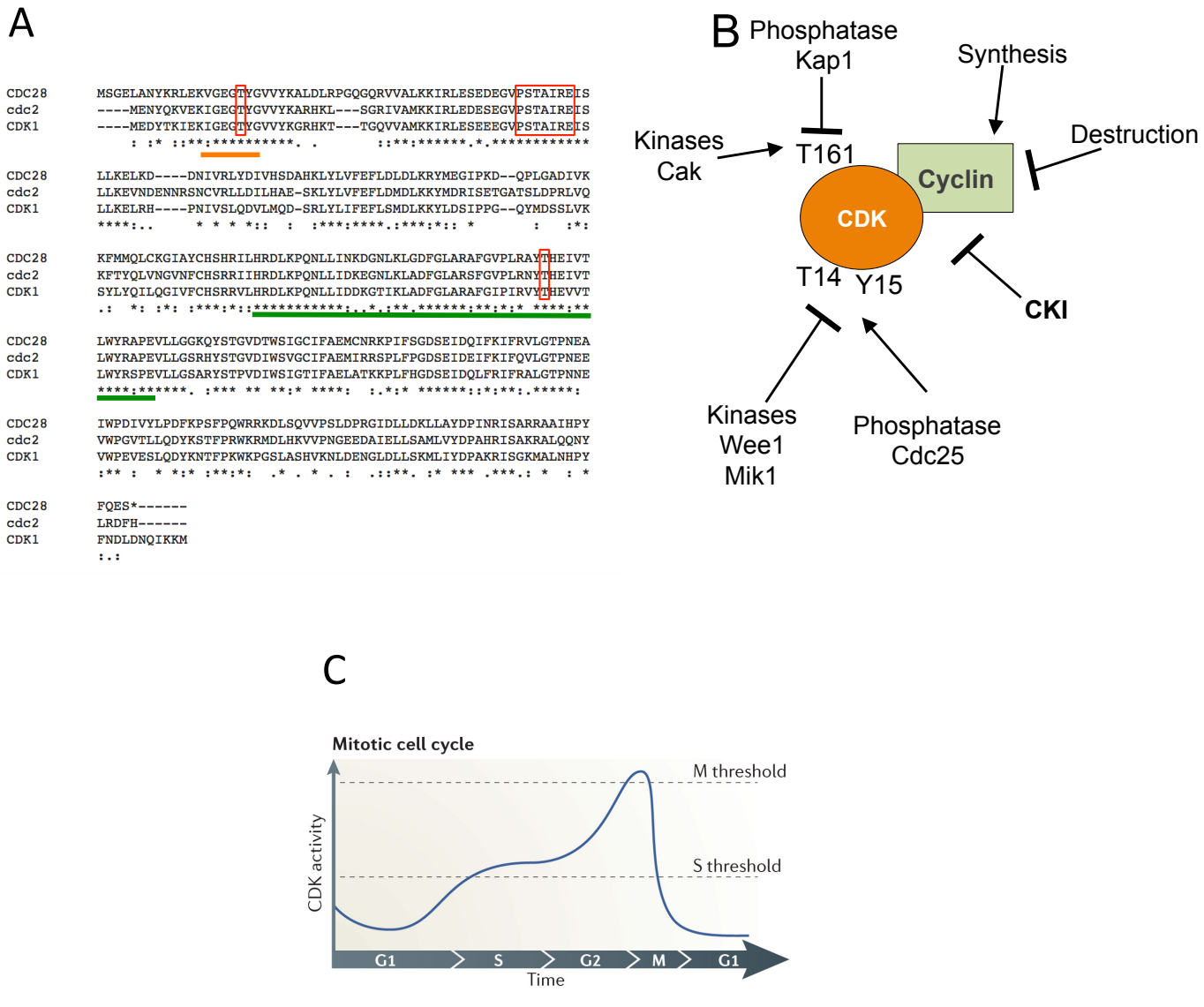


**Figure 2 : A.** Alignment of Cdc2 (fission yeast), CDC28 (budding yeast) and CDK1 (Human) sequences showing a high conservation across species. Inhibitory threonine, PSTAIRE domain and activating threonine are framed. Orange lane and green lane show ATP binding site and T-loop, respectively. **B.** CDK-Cyclin activity is regulated at multiple levels. **C.** S phase and M phase initiation are triggered by different thresholds of cyclin-dependent kinase (CDK) activity, regardless of which cyclin–CDK complex provides the activity (Edgar, Zielke, and Gutierrez 2014 )

(T167 in fission yeast, T169 in budding yeast and T161 in mammals), whereas phosphorylation on tyrosine 15 (and threonine 14 in mammalian cells) induced by Wee1/Mik1 kinase inhibits CDK activity. In addition to appropriate phosphorylation state of CDK, binding to a cyclin is required for the activation (Russo, Jeffrey, and Pavletich 1996). This regulation is achieved by controlling cyclin expression and subcellular localization during cell cycle progression. In addition CDK activity can also be modulated by direct binding to CKI (CDK inhibitors).

Different processes define substrate specificity of CDKs. On the one hand, phosphorylation by CDKs occurs at consensus sites [S/T]*PX[K/R] on substrates in which S/T is the phosphorylated residue. On the other hand, cyclins contain a hydrophobic patch that can bind LP or RXL motif on specific substrates during G1 and S phase respectively (Kõivomägi and al. 2011; Loog and Morgan 2005; Schulman, Lindstrom, and Harlow 1998). CDK can bind different cyclins leading to the formation of complexes with various specificities. Consistently, many experiments in mice and yeast suggested that cyclin couldn't be interchangeable. However, Paul Nurse and co-workers have demonstrated with an elegant method that progression through the cell cycle can be recapitulated only by modulating an engineered monomolecular cyclin-dependent protein kinase module lacking much of the canonical regulation (Coudreuse and Nurse 2010). Their results strongly suggest that the cell cycle is essentially driven by reaching different thresholds of Cyclin-Dependent Kinase activity, whatever which cyclin–CDK complex provides the activity (Figure 2C).

## C. Interphase

### *1) G1/S transition: the START checkpoint*

In fission yeast, Cdc2 in association with the Cig2 cyclin ensures the G1/S transition (START checkpoint). The CKI Rum1 directly binds Cdc2-Cig2 and inhibits the complex. Rum1 phosphorylation by Cdc2-Cig1 and Cdc2-Puc1 induces its degradation to ensure sufficient Cdc2-Cig2 activity (Figure 3A). Other CDKs are also implicated in G1/S transition by sensing output signals as the well-known Pho85 kinase in budding yeast. Pho85 has many roles such as the control of phosphate uptake, cell polarization and cell cycle transition (Huang, Friesen, and Andrews 2007). Fission yeast sequence homologous of Pho85 is Pef1. Pef1 has been described as a CDK by its high degree of sequence homology with Cdc2

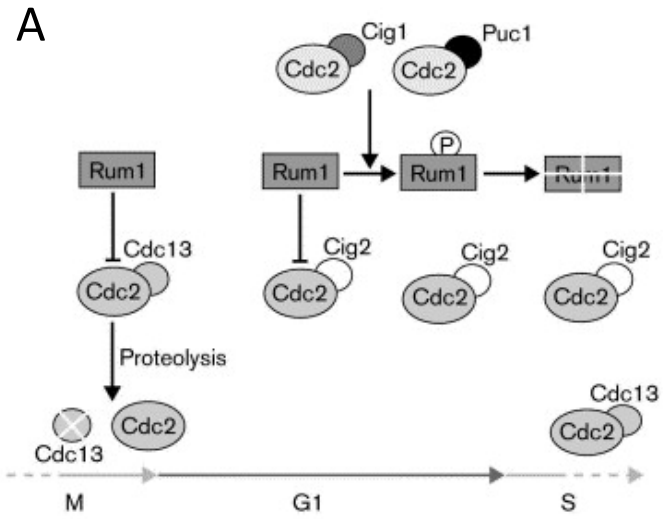


B

```
cdc2      MENYQKVEKIGEGTYGVVYKARHKLSGRIVAMKKIRLEDESEGVPSTAIREISLLKEVND
Pef1      -MNYQRLEKLGEGTYAHVYKGQNRVTGEIVALKVIRID-ADEGTPSTAIREISLMKELRH
            ***::**:*****. ***.:.:::*.***:* **::  .**.**********:**:..

cdc2      ENNRSNCVRLLDILHAESKLYLVFEFLDMDLKKYMDRISETGATSLDPRLVQKFTYQLVN
Pef1      P----NIMSLSDVLQTENKLMLVFEYMEKDLKKYMDTYGNQGA--LPPSQVKNFTQQLLK
               * : * *:*::*.** ****::: *******  .: **  * *  *::** **::

cdc2      GVNFCHSRRIIHRDLKPQNLLIDKEGNLKLADFGLARSFGVPLRNYTHEIVTLWYRAPEV
Pef1      GISFCHENRVLHRDLKPQNLLINSRGELKLADFGLARSIGIPVNTFSNEVVTLWYRAPDV
          *:.***..*::***********:..*:**********:*:*:..::.*:*********:*

cdc2      LLGSRHYSTGVDIWSVGCIFAEMIRRSPLFPGDSEIDEIFKIFQVLGTPNEEVWPGVTLL
Pef1      LLGSRVYSTSIDIWSVGCIMAEMATGRPLFAGSNNEDQLLKIFRLLGTPTEQSWPGISLL
          ***** ***.:*********:***    *** *..: *:::***::****.*: ***::**

cdc2      QDYKSTFPRWKRMDLHKVVPNGEEDAIELLSAMLVYDPAHRISAKRALQQNYLRDFH
Pef1      PEYKPTFPIYKAQDLAYLFPTFDPLGLDLLRRMLRLQPELRTTGQDALQHAWFLTA-
           :** *** :*  **  :.*. :  .::**  **  :*  * :.: ***: ::
```

**Figure 3 : The G1-S transition. A.** G1/S transition or START checkpoint (Moser and Russell 2000). **B.** Cdc2 and Pef1 alignment. All structural Cdc2 features are conserved in Pef1 kinase with the exception of the activating threonine which is replaced by a serine residue.

(Figure 3B). Pef1 in association with its cyclin partner Pas1 stimulates the G1-S transition by specifically activating the Res2p-Cdc10p complex. Contrary to Pho85, Pef1 is not implicated in phosphate regulation (K. Tanaka and Okayama 2000). Tor1 and Tor2 are also two kinases (in budding yeast, fission yeast and mammalian cells) involved in the control of cell cycle start in response to nutriment availability. Collectively, the phosphorylation events induced by these different kinases lead to the activation of the MBF (*MluI* cell cycle box-binding factor) transcription factor (Ayté and al. 2001; K. Tanaka and Okayama 2000; Connolly, Caligiuri, and Beach 1997). MBF is made of Cdc10, Res1 and Res2 in fission yeast. Its association with Rep2 protein activates the cell-cycle-dependent transcription of genes required for S phase like *cdc18* a gene essential for DNA replication (Muzi Falconi, Brown, and Kelly 1996). The Pef1-Pas1 complex has also been shown to also be able to activate MBF independently of Rep2 (K. Tanaka and Okayama 2000).

### *2) S phase: DNA replication*

Duplication of the genetic material takes place during S phase and is referred as DNA replication. This process that requires components highly conserved across species can be divided in two major steps: the recruitment of replication factors at replication origins (the licensing) and the replication *per se* by processing proteins (Figure 4A).

Replication origins are "licensed" in G1 by the assembly of pre-replicative complexes (pre-RCs) consisting of ORC (the origin recognition complex), Cdc6, Cdt1 and minichromosome maintenance (MCM) proteins (for review Sclafani and Holzen 2007). Later on, the activity of CDK and Dbf4–Cdc7 (DDK) kinases promote the loading of additional replication proteins such as Cdc45 and GINS (Go, Ichi, Nii, San) to unwind DNA for DNA polymerase loading. The recruitment of other proteins such as proteins of the RFC (replication factor C), PCNA (proliferating cell nuclear antigen), RPA (replication protein A) and other DNA polymerases) allows formation of two functional replication forks that move in opposite directions from the activated origin. DNA replication occurs on both DNA strands (leading and lagging strands) but due to the directionality of DNA synthesis (5'->3'), replication of the lagging strand is discontinuous and requires assembly of Okazaki fragments and additional replication factors like Fen1 (Flap Endonuclease 1), Dna2 and DNA polymerase δ (for review Fragkos and al. 2015) (Figure 4B).

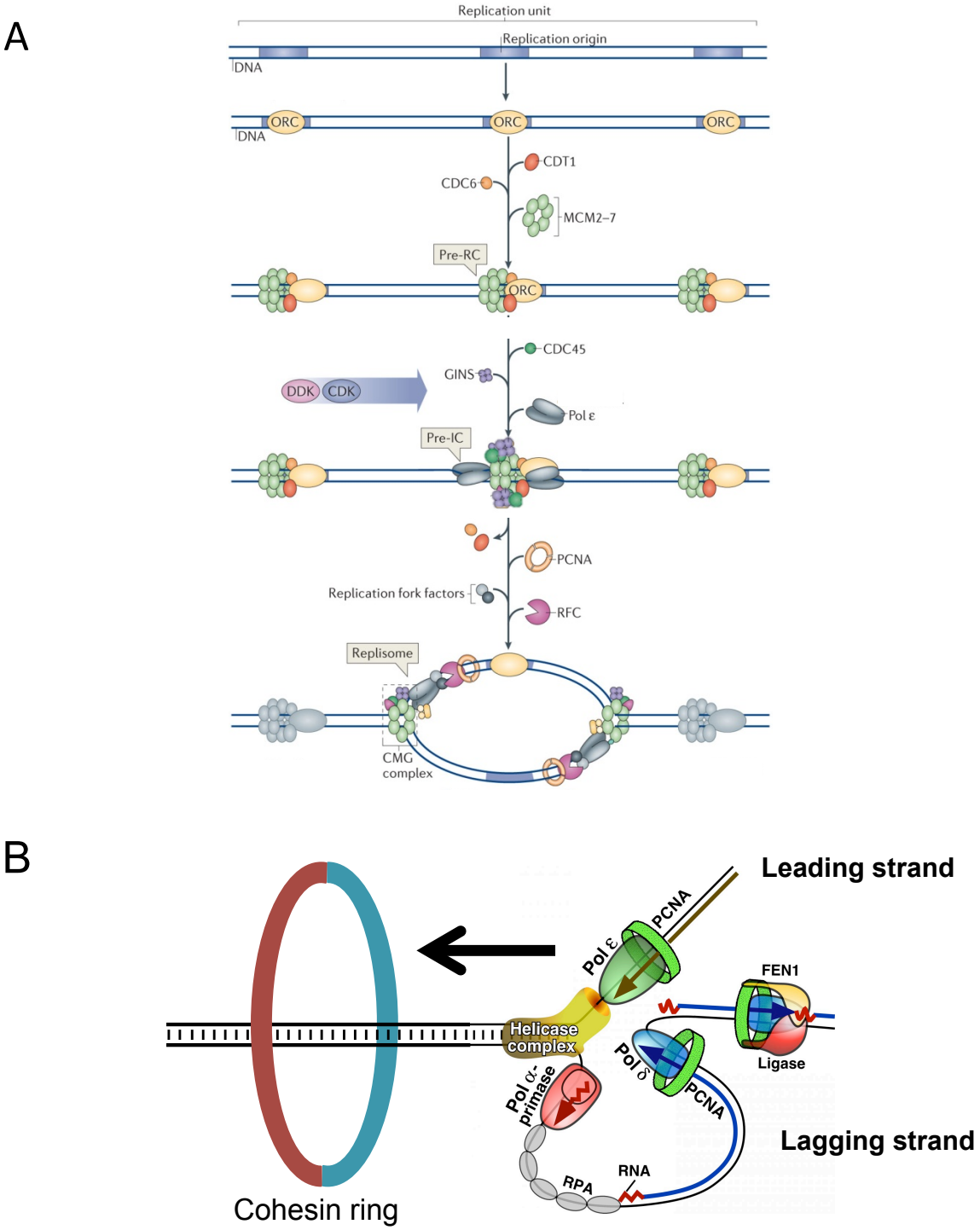


**Figure 4 : DNA replication**. **A.** Licensing of replication origins is restricted to the G1 phase of the cell cycle and results from the sequential loading of pre-replication complex (pre-RC) proteins. The ORC complex is first recruited on all potential origins in the genome. ORC recruitment is followed by the binding of CDC6 and CDT1. Loading of MCM helicase complex is the last step of the licensing reaction. Origin activation involves the formation of a pre-initiation complex (pre-IC) and activation of the MCM helicase complex. Assembly of the pre-IC is triggered at the G1–S phase transition by DDK and CDKs that phosphorylate several replication factors (of which CDC45, GINS, and DNA polymerase ε (Pol ε) are the most important) to promote their loading on origins. MCM complex phosphorylation results in helicase activation and DNA unwinding. Helicase activation induces the recruitment of other proteins (such as RFC proteins, PCNA, RPA and other DNA polymerases) that convert the pre-IC into two functional replication forks that move in opposite directions from the activated origin, with the replisome at each replication fork (adapted from “DNA replication origin activation in space and time”, Michalis Fragkos, 2015). **B.** Asymmetry of DNA replication : DNA polymerase III replicates the leading strand. However, the lagging strand replication requires the synthesis of RNA primers by primase activity enabling DNA polymerase III to add DNA nucleotides. These incomplete DNA portions are called Okazaki fragments. DNA polymerase I replaces the RNA with DNA along the chain, filing the gaps between Okazaki fragments, but leaves unconnected "nicks”. To complete the strand DNA ligase (Fen1) links the nicks together (adapted from Burgers lab home page).

DNA replication produces two identical DNA molecules named sister chromatids that are paired by the cohesin complex. The mechanism by which cohesin establishes sister chromatid cohesion during DNA replication remains largely unknown. It has been proposed that the replication fork might pass through cohesin rings, or alternatively cohesin might sequentially embrace two replicated DNAs in the wake of the replication fork (Lengronne and al. 2006). What it is clear is that DNA replication and sister chromatid cohesion are intimately linked to each other and that both of these processes must be correctly achieved to preserve genomic integrity and allow correct genetic inheritance.

### *3) G2/M transition*

After complete DNA replication and critical cell size accomplishment, M-phase is induced by increasing Cdc2-Cdc13 (also called MPF for Maturation Promoting Factor) kinase activity. Cdc13 binds Cdc2 kinase from S phase, but a conserved phosphorylation on tyrosine 15 induced by Wee1/Mik1 kinases inhibits Cdc2-Cdc13 activity. An inhibitory phosphorylation of threonine 14 by Mik1 has also been described in mammalian cells (Liu and al. 1997). At the G2/M transition, the conserved phosphatase Cdc25 dephosphorylates Y15 (and T14) to ensure activation of MPF and mitotic entry. The inhibitory phosphorylation of Wee1 by Nim1 (Coleman, Tang, and Dunphy 1993), and the activating phosphorylation of Cdc25 by MPF (positive feedback loop) leads to the amplification of MPF activity that reaches a threshold allowing the transition from G2 to mitosis (Figure 5).

## D. Mitosis

### *1) The different steps of mitosis*

The process of mitosis is divided into distinct phases that are largely defined by the organization and behaviour of the chromosomes (Figure 6A). During the prophase stage, the chromatin becomes progressively condensed and chromosomes appear as two individualized sister chromatids that are linked together by cohesin. At this time, the interphase microtubule network has been depolymerised and microtubules are progressively organized to form a mitotic spindle emanating from the two centrosomes.

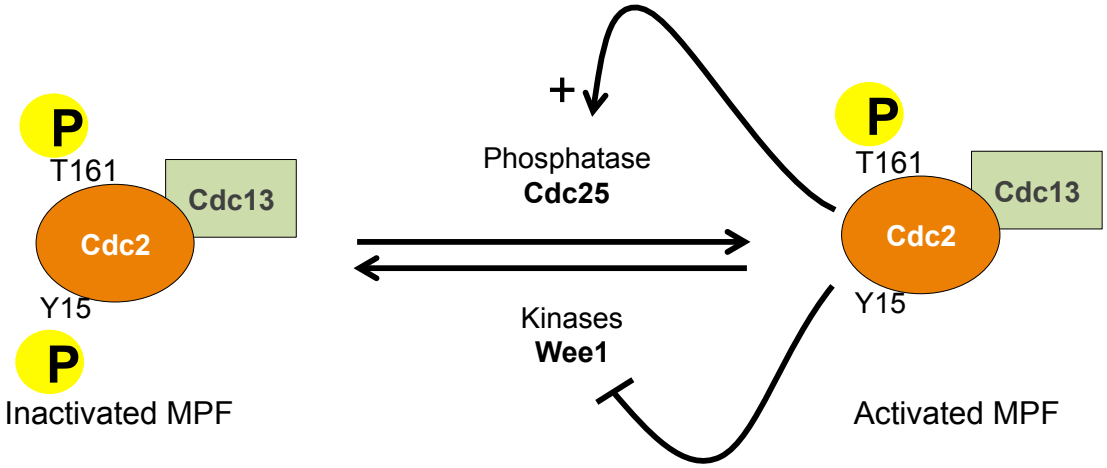


**Figure 5 : The G2-M transition**. Cdc2 bound to cyclin B (Cdc2-Cdc13) is phosphorylated on the "activating" threonine 161 by CAK but the kinase is kept inactive by the inhibitory phosphorylation of the tyrosine 15 by Wee1-like kinases. At the G2-M transition, Cdc25 dephosphorylates Cdc2 on its tyrosine 15 leading to Cdc2-Cdc13 activation which in turn phosphorylates Cdc25 and Wee1 to respectively increase and decrease their activities. These two feedback loops result in the abrupt and irreversible activation of Cdc2 and in entry into mitosis (P = phosphorylated)**.**

Nuclear envelope breakdown marks the transition between prophase and prometaphase, during which the attachment of the microtubules to the chromosomes begins. In Fungi, the nuclear membrane persists all along mitosis (closed mitosis). During prometaphase, microtubule fibers capture chromosomes through their binding to kinetochores, which are protein complexes assembled onto centromeric DNA. Sister kinetochores connect to opposite spindle poles leading to chromosome bi-orientation called amphitelic attachment (Figure 6B). Chromosomes then exhibit a complex pattern of movements that is often described as 'the dance of chromosomes' in classic cytology literature. These seemingly chaotic movements result in the grouping of chromosomes to the spindle equator.

Metaphase is the stage at which all chromosomes are aligned on the mitotic spindle. Sister chromatid cohesion is of fundamental importance for this process as it counteracts the pulling forces of microtubules toward the spindle poles. Shortly after metaphase alignment, the cohesion between sister's chromatids is irreversibly destroyed by cohesin cleavage by a site-specific protease called "Separase" that is conserved in all Eukaryotes.

Sister chromatid pairs then split and separate as the cell enters anaphase. Sister chromatids move poleward (anaphase A) and the poles separate from each other (anaphase B). During the next stage, telophase, the chromosomes de-condense as the nuclear envelope reforms around the two daughter nuclei. The cell is finally divided into two by cytokinesis (Walczak, Cai, andKhodjakov 2010).

### *2) Control of the metaphase to anaphase transition*

Faithful chromosome segregation during mitosis is governed by the Spindle Assembly Checkpoint (SAC), a surveillance mechanism that senses kinetochore attachment to spindle microtubules and prevents progression through anaphase until all chromosomes are properly bioriented. A large number of proteins are implicated including Mad1, Mad2, Mad3 (Mitotic Arrest Deficient), Bub1, Bub3 (Budding Uninhibited by Benzimydazole) and Mps1 (MonoPolar Spinlde 1). This checkpoint operates by inhibiting the anaphase-promoting complex/cyclosome (APC/C) and thereby anaphase onset. Indeed, APC/C is responsible for Separase activation and thereby cohesin cleavage and also responsible for Cdc13 cyclin degradation, the two main events involved in metaphase to anaphase transition (Figure 7).

A

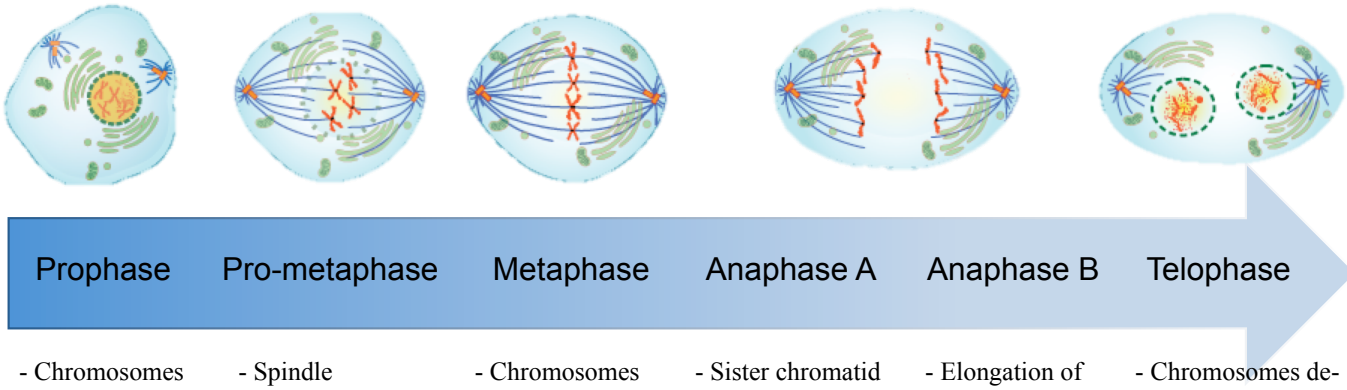

| Prophase | Pro-metaphase | Metaphase | Anaphase A | Anaphase B | Telophase |
|---|---|---|---|---|---|
| - Chromosomes condense<br><br>- Spindle microtubules emerge from the centrosomes | - Spindle microtubules attach to kinetochores<br><br>- Centrosomes move toward opposite poles | - Chromosomes line up at the metaphase plate<br><br>- Sister-chromatid pairs are bilaterally attached to spindle microtubules (amphitelic attachment) | - Sister chromatid cohesion is destroyed | - Elongation of spindle microtubules | - Chromosomes de-condense<br><br>- Nuclear envelope material surrounds each set of chromosomes<br><br>- The mitotic spindle breaks down |

B

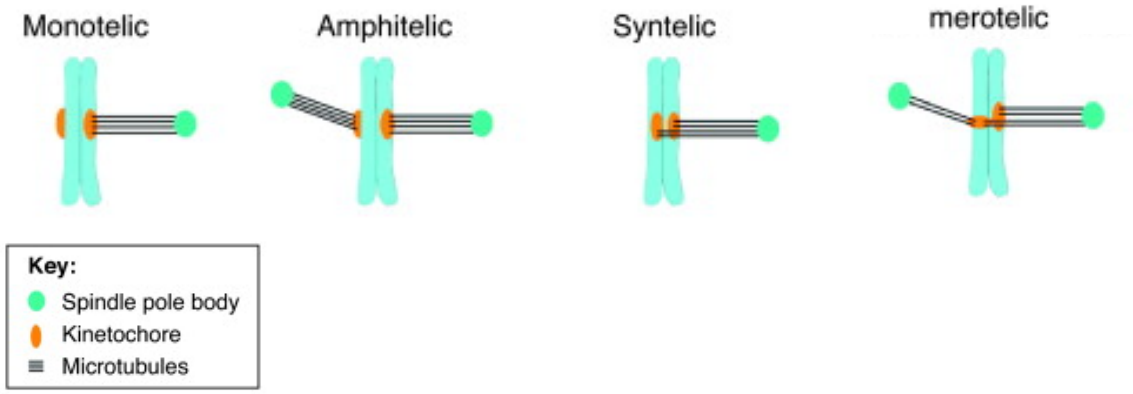


**Figure 6 : A.** The different steps of mitosis. **B.** Types of kinetochore attachments during mitosis. Monotelic attachment: only one of the two sister kinetochores is attached to spindle microtubules. Amphitelic attachment: sister kinetochores are attached to microtubules emanating from opposite spindle poles. Monotelic kinetochore attachment is an intermediate state preceding proper amphitelic attachment. There are two types of erroneous kinetochore attachments: syntelic attachment, where both sister kinetochores interact with microtubules emanating from the same spindle pole, and merotelic attachment, where a single kinetochore is connected to both spindle poles. To segregate chromosomes properly, erroneous kinetochore attachments should be corrected and amphitelic attachments stabilized ( adapted from Gregan, 2011).

The SAC monitors whether kinetochores are associated with microtubules or not. A single unattached kinetochore (monotelic attachment) is sufficient to activate the SAC (Rieder and al. 1995, Guse and al. 2011). Unattached kinetochores serve as a scaffold for recruiting SAC proteins and generate the inhibitory signal. It has long been debated whether or not lack of tension across sister chromatids (and/or intra-kinetochore tension) can also be sensed by this checkpoint (Khodjakov and Pines 2010; Maresca and Salmon 2010). Sister chromatid cohesion is a major contributor to the establishment of tension, as it provides the counterforce that resists microtubule-pulling forces upon spindle attachment. As a result, correctly attached kinetochores become stretched. It has been proposed that kinetochore stretching generates a physical distance between Aurora B kinase (localized within the inner centromere) and its substrates (kinetochore proteins). In absence of tension (monopolar attachment for instance), Aurora B would phosphorylate its substrates and lead to microtubule instability ensuring SAC activation. Multiple cycles of attachment / correction would occur until the correct bilateral attachment is made. However, some types of faulty attachments may escape. Merotelic attachments, in which a single kinetochore is attached to microtubules emanating from both spindle poles, may generate sufficient tension across sister kinetochores to escape detection. Failure to correct merotely causes chromatids to lag on the mitotic spindle hindering their timely correct segregation.

# *II. Cohesin structure and its interaction with DNA*

## A. The cohesin complex

### *1) Structure of the cohesin complex*

The cohesin complex is made of four core subunits: Smc1, Smc3, Scc1 and Scc3 (Psm1, Psm3, Rad21 and Psc3 respectively in *S. pombe)* (Figure 8). Together these proteins form a ring-like structure with a 45-50 nm diameter as seen by electron microscopy (Anderson and al. 2002; Huis in ’t Veld and al. 2014). The proteins Pds5 (precocious dissociation of sister protein 5) and Rad61 (Pds5 and Wpl1 respectively in *S.pombe*) are regulatory factors that interact with cohesin to modulate its function. The four core proteins have a 1:1:1:1 stoichiometry whereas Pds5 and Wpl1 are sub-stoichiometric (Holzmann and al. 2011).

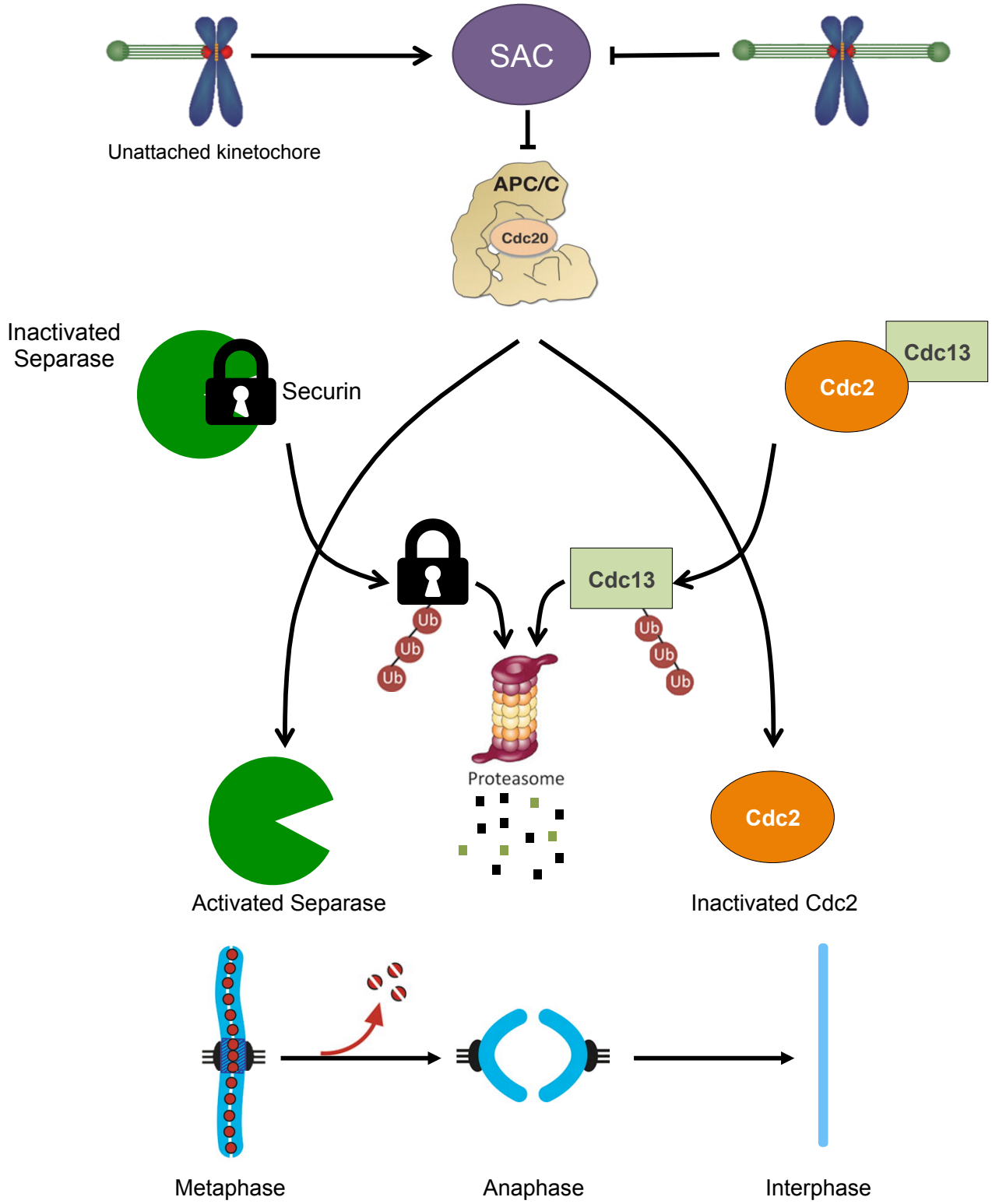


**Figure 7 : The metaphase to anaphase transition.** The Anaphase Promoting Complex or Cyclosome (APC/C) is an E3 ubiquitin-ligase that targets specific proteins for degradation by the proteasome. The activity of APC/C in conjunction with its accessory protein Cdc20 is controlled by the spindle assembly checkpoint (SAC). This multi-component surveillance mechanism creates a diffusible "wait anaphase signal", which inhibits APC/C-Cdc20 as long as chromosomes are not properly connected with the mitotic spindle apparatus. APC/C activation leads to the degradation of Securin and Cdc13 cyclin at the metaphase-to-anaphase transition. Separase then cleaves cohesin and thereby destroys cohesion enabling sister chromatids to separate. Cdc2 inactivation leads to mitotic exit.

Smc1 and Smc3 are ABC-like ATPases that belong to the SMC protein family (Structural Maintenance of Chromosome). In Eukaryotes, there are at least six different Smc proteins that form three heterodimers in specific combinations: The Smc2–Smc4 pair is part of the condensin complex and plays an essential function in chromosome condensation and segregation. The Smc5-Smc6 pair is part of a complex mainly involved in DNA repair and checkpoint responses but whose exact functions remain largely unknown (Lehmann, 2005). Lastly, the Smc1-Smc3 heterodimer is part of the cohesin complex. Smc1 and Smc3 like the other Smc proteins are flexible coiled-coil proteins that fold back on themselves to yield molecules with a "hinge" domain at one end and a globular Nucleotide Binding Domain (NBD) at the other (Figure 9). The hinge domains bind tightly together whereas a kleisin protein, Scc1/Rad21 for the cohesin complex, connects the Smc heads. The Smc1–3 mouse hinge crystal structure has been described as a doughnut shape with a channel in the middle (Kurze and al. 2011)(Figure 10A). The residues within this channel form a positively charged cavity and it has been suggested that it might be a DNA-binding site required for cohesin binding to DNA (Gruber and al. 2006) . The NBD domains from each Smc protein can bind together and hydrolyse Adenosine triphosphate (ATP) in a sandwich dimer mode. In these structures, ATP binds to a pocket formed by the Walker A and Walker B motifs from one Smc subunit (from N-terminal and C-terminal respectively), and makes a contact with the C motif from the second subunit emanating from its C-terminal domain (Figure 9).

The kleisin Scc1/Rad21 interacts with each of the two Smc proteins in an asymmetric way to form the cohesin ring (Figure 10B-C). This has been confirmed by structure analysis by crystallography and *in vivo* cross-linking methods that allowed the mapping of these interactions. The C-terminal domain of Scc1 forms a winged helix domain (WHD) that contacts the globular domain of Smc1 (Haering and al. 2004). The Scc1's N-terminal domain binds to the coiled-coil emerging from Smc3's ATPase head (Gligoris and al. 2014; Huis in 't Veld and al. 2014) . The N-terminal domain of Scc1 is composed by three alpha helices ($\alpha$1, $\alpha$2 and $\alpha$3). The $\alpha$2 and $\alpha$3 helices contact the coiled-coil structure of Smc3 protein to form a compact four-helix bundle. Finally, it has been shown that the central part of the kleisin Scc1/Rad21 plays a crucial role in the recruitment of Scc3 but also Pds5 and Wapl to the ring (Intyre and al. 2007; Roig and al. 2014; Orgil and al. 2015; Lee and al. 2016; Muir and al. 2016).

A

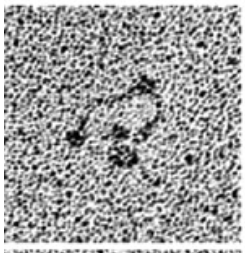

100 nm

B

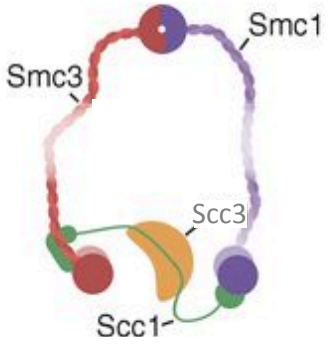


50nm

C

| | | S. cerevisiae (Budding yeasts) | S. pombe (Fission yeasts) | A. thaliana (Plants) | C. elegans (Nematodes) | D. melanogaster (Insects) | H. sapiens (Human) |
|---|---|---|---|---|---|---|---|
| **Cohesin** | | | | | | | |
| Subunits | κ-SMC | Smc1 | Psm1 (Smc1) | SMC1 (TTN8) | HIM-1 (SMC-1) | Smc1 | SMC1α, SMC1β* |
| | ν-SMC | Smc3 | Psm3 (Smc3) | SMC3 | SMC-3 | Smc3 | SMC3 |
| | α-kleisin | Scc1 (Mcd1), Rec8* | Rad21, Rec8* | SYN2, SYN3, SYN4, SYN1* | SCC-1 (COH-2), COH-1, REC-8*, COH-3/4* | Rad21, C(2)M?* | SCC1, REC8*, RAD21L* |
| | HEAT-A | Pds5 | Pds5 | PDS5 | EVL-14 | Pds5 | PDS5A, PDS5B |
| | HEAT-B | Scc3 (Irr1) | Psc3, Rec11* | SCC3 | SCC-3 | SA, SA-2 (SNM)* | SA1, SA2, SA3* |
| Regulators | Kollerin (loading complex) | Scc2 | Mis4 | SCC2 | PQN-85 (SCC-2) | Nipped-B | NIPBL (SCC2) |
| | | Scc4 | Ssl3 | – | MAU-2 | Mau-2 | MAU2 (SCC4) |
| | Acetyl-transferase | Eco1 (Ctf7) | Eso1 | ECO1 (CTF7) | F08F8.4 | Eco (Deco) + San | ESCO1, ESCO2 |
| | Deacetylase | Hos1 | – | – | – | – | HDAC8 |
| | Stabilizer | – | – | – | – | Dalmatian | Sororin (CDCA5) |
| | Destabilizer | Wpl1 (Rad61) | Wpl1 | WAPL | WAPL-1 | Wapl | WAPL |

**Figure 8 : Cohesin forms a ring. A.** Cohesin ring seen by electron microscopy (Gruber 2006) **B.** Schematic view of the cohesin ring. **C.** Name of conserved structural cohesin proteins and cohesin regulatory subunits across species. (Haering CH and Gruber S 2016, * Meiosis specific)

### *2) Topological binding of cohesin to chromatin*

Cohesin has been extensively studied for its crucial function in sister chromatid cohesion. Cohesion is made during S phase and maintained until the metaphase to anaphase transition. At this stage, cohesion between sister chromatids is lost because of the cleavage of the Scc1/Rad21 kleisin by the proteolytic enzyme Separase. The discovery that cohesin's subunits together create a gigantic ring whose integrity is destroyed by Scc1 cleavage at the onset of anaphase has raised the idea that sister DNAs might be entrapped inside cohesin's ring. Strong experimental evidences support this model. Indeed, it has been demonstrated that cohesin binding to chromatin resists to high salt wash but that DNA nuclease digestion allowed cohesin release from DNA (Ciosk and al. 2000). Reciprocally, opening of the cohesin ring through an artificial site-specific proteolytic cleavage in the coiled-coil of Smc3 is sufficient to release cohesin from chromosomes and destroy sister chromatid cohesion (Gruber, Haering, and Nasmyth 2003; F. Uhlmann, Lottspeich, and Nasmyth 1999; F. Uhlmann and al. 2000; Gruber, Haering, and Nasmyth 2003; Ivanov and Nasmyth 2005; Ivanov and Nasmyth 2007). Linearization of circular minichromosomes releases their association with cohesin *in vitro* (Ivanov and Nasmyth 2005), and covalent connection of the three protein interfaces renders minichromosome-cohesion resistant to protein denaturation (Haering and al. 2008). Altogether, these data suggest that cohesin rings topologically interact with chromatin and have led to the hypothesis that sister chromatid cohesion might be the result of sister DNAs entrapment inside a cohesin ring.

Whether sister DNAs are held together by individual cohesin complexes (the “strong” ring model) or by two or more complexes that interact with each other (handcuff and bracelets models) remains under debate (Figure 11). The handcuff model is supported by co-immunoprecipitation experiments performed in human cells where it has been shown that Smc1, Smc3 and Rad21 interact with themselves in a Scc3-dependent manner (N. Zhang and al. 2008). More recently, experiments performed in budding yeast demonstrated that co-expression of two mutant alleles of Scc1 (each being deficient for sister chromatid cohesion) restores cohesion (Eng, Guacci, and Koshland 2016). Similar intra-allelic complementation effects have also been obtained with *smc3* supporting a model in which cohesin ring entraps one DNA molecule and oligomerization of cohesin ensures cohesion (Figure 11C). Finally, cohesin-cohesin interaction has also been suggested by high resolution ChIP-sequencing analysis (Nagy and al. 2016). Because of the numerous functions of cohesin it could be envisaged that different cohesin binding modes might co-exist in the cell.

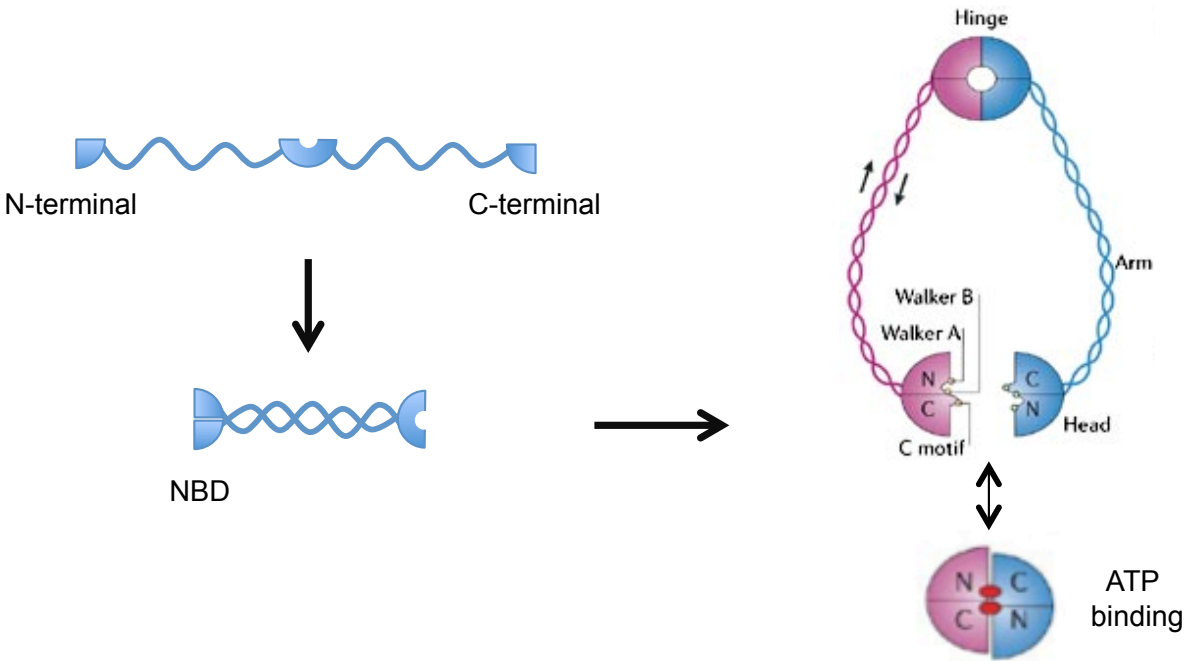


**Figure 9 : SMC proteins architecture.** Smc proteins fold back on themselves to form a Nucleotide Binding Domain (NBD), a long coiled-coil and a hemi-hinge domain. Dimerization of two Smc proteins leads to two functional ATP binding domains and a hinge domain separated by a long coiled-coil domain describing a V-shape structure (Nasmyth K and al 2005).

## B. DNA capture by the cohesin ring: a reversible event

### *1) Cohesin loading*

DNA capture by the cohesin ring, called the loading reaction, requires ATP binding and hydrolysis by the Smc proteins. Indeed, mutants in ATPase Walker A or Walker B domain of Smc1 or Smc3 that inhibit ATP binding failed to load cohesin *in vivo* and *in vitro* (Arumugam and al. 2003; Lehane, and Uhlmann 2003; Arumugam and al. 2006; Murayama and Uhlmann 2014; Weitzer). Mutations in the C-loop domain of Smc1 or Smc3 that prevent ATP hydrolysis without modifying its binding failed to ensure correct cohesin binding to chromatin (Hu and al. 2011).

In addition to ATP binding and hydrolysis, capture of DNA molecules by the cohesin ring has been shown to require the opening of an "entry gate" located at the Smc1-Smc3 hinge interface. Nasmyth and co-workers have shown that covalently closed Smc1-Scc1 and Smc3-Scc1 interfaces do not block cohesin loading. By contrast, cohesin binding to chromatin was completely inhibited by the artificial closing of Smc1-Smc3 interface at their hinge domains. These results strongly suggest that the opening of the Smc1-Smc3 hinge interface is required for cohesin binding to chromatin (Figure 12A). Based on ABC-like transporter structure of Smc proteins, it has been proposed a model in which ATP hydrolysis induced a conformational change on the Smcs V-shaped structure that leads to a transient dissociation of hinge domains allowing DNA entry into the ring (Gruber and al. 2006).

In budding yeast, DNA capture by cohesin has been shown to require the action of a separate complex, the loading complex, which is made of two essential proteins: Scc2 and Scc4 (Ciosk and al. 2000). Orthologues of Scc2 are found in numerous species including fission yeast (Mis4)(Furuya, Takahashi, and Yanagida 1998), Drosophila (Nipped-B) and human (NIPBL also known as Delangin). Orthologues of Scc4 have also been identified. The fission yeast counterpart Ssl3 has been discovered by our group from a genetic screen (Pascal Bernard and al. 2006). At the same time, another group has shown that Scc4 and Ssl3 are members of a family of homologous proteins found in other ascomycetes, but also in metazoan and plants (Watrin and al. 2006). Like their budding yeast counterparts, these loading factors are essential for cohesin association with chromosomes.

The C-terminal region of Scc2 contains HEAT (Huntingtin, Elongation factor 3, A subunit of PP2A, and lipid kinase TOR) repeats characterized by multiple consecutive α-helix

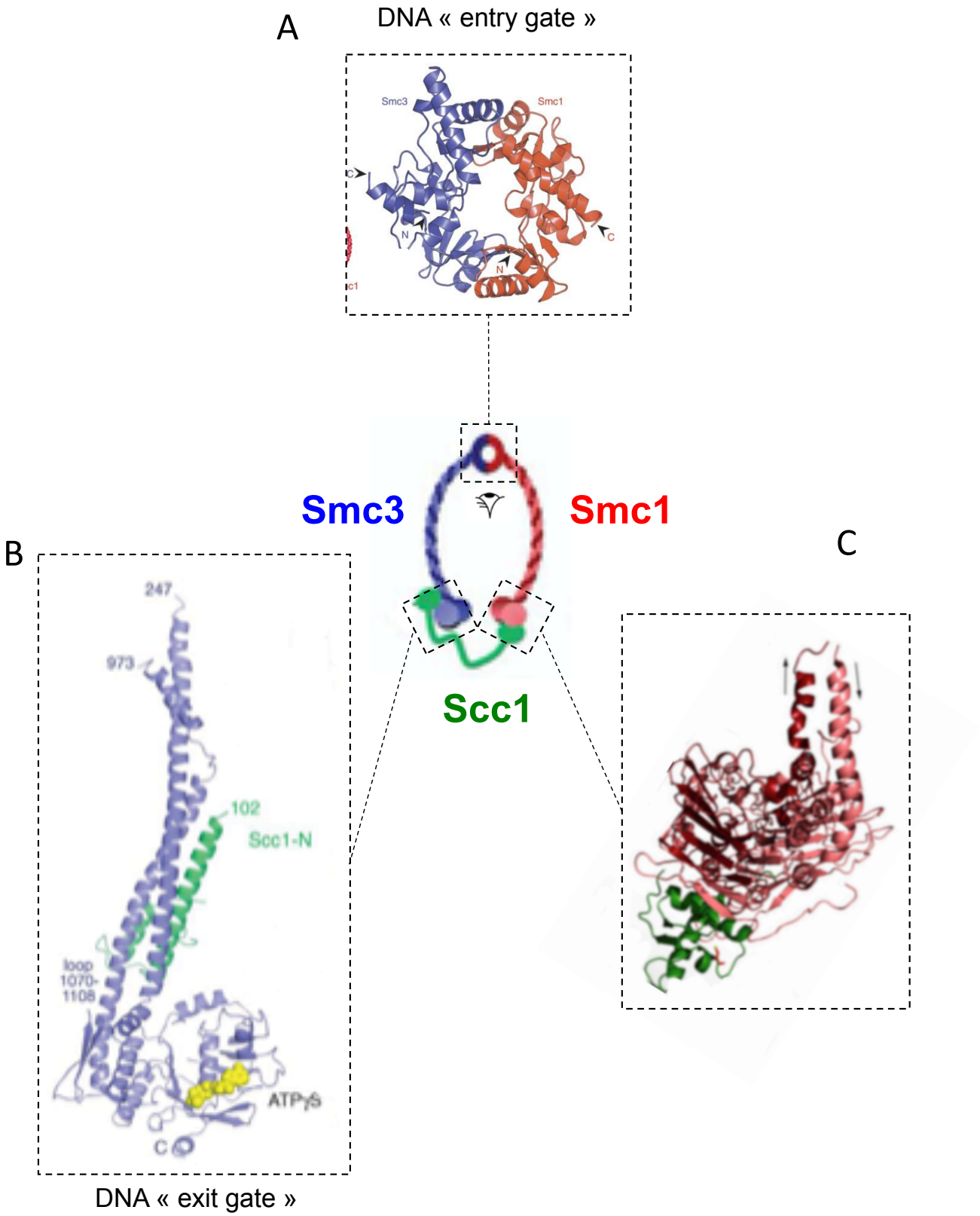


**Figure 10 : One ring, multiples interfaces. A.** Smc1-Smc3 interface describes a hinge (adapted from Kurze and al. 2011). **B.** Smc3-Scc1 interface. Scc1 (green) contacts the coiled-coil domain of Smc3 (blue) emanating from its NBD (adapted from Gligoris and al. 2014 ). **C.** Smc1-Scc1 interface. C-terminal domain of Scc1 forms a winged helix domain and contacts the globular domain of Smc1 (adapted from Deardoff and al. 2012).

that form a solenoid or super helix (Andrade and al. 2001). The N-terminal domain of Scc2 is predicted as unstructured. Scc4 is a TPR (tetra-trico-peptide repeats) protein describing a plate structure with convex and concave phase. Scc4 encloses the N-terminal domain of Scc2 suggesting that Scc4 acts as chaperone to fold the N-terminal domain of Scc2 (Chao and al. 2015; Hinshaw and al. 2015). The Scc2-Scc4 complex has three distinct domains. A globular domain which consists of Scc2-N-terminal and Scc4, a central body and a hook-like tail domain composed by HEAT repeats of Scc2 (Figure 12B).

Recently, the cohesin loading reaction has been recapitulated *in vitro* by using recombinant fission yeast proteins (Murayama and Uhlmann 2014). In this system, cohesin by itself has the ability to hydrolyse ATP and to bind DNA but the reaction is strongly enhanced by addition of the cohesin loader. The cohesin loader makes multiple contacts with the cohesin components leading to the suggestion that it may help conformational changes required for DNA entry inside the ring. Interestingly, Mis4 (Scc2) alone was sufficient to ensure cohesin binding to DNA *in vitro*, this contrast with the essential function of Ssl3 (Scc4) *in vivo*. In the fission yeast, Mis4-GFP forms punctate foci within the nucleus. These are dispersed in a *ssl3-ts* mutant at the restrictive temperature suggesting that Ssl3 might target Mis4 to specific loci (Bernard and al. 2006). Moreover, *in vitro*, cohesin binding displayed no DNA sequence specificity whereas *in vivo* cohesin binding to chromatin is spatially regulated and cohesin accumulates around centromeres and at discrete sites along the chromosomes (Murayama and Uhlmann 2014). It has been proposed that Ssl3 might be essential for controlling cohesin targeting to specific loci.

### *2) Cohesin unloading*

DNA capture by the cohesin ring is a reversible event. Indeed, It has been shown that once captured, DNA can escape from the cohesin ring in an unloading reaction that depends on the Wapl protein (Wings Apart-Like) which together with Pds5 associate with cohesin onto chromatin and promotes its dissociation (Gandhi, Gillespie, and Hirano 2006; Kueng and al. 2006) (Figure 12A).

Experiments performed in yeast, drosophila and human cells have shown that cohesin release from DNA requires the opening of the Smc3-Scc1 interface, the so called “exit gate” by opposition to the “entry gate" (Huis in ’t Veld and al. 2014; Eichinger and al. 2013; Chan

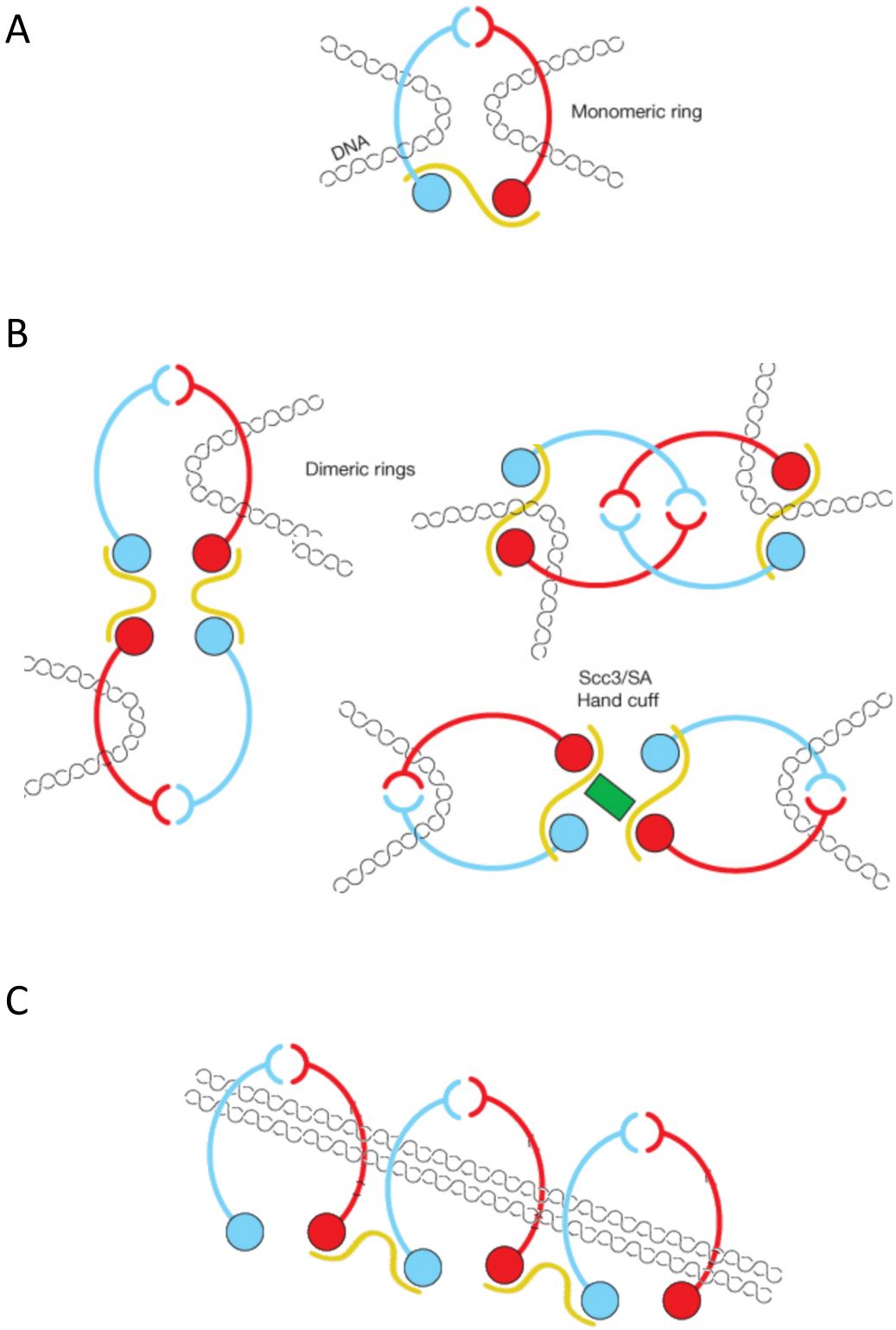


**Figure 11 : Cohesin-DNA interaction models A.** The embrace model. Single monomeric cohesin ring entraps sister DNAs. **B.** Handcuff models : cohesin forms dimeric rings, either by virtue of N- and C-terminal kleisin domains binding to NBDs from different Smc1–Smc3 heterodimers or through cohesin ring concatenation or sister DNAs are entrapped inside separate cohesin rings that are connected by binding to the same Scc3/SA subunit (adapted from Nasmyth K. 2011) **C.** The bracelet model. Smc1–Smc3 heterodimers are linked together by kleisin to form an oligomeric bracelet that winds around sisters and does not in fact form a closed ring.

and al. 2012). This observation has led to the idea that Wapl/Pds5 might promote cohesin release by disrupting the Smc3-Scc1 interface. Two sets of recent data strongly support this hypothesis. *In vivo*, the N-terminal part of Scc1 still remains bound to Smc3 after Scc1 cleavage at anaphase in *wpl1* deleted strains (Beckouët and al. 2016). This suggests that Wpl1 function is required to disrupt the Smc3-Scc1 interaction. The unloading reaction has also been recapitulated *in vitro*. In these experiments, Wapl has been shown to disrupt the Smc3-Scc1 interface and promote DNA release from cohesin (Murayama and Uhlmann 2015). This reaction requires the disengagement of Smc heads by ATP hydrolysis, then subsequently the Smc1-Smc3 heads must re-bind ATP to allow Wapl dependent opening of Smc3-Scc1 interface. From these data it was proposed that the first cycle of ATP hydrolysis would enable the disengagement of the SMCs head, allowing DNA to pass this first gate. Wpl1-mediated disruption of the Smc3-Rad21 interface would then allow DNA exit from cohesin (Figure 12).

As loading and unloading reactions may occur simultaneously, the steady state amount of DNA-bound cohesin should result from the equilibrium between the loading and unloading reactions. *In vivo* experiments are consistent with this notion. FRAP experiments on rat G1 cells have revealed that cohesin has a residence time of about 24+-5min on DNA (Gerlich and al. 2006). A similar value was measured in fission yeast by measuring cohesin release from DNA upon inactivation of the cohesin loader Mis4 in G1 cells (Vaur et al. 2012). The DNA trapping function (for how long DNA is captured by cohesin) can therefore be regulated by modulating DNA entry and exit. This feature provides a fantastic device for regulating biological processes in space and time by modulating where and when DNA trapping must take place.

### *3) Cohesin localisation on chromatin*

Cohesin is not randomly located onto chromosomes (Figure 13A). Initial reports in budding yeast described a predominant enrichment at centromeric regions and a less pronounced accumulation at specific sites along chromosome arms. These are distributed every 10-15kb and were named CARs for Cohesin Associated Regions (Blat and Kleckner 1999; Megee and al. 1999; T. Tanaka and al. 1999). These data have been confirmed by genome wide analyses of cohesin positioning in budding and fission yeasts that revealed that

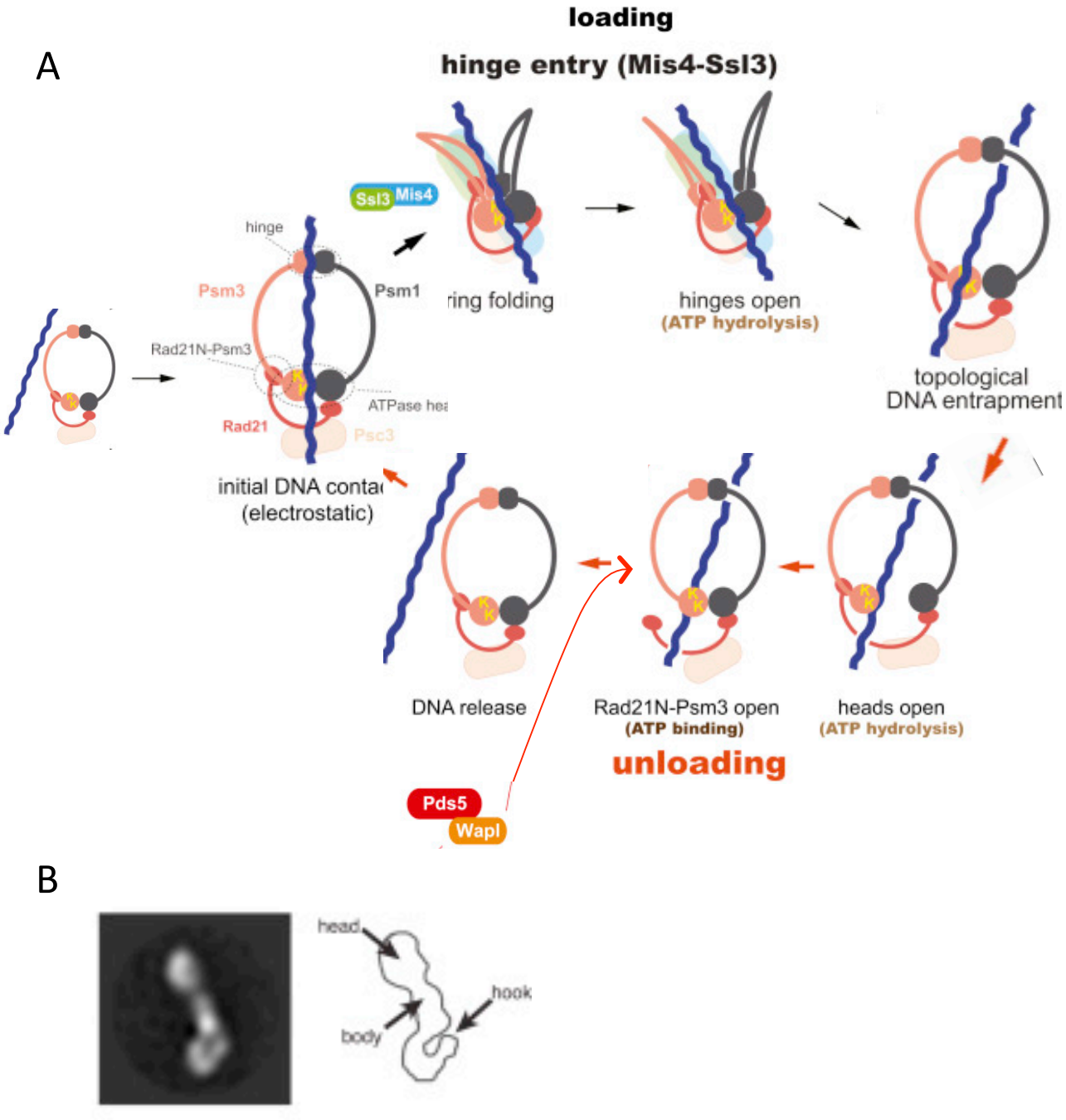


**Figure 12 : Cohesin loading and unloading onto DNA. A.** Cohesin loading model: The Psm1 and Psm3 coiled coils might enable interactions of SMC hinge and head domains from the same cohesin ring, creating a DNA binding surface formed by sequences from both hinge and head domains. Upon contact with DNA, binding to or hydrolysis of ATP by the ABC ATPase would generate a conformational change in the SMC heads transmitted to hinge domains via the coiled-coils, the DNA double helix, and/or direct interactions between head and hinge domains, causing disruption of one of the two hinge-hinge contact sites and DNA entry. Cohesin loading onto DNA is stimulated by the loading complex (Mis4-Ssl3 in fission yeast). The cohesin loader makes contact with all four cohesin subunits and would facilitate the conformational changes required for DNA capture by cohesin.
Cohesin unloading model: DNA escape from cohesin would require the passage of two interfaces. ATP hydrolysis would trigger SMC heads disengagement, allowing DNA to pass the first gate. The SMCs would rebind ATP and the Psm3-Rad21 interface would be opened by the concerted action of Wpl1, Pds5 and Psc3 (adapted from Murayama.Y, 2015). **B.** Electronic microscopy image of full-length Scc2-Scc4 complex. It can be divided into a globular head domain, a central body, and a C-terminal hook domain (William C.H. Chao and al, 2015).

cohesin occupies a large block around centromeres and discrete sites along chromosome arms often situated in the intergenic regions of convergent RNA-polymerase-II-transcribed genes (Lengronne and al. 2004; Schmidt, Brookes, and Uhlmann 2009).

The budding yeast cohesin loader Scc2/Scc4 is found at core centromeres and along chromosome arms at tDNAs, rDNAs and throughout the transcription units of highly transcribed genes, sites largely distinct from those occupied by the cohesin complex. It has been suggested that cohesin rings are loaded onto chromosomes at the sites occupied by the cohesin loader from where they slide away once the loading reaction is achieved (Figure 13 B-C).

Experiments performed in budding yeast have shown that cohesin is recruited to core centromeres under the influence of the kinetochore-specific CTF19 complex and then displaced to peri-centromeric regions (Fernius and Marston 2009). Similarly, in fission yeast, the cohesin loader is found within the core centromere whereas cohesin accumulates within peri-centromeric heterochromatin. In fission yeast, cohesin localization at heterochromatic region (centromere, telomere and mating type region) is largely dependent on HP1 (Heterochromatin Protein 1) homologue Swi6 protein (Bernard and al. 2001; Nonaka and al. 2002; Schmidt, Brookes, and Uhlmann 2009).

In budding yeast, chromosome arm's cohesin is first loaded at transcriptionally active regions occupied by Scc2/Scc4 and then displaced in a transcription dependent manner to accumulate at more permanent positions. It has been suggested that cohesin slides across genes, being pushed by the transcription machinery (Glynn and al. 2004; Lengronne and al. 2004; Ocampo-Hafalla and al. 2016). According to this idea, Koshland and colleagues demonstrated that the DNA motor protein FtsK, which is a highly processive translocase capable of dislodging proteins from DNA can push cohesin along DNA *in vitro* (Stigler and al. 2016). In Drosophila, the distribution of Nipped-B is almost undistinguishable from that of cohesin and coincides with RNA polymerase II sites. In the fission yeast, cohesin and the Ssl3-Mis4 loading complex show aspects reminiscent of both budding yeast and Drosophila (Schmidt, Brookes, and Uhlmann 2009). In mammalian cells, cohesin colocalizes and directly contact the CTCF insulator factor (Wendt and al. 2008; Xiao, Wallace, and Felsenfeld 2011).

A key question is how the cohesin loader binding sites are defined. As previously mentioned cohesin loading did not show DNA sequence preference *in vitro*. Indeed, no difference was obtained when cohesin loading reactions were performed using DNA

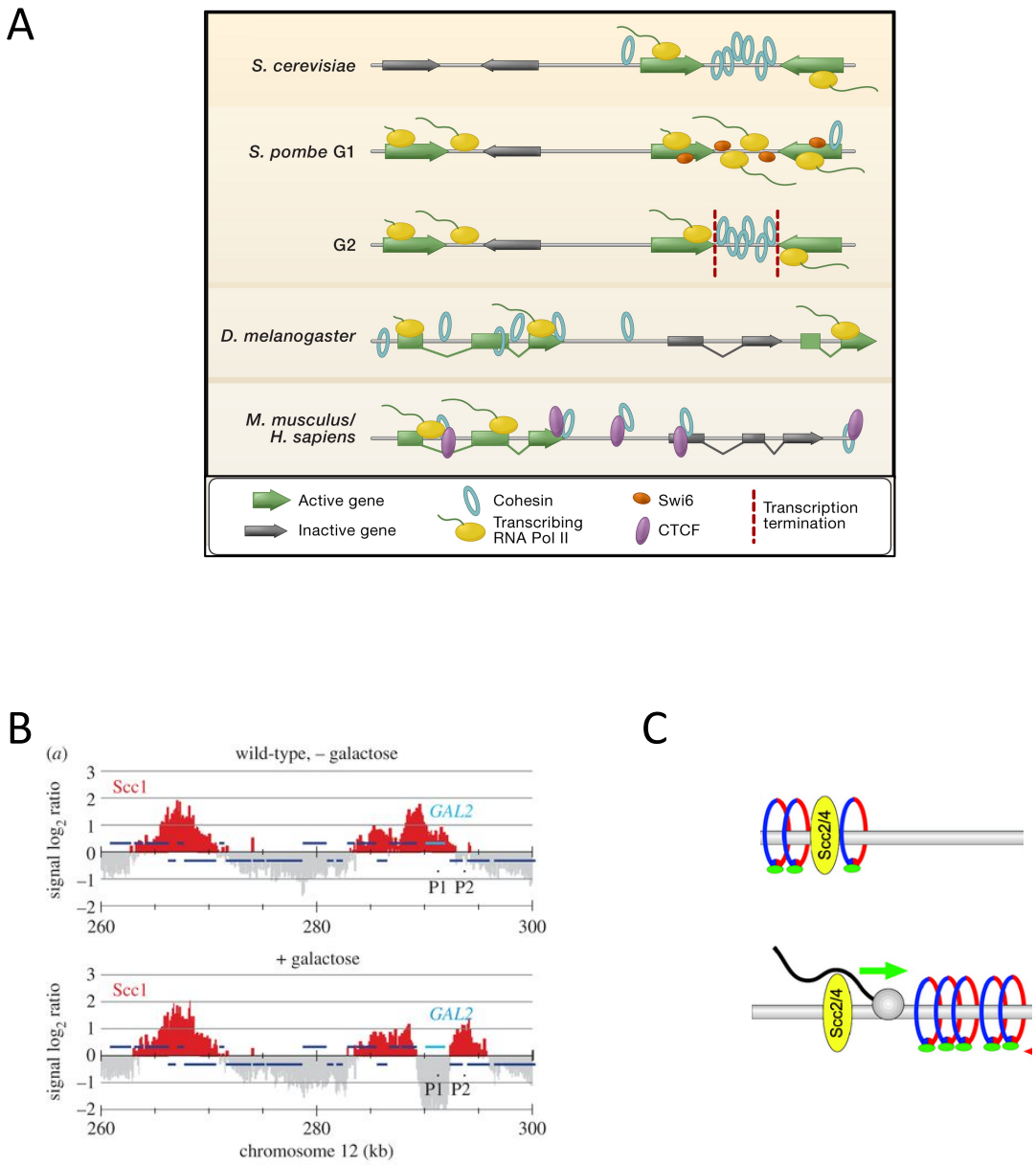


**Figure 13 : Cohesin binding and sliding on DNA. A.** Cohesin localisation in various eukaryotes : In budding yeast, cohesin mainly associates between convergently transcribed genes. Fission yeast shows read-through transcription at convergent genes in G1. Swi6 association might recruit cohesin to these regions. In G2, heterochromatin marks at these regions are mainly lost, and a model proposes that cohesin accumulation between convergently transcribed genes leads to transcriptional termination in G2. In Drosophila, cohesin associates both with gene-rich and intergenic regions. Only a subset of transcriptionally active genes is bound. In mammalian cells cohesin co-localises with the CTCF insulator protein at both genic and intergenic regions, although binding along genes is slightly enriched. Adapted from Peric-Hupkes & van Steensel, 2008. **B.** Scc1 ChIP-on-chip experiment showing cohesin displacement on *gal2* core gene upon activation by galactose addition (Ocampo-Hafalla M. and al, 2016) **C.** Model illustration (Kim Nasmyth and Christian H. Haering 2005).

sequences that are *in vivo* enriched or free from cohesin loader and cohesin (Murayama and Uhlmann 2014). *In vivo*, the possibility of such consensus DNA sequence motif has been largely addressed by genome wide analysis (Blat and Kleckner 1999; Lopez-Serra and al. 2014a). In budding yeast, Oligo (A)-containing motifs, B-box motifs bound by TFIIIC at tRNA genes only and three others motifs have been described but they do not contain any conserved features. From that, it has been proposed that cohesin loader and cohesin distribution might rely on some specific chromatin factors. The tight relationship between transcription and cohesin loading and further positioning has led to hypothesize that transcription factors might be involved in such a process. In fission yeast, Mis4 and Ssl3 co-localize with Sfc6 an RNA polymerase III subunit (Schmidt, Brookes, and Uhlmann 2009). Other factors appear important to address the cohesin loader on chromatin such as the previously mentioned CTF19 kinetochore complex in a mechanism dependent of DDK4 (Dbf4-dependent kinase) activity in budding yeast (Fernius and al. 2013; Natsume and al. 2013) , or replicator factors (Pre-RC complexes) in *Xenopus* eggs extracts (Takahashi and al. 2004). Moreover, in budding yeast, the Chl1 protein was shown to be required at G1-S phase transition to ensure proper Scc2 binding to chromatin and in a concomitant way Scc1 binding (Rudra and Skibbens 2013; Samora and al. 2016). Finally, budding yeast genome wide analysis has revealed that localization of the cohesin loader Scc2-Scc4 overlapped with those of the chromatin-remodelling (RSC) complex. Inactivation of Sth1 RCS component leads to loss of Scc2 binding to chromatin at transcriptional start sites (TSS) and nucleosome re-positioning at these sites. This suggests a mechanism by which RCS complex allows cohesin loader recruitment at TSS by maintaining a nucleosomes depleted region (Lopez-Serra and al. 2014b). Interestingly, recent work reports that RCS complex is required to facilitate condensin loading by nucleosome eviction in fission yeast (Toselli-Mollereau and al. 2016) suggesting it might be more a general mechanism used for the loading of all Smcs complexes.

# *III. Cohesin's functions*

## A. Sister chromatid cohesion

The best-known function of cohesin is sister chromatid cohesion, an essential process for correct chromosome segregation. Cohesin is thought to tether sister-chromatids together as they emerge from the replication fork and until nuclear division. The first essential function of

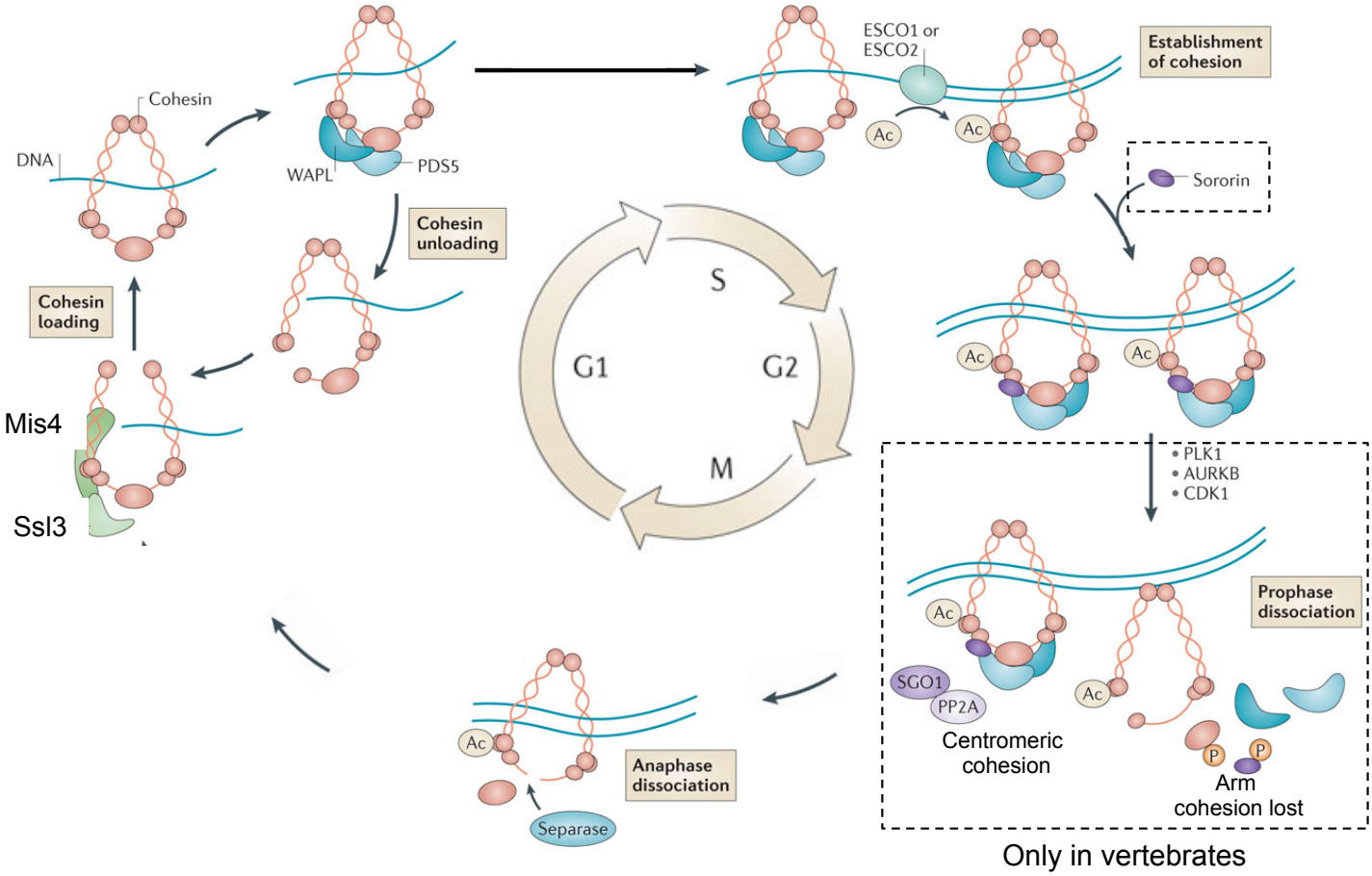


**Figure 14 : The cohesion cycle.** Cohesin is dynamically associated with chromatin in G1as a consequence of repeated cycles of loading and unloading. During DNA replication, the cohesin acetyltransferase Eso1 acetylates (Ac) K105 and K106 in the N-terminal domain of SMC3 which would inhibit cohesin unloading.
Dotted box : In vertebrates, the acetyl-transferases trigger Sororin binding to chromatin. Sororin is thought to displace WAPL from PDS5 thereby inhibiting the unloading reaction. Sororin-bound acetylated cohesin complexes encircling sister chromatids are stably bound to chromatin. In prophase, most cohesin dissociates from chromatin when Polo-like kinase 1 (PLK1) phosphorylates (P) the SA subunit. Sororin is released from cohesin after being phosphorylated by Aurora B (AURKB) and Cyclin-Dependent Kinase 1 (CDK1), thereby re-activating WAPL-dependent cohesin release from DNA. Concomitantly, Shugoshin 1 (SGO1) and its partner protein phosphatase 2A (PP2A) accumulate at centromeres to counteract the above-mentioned phosphorylation events and prevent cohesin dissociation. Centromeric cohesin remains on chromatin until anaphase onset. Finally, Rad21 cleavage by Separase at anaphase stage destroys the integrity of the cohesin ring, allowing sister-chromatid separation and segregation.
Adapted from *Nature reviews cancer, 2014*, Losada, A., Cohesin in cancer: chromosome segregation and beyond.

sister chromatid cohesion is to keep the information "these two DNA molecules are identical". By joining sister-chromatids together cohesin ensures that a pair of chromatids is made of two identical DNA molecules. Thus, when the mitotic spindle attaches a pair of chromatids and segregates them, these are necessarily sister-DNA molecules. The corollary being that a precocious separation of sisters (*ie* before or during the early mitotic stages) will lead to the random segregation of chromatids and the generation of aneuploid daughter cells. As mentioned earlier, the second essential function of cohesin is to oppose the splitting forces exerted by spindle microtubules as to generate tension within kinetochores that is taken into account by the SAC.

### *1) The cohesion cycle*

- *The dynamic behaviour of cohesin*

FRAP experiments in living rat cells revealed that cohesin has a residence time of about 24+-5min in G1 (Gerlich and al. 2006). In fission yeast cohesin association with G1 chromosomes requires continued activity of the cohesin loader, suggesting that repeated loading cycles maintain cohesin binding (Bernard and al. 2008). In G1 human cells approximately 40% of cohesin is chromatin bound with a residence time of several minutes (Ladurner and al. 2014). This dynamic mode of interaction with chromatid depends on a functional cohesin loader and ATP hydrolysis (Ladurner and al. 2014). A "transient binding mode" with a residence time on chromatin of less than 1 minute is also described but doesn't requires ATP hydrolysis. These data suggested a docking reaction on DNA induced by the cohesin loader (transient interaction), and a topological entrapment require ATP hydrolysis (dynamic interaction). As mentioned earlier, cohesin release from DNA is stimulated by Wpl1 (Kueng and al. 2006; Gandhi, Gillespie, and Hirano 2006). Wapl RNAi increases cohesin-residence time by more than 20 fold in G1 cells (Tedeschi and al. 2013; Kueng and al. 2006). Moreover, Wpl1 knock-out in mouse embryonic fibroblasts or in budding yeast abolishes cohesin turn over on chromatin (Lopez-Serra and al. 2013; Chan and al. 2012) (Figure14).

- *The generation of sister-chromatid cohesion in S phase*

Several observations indicate that sister-chromatid cohesion is created in a process coupled with DNA replication. Cohesin can be loaded after S-phase and does bind DNA but only those deposited before or at the beginning of S phase are competent to generate

cohesion. Budding and fission yeast genetics indicated that mutations within components of the replisome generate cohesion defects, suggesting that the replisome is involved in the generation of cohesive structures (Mayer and al. 2001; Lengronne and al. 2006; Samora and al. 2016). How cohesion is actually created is unknown. One study from Frank Uhlmann's laboratory suggested that indeed cohesion is generated with cohesin loaded before the passage of the replication fork (Lengronne and al. 2006). The replisome may pass through cohesin rings or alternatively, cohesin may be remodelled to allow passage of the fork and the capture of the two sisters. Single-molecule imaging revealed that *in vitro*, cohesin cannot travel through small obstacles (~19,5nm in diameter), suggesting that the replisome is unlikely to pass through cohesin rings (Stigler and al. 2016).

Although this critical aspect remains largely unknown, progress has been made towards the understanding of how cohesion is maintained following S phase. FRAP experiments have shown that a new population of cohesin is created during S phase with a residence time >6h (Gerlich and al. 2006). Similarly in fission yeast, inactivation of the cohesin loader in G2 cells revealed two cohesin populations (Feytout and al. 2011). One is not stably bound to DNA and resembles G1 cohesin while the other is stably bound (no dissociation was observed during a 5 hours experiment). This stable cohesin fraction ensures sister-chromatid cohesion as monitored by FISH during the G2 arrest and cells segregated their chromosomes normally when released from into mitosis. These observations suggested that a sub-population of cohesin is modified during S-phase to become stably bound to DNA. The major question was to understand how cohesin became stable on DNA.

A major player is an acetyl-transferase called Eco1 in budding yeast. It was originally identified as a thermosensitive mutant (*eco1-1*) defective for sister-chromatid cohesion (Tóth and al. 1999). Inactivation of Eco1 in G1 does not prevent DNA replication nor cohesin loading onto chromosomes; however, sister-chromatids separate shortly after DNA replication leading to a lethal mitosis. By contrast, inactivation of Eco1 after S-phase does not affect sister-chromatid cohesion and chromosome segregation during the ensuing mitosis, indicating that Eco1 is dispensable for cohesion maintenance.

Eco1 homologues are found in fission yeast (K. Tanaka and al. 2000), Drosophila (Williams and al. 2003), Xenopus (Takagi and al. 2008) and Human cells (Vega and al. 2005; Bellows and al. 2003; Hou and Zou 2005). Its GCN5-Related N-Acetyltransferase superfamily appartenance (Ivanov and al. 2002) suggests that Eco1 can acetylate proteins.

- Replisome passage through the cohesin ring :

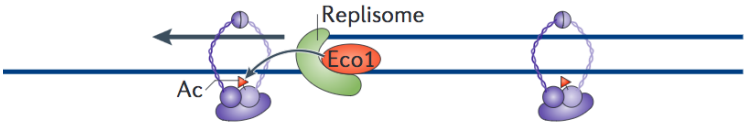


- Cohesin reloading in the wake of the fork :

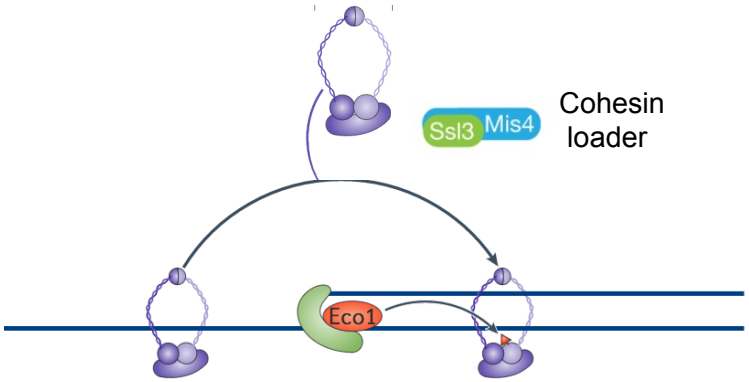


**Figure 15 : Model of cohesion establishment at the replication fork.** Two models for the establishment of sister chromatid cohesion during DNA replication :Replisome passage through the cohesin ring is an efficient way to co-entrap sister chromatids. Acetylation (Ac) at any time before or around the time of DNA replication would ensure stable sister chromatid cohesion. Cohesin reloading in the wake of the fork means that cohesin loads onto DNA and co-entraps sister chromatids, as they lie close to each other just behind the replication fork. In this case, cohesin loader is required and acetylation must occur following cohesin loading onto both sister chromatids.

Indeed, Eco1 acetylates two conserved lysine residues within the Smc3 head domain (K112 K113 in budding yeast, K105 K106 in *S.pombe* (Feytout and al. 2011), Xenopus (Higashi and al. 2012) and Human cells (J. Zhang and al. 2008) and this event is thought to stabilize cohesin interaction with DNA by inhibiting Wpl1-dependent DNA exit from cohesin.

Historically, Wpl1 was known to promote cohesin release from DNA and the deletion of *wpl1* allowed cell survival in the absence of the otherwise essential *eco1* gene. Similarly, acetyl-mimicking mutations within Smc3 bypassed Eco1 requirement, suggesting that Smc3 acetylation counteracted Wpl1 (Rolef Ben-Shahar and al. 2008). A key finding was that the artificial covalent linkage between Smc3 and Scc1 (a Smc3-Scc1 fusion protein) also allowed cell viability in the absence of Eco1 (Huis in 't Veld and al. 2014; Eichinger and al. 2013; Chan and al. 2012). This suggested that Wpl1 might open cohesin by opening the Smc3 / Scc1 interface and that Smc3 acetylation would inhibit this reaction.

*In vivo*, Smc3 acetylation increases covalent cross-linking between Smc3 and Scc1 N-terminal domain and this requires Smc heads interaction without ATP hydrolysis (Beckouët and al. 2016). *In vitro*, cohesin dissociation from DNA is reduced if K106 of Psm3 (fission yeast proteins) is replaced by glutamine that mimics the acetylated state (Murayama and Uhlmann 2015).

The mechanism by which Smc3 acetylation renders cohesin rings insensitive to Wapl is only partially understood. In budding yeast, it was reported that acetylation could block the Smc1/3 head engagement that is required to induce N-Scc1 and Smc3 disengagement (Beckouët and al. 2016). Moreover, there appears to be a difference between yeast and animal cells because in the latter, Smc3 acetylation causes the recruitment of Sororin, which counteracts Wapl by preventing its binding to Pds5 (Lafont, Song, and Rankin 2010; Nishiyama and al. 2010). Yeasts have no known Sororin orthologous, and it was proposed that its function would be performed by specific domains of other cohesin subunits.

The establishment of sister chromatid cohesion is intimately linked with DNA replication, implying a local regulation of the cohesin acetyl transferase. Interestingly, Eco1 interacts with PCNA (Skibbens and al. 1999; Maradeo and Skibbens 2009), and Ctf18 (Terret and al. 2009; Lengronne and al. 2006) and may travel with the replication fork suggesting acetylation may take place in the wake of the replication machinery (Figure 15).

- *Keep cohesin associated with DNA: cohesion maintenance*

Sister-chromatid cohesion must persist throughout the G2 phase and until nuclear division, a time frame ranging from hours to decades in human oocytes. Experiments in budding and fission yeast indicated that Pds5 has a crucial role in this process. In fission yeast, *pds5* is not essential for cell viability. However, cohesion is lost when cells experience an extended G2 phase. The stable cohesin fraction is not made and cohesin is progressively lost from chromosomes (Vaur et al. 2012; Panizza et al. 2000). Thus Pds5 has opposite activities. Pds5 acts with Wpl1 to promote cohesin release but is required for the maintenance of sister-chromatid cohesion, presumably through the stabilization of cohesin interaction with DNA. In addition, it was discovered in fission yeast that Pds5 is required for Psm3 acetylation, an observation subsequently made in budding yeast and mouse cells (Vaur et al. 2012; Chan et al. 2013; Carretero et al. 2013). Pds5 is thus an enigmatic protein. Several structural studies indicate that Pds5 is a large HEAT repeat protein making multiple contacts with the cohesin ring (Smc3-Smc1 and Scc1), Wpl1 and Scc3 (Lee and al. 2016a; Muir and al. 2016). However, the mechanism allowing Pds5 to switch function from cohesin release to cohesin stabilization is unknown.

- *Cohesin removal from chromosome and cohesion loss*

Cohesin rings that have been locked in S phase stably hold sister chromatids together until the start of mitosis. In budding yeast, all cohesive cohesin is maintained until the metaphase-to-anaphase transition. However in animal cells, cohesin removal activity along chromosome arms is observed in prophase and pro-metaphase (Figure 14). This prophase dissolution pathway (PDP) leads to the formation of the characteristic X-shaped chromosomes when cells experience a prolonged prophase or metaphase arrest. Cohesin removal from DNA at this step is largely dependent of Wpl1 activity, presumably through the opening of the cohesin exit gate (Waizenegger and al. 2000). In the mean time, centromeric cohesin is protected from the PDP. In mitosis, the SA cohesin subunit and Sororin deposited on chromosome arms are phosphorylated by mitotic kinases such as CDK1, PLK1 and Aurora B leading to Sororin inactivation and allowing Wpl1-dependent cohesin removal from DNA. At centromere, SGO1 (Shugoshin in full, which stands for ‘‘guardian spirit’’ in japanese) is recruited by two phosphorylation marks. The first entails CDK1-dependent phosphorylation of SGO1, which allows it to bind to cohesin along the entire length of chromosomes (Liu and al, 2013b). The second is Bub1-mediated phosphorylation of histone H2A. As Bub1 locates to

centromeres, this allows the concentration of SGO1 at centromeres (Kawashima and al., 2010). SGO1 binding to PPA2 phosphatase counteracts the phosphorylation of centromeric cohesin and inhibit cohesin release activity.

The Metaphase-anaphase transition is an irreversible event. As previously mentioned, Securin degradation activates Separase which cleaves the Scc1 cohesin subunit at two conserved consensus sites (EXXR (X, any residue) and cleaves after R) (Uhlmann, Lottspeich, and Nasmyth 1999). Scc1 cleavage breaks the ring-like structure, allowing sisters to be pulled apart. The cleavage is enhanced by the phosphorylation of Scc1 by the budding yeast orthologous of Plk1, Cdc5 (Alexandru and al. 2001), and the resulting proteolytic fragments of Scc1 are degraded by the ubiquitin-dependent N-end rule pathway (Rao and al. 2001). Deacetylation of Smc3 by Hos1 in yeast and by HDAC8 in humans occurs after kleisin cleavage and may prepare cohesin complexes for their next acetylation cycle (Beckouet and al., 2010; Borges and al., 2010;Deardorff and al., 2012; Xiong and al., 2010).

- *Meiosis*

In meiosis, a single round of DNA replication is followed by two rounds of successive chromosome segregations called meiosis I and meiosis II. In meiosis I, homologs (a pair of sister chromatids) connected by chiasmata are segregated to opposite poles, while sister chromatids are segregated to the same pole. This type of segregation is called reductional segregation). At the same time, deliberate DNA double-strand breaks are formed and resolved in a way that leads to recombination. During the following meiosis II, sister chromatids can separate to opposite poles as they do in mitosis. Subsequent segregation of homologous chromosomes and sister chromatids is coordinated by the sequential loss of a specialized meiotic cohesin from the arms prior to the first meiotic division, and then from centromere regions prior to the second division. The cohesin complex in meiosis differs from that in mitosis. A meiotic counterpart, Rec8, replaces Scc1/Rad21 kleisin subunit (Watanabe 2004). In fission yeast, Psc3 subunit is replaced along arms chromosome, but not at centromeres, by a second meiosis specific subunit called Rec11 (Kitajima and al. 2003). By contrast to vegetative cells in which cohesin localizes preferentially to the peri-centromeric regions, meiosis Rec8-containing cohesin localizes additionally to the core centromeres. The abolishment of Rec8 only at the core centromere results in equational rather than reductional

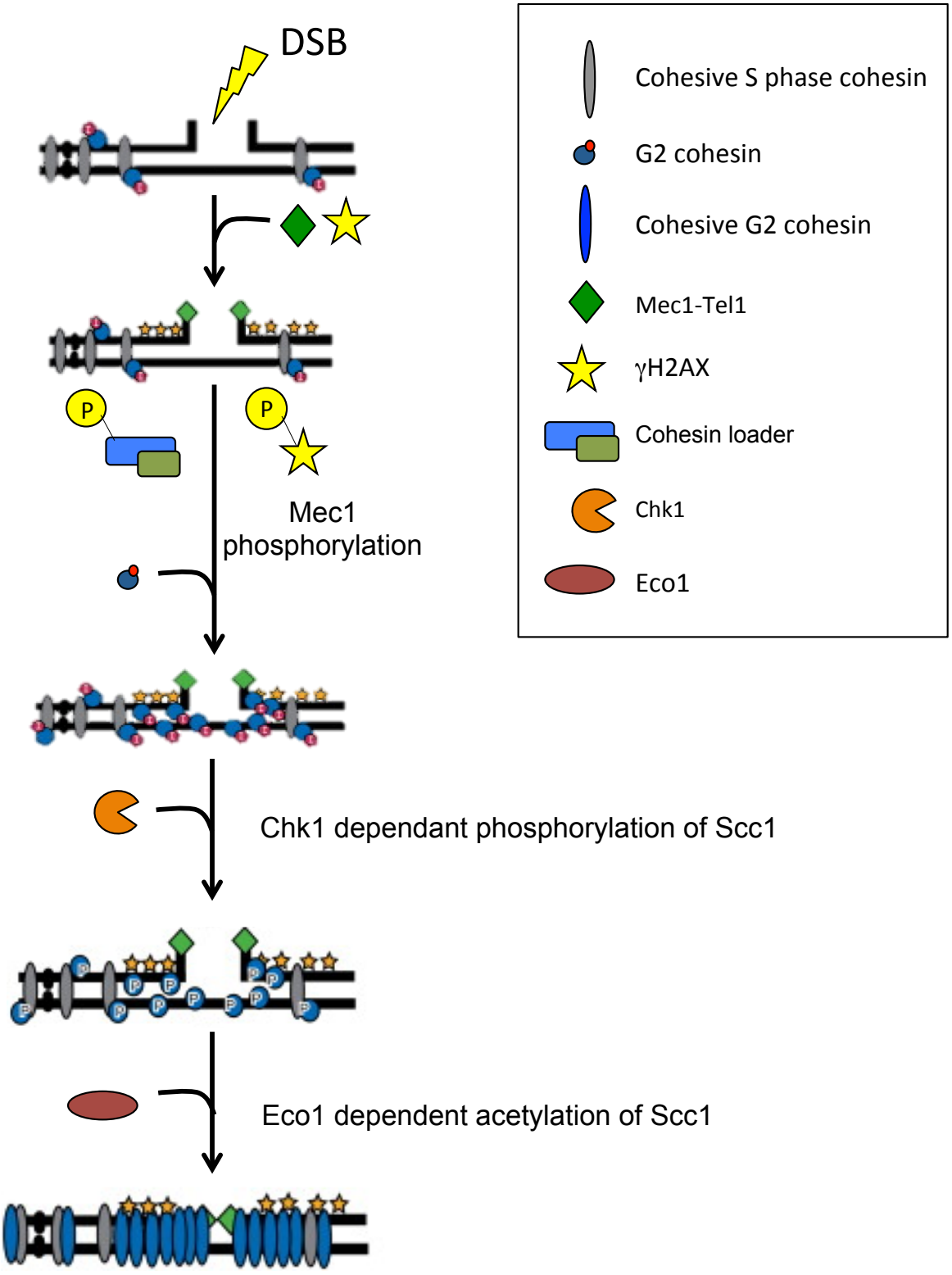


**Figure 16 : DNA Double Strand Break Induced Cohesion .** In the event of a double strand break (DSB) in G2/M, cohesins are recruited to a large (~100 kb) region surrounding the break site in a process dependent on DSB sensors/transducers (Mec1 and Tel1). The Mec1/Tel1 DNA damage checkpoint proteins phosphorylate (P) the histone variant H2AX and cohesin loader which loads cohesin onto the phospho-H2AX domain. Cohesin is then converted to a cohesive state both at the break site and at CAR sites throughout the genome. This cohesion generation pathway requires Chk1 that phosphorylates cohesin on the Scc1 subunit (S83) . Scc1 phosphorylation primes for Eco1-dependent acetylation of two lysine residues in Scc1, K84 and K210 (adapted from Jill M. 2008).

division at meiosis I, advocating a model whereby the establishment of cohesion at the core centromere conjoins the two kinetochore domains at meiosis I, whereas the core regions may open to opposite sides when not establishing this cohesion (Sakuno, Tada, and Watanabe 2009).

### *2) Cohesin function in DNA repair*

The establishment of sister-chromatid cohesion is normally restricted to the S phase of the cell cycle. However, an alternative pathway is activated when cells experience a DNA double strand break (DSB) (Sjögren and Nasmyth 2001; Sjögren and Ström 2010; Ström and al. 2004; Heidinger-Pauli, Ünal, and Koshland 2009). In response to a DSB the DNA damaged checkpoint is switched on, causing a delay in cell cycle progression until repair is completed. In the S and G2 phases of the cell cycle, repair occurs preferentially via homologous recombination (HR) using the undamaged sister chromatid as a template. Cohesion formed during S phase (S-phase cohesion) is required for post-replicative repair of DSBs via HR. In addition to S phase cohesion, it was shown in budding yeast that recruitment of cohesin around the DSB and *de novo* formation of cohesion is important for DSB repair. Strikingly, a single DSB also triggers neo-cohesion genome-wide. This pathway, called damage induced (DI)-cohesion, is depicted in Figure 16 and detailed below.

In a normal, unperturbed S phase, a fraction of cohesin becomes sheltered from Wapl ensuring long-term cohesion between sister-chromatids during the G2 phase. In the mean time, cohesin loading still occurs but this pool of cohesin remains Wapl-sensitive and does not create a stable link between sisters. In the event of a DSB, this cohesin sub-population becomes cohesive. In addition to this genome-wide response, cohesin is specifically deposited around the break site, in a manner dependent on ATM/ATR, phosphorylated histone H2A (H2AX) and the cohesin loader. As for S-phase cohesion, the acetyl-transferase Eco1 is central to the DI-cohesion pathway and again, Eco1 acts by counteracting Wpl1. DI-cohesion is abolished in *eco1* mutants and conversely DI-cohesion is permanently activated when the *wpl1* gene is deleted, even in the absence of a DSB. However the pathway is different from S phase. Elegant experiments have shown that the kleisin subunit Scc1 is the Eco1 target for DI-cohesion (Heidinger-Pauli, Ünal, and Koshland 2009). In the event of a DSB, ATR (Mec1) activates Chk1, which phosphorylates the kleisin subunit Scc1 on the conserved S83 residue. Phosphorylated S83 is thought to prime Eco1-dependent acetylation of two critical lysine

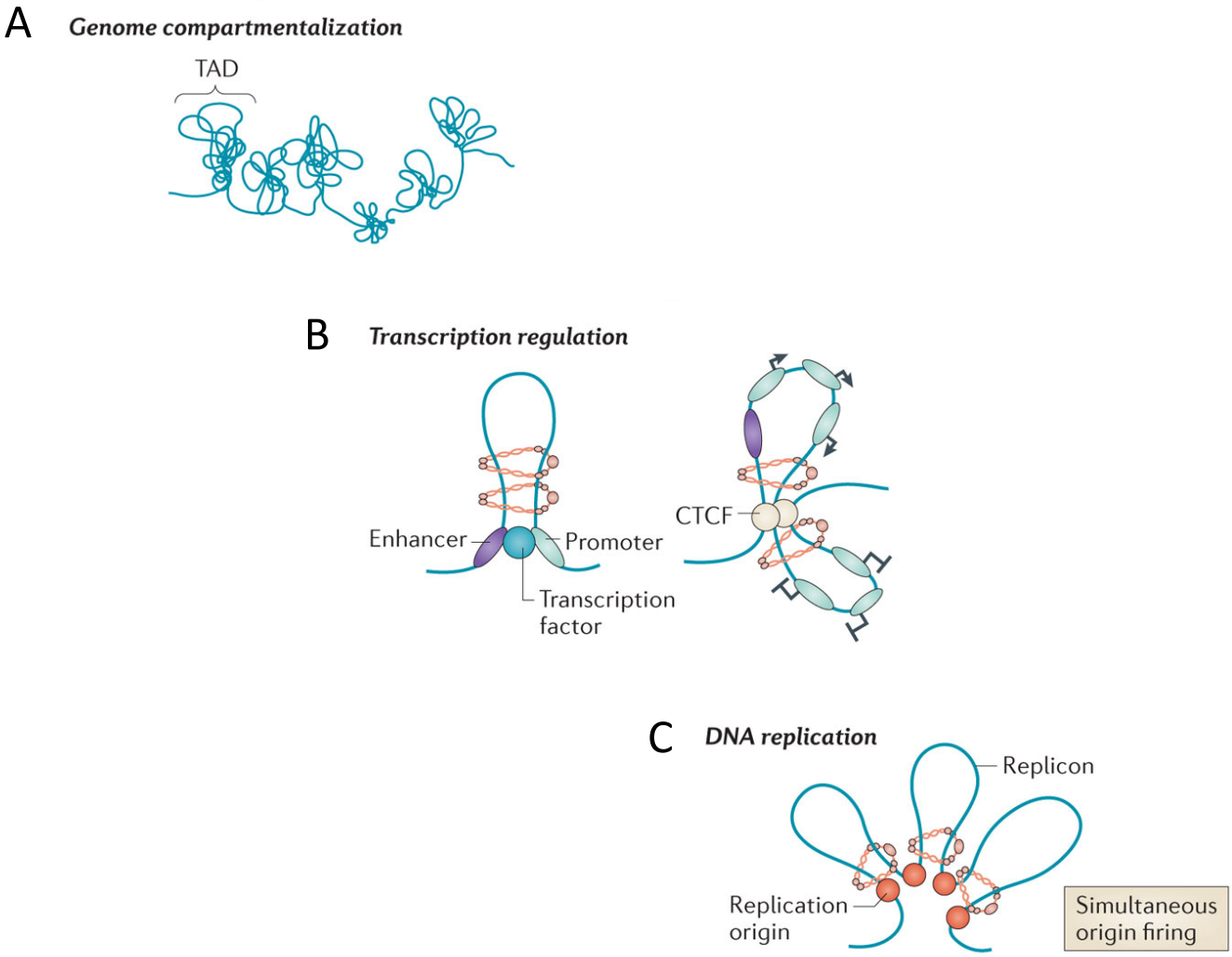


**Figure 17 : Cohesin as a global organizer of chromosome structure**. **A.** The chromosomes are partitioned into discrete units known as Topologically Associating Domains (TADs) that range from 100 kb to 1 Mb. TADs confine regulatory activities (for example, enhancers) to a specific domain. **B.** Within a domain, cohesin can promote transcription by facilitating the interaction between an enhancer and a promoter or contribute to the transcriptional regulation of gene clusters. **C.** Cohesin organizes chromatin loops at replication factories, thereby facilitating simultaneous firing of the clustered origins.
Adapted from *Nature reviews cancer, 2014*, Losada, A., Cohesin in cancer: chromosome segregation and beyond.

residues in Scc1, K84 and K210. Although these modifications have not been demonstrated, in depth analysis of Scc1 mutants was consistent with this model. For instance, the S83D phosphomimic bypassed the need for Chk1 or DSB for the creation of cohesion in G2 but did not bypass Eco1 requirement. By contrast an acetyl-mimic of Scc1 (K84Q K210Q) generated cohesion in G2 even when Eco1 was inactivated.

To summarize, S-phase and DI-cohesion are two distinct pathways that generate sister-chromatid cohesion presumably by preventing Wpl1 from dissociating cohesin from DNA. The common key player is the cohesin acetyl-transferase but the targets are different: Smc3 in S phase and Scc1 for DI-cohesion. Intriguingly, they cannot be substituted. Smc3 acetyl-mimic can bypass Eco1 for S-phase cohesion but not for DI-cohesion and conversely, Scc1 acetyl-mimic can bypass Eco1 for DI-cohesion but not for S-phase cohesion. The reason for this is unknown and highlight that much remains to be known for a better understanding of cohesin regulation.

## B. Cohesin influences 3D architecture of chromatin

Cohesin appears now as an organizer of chromatin in interphase cells. This organization is based on a hierarchy of chromatin loops by creating long-range interactions that underly most aspects of genome function, including DNA replication and transcriptional regulation (Figure 17). Mechanistically, it has been hypothesized that cohesin encircles juxtaposed genomic DNA in a manner similar to cohesin function in sister chromatid cohesion. Indeed, in human cells cohesin mediated DNA looping is required to organize replication factories and to promote their efficient firing. This would facilitate the local concentration of the initiator proteins and kinases required to activate origins facilitating simultaneous firing of the clustered origins. Depletion of Rad21 results in slow S-phase progression correlated with the formation of larger chromatin loops in G1 and a reduced frequency of origin firing during S phase (Guillou and al. 2010). In mouse, cohesin influences the architecture of the immunoglobulin loci during B lymphocyte development and facilitates V(D)J recombination (Variable, Diversity and Joining) (for review Feeney and Verma-Gaur 2012)

By promoting higher-order structures (Topologically Associated Domain TAD) within the interphase nucleus, cohesin has been shown to regulate gene transcription in organisms

ranging from yeast to human. In budding yeast, cohesin contributes to gene regulation by defining their position within the nucleus (Gard and al., 2009). In fission yeast, cohesin promotes gene-proximal transcription termination between the convergent genes by blocking readthrough transcription (Gullerova and Proudfoot 2008; Schmidt, Brookes, and Uhlmann 2009). In *Drosophila*, cohesin alteration in postmitotic mushroom body γ-neurons results in axon pruning defects partially due to a lack of expression of the ecdysone receptor (Pauli and al. 2008). Moreover, a large number of studies have shown that cohesin collaborates with numerous factor like CTCF (CCCTC-binding-factor) and ER estrogen receptor but also with Mediator or Polycomb to regulate gene transcription by allowing or preventing communication between enhancers or promoters (for review Merkenschlager and Nora 2016).

In human cells, dysregulation of cohesin function has been shown to cause a severe developmental syndrome named Cornelia de Lange syndrome (CdLS). The genome wide transcriptional profiling of cell lines derived from CdLS patients has revealed numerous expression changes, both up and down regulation, as well as reduced level of cohesin association in the promoter of affected genes regions (Liu and al., 2009). In CdLS, more than half of patients present heterozygous mutations in the gene encoding the cohesin loader NIPBL whereas mutation in the gene encoding Smc1, Smc3 and Rad21 have been found at lower frequency (Remeseiro, Cuadrado, and Losada 2013). Importantly, cells from CdLS patients show no detectable cohesion defects, although they display an increased sensitivity to DNA damage. Similarly, Drosophila and zebrafish mutants with reduced amounts of cohesin or cohesin loader also display altered gene expression and development defects, but no apparent chromosome segregation defects (Muto at al, 2011).

Over the last decade, research on cohesin complexes has provided important insight into many aspects of chromosome biology. Although cohesin was discovered through its sister chromatid cohesion function, recent work has revealed that understanding cohesin function is essential for the elucidation of DNA damage response pathways, mechanisms of gene regulation, and the etiology of several human diseases. Fundamental knowledge is therefore of crucial importance to fully understand cohesion functions. In particular, understanding how, when, where and for how long cohesin will hold that particular DNA strands is a challenge for the future.

# Chapter I: Materials and methods

## *I. Biological material*

Fission yeast has been used as a model organism for decades since it is easy to cross, manipulate and grow, even in large scale. In over 50 years of fission yeast research, a large portfolio of techniques has been developed, including rapid forward and reverse genetics, biochemistry, proteomics and genome-wide analysis. *Schizosaccharomyces pombe* was first found in millet beer brewed in East Africa and later isolated from French wine (Jeffares and al., 2015). The unicellular eukaryote forms rod-shaped cells 3-4 µm in diameter and 7-15 µm in length (Mitchison and Nurse, 1985). Haploid genome size is 14.1Mb distributed on three chromosomes and genome sequence was published in 2002 (Wood and al., 2002). The biological cycle is haplodiplontic with a predominant haploid cycle. Haploid cells divide symmetrically into two daughter cells of equal size with a typical eukaryotic cell cycle with four different stages: G1, S, G2 and M. The G2 phase is predominant. In exponentially growing cultures, about 80% cells are in G2. In rich medium at 25°C, the duration of a cell cycle is about 3.5 hours for wild-type cells. The cell population grows exponentially until ~2-4x$10^7$ cells /ml and rich saturation for a cell density around 2-3x$10^8$ cells/ml. Physiological experiments are usually carried out using actively dividing cells (~5x$10^6$ cells /ml).

Mating occurs when homothallic cells or cells from opposite mating types are nitrogen starved. Cells arrest in G1, mate and undergo meiosis to form tetrads after ~2 days at 26°C. All strains are listed in Table 1.

## *II. Methods*

### A. Culture methods

#### *1) Culture media*

Table 2 shows the composition of the media. Agar was added at 20g/L to obtain solid media. Sterilisation was made by autoclaving at 110°C during 30min. The inhibitor 1-NA-PP*1* (CAS № 221243-82-9, Cayman Chemical, stock solution 25mg/ml in DMSO) was added at 25µg/ml and tetracycline (anydrotetracycline hydrochloride SIGMA, stock solution 10mg/ml in DMSO) was added at 5µg/ml. YES+A medium is defined as rich medium, $EMM_2$

# Table 1: Strain list

**Chapter II: The Pef1 Cyclin Dependent kinase regulates sister-chromatid cohesion through the phosphorylation of the cohesin kleisin subunit**

**Figure 18A-B:**

3820: *h*$^{+}$

2730: *h*$^{+}$ *mis4-367*

6246: *h*$^{+}$ *ura4-D18 pef1Δ::ura4*$^{+}$

3652: *h*$^{+}$ *ura4-D18 mis4-367 pef1Δ::ura4*$^{+}$

3647: *h*$^{+}$ *ura4-D18 pas1Δ::ura4*$^{+}$

3649: *h*$^{+}$ *ura4-D18 mis4-367 pas1Δ::ura4*$^{+}$

4623: *h*$^{+}$ *natR-eso1-H17*

6725: *h*$^{+}$ *pef1Δ::hygR natR-eso1-H17*

3820: *h*$^{+}$

2730: *h*$^{+}$ *mis4-367*

3652: *h*$^{+}$ *ura4-D18 mis4-367 pef1Δ::ura4*$^{+}$

7639: *h*$^{+}$ *mis4-242*

7638: *h*$^{+}$ *mis4-242 pef1Δ::natR*

8112: *h*$^{+}$ *leu1-32 ura4-D18 or ura4*$^{+}$ *ssl3Δ::ura4*$^{+}$ *ars1-ssl3-29ts-LEU2*

8114: *h*$^{+}$ *leu1-32 ura4-D18 or ura4*$^{+}$ *pef1Δ::hygR ssl3Δ::ura4*$^{+}$ *ars1-ssl3-29ts-LEU2*

6246: *h*$^{+}$ *ura4-D18 pef1Δ::ura4*$^{+}$

**Figure 19**

A.

2: *h*$^{-}$

2729: *h*$^{-}$ *mis4-367*

6747: *h*$^{-}$ *mis4-367 pef1-F78A*

6749: *h*$^{-}$ *mis4-367 pef1-F78G*

B-C-D.

2: *h*$^{-}$

as synthetic medium. $EMM_2$-N is used for genetic crosses and to synchronize cells in G1 using liquid medium.

### *2) Growth conditions*

Cellular concentration was calculated with a Thomas counting slide. Cells were grown at 25°C within Erlenmeyer flasks with shaking (200rpm).

*- G1 arrest by overexpression of Res1-Cter*

G1 arrest was achieved using overexpression of C-terminal part of Res1 that binds to and sequesters Cdc10. The overexpression is driven by the thiamine repressible *nmt* promoter (*nmt-res1Cter*) (Bernard and al. 2008).

Cells were grown in $EMM_2$ 20µM thiamine to late log phase (~$10^7$ cells /ml), washed three times with $EMM_2$ by centrifugation (1min, 1300g). Cultures were set up in $EMM_2$ at $4x10^5$cells/ml at 25°C. G1 arrest was achieved after seven generations (approximately 30h) and confirmed by FACS analysis of DNA content.

*- G1 arrest using cdc10-129*

*cdc10-129* cells were grown exponentially in $EMM_2$ medium at 25°C before temperature shift to 36.5°C, the restrictive temperature for *cdc10-129*. After 4 hours at the restrictive temperature, the cells appeared uniformly elongated, and the septation index was close to 0. The arrest was further monitored by FACS analysis of DNA content.

*- G1 arrest by nitrogen starvation and synchronous release*

In response to nitrogen starvation, fission yeast cells arrest in G1. Exponential cells were cultured in $EMM_2$ at 25°C to late log phase. Cells were centrifuged (1min, 1300g) and washed three times with $EMM_2$-N. A volume of cells corresponding to $1x10^7$cells/ml was grown 18h in $EMM_2$-N at 25°C. All cells had acquired a small round shape, the typical phenotype for nitrogen-starved cells. Cultures were centrifuged (1min, 1300g) and washed once with YES+A and re-suspended in YES+A to $1x10^7$cells/ml. Cells aliquots were taken at different times to monitor cell cycle arrest and release by FACS analysis of DNA content.

2729: *h⁻ mis4-367*

6747: *h⁻ mis4-367 pef1-F78A*

E-F-G-H-I

2: *h⁻*

2729: *h⁻ mis4-367*

3651: *h⁻ ura4-D18 mis4-367 pef1Δ::ura4⁺*

6245: *h⁻ ura4-D18 pef1Δ::ura4⁺*

6747: *h⁻ mis4-367 pef1-F78A*

**Figure 20:**

6747: *h⁻ mis4-367 pef1-F78A*

**Figure 21:**

A

2: *h⁻*

6400: *h⁻ pef1-GFP-natR*

B

2804: *h⁻ leu1-32 mis4-3HA-LEU2*

6940: *h⁻ leu1-32 mis4-3HA-LEU2 pef1-GFP-natR*

C

2: *h⁻*

3638: *h⁻ leu1-32 ura4-D18 pef1Δ::ura4⁺*

3985: *h⁻ cdc10-129*

5545: *h⁻ cdc10-129 ura4-D18 pef1Δ::ura4⁺*

D

2: *h⁻*

6148: *h⁻ rad21FLAG3-KanR*

7326: *h⁻ rad21FLAG3-KanR pef1-F78A*

*- S-phase arrest by hydroxyurea treatment and synchronous release*

Cells were grown in YES+A medium to mid-log phase at 25°C at which time HU was added to 20mM. Cells were further incubated for 4h15 at 36.5°C to induce S-phase arrest. Cells were collected, the HU-containing medium was removed and cells were incubated for 1h45 at 36.5°C in fresh YES+A medium equilibrated at 36.5°C. Cell-cycle arrest was monitored by measuring DNA content by flow cytometry and determination of the septation index.

## B. Genetic analysis

### *1) Crosses*

Crosses were made by mixing two strains of opposite mating type ($h^+$ and $h^-$) on $EMM_2$-N solid media for 2 days at 26°C.

### *2) Random spore analysis*

A loopful of the cross was dispersed into 200µl of distilled water and 1.5µl of cytohelicase 0.5% (v/v) was added and incubated for 6 hours at 32°C or 25°C. SDS was added to 0.5% and spore density was determined using a Thomas microscope slide. Spores were spread on appropriate media with glass beads (generally 300 spores per plate). Colonies were then replica plated onto appropriate plates to select for the desired phenotypes.

### *3) Spotting assay*

Cells were cultured on solid media at 25°C. Equivalent amount of cells were picked up and re-suspended into 100µl YES+A. Serial dilutions at $1/5^e$ were made in YES+A using a 96 wells microtitration plate and spotted with a manual replicator on appropriate media. Plates were incubated at indicated temperatures during 2-3 days.

E

2: *h*$^-$

6400: *h*$^-$ *pef1-GFP-natR*

**Figure 22:**

A

3789: *h*$^-$ *rad21-9PK-KanR*

B

3820: *h*$^+$

2730: *h*$^+$ *mis4-367*

9082: *h*$^+$ *rad21-163A*

9080: *h*$^+$ *mis4-367 rad21-163A*

9221: *h*$^+$ *rad21-164A*

9219: *h*$^+$ *mis4-367 rad21-164A*

9264: *h*$^+$ *mis4-367 rad21-164A*

8955: *h*$^+$ *mis4-367 rad21-S163AS164A*

3820: *h*$^+$

2730: *h*$^+$ *mis4-367*

6848: *h*$^+$ *mis4-367 pef1Δ::natR*

9003: *h*$^+$ *mis4-367 rad21-163E164E pef1Δ::natR*

8949: *h*$^+$ *mis4-367 rad21-163E164E*

9005: *h*$^+$ *mis4-367 rad21-163A164A pef1Δ::natR*

8955: *h*$^+$ *mis4-367 rad21-163A164A*

2730: *h*$^+$ *mis4-367*

C

2: *h*$^-$

6400: *h*$^-$ *pef1-GFP-natR*

### *4) Transformation*

Cells were grown in YES+A to a density of 1-2x$10^7$ cells/ml. Cells were centrifuged (1300g, 1min), and washed twice with 1ml of LiAc buffer (0.1M Li-acetate pH4.9). Cells were suspended in LiAc to $10^9$ cells/ml and distributed into 150µl aliquots (for one transformation) and incubated 45min at 32°C. DNA was added (15µl) and mixed by vortexing. One volume of 370µl of 50 % (w/v) PEG pH7.5 pre-warmed at 32°C was added, mixed by vortexing and incubated at 32°C for 60 minutes. Heat shock was done at 43°C for 15 minutes followed by 10 min at room temperature. Cells were centrifuged and re-suspended in 0.5ml YES+A and cultured over-night in 5ml YES+A (25°C, 200rpm). The culture was centrifuged (1300g, 1min); cells re-suspended in 1ml of fresh YES+A and spread onto appropriate selection media.

### *5) Ectopic Rad21-FLAG strain construction*

The tetO7-Rad21-FLAG allele was integrated on chromosome III at position 171385 (Fennessy and al. 2014) and constructed as follows. A DNA fragment carrying hphMX-tetO7-Pcyc1 was amplified by PCR using pFA6a-hphMX-tetO7-Pcyc1-3xFLAG as template and oligonucleotides primer tet0-fw-chrIII (TATGTAACGGATTGGGATGTGTGTTTTATATGTGTATGAAATGTACATACTGTATAAGTAGTGTAGATATGCTTGTTAAAGAATTCGAGCTCGTTTAAAC)

and Primer tet0-rev-chrIII

(AAGTCCGAGTTAAACTAGAGTCTGACTTAAAACCAGTGCAATGCCTCCATTAACATGATCACATATGTTGGGATTAACTCCATATTAATTAACCTCCAGG).

The PCR product was transformed in an *h- ura4-D18* strain to obtain *h- ura4-D18 hphMX-tetO7- Pcyc1-3xFLAG* strain. Correct integration was checked by PCR.

Next, a DNA fragment carrying rad21-kanMX was amplified by PCR using pFA6a-Gly11-3TEV-rad21-kanMX as template and oligonucleotides primer tet07_rad21_fw

(CACGCAAACACAAATACACACACTAAATTACCGGATCAATTCGGGGGATCCGTTTATCATCCTGGAGGTTAATTAATATGTTCTATTCAGAGGCCATTCT) and primer tet07_rad21 rev

**Figure 23:**

A

2: *h*$^-$

2965: *h*$^-$ *mis4-367*

6849: *h*$^-$ *mis4-367 pef1Δ::natR*

4009: *h*$^-$ *ura4-D18 or ura4*$^+$ *mis4-367 pef1Δ::ura4*$^+$ *wpl1Δ::kanR*

2: *h*$^-$

2729: *h*$^-$ *mis4-367*

*3060: h- wpl1Δ::kanR*

*3474: h*$^-$ *mis4-367 wpl1Δ::kanR*

2: *h*$^-$

2729: *h*$^-$ *mis4-367*

6943: *mis4-367 psm3-Gly11-TEV3-rad21-kanR*

6929: *h*$^-$ *mis4-367 pef1Δ::natR psm3-Gly11-TEV3-rad21-kanR*

6849: *h*$^-$ *mis4-367 pef1Δ::natR*

6638: *h*$^-$ *pef1Δ::natR*

6926: *h*$^+$ *pef1Δ::natR psm3-Gly11-TEV3-rad21-kanR*

6928: *h*$^-$ *psm3-Gly11-TEV3-rad21-kanR*

B

2758: *h*$^-$ *mis4-367 ura4*$^+$*-pREP2res1*

3328: *h*$^-$ *mis4-367 rad21-9PK-kanR ura4*$^+$*-pREP2res1*

3730: *h*$^-$ *mis4-367 pef1Δ::ura4*$^+$ *rad21-9PK-kanR ura4*$^+$*-pREP2res1*

**Figure 24:**

A-B

3985: *h*$^-$ *cdc10-129*

6393: *h*$^-$ *cdc10-129 rad21FLAG3-kanR*

8147: *h*$^-$ *mis4-367 cdc10-129 rad21FLAG3-kanR*

(AAGTCCGAGTTAAACTAGAGTCTGACTTAAAACCAGTGCAATGCCTCCATTAAC
ATGATCACATATGTTGGGATTAACTCCGACAGCAGTATAGCGACCAGC).

The PCR product was transformed in the *h- ura4-D18 hphMX-tetO7- Pcyc1-3xFLAG* stain described above to obtain *h- ura4-D18 hphMX-tetO7- rad21-KanMX* strain. Correct integration was checked by PCR.

Next, a DNA fragment carrying GFP-natMX was amplified by PCR using pFA6a-GFP(S65T)-natMX4 as template with primer rad21_6Gly_GFP_fw

(ATGTTGCCATTCAGAACGAAATCACGCTTACTGCTAAACGTGGAATGCTACTTTC
ATCACTAGGGGGAGGCGGGGGTGGAAGTAAAGGAGAAGAACTTTT) and primer tet07_rad21 rev

(AAGTCCGAGTTAAACTAGAGTCTGACTTAAAACCAGTGCAATGCCTCCATTAAC
ATGATCACATATGTTGGGATTAACTCCGACAGCAGTATAGCGACCAGC).

The PCR product was transformed in the *h- ura4-D18 hphMX-tetO7-rad21-KanMX* strain described above to obtain a *h- ura4-D18 hphMX-tetO7-rad21-GFP(S65T)-NatMX* strain. Correct integration was checked by PCR

Next, genomic DNA of *h- rad21-FLAG3-KanMX* strain was amplified by PCR using oligonucleotides primer Rad21_FLAG_FW

(ATCTGTCAAGCAGGATGTTGCCATTCAGAACGAAATCACGCTTACTGCTAAACGT
GGAATGCTACTTTCATCACTATGCGGCCGCGACTACAAAGACCAT) and primer tet07_rad21 rev

(AAGTCCGAGTTAAACTAGAGTCTGACTTAAAACCAGTGCAATGCCTCCATTAAC
ATGATCACATATGTTGGGATTAACTCCGACAGCAGTATAGCGACCAGC).

The PCR product was transformed in the *h- ura4-D18 hphMX-tetO7-rad21-GFP(S65T)-NatMX* strain to obtain a *h- ura4-D18 hphMX-tetO7-rad21-FLAG3-KanMX* strain. Correct integration was checked by PCR.

The tetracycline sensitive repressor gene (ura4$^{+}$-tet$^{ON}$:TetR-tup11D70 integrated at the ura4 locus (Zilio, Wehrkamp-Richter, and Boddy 2013)) was introduced by crossing to obtain the following strain *ura4-D18* ura4$^{+}$-tet$^{ON}$ *hphMX-tetO7-rad21-FLAG3-KANMX* in which addition of tetracycline allowed expression of the ectopic Rad21-FLAG.

8149: *h⁻ mis4-367 pef1-F78A cdc10-129 rad21FLAG3-kanR*

C

4961: *h⁻ mis4-367 cdc10-129*

8007: *h⁻ mis4-367 pef1-F78A cdc10-129*

**Figure 25:**

2: *h⁻*

6881: *h⁻ mis4-367 rad21FLAG3-kanR*

7324: *h⁻ mis4-367 pef1-F78A rad21FLAG3-kanR*

7326: *h⁻ pef1-F78A rad21FLAG3-kanR*

**Figure 26:**

6701: *h⁻ pef1-F78A rad21-9PK-kanR*

6747: *h⁻ mis4-367 pef1-F78A*

6923: *h⁻ mis4-367 pef1-F78A rad21-9PK-kanR*

**Figure 27:**

2: *h⁻*

6881: *h⁻ mis4-367 rad21FLAG3-kanR*

7326: *h⁻ pef1-F78A rad21FLAG3-kanR*

7324: *h⁻ mis4-367 pef1-F78A rad21FLAG3-kanR*

**Figure 28:**

2: *h⁻*

2729: *h⁻ mis4-367*

6849: *h⁻ mis4-367 pef1Δ::natR*

6777: *h⁻ ura4⁺-Tet$^{ON}$*

7548: *h⁻ ura4⁺-Tet$^{ON}$ NCRNA458::hygR-tet07-rad21-FLAG3kanR*

7567: *h⁻ ura4⁺-Tet$^{ON}$ rad21Δ::ura4⁺ NCRNA458::hygR-tet07-rad21-FLAG3-kanR*

7580: *h⁻ ura4⁺-Tet$^{ON}$ rad21Δ::ura4⁺ mis4-367 NCRNA458::hygR-tet07-rad21-FLAG3-kanR*

Sequencing of the *hphMX-tetO7-rad21-FLAG3-KANMX* construction revealed a frame shift mutation resulting in the modification of the last four amino acids of the Rad21 protein ($^{623}$MLLS$^{626}$ to $^{623}$NATF$^{626}$) that does not affect its functionality as judged by its ability to support viability in absence of the essential endogenous Rad21 gene (*rad21Δ hphMX-tetO-rad21-FLAG3-KANMX tet*-ON strain in tetracycline condition, see Figure 28).

## C. FACs analysis of DNA content.

### *1) Ethanol fixation*

A sample of $5x10^7$ cells grown in liquid media was withdrawn, $NaN_3$ was added (1mM final concentration) and cells washed with cold sterile water by centrifugation (1min, 1300g). The supernatant was removed and the pellet was re-suspended in 1ml of cold ethanol 70% (-20°C). Fixed cells were stored at 4°C.

### *2) DNA labelling*

Fixed cells (100µL) were spun down and re-suspended in 400µl of Na-citrate 50mM. Cells were centrifuged (1min, 1300g) and supernatant was discarded. The cell pellet was re-suspended in 500µl of Na-citrate 50mM 0.1µg/ml RNAse A and incubated at 37°C for two hours. One volume of Na-citrate 50mM, 2µm SYTOX green was added.

For cells released from nitrogen-starved media, the protocol was modified as follows. One volume of 500µl of fixed cells was centrifuged (10min, 14000g) and supernatant was discarded. The cell pellet was re-suspended in 1ml of Na-citrate 50mM, incubated during 10min with regular vortexing. Cells were washed with 500µL Na-citrate 50mM, re-suspended in HCl 0.1N, pepsin 2mg/ml and incubated at room temperature during 1 hour. Cells were washed twice with Na-citrate 50mM, re-suspended in 100µL Na-citrate 50mM RNAse A 20µg/mL, incubated one hour at 37°C and over-night at 4°C. The nuclei were stained by the addition of 400µl Na-citrate 50mM 0.125µg/mL SYTOX green.

7580: *h⁻ ura4⁺-Tet$^{ON}$ rad21Δ::ura4⁺ mis4-367 pef1Δ::natR NCRNA458::hygR-tet07-rad21-FLAG3-kanR*

**Figure 29:**

7818: *h⁻ mis4-367 cdc10-129 NCRNA458::hygR-tet07-rad21-FLAG3-kanR ura4⁺-Tet$^{ON}$*

7835: *h⁻ mis4-367 pef1-F78A cdc10-129 NCRNA458::hygR-tet07-rad21-FLAG3-kanR ura4⁺-Tet$^{ON}$*

**Figure 30:**

7791: *h⁻ cdc10-129 NCRNA458::hygR-tet07-rad21-FLAG3-kanR ura4⁺-Tet$^{ON}$*

7839: *h⁻ pef1-F78A cdc10-129 NCRNA458::hygR-tet07-rad21-FLAG3-kanR ura4⁺-Tet$^{ON}$*

**Figure 37:**

6393: *h⁻ cdc10-129 mis4⁺ rad21-FLAG*

7818: *h⁻ mis4-367 cdc10-129 NCRNA458::hygR-tet07-rad21-FLAG3-kanR ura4⁺-Tet$^{ON}$*

7835: *h⁻ mis4-367 pef1-F78A cdc10-129 NCRNA458::hygR-tet07-rad21-FLAG3-kanR ura4⁺-Tet$^{ON}$*

7791: *h⁻ cdc10-129 NCRNA458::hygR-tet07-rad21-FLAG3-kanR ura4⁺-Tet$^{ON}$*

7839: *h⁻ pef1-F78A cdc10-129 NCRNA458::hygR-tet07-rad21-FLAG3-kanR ura4⁺-Tet$^{ON}$*

### *3) Flow cytometry*

Labelled cells were sonicated 10-15sec at 20m/sec and DNA content was measured using an Accuri C6 Flow cytometer on 30000 cells. Figures were mounted using FlowJo.

## D. Analysis of chromatin proteins

### *1) Nuclear spreading and indirect immunofluorescence*

- *Spheroplasts preparation*

The protocol is derived from (Schmidt, Brookes, and Uhlmann 2009). Cell cultures (~5x$10^6$ cells/mL) were arrested by $NaN_3$ 1mM and cooling on ice. One volume corresponding to 5x$10^7$ cells was centrifuged (1min, 1300g) and washed once with 1ml of cold (4°C) distilled water and once with 900µL of cold sorbitol 1.2M. Samples were centrifuged (1min, 1300g) and the cell pellet was re-suspended in 300µl of lysing enzymes (6.7mg/mL of *Trichoderma harzianum* lysing enzymes, Sigma L1412 in SP2 buffer: 1.2M sorbitol; Tri-sodium citrate 50mM; $Na_2HPO_4$ 50mM, pH5.6) and incubated at 30°C to digest the cell wall. Enzymatic digestion was monitored by SDS lysis (2µL of cells + 1µL of SDS 10%) and observation was made using a bench microscope and a 40X objective. When ~95% of cells were lysed by SDS, the reaction was stopped by transferring samples on ice. Spheroplasts were deposited onto 1 ml ice-cold sucrose cushion (15% sucrose, 1.2M sorbitol, 10mM Tris-HCl, pH 7.5) and spun down (4min, 500g, 4°C). The pellet was washed once in ice-cold Sorb/Tris (1.2M sorbitol 10mM Tris–HCl, pH7.5) and once in ice-cold Sorb/MES (0.1M MES hydrate (2-(*N*-morpholino) ethane sulfonic acid), 1mM EDTA, 0.5mM $MgCl_2$, 1M sorbitol, pH6.4). Finally, spheroplasts were re-suspended in 600µL of ice-cold Sorb/MES and kept on ice until spreading.

- *Chromatin spreading*

Lysis of the spheroplasts is performed onto an acid washed microscope slide. Twenty microliters of spheroplasts were deposited on the slide followed by the rapid addition of 40µL fixative solution (4% paraformaldehyde; 3.4% sucrose), 80µL of detergent solution (1% Lipsol), and 80µL of fixative. The mixture was immediately spread onto the slide using a Pasteur pipette. Slides are allowed to dry over-night at room temperature under a fume hood.

**Chapter III. Wpl1 anti-cohesion function requires de-phosphorylation of cohesin by Protein Phosphatase 4**

**Figure 1A**

3820 *h$^{+}$*

5912 *h$^{+}$ natR-eso1-H17*

6577 *h$^{+}$ natR-eso1-H17 psy2D::hygR*

6093 *h$^{+}$ natR-eso1-H17 pph3D::hygR*

6726 *h$^{+}$ natR-eso1-H17 pph3D::kanR psy2D::hygR*

9251 *h$^{-}$ natR-eso1-H17 wpl1D::hygR pph3D::kanR psy2D::hygR*

4044 *h$^{+}$ natR-eso1-H17 wpl1D::kanR*

**Figure 1B** Progeny from the following crosses: 6979x7589 and 6982x7589

6979 *h$^{-}$ ura4-D18 wpl1D::hygR eso1D::ura4$^{+}$*

7589 *h$^{+}$ ura4-D18 psy2D::hygR*

6982 *h$^{-}$ ura4-D18 wpl1D::hygR eso1D::ura4$^{+}$ pph3D::kanR*

**Figure 1C**

7316 *h$^{-}$ cdc25-22 hygR-tetO7-wpl1-13myc-kanR ura4$^{+}$-Tet$^{ON}$ eso1D::natR*

7344 *h$^{-}$ cdc25-22 hygR-tetO7-wpl1-13myc-kanR ura4$^{+}$-Tet$^{ON}$*

7348 *h$^{-}$ cdc25-22 hygR-tetO7-wpl1-13myc-kanR ura4$^{+}$-Tet$^{ON}$ eso1D::natR psy2D::hygR*

**Figure 1D**

8886 *h$^{-}$ cdc25-22 wee1-as8-kanR cut9$^{ts}$ hygR-tetO7-wpl1-13myc-kanR ura4$^{+}$-Tet$^{ON}$ eso1D::natR*

8928 *h$^{-}$ cdc25-22 wee1-as8-kanR cut9$^{ts}$ hygR-tetO7-wpl1-13myc-kanR ura4$^{+}$-Tet$^{ON}$ eso1D::natR pph3D::hygR*

**Figure 2A**

4292 *h$^{-}$ wpl1-13myc-hygR*

6897 *h$^{-}$ wpl1-13myc-hygR psy2-6Gly-3FLAG-kanR*

**Figure 2B**

- *Indirect immunofluorescence*

To eliminate cellular debris and soluble proteins, glass slides were washed four times during one hour in PBS (136.9mM NaCl; 2.68mM KCl; 8.1mM Na2HPO4; 1.47mM KH2PO4; pH7.2) with gentle shaking. PBS was removed and 100µL of Blocking buffer (BB: 0.5% gelatin from porcin skin; 0.5% BSA on PBS) was added and coated with a coverslip. For the immunodetection of FLAG-tagged proteins, the blocking buffer was 1% BSA in PBS (BB1%). Slides were incubated in a wet chamber at 26°C for 30min. The coverslip was removed, and 95µL of antibody dilution was added (Anti-PK antibody: mouse monoclonal (ABD serotec clone SV5-Pk1: 1mg/mL): D500 in BB, anti-GFP antibody: rabbit polyclonal (Invitrogen A11122: 2mg/mL): D800 in BB, anti-FLAG antibody: mouse monoclonal (Sigma clone M2: 1mg/mL): D500 in BB1%). A new coverslip was added and slides were incubated in a wet chamber at 26°C during 3 hours. The coverslip was removed, and slides were washed three times during 10min with PBS with gentle shaking. PBS was removed, and 100µL of blocking buffer was added during 10min at room temperature. The coverslip was removed and100µL of secondary antibody solution was added (anti-mouse FITC antibody (Sigma F2883) D400 in BB; anti-mouse CY3 antibody (Sigma C2181) D400 in BB; anti-mouse CY3 antibody (Jackson ImmunoResearch) D1000 in BB1%; anti-rabbit FITC antibody (Sigma F0382) D400 in BB), a coverslip was added and slides were incubated 2h at 26°C in a wet chamber and over-night at 4°C. Slides were transferred 1 hour at 26°C and incubated 1 hour on PBS to reduce viscosity of BB. Coverslips were removed and slides washed three times in PBS during 30min with gentle shaking. PBS was completely removed and 50µL of mounting solution (2/3 BB or BB1%; 1/3 Vectashield (Vector laboratory); 0.2µg/µl DAPI) was added and a coverslip was deposited.

- *Imaging and quantification*

Fluorescence images were acquired with a Leica DMRD microscope equipped with a cooled CCD camera and a 63X objective. Signals were quantified using Metamorph software. Signal intensity was measured in a square surface containing the spread nucleus. Background signal was measured by moving the square surface in an adjacent region devoid of nuclei. The background value was subtracted for each nucleus. The signal was quantified for at least fifty nuclei for each sample. The mean and the confidence interval of the mean were calculated with $\alpha$=0.05.

2 *h*$^{-}$

6690 *h*$^{-}$ *psy2-6Gly-3FLAG-kanR*

**Figure 2C**

2 *h*$^{-}$

3738 *h*$^{-}$ *pds5D::natR*

6096 *h*$^{-}$ *pph3D::hygR*

3060 *h*$^{-}$ *wpl1D::kanR*

**Figure 2D**

3789 *h*$^{-}$ *rad21-9PK-kanR*

6284 *h*$^{-}$ *rad21-9PK-kanR pph3D::hygR*

**Figure 2E**

7316 *h*$^{-}$ *cdc25-22 hygR-tetO7-wpl1-13myc-kanR ura4*$^{+}$*-Tet*$^{ON}$ *eso1D::natR*

7344 *h*$^{-}$ *cdc25-22 hygR-tetO7-wpl1-13myc-kanR ura4*$^{+}$*-Tet*$^{ON}$

7348 *h*$^{-}$ *cdc25-22 hygR-tetO7-wpl1-13myc-kanR ura4*$^{+}$*-Tet*$^{ON}$ *eso1D::natR psy2D::hygR*

**Figure 3A**

3820 *h*$^{+}$

8824 *h*$^{+}$*rad21-163E164E*

8830 *h*$^{+}$ *pph3D::hygR rad21-163E164E*

6095 *h*$^{+}$ *pph3D::hygR*

5912 *h*$^{+}$*natR-eso1-H17*

8820 *h*$^{+}$*natR-eso1-H17 rad21-163E164E*

8828 *h*$^{+}$*natR-eso1-H17 rad21-163E164E pph3D::hygR*

6093 *h*$^{+}$*natR-eso1-H17 pph3D::hygR*

3820 *h*$^{+}$

8897 *h*$^{+}$*rad21-163A164A*

8903 *h*$^{+}$ *pph3D::hygR rad21-163A164A*

6095 *h*$^{+}$ *pph3D::hygR*

5912 *h*$^{+}$*natR-eso1-H17*

## *2) Chromatin Immunoprecipitation (ChIP)*

The procedure is essentially as described in (Feytout and al. 2011)

- *Formaldehyde fixation*

Cells were fixed by adding formaldehyde to the culture (2.54% final) during 15min at 36.5°C with shaking (200rpm). Fixation was stopped by addition of 125mM glycine and transfer on ice for 15min. One volume of culture corresponding to $2x10^8$ cells was centrifuged (1min, 1300g) and cells washed twice with ice-cold PBS (136.9mM NaCl; 2.68mM KCl; 8.1mM Na2HPO4; 1.47mM KH2PO4; pH7.2) and once with 1mL of PBS. The cell pellet was frozen on dry ice and stored at -80°C.

- *Cell lysis*

A volume of 125µL of lysis buffer (50mM HEPES-KOH, pH7.6; 140mM NaCl, 1mM EDTA; 1% triton X-100 (v/v); 0.1% sodium deoxycholate (w/v), 1mM PMSF (Phenyl Methyl Sulfonyl Fluoride) and one tab of protease inhibitors (Protease inhibitors "complete EDTA free" Roche) for 10mL) freshly made and stored on ice, was added and the cell pellet was re-suspended by vortexing. A 500µl volume of acid-washed glass glass beads (SIGMA G-8772 425-600µm) was added and cell lysis was performed using a CryoFastPrep (3 rounds of 30 seconds at the maximum power 6.5m/s). To separate the chromatin extract from the glass beads, the bottom of the tubes were punctured with a flame-heated needle. Punctured tubes were inserted in a 15ml Falcon and centrifuged (1min, 1300g, 4°C). The lysates were collected and the volume was increased by the addition of 325µL of ice-cold lysis buffer.

- *Chromatin sonication and clarification*

Cells lysates were sonicated in a water tank at 0-1°C for seven cycles of 30 sec ON 30 sec OFF at 20KHz (Bioruptor, Diagenode). Under these conditions chromatin is shared to ~1000bp fragments. Lysates were clarified by centrifugation (10min 10000g 4°C) and the supernatant used for the immunoprecipitation.

- *Chromatin Immunoprecipitation*

Immunoprecipitation was made using magnetics beads (Ademtech, coated with protein G, 04342). For one immunoprecipitation, 25µl of magnetics beads were used. One volume of beads was mixed with 9 volumes of blocking buffer (Ademtech) during 15 minutes with

**Figure 4**

7821 *h$^-$ cdc25-22 mis4-367 wee1-as8-kanR cut9$^{ts}$ hygR-tetO7-wpl1-13myc-kanR ura4$^+$-Tet$^{ON}$*

7782 *h$^-$ cdc25-22 mis4-367 wee1-as8-kanR cut9$^{ts}$ hygR-tetO7-wpl1-13myc-kanR ura4$^+$-Tet$^{ON}$ rad21-9PK-kanR eso1D::natR*

7847 *h$^-$ cdc25-22 mis4-367 wee1-as8-kanR cut9$^{ts}$ hygR-tetO7-wpl1-13myc-kanR ura4$^+$-Tet$^{ON}$ rad21-9PK-kanR eso1D::natR psy2D::hygR*

7904 *h$^-$ cdc25-22 mis4-367 wee1-as8-kanR cut9$^{ts}$ hygR-tetO7-wpl1-13myc-kanR ura4$^+$-Tet$^{ON}$ rad21-9PK-kanR*

7882 *h$^-$ cdc25-22 mis4-367 wee1-as8-kanR cut9$^{ts}$ ura4$^+$-Tet$^{ON}$ rad21-9PK-kanR eso1D::natR wpl1D::kanR*

7883 *h- cdc25-22 mis4-367 wee1-as8-kanR cut9$^{ts}$ rad21-9PK-kanR wpl1D::kanR*

9214 *h$^-$ cdc25-22 mis4-367 psy2D::hygR wee1-as8-kanR cut9$^{ts}$ hygR-tetO7-wpl1-13myc-kanR ura4$^+$-Tet$^{ON}$ rad21-9PK-kanR*

9294 *h$^-$ cdc25-22 mis4-367 psy2D::hygR wee1-as8-kanR cut9$^{ts}$ hygR-tetO7-wpl1-13myc-kanR ura4$^+$-Tet$^{ON}$ rad21-163A164A-9PK-kanR*

**Figure S1**

3820 *h$^+$*

5659 *h$^+$ wpl1$^+$-hygR natR-eso1-H17*

5640 *h$^+$ wpl1$^+$-hygR natR-eso1-H17 pds5$^{G755V\text{-}STOP}$*

5647 *h$^+$ wpl1$^+$-hygR natR-eso1-H17 pds5$^{K686\text{-}STOP}$*

5825 *h$^+$ wpl1$^+$-hygR natR-eso1-H17 psc3$^{T217M}$*

5827 *h$^+$ wpl1$^+$-hygR natR-eso1-H17 psc3$^{Q153E}$*

5834 *h$^+$ wpl1$^+$-hygR natR-eso1-H17 psc3$^{L149P}$*

5978 *h$^+$ wpl1$^+$-hygR natR-eso1-H17 psm3$^{G103V}$*

1520s *h$^+$ wpl1$^+$-hygR natR-eso1-H17 psm3$^{K106N}$*

5823 *h$^+$ wpl1$^+$-hygR natR-eso1-H17 pph3$^{R111W}$*

**Figure S2**

3789 *h$^-$ rad21-9PK-kanR*

6284 *h$^-$ rad21-9PK-kanR pph3D::hygR*

gentle shaking. The liquid was removed by magnetization and five beads volume of IP buffer and 2µg of anti-FLAG antibody (F1804, SIGMA) were added and incubated one hour at room temperature on a rotating mixer.

Thirty-five microliters of chromatin extract were removed and stored on ice (input fraction) and 350µl were used for the immunoprecipitation (IP) by mixing with 127µl of beads-antibody mix and 550µl of IP buffer. Samples were incubated over-night on a rotating mixer at 4°C.

- *Washes*

All IP samples were washed five times with 300µl of washing solution followed by 10 min incubation on a rotating mixer at room temperature. First wash was performed with 20mM Tris-HCl; 150mM NaCl; 2mM EDTA; 1% triton X-100; 0.1% SDS. The second wash with 20mM Tris-HCl; 500mM NaCl; 2mM EDTA; 1% triton X-100; 0.1% SDS and third wash with 10mM Tris-HCl; 1mM EDTA; 1% sodium deoxycholate; 1% igepal and 25mM LiCl. The two final washes were made with TE (10mM Tris-HCl; 1mM EDTA) without incubation time.

Finally, 290µl of TES (50mM Tris-HCl; 1mM EDTA; 0.5% SDS) were added on the beads and 255µl on input samples. Proteins were removed by adding 10µl of proteinase K 10mg/ml (Boehringer Mannhein) to all samples (IP and input), and 2 hours incubation at 37°C on a rotating mixer. IPs samples were magnetized to remove beads then all the samples (IP and input) were incubated at 65°C over-night to reverse the cross-links.

- *DNA purification*

DNA purification was made by using ChIP DNA clean and concentrator columns (Zymo research, D5205) according to manufacturer's instructions. ChIP DNA Binding Buffer (600µl) was mixed with 120µl of sample (IP and input) and transferred into a Zyo-Spin column (Zymo research, D5205). Samples were centrifuged (30sec, 10000g). DNA was washed twice with 200µl of washing buffer and centrifuged (30sec, 10000g). Immunoprecipitated DNA was eluted with 50µl of Tris-HCl 10mM and input samples with 100µl of Tris-HCl 10mM.

**Figure S4**

2960 *h⁻ leu1-32 eso1-H17*

**Figure S5B**

8211 *h⁻ natR-eso1-H17 rad21-RV20B*

8217 *h⁻ natR-eso1-H17 rad21-RV38R*

8229 *h⁻ natR-eso1-H17 rad21-RV43D*

8389 *h⁻ natR-eso1-H17 rad21-RV25E1*

8433 *h⁻ natR-eso1-H17 rad21-RV63G1*

5913 *h⁻ natR-eso1-H17*

2 *h⁻*

8373 *h⁻ natR-eso1-H17 rad21-RV43C*

8381 *h⁻ natR-eso1-H17 rad21-RV38S*

8441 *h⁻ leu1 natR-eso1-H17 rad21-RV33C2*

8520 *h⁻ leu1 natR-eso1-H17 rad21-RV79W1*

**Figure S5C**

3820 *h⁺*

5912 *h⁺natR-eso1-H17*

8699 *h⁺natR-eso1-H17 rad21-163E*

8708 *h⁺natR-eso1-H17 rad21-163E164E*

8711 *h⁺natR-eso1-H17 rad21-163E164E165E*

3820 *h⁺*

5912 *h⁺natR-eso1-H17*

8808 *h⁺natR-eso1-H17 rad21-163E*

9305 *h⁺natR-eso1-H17 rad21-164E*

9309 *h⁺natR-eso1-H17 rad21-165E*

8820 *h⁺natR-eso1-H17 rad21-163E164E*

9332 *h⁺natR-eso1-H17 rad21-164E165E*

9307 *h⁺natR-eso1-H17 rad21-163E165E*

- *DNA quantification by real time PCR*

Real time PCR reactions were set up in 96-Well PCR plates by mixing 2µl of DNA and 18µl of MIX (10µl "Abgene SYBER MIX", 5µl H20 and 3µl primers 2µM) for a total volume of 20µl. The plate was sealed and PCR were run in a MX3000P thermocycler (Stratagene) using the following conditions. One step 95°C for 15 min followed by 40 cycles (15 sec 95°C- 1min 60°C).

Serial dilutions of genomic DNA (50ng/µl to $5x10^{-4}$ng/µl) were used to construct the standard curve. The %IP is calculated as the ratio IP/Input.

## *3) Chromatin Immunoprecipitation and sequencing (ChIP-seq)*

- *Formaldehyde fixation*

Cells were fixed by adding formaldehyde into the cultures (1% final) during 15min at 36.5°C with shaking (200rpm). Fixation was stopped by addition of 125mM glycine and transfer on ice for 15min. One volume of culture corresponding to $2x10^8$ cells was centrifuged (1min, 1300g) and cells washed twice with acid-washed PBS buffer (136.9mM NaCl; 2.68mM KCl; 8.1mM Na2HPO4; 1.47mM KH2PO4; pH 7.2) and once with 1mL of PBS, 1mM PMSF and protease inhibitor (Sigma). Cell Pellets were frozen on dry ice and stored at -80°C.

- *Cell lysis*

A volume of 125µL of lysis buffer (50mM HEPES-KOH, pH7.6; 140mM NaCl, 1mM EDTA; 1% triton X-100 (v/v); 0.1% sodium deoxycholate (w/v), 1mM PMSF (Phenyl Methyl Sulfonyl Fluoride and one tab of protease inhibitors (Protease inhibitors "complete EDTA free" Roche) for 10mL) freshly made and stored on ice was added and the cell pellet was re-suspended by vortexing. A 500µl volume of ice-cold glass beads (SIGMA G-8772 425-600µm) was added and cell lysis was performed using a CryoFastPrep (4 rounds of 30 seconds at the maximum power 6.5m/s). To separate the chromatin extract from the glass beads, the bottom of the tubes were punctured with a flame-heated needle. Punctured tubes were inserted in a 15ml Falcon and centrifuged (1min, 1300g, 4°C). The lysates were collected and the volume was increased by the addition of 175µL of ice-cold lysis buffer and transferred on TPX tubes (Diagenode, C30010016).

# Table 2: Fission yeast media

Rich media Yes+Ade:

0.5% yeast extract (w/v)
3% glucose (w/v)
150mg/L adenine
100mg/L uracil, leucine and histidine

Synthetic media $EMM_2$ (Edinburgh minimal medium):

3g/l potassium hydrogen phthalate
5.55 g/L $Na_2HPO_4$, $12H_2O$
5 g/L $NH_4Cl$
2% (w/v) glucose
20ml/L salts solution
1ml/L vitamins solution
0.1ml/L minerals solution

Synthetic media $EMM_2$-N (Edinburgh minimal medium without nitrogen):

3g/l de potassium hydrogen phthalate
5.55 g/L $Na_2HPO_4$, $12H_2O$
2% (w/v) glucose
20ml/L salts solution
1ml/L vitamins solution
0.1ml/L minerals solution

50X Salt stock:

52.5g/L $MgCl_2$, $6H_2O$
0.735g/L $CaCl_2$, $2H_2O$
50g/L KCl
2g/L $Na_2SO_4$

1 000X vitamin stock:

1g/L pantothenic acid
10g/L nicotinic acid
10g/L myo-inositol
10mg/L biotin

10 000X mineral stock:

5g/L boric acid
4g/L $MnSO_4$
4g/L $ZnSO_4$, $7H_2O$
2g/L $FeCl_2$, $6H_2O$
0.4g/L molybdic acid
1g/L de KI
0.4 g/L $CuSO_4$, $5H_2O$
10g/L citric acid

- *Chromatin sonication and clarification*

Cells lysates were sonicated in a water tank at 0°C during 15 cycles of 30 sec ON 30 sec OFF with the Bioruptor Pico sonicator. These conditions allowed production of chromatin fragments around 250pb-300pb. Lysates were centrifuged (10min, 10000g, 4°C) and the supernatant used for the immunoprecipitation.

- *Chromatin Immunoprecipitation*

Immunoprecipitation was made using magnetics beads (Ademtech, protein G, 04342). For one immunoprecipitation, 25µl of magnetics beads were used. One volume of beads was mixed with 9 volumes of blocking buffer (Ademtech) during 15 minutes with agitation. Supernatant was removed by magnetization and five volume of IP buffer and 2µg of anti-FLAG antibody (F1804, SIGMA) were added and incubated one hour at room temperature on a rotating mixer.

Three cells pellets were used per experimental condition. Sonicated lysates were mixed. The immunoprecipitation (IP) was made using 290µl of extract and 29 µl were spared for the input (IN). Immunoprecipitation samples were mixed with 127µl of beads-antibody mix and 548µl of IP buffer. Samples were incubated over-night on a rotating mixer at 4°C.

- *Washes*

IPs were washed five times with 300µl of washing solution and 10 min incubation on a rotating mixer at room temperature. First wash used 20mM Tris-HCl; 150mM NaCl; 2mM EDTA; 1% triton X-100; 0.1% SDS. The second wash with 20mM Tris-HCl; 500mM NaCl; 2mM EDTA; 1% triton X-100; 0.1% SDS, and third wash with 10mM Tris-HCl; 1mM EDTA; 1% sodium deoxycholate; 1% igepal and 25mM LiCl. The two final washes were made with TE (10mM Tris-HCl; 1mM EDTA) without incubation time.

Finally, 290µl of TES (10mM Tris-HCl; 1mM EDTA; 0.5% SDS) were added on the beads and 261µl on input samples. Proteins were removed by adding 10µl of proteinase K 10mg/ml (Boehringer Mannhein) to samples (IP and IN) and 2 hours incubation at 37°C on a rotating mixer. IPs samples were magnetized to remove beads then all the samples (IP and input) were incubated at 65°C over-night to reverse the cross-links.

- *DNA purification*

DNA purification was made by using Qiaquick PCR purification kit columns (Qiagen, 28106) according to manufacturer's instructions. PB buffer (1500µl) was mixed with 300µl of sample (IP and input) and loaded onto the column. Samples were centrifuged (30sec, 10000g). Washing buffer (750µl) was added and the column spun twice (30sec, 10000g) and kept at room temperature for 5min. Immunoprecipitated DNA was eluted in 27µl of Tris-HCl 10mM pH8 and mixed with its corresponding duplicate. Input was eluted with 100µl of Tris-HCl 10mM pH8.

- *Library preparation and sequencing*

BEA core facility group at Karolinska Institute made library preparation and sequencing. Library was prepared by the Thruplex protocol (Rubicon Genomics) from 250-350pb DNA in which short tags were added (6nt). This process allowed multiplexed sequencing by Illumina sequencer. Single reads (50pb) were generated and data available as FASTQ files.

- Bioinformatics analysis

FASTQ files were aligned on the *S. pombe* genome (ASM294v2) with bowtie2 (default parameters) to obtain BAM files. Data visualization and analysis were performed with SeqMonk. Peaks calling MACS (default parameters, DNA size 300pb, p-value>$10^{-5}$) was used to identify regions of Rad21-FLAG enriched in the aligned data over a whole-genome input DNA sample that was processed and sequenced in parallel. Sequenced input is used to normalize each sample and quantitation is made per million reads or Log value (by relative quantitation using Input signal as reference).

## E. Protein analysis

### *1) Total protein extract*

One volume of culture corresponding to 5x$10^8$ cells was centrifuged (1min, 1300g) and cells washed twice with ice-cold PBS buffer (136.9mM NaCl; 2.68mM KCl; 8.1mM Na2HPO4; 1.47mM KH2PO4; pH7.2) and once with 1mL of PBS, 1mM PMSF. The cell pellet was frozen on dry ice and stored at -80°C.

A volume of 125µL of lysis buffer freshly made and stored on ice (50mM HEPES-KOH, pH7.6; 100mM KCl; 2.5mM $MgCl_2$; 0.25% triton X-100 (v/v); 1mM dithiothreitol [DTT]; 0.1% SDS, 10mM sodium butyrate, 10% glycerol and protease inhibitors 1mM PMSF; 1mM Na-vanadate; 20mM beta-glycerophosphate and 50µl of inhibitor cocktail (SIGMA p8215) for 10mL) was added and the cell pellet was re-suspended by vortexing. A 500µl volume of acid-washed glass beads (SIGMA G-8772 425-600µm) was added and cell lysis was performed using a CryoFastPrep (2 rounds of 20 seconds at the maximum power 6.5m/s). To recover the extract, the bottom of tubes was punctured with a flame-heated needle. Punctured tubes were inserted in a 15ml Falcon and centrifuged (1min, 1300g, 4°C). Lysates were collected and the volume was increased by the addition of 275µL of ice-cold lysis buffer. Lysates were centrifuged twice (10min, 10000g, 4°C) and 350µL of supernatant were collected.

- *Co-Immunoprecipitation from crude extracts*

From total extract, a fraction (1/10 volume) was taken as input (IN) and the remaining 9/10 used for the immunoprecipitation (IP). Fifty microliters of magnetics beads in lysis buffer were added (coated with protein A or G, microMACS) and 2µg of antibody (anti-GFP antibody rabbit polyclonal (2mg/ml, A11122, Invitrogen); anti-GFP antibody mouse monoclonal (clones 7.1 and 13.1 at 0.4mg/ml, Roche), anti-FLAG antibody mouse monoclonal (Sigma clone M2 1mg/mL). All samples were incubated at 4°C during 1 hour in the dark. Immunoprecipitates were collected using microMACS columns on a magnetic rack and the flow-through fraction was collected (FT). Beads were washed 5 times with wash solution (50mM HEPES-KOH, pH7.6; 75mM KCl; 1mM $MgCl_2$; 1mM EDTA; 0.1% triton X-100 (v/v); 1mM dithiothreitol [DTT]; 10mM sodium butyrate, 10% glycerol). A volume of 20µl (void volume of the column) of hot Laemmli buffer (95°C) was added for 5min. The IP fraction was collected by addition of 50µl of hot Laemmli (95°C). Input (IN) and FT fractions were adjusted to 1X Laemmli buffer, boiled for 5 min and all samples analysed immediately or stored at -20°C.

- *Protein electrophoresis*

Proteins were separated by their molecular weight using polyacrylamide gel electrophoresis under denaturing conditions (SDS-PAGE) in TGS buffer (25mM Tris; 250mM glycine; 0.1% SDS).

- *Western blotting*

Protein transfer was made by electric transfer using semi-dry conditions. Two types of membranes were used, nitrocellulose (Amersham) or PVDF for low molecular weight proteins. Three Whatman papers soaked with transfer buffer (39mM glycine; 48mM Tris; 20% ethanol (v/v); 3.7% SDS) were deposited on the cathode of the apparatus (Amersham Hoefer 77TE). Membrane soaked in transfer buffer was deposited on the Whatman papers followed by the acrylamide gel and 4 Whatman papers soaked in transfer buffer. Transfer was done one hour at 0.8mA/cm$^2$ (40mA).

- *Immuno-detection*

The membrane was incubated in TBST-milk (20mM Tris; 137mM NaCl; 0.1% tween-20; 5% milk (w/v)) during 30 minutes at room temperature with shaking and over-night at 4°C with shaking in TBST 5% milk containing the primary antibody. The antibodies and concentrations used are listed below.

- Anti-GFP antibody, mouse monoclonal (clones 7.1 and 13.1 at 0.4mg/ml, Roche) 1/1000$^{th}$;
- Anti-FLAG antibody, mouse monoclonal (clone M2: 1mg/mL, Sigma) 1/4000$^{th}$;
- Anti-tubulin TAT1 antibody, mouse monoclonal (Woods and al. 1989), 1/10000$^{th}$;
- Anti H3 antibody, rabbit polyclonal (1000mg/ml, Abcam), 1/1000$^{th}$;
- Anti Psm3 antibody (400µg/ml, rabbit immunisation with 631 N-ter residues of Psm3, and affinity purified with recombinant protein, (Feytout and al. 2011), 1/2000$^{th}$;
- Anti Psm1 antibody (rabbit immunisation with 630 N-ter residues of Psm1, and affinity purified with recombinant protein, (Feytout and al. 2011), 1/5000$^{th}$;
- Anti Rad21 antibody (900µg/ml, rabbit immunisation with 413 C-ter residues of Rad21, and affinity purified with recombinant protein, (Feytout and al. 2011), 1/2000$^{th}$;
- Anti HA antibody, mouse monoclonal (1mg/ml, Covance 16B12) 1/2000$^{th}$;
- Anti thiophosphate-ester antibody, rabbit monoclonal (clone 51-8, Abcam) 1/10000$^{th}$
- Anti myc antibody, mouse monoclonal (200µg/ml, clone 9E10, Santa Cruz) 1/2000$^{th}$

The membrane was washed three times at room temperature during 30min in TBST followed by an one hour incubation time with the appropriate secondary antibody in TBST

5% milk (anti mouse peroxidase antibody (A5906, SIGMA) diluted at 1/10000; anti-rabbit peroxidase antibody (NA9340) diluted at 1/10000). Finally, the membrane was washed three times at room temperature in TBST during 30min. Proteins were revealed by $ECL^+$ kit (Amersham) or Western Lightning® Plus-ECL (NEL105001EA).

## *2) Cellular fractionation*

- *Spheroplast preparation*

Cells grown to mid log phase (~$5x10^6$ cells/mL) were arrested by adding 1mM sodium azide and cooling on ice. One volume corresponding to $2x10^8$ cells was centrifuged (1min, 1300g, 4°C) and washed with 30ml of cold distilled water and 30mL of cold sorbitol 1.2M. Samples were centrifuged (8min, 1300g, 4°C) and the cell pellet was re-suspended in 1000µl of lysing enzymes (6,7mg/mL of *Trichoderma harzianum* lysing enzymes, Sigma L1412 in SP2: 1.2M sorbitol; Tri-sodium citrate 50mM; $Na_2HPO_4$ 50mM, pH5.6) and incubated at 30°C to digest the cell wall. Enzymatic digestion was monitored by SDS lysis (2µL of cells + 1µL of SDS 10%) and microscopic observation. When ~95% of cells were lysed by SDS, the reaction was stopped by transferring samples on ice. Spheroplasts were deposited onto 1 ml sucrose cushion (15% sucrose, 1.2M sorbitol, 10mM Tris–HCl, pH7.5) and spun (4min, 500g, 4°C). The pellet was washed once in ice-cold Sorb/Tris (1.2M sorbitol 10mM Tris–HCl, pH7.5), frozen on dry ice and stored at -80°C.

- *Protein fractionation*

Spheroplasts were re-suspended in 300µl of AX buffer (20mM Hepes/KOH pH 7.9; 1.5mM Mg-Acetate; 50mM K-Acetate; 0.5mM DTT; 10% glycerol; 1% Triton-X 100, and protease inhibitors (1mM PMSF, 20µg/ml leupeptin, 40µg/ml aprotinin, 10µg/ml pepstatin A, 2mM benzamidine, 2.4µl of chymostatin and 0.25mM sodium vanadate) by delicate pipetting and occasional vortexing. A volume of 40µl was spared as the total fraction. Lysate was deposited onto 200µl of AXS buffer (AX; 30% sucrose) and centrifuged (15min, 13000g, 4°C). Supernatant was spared as soluble fraction containing cytosolic and nucleo-soluble proteins. Pellet was suspended with AX buffer and deposited on 200µl of AXS buffer. Samples were centrifuged (15min, 13000g, 4°C). Supernatant was kept as the "wash fraction" and the chromatin pellet was re-suspended in 200µl of AX buffer (chromatin fraction).

## F. Cytological analysis

### *1) Immunofluorescence anti-tubulin and FISH*

Cells were fixed and processed for tubulin staining using the TAT1 antibody as described (Woods and al. 1989). Fluorescence in situ Hybridization was performed as described (Steglich and al. 2015) using the centromere proximal c1228 cosmid as a probe (Mizukami and al. 1993).Cells were imaged using a Leica DMRXA microscope and a 100X objective. Distances between FISH signals were measured from maximum projections of images created from z-series of eight 0.4-µm steps using MetaMorph software.

## G. Biochemical analysis

### *1) In vitro production of proteins*

The proteins were produced using protocols, equipment, reagents and expertise kindly provided by Dr Marie-France Giraud (IBGC). The *wpl1* and *rad21* open reading frames were cloned in pGADT7, a kind gift from Yoshinori Watanabe.

Bacterial S30 extracts were prepared from BL21 (DE3) Star cells according to the protocol developed by Schwarz (Nature Protocols, 2007). 921.1µL of "Master Mix" were obtained by mixing 9µL of 10% (w/v) sodium azide, 90µL of 40% (w/v) PEG 8000, 67.9µL of 4M potassium acetate, 18.2µL of 1M magnesium acetate, 66µL of 2.5M HEPES, 36µL of a solution containing 1 tablet of protease inhibitor cocktail (Complete, Roche)/1mL, 18µL of 1% (w/v) folinic acid, 7.2µL of 0.5 M DTT, 24µL of NTP mix (60mM GTP, 60mM CTP, 60mM UTP, 90mM ATP), 36µL of 1M phosphoenol pyruate, 36µL of 1M acetyl phosphate, 225µL of a stock solution containing 4mM of each amino acid, 107.8µL of a solution containing 16.7mM of each of the following amino acids (R,C,W,M, D and E) and 180µL of dd$H_2O$. Assays were performed in a Fliptube®, in which 100µL of the "Reaction Mix" (0.4µL of pyruvate kinase at 2000U/mL, 1.2µL of *E. coli* tRNAs at 40 mg/mL, 1.4µL of T7 RNA Polymerase at 400U/µL, 0.9µL of RNAguard at 32U/µL, 7.5µL of plasmid at 200 ng/µL, 35µL of "S30" extract and 51.2µL of "Master Mix") were placed into the cap of the tube. The cap was covered with a dialysis membrane (SpectraPore7, Molecular Weight Cut Off (MWCO): 10000 Da). The tube was cut at its bottom and assembled onto the cap. 1700µL of "Feeding Mix" (870µL of "Master Mix", 595µL of "S30 buffer" (14mM magnesium acetate,

0.6mM potassium acetate, 0.5mM DTT, 10mM Tris-acetate pH8.2), 212µL of a solution containing 4mM of each amino acid and 23µL of dd$H_2O$) were added through the bottom hole. Incubations were performed at 28°C, at 50-75 rpm during 20 hours.

### *2) In vitro phosphorylation*

- *Immunoprecipitation of Pef1-GFP*

Immunoprecipitation was made as previously described (E.1.*Co-Immunoprecipitation from crude extracts*) with modifications. After immunoprecipitation, samples were deposited onto microMACS columns on the magnetic rack and beads washed twice with wash buffer and three times with kinase buffer 2.5X (120mM Tris-HCl pH7.5; 25mM MgCl2; 2mM EGTA, 2mM DTT). MicroMACS columns were removed from the magnet and beads with immune-complexes were eluted with 40µl 2.5X kinase buffer; 30µL were used for the phosphorylation assay and 10µl analysed by Western Blotting to check the amount of IP'ed Pef1-GFP.

- *Phosphorylation reaction and alkylation*

A fraction of the supernatant of *in vitro* produced Rad21 (45µl) was mixed with beads-immune-complexes (30µl) of Pef1-GFP or no tag control. ATPγS (1mM final) was added to start the reaction. *In vitro* phosphorylation was performed at 30°C during 1 hour with 1min shaking (300rpm) every 10min. The reaction was stopped by adding EDTA (20mM final). PNBM (p-Nitrobenzyl mesylate) was added (5mM final) to alkylate thio-phosphorylated proteins and the samples incubated for 2 hours at 21°C on a rotating wheel.

- *Recovery of Thio-phosphorylated proteins*

Samples were deposited on microMACS columns equilibrated with kinase buffer. The Flow-Through was collected as fraction containing thio-phosphorylated proteins and analysed by SDS-PAGE.

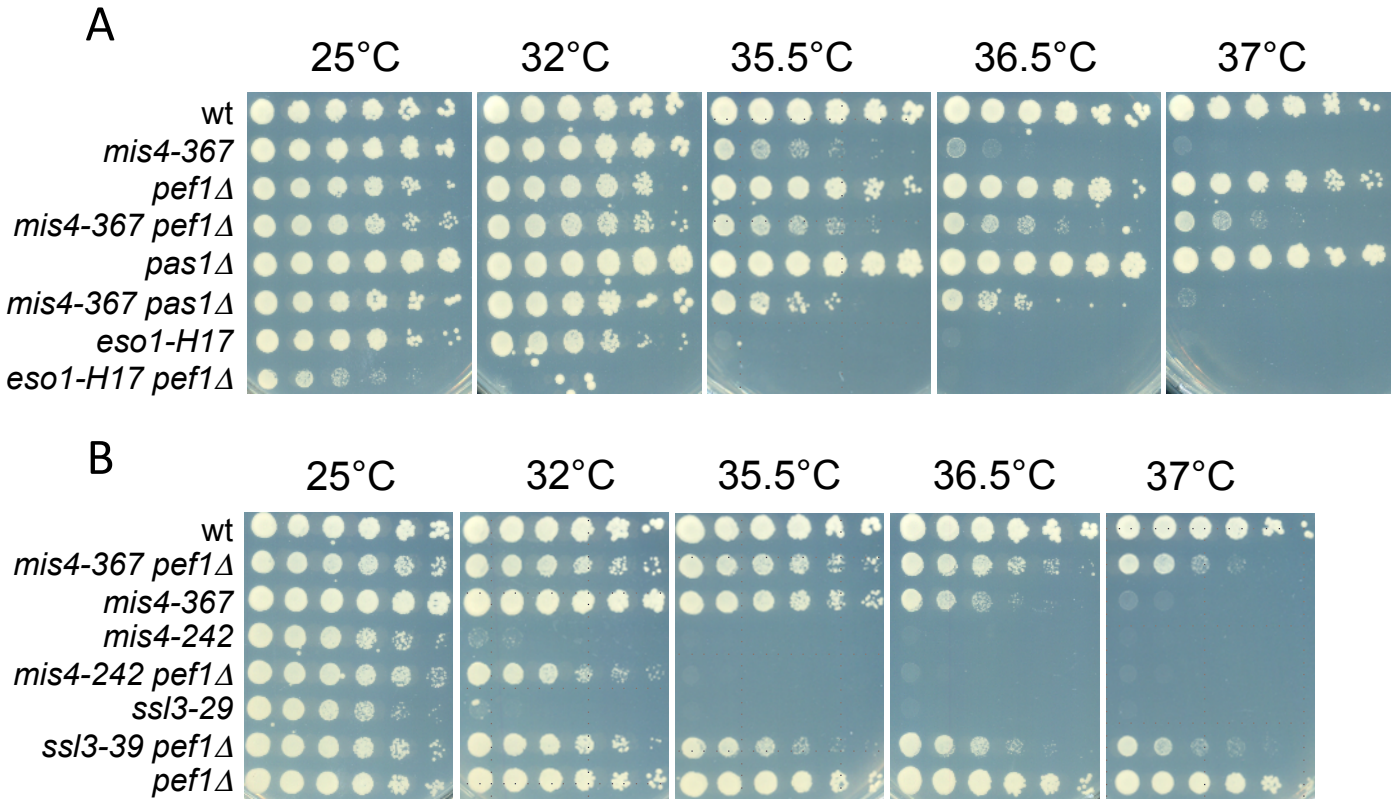


**Figure 18 : A.** Deletion of *pef1* or *pas1* suppresses the thermosensitive phenotype of *mis4-367*. **B.** The thermosensitive phenotype of cohesin loader mutants is suppressed by *pef1Δ*. Serial dilutions of cells were spotted on YES medium and incubated at the indicated temperatures.

# Chapter II: The Pef1 Cyclin Dependent kinase regulates sister-chromatid cohesion through the phosphorylation of the cohesin kleisin subunit

## *I. Loss of function of the Pef1 CDK suppresses cohesin loader deficiency*

To identify proteins that may regulate cohesin binding to chromatin in *S.pombe*, a genetic screen was performed in the laboratory by Amélie Feytout, searching for suppressors of the thermosensitive phenotype of *mis4-367* (Feytout 2010*)*. Eleven mutants were isolated that distributed into 4 linkage groups. Groups 1 and 2 were composed by 3 and 6 mutants respectively and groups 3 and 4 were each defined by a single suppressor. Genetic mapping and tiling array hybridization were used to identify the mutated gene in group 1. A single base substitution (A443G) was found within the *pef1* coding sequence. The mutation (N146S) is located within the catalytic site of the kinase. DNA sequencing of the *pef1* open reading frame confirmed the mutation. Another mutant from group 1 had the very same mutation (A443G) and the third had a G487T mutation (G62W).

To ask whether suppression required *pef1* loss of function, a *pef1*-deleted allele was generated. As shown in figure 18A, *pef1* deletion suppressed *mis4-367* thermosensitivity. Deletion of the *pas1* gene behaved similarly, consistent with Pas1 being the major cyclin partner of Pef1 (K. Tanaka and Okayama 2000). Still, the level of suppression is lower, consistent with the notion that Pef1 may bind another cyclin (Chen and al. 2013). Interestingly, the suppressing effect was not restricted to the *mis4-367* allele. The growth assay shown in Figure 18B shows that *pef1*Δ efficiently suppressed *ssl3-29* (Bernard and al. 2006) and partially suppressed *mis4-242* (Toyoda and al. 2002). However *pef1* deletion could not rescue the lethal phenotype of a *mis4* deleted strain (not shown), arguing that suppression requires a residual activity of the cohesin loader. A negative interaction was observed between *pef1*Δ and *eso1-H17* (Figure 18A). This indicates that *pef1* loss of function

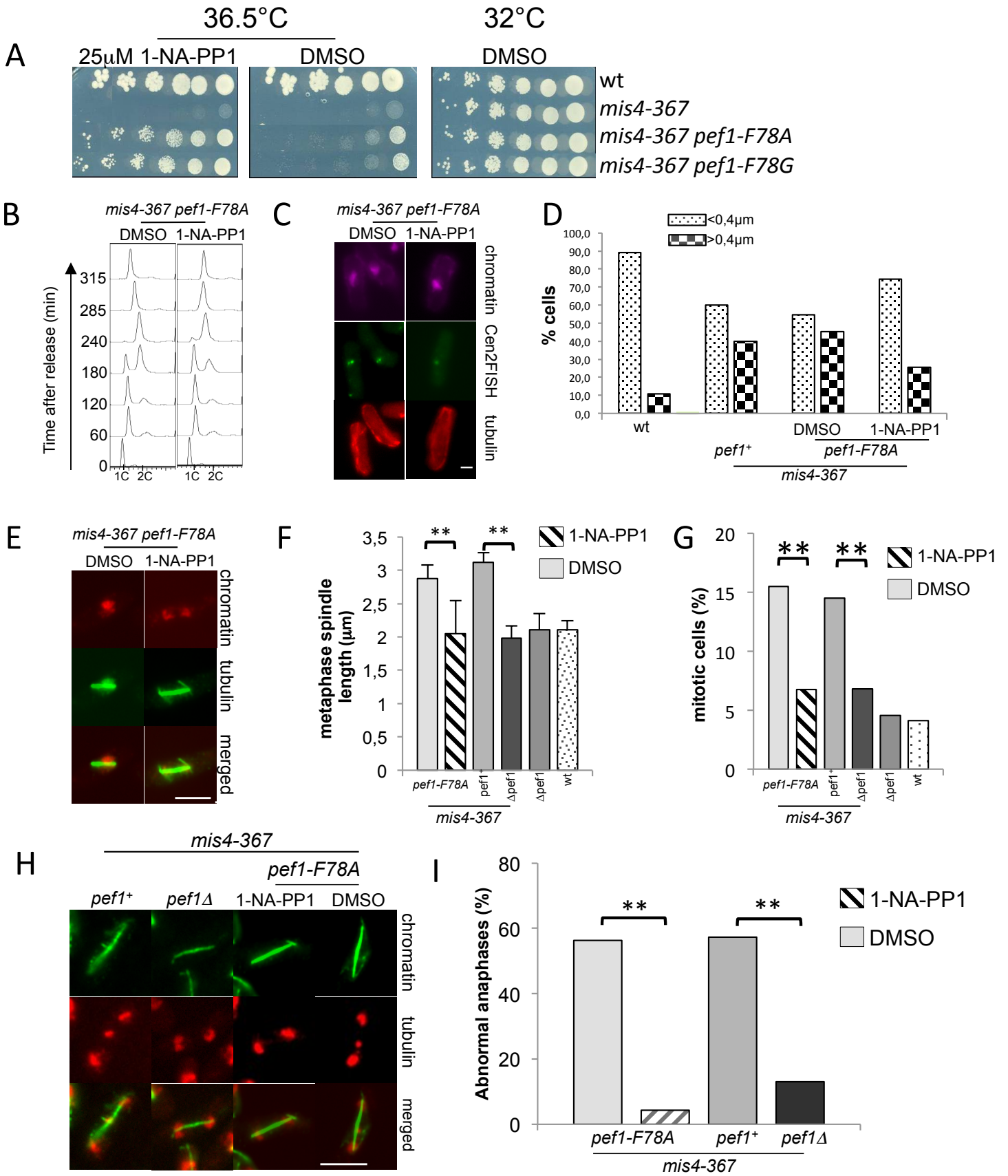


**Figure 19. inhibition of Pef1 kinase activity largely restores sister-chromatid cohesion and chromosome segregation in *mis4-367* cells**. **A.** Serial dilutions of cells were spotted on YES medium (with 1-NA-PP1 or DMSO) and incubated at the indicated temperatures. **B-D**. cen2FISH on G2 cells. Nitrogen starved cells were released into rich medium at the restrictive temperature with or without 1-NA-PP1. **B.** DNA content analysis was monitored by flow cytometry and cells were collected at 315min after release. **C.** Images show examples of typical G2 cells with separated and unseparated cen2FISH dots. Bar=2µm. **D.** Percentage of cells showing separated dots. **E-I.** Exponentially growing cells at 25°C were shifted to the restrictive temperature (36.5°C) during 1 cell cycle (cell density was doubled). For *mis4-367 pef1-f78A* strains 1-NA-PP1(25mM, PP1) or DMSO was added at the time of temperature shift. Cytological analysis of cells undergoing their first mitosis upon temperature shift **E-F.** Spindle length was measured on mono-nucleated cells (** $p<0.01$, t test). Bar=2µm. **G.** Percentage of mitotic cells was determined from the examination of 1800-2200 cells (** $p<0.01$, $\chi^2$ test) . **H-I.** The mitotic spindles were stained (tubulin, green) and DNA was stained with DAPI (red, pseudocolour). Bar=5µm. The frequency of abnormal anaphases was determined from the examination of 50–100 anaphases per sample. Abnormal anaphases were defined as cells with a spindle length >3µm displaying DAPI-stained material that had not reached the spindle poles (** $p<0.01$, $\chi^2$ test).

is not a general suppressor of thermosensitive mutants and further implicates Pef1 in the pathway of sister-chromatid cohesion.

## *II. Inhibition of Pef1 kinase activity in mis4-367 cells restores sister-chromatid cohesion and chromosome segregation*

To ask whether Pef1 acts through its kinase activity, analogue sensitive (as) versions of the CDK were generated. The gatekeeper Phe-78 residue within the ATP binding pocket of the CDK was mutated to glycine or alanine according to the chemical-genetic approach developed by Shokat and co-workers (Gregan and al. 2007). As shown in figure 19A, 1-NA-PP1 addition suppressed *mis4-367* thermosensitivity in a *pef1-F78A* dependent manner, arguing that inhibition of Pef1 kinase activity is responsible for the suppression. To evaluate the level of suppression mediated by Pef1 inhibition we examined well-known phenotypes displayed by cohesin loader mutants. Inactivation of the cohesin loader before S phase prevents the establishment of sister-chromatid cohesion. We employed DNA FISH to directly monitor cohesion after S phase using a probe proximal to the centromere of chromosome 2.

Cells were synchronized in G1 by nitrogen starvation and released into the cell cycle at the restrictive temperature for *mis4-367* with or without 1-NA-PP1 (Figure 19B). Cells were collected when S phase was completed as judged by DNA content analysis and before mitosis, as verified by the absence of a mitotic spindle and the presence of an interphase array of microtubules. In wild-type, most cells displayed closely apposed cen2FISH signals with only 10% of the cell population showing FISH signals separated by more than 0.4µm (Figure 19D). By contrast in *mis4-367* cells, this population was increased to 40%. Similarly, ~45% of cells showed separated FISH signals in *mis4-367 pef1-F78A* without kinase inhibition (DMSO). Importantly, this population was reduced to 26% when 1-NA-PP1 was added. The suppression is not complete since the frequency of separated signals was not back to wild-type level but the effect is statistically significant.

To see whether sister-chromatid cohesion was functionally restored we looked at mitotic phenotypes. When cells enter mitosis with precociously separated sister-chromatids,

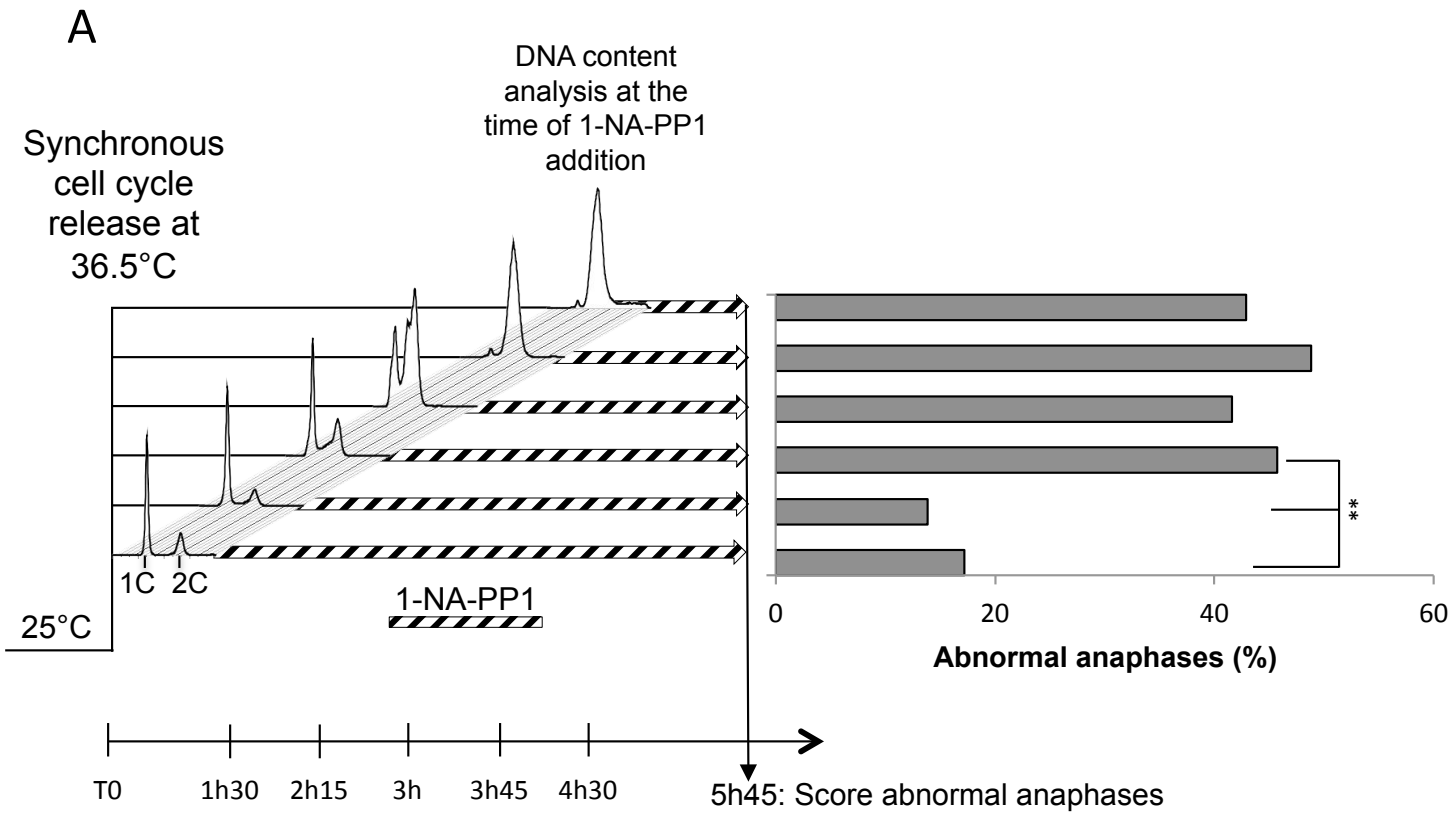


**Figure 20. Pef1 kinase inhibition must occur before S phase to suppress *mis4-367* chromosome segregation defects**. Cells (*mis4-367 pef1-F78A*) were arrested in G1 by nitrogen starvation and released into rich medium at restrictive temperature for *mis4-367*. 1-NA-PP1 was added at various time points (T0, 1h30, 2h15, 3h, 3h45 and 4h30). DNA content analysis was monitored by flow cytometry to determine the cell cycle stages at which 1-NA-PP1 was added. At time 5h45, cytological analysis of cells undergoing their first mitosis was performed. The frequency of abnormal anaphases was determined from the examination of 50–100 anaphases per sample. Abnormal anaphases were defined as cells with a spindle length >3µm displaying DAPI-stained material that had not reached the spindle poles (** $p<0.01$, $\chi^2$ test).

kinetochore capture by microtubules fail to generate tension within kinetochores resulting in the activation of the spindle assembly checkpoint and a delay in anaphase onset. Spindle forces are not counteracted by sister-chromatid cohesion resulting in metaphase cells with a longer spindle. Finally when anaphase is triggered sister-chromatids lag on the spindle as a result of single kinetochores being captured by microtubules emanating from opposite spindle poles (merotely).

To examine these phenotypes, cycling *mis4-367 pef1-F78A* cells were shifted to the restrictive temperature for one cell cycle (one doubling of the cell number) to ensure that all cells accomplished S phase at the restrictive temperature. Cells were fixed and stained for tubulin to visualize the mitotic spindle. During *S. pombe* mitosis, the length of the spindle defines 3 phases (Nabeshima and al., 1998). Spindle formation (phase 1) with a spindle from 0 to 2 µm long. During phase 2 spindle length is constant (2.5 µm). Phase 2 includes metaphase and anaphase A. During phase 3 (anaphase B) the spindle elongates.

As shown in figure 19 E-G, the frequency of mitotic cells was increased in *mis4-367* cells as well as the length of the spindle and both defects were efficiently corrected by *pef1*Δ or *pef1-F78A* inhibition. Finally, ~56% of *mis4-367* anaphase cells displayed lagging chromatids, a defect largely corrected by inhibition of the Pef1-F78A kinase (Figure 19 H-I).

We conclude that inhibition of Pef1 kinase activity largely restores sister-chromatid cohesion and chromosome segregation in *mis4-367* cells.

## *III. Pef1 kinase inhibition must occur before S phase to rescue chromosome segregation in mis4-367 cells*

Experiments using conditional mutants have shown that the cohesin loading complex is required in G1/S phase for cohesion establishment (Ciosk and al. 2000; Furuya, Takahashi, and Yanagida 1998), suggesting that Pef1 kinase activity may be crucial at that stage of the cell cycle.

To address this question, *mis4-367 pef1-F78A* cells were synchronized in G1 by nitrogen starvation. The culture was divided into 6 samples and cells released in the cell cycle

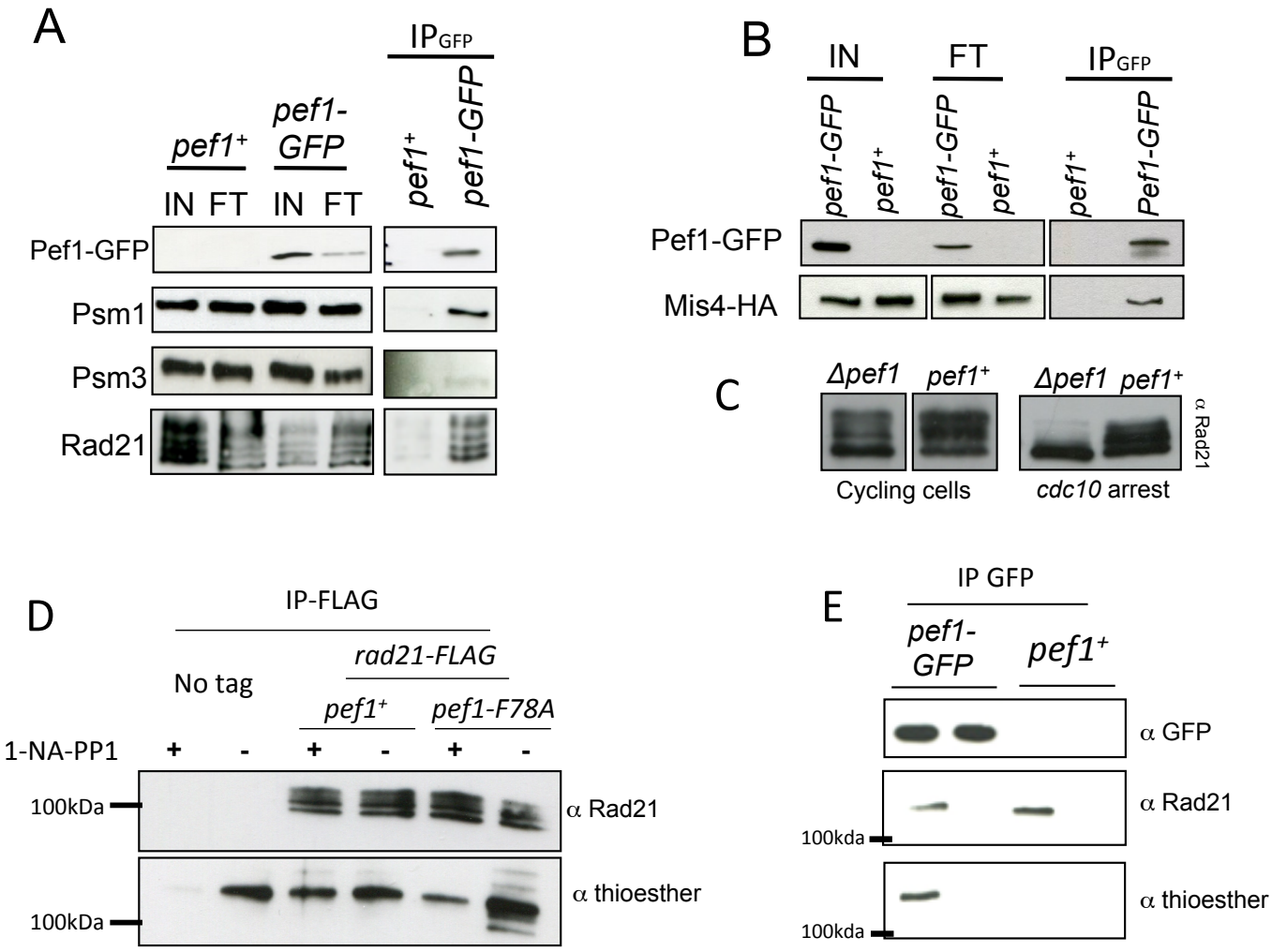


**Figure 21 : Pef1 co-immunoprecipitates cohesin and its loader and phosphorylates Rad21 *in vitro***. **A.** Exponentially growing cells expressing Pef1-GFP were lysed and lysates subjected to immunoprecipitation with anti-GFP antibodies. Co-immunoprecipitated proteins (IP) were analysed by Western blotting using anti-Rad21, anti-Psm1, anti Psm3 and anti-GFP antibodies. I, input; FT, Flow Through **B.** Exponentially growing cells expressing Pef1-GFP and Mis4-HA were lysed and lysates subjected to immunoprecipitation with anti-GFP antibodies. Co-immunoprecipitated proteins were analyzed by Western blotting using anti-HA. **C.** Exponentially growing cells, or G1 arrested cells (*cdc10-129*) from *pef1*$^+$ or *pef1Δ* strains were lysed and total protein extracts were probed with anti-Rad21 antibodies (Amélie Feytout) **D.** *In vitro* phosphorylation assay was made by mixing extracts from cycling cells containing Rad21-FLAG with anti-GFP immunoprecipitates from *pef1-GFP* or *pef1*$^+$ cycling cells. Anti-FLAG immunoprecipitates were analysed by Western blotting using anti-GFP, anti-Rad21 and anti-thioesther antibodies **E.** *In vitro* phosphorylation assay was made by mixing Rad21 produced *in vitro* with anti-GFP immunoprecipitates from *pef1-GFP* or *pef1*$^+$ cycling cells. Proteins were analysed by Western blotting using anti-GFP, anti-Rad21 and anti-thioesther antibodies.

at the restrictive temperature. At various time during cell cycle progression 1-NA-PP1 was added. At time 5h45, cells were collected, stained for tubulin to score anaphase cells with lagging chromatids. As expected, a high rate of anaphase cells with lagging chromatids was observed when no inhibitor was added (DMSO, Figure 20). Similarly, 1-NA-PP1 addition during S or G2 phase didn't suppressed chromosome segregation defects. However, Pef1 kinase inhibition before DNA replication reduced the frequency of abnormal anaphases. Therefore Pef1 kinase inhibition must occur during the pre-replicative stage when Mis4 exerts its essential function to suppress *mis4-367* chromosome segregation defects.

## *IV. Rad21 is a Pef1 target*

The putative phosphorylation site of CDK with the minimal consensus sequence [S/T]*PX[K/R] in which S/T is the phosphorylated residue is found in the majority of cohesion proteins. In an attempt to see whether Pef1 may phosphorylate cohesin subunits *in vivo*, a GFP-tagged version of Pef1 CDK was immunoprecipitated from cycling cells and probed with anti-cohesin antibodies. As shown in figure 21, all three core cohesin components (Rad21, Psm1 and Psm3) co-immunoprecipitated with Pef1. A similar experiment made with a *mis4-HA pef1-GFP* strain (Figure 21B) indicates that Pef1 also co-immunoprecipitated the cohesin loader subunit Mis4. These data suggest that Pef1 might directly contact cohesin ring and its loader and might phosphorylate one of those proteins to control cohesin ability to bind chromatin.

By comparing the electrophoretic mobility of the best-known cohesion proteins in *pef1*$^{+}$ versus *pef1*Δ strains, we didn't detect any modification except for the kleisin Rad21 whose migration was strongly altered. Rad21 protein was detected as several phospho-isoforms as previously described (Birkenbihl and Subramani 1995). As shown in figure 21C, in *pef1* deleted cycling cells, the hypo-phosphorylated form was more prominent and in G1-arrested cells, Rad21 was almost exclusively detected in a hypo-phosphorylated state, indicating that Pef1 kinase activity regulates the phosphorylation status of the Rad21 cohesin subunit.

To test whether Rad21 is directly phosphorylated by Pef1 CDK, we performed an *in vitro* kinase assay. The Rad21-FLAG protein immunoprecipitated from a wild type strain was

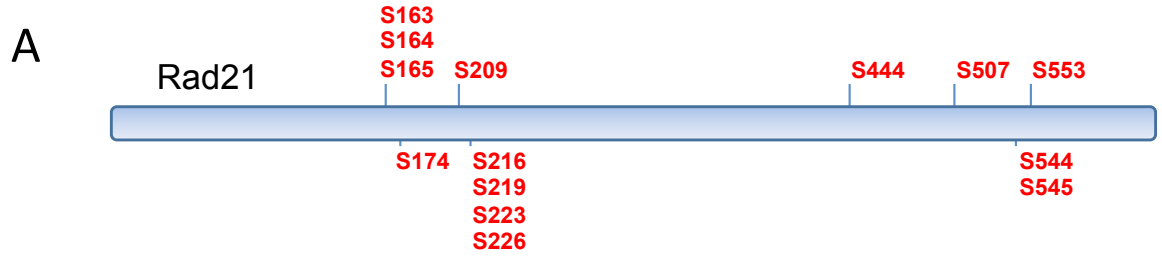


3789 (*pph3*$^{+}$) Total aa: 628 **Covered: 569** Coverage 90.6% P Phospho (S,T) probability 95-100%

MFYSEAILSK KGPLAKVWLA AHWEKKLSKV QTLHTSIEQS VHAIVTEETA PMALRLSGQL MLGVVRIYSR KARYLLEDCT
EALMRLKMSE QPGQVDMIEP ATALQSLKGK DAVTQSANLT LPETITEFDL LVPDSTFDFQ WSQLLRTPSR SSNTLELHSL
PISSSPSFPS SQLSIEAGRN AQVESGFSLG ESFAHVGNDM QFHLPISNSG AATPRSVHSD NQSQISIEVG RDAPAAAATD
LSGIIGPQMT KSPASSVTHF STPSMLPIGG TSLDDELLAP VDDLNLDLGL DDLLGDEQGA NAPAIEADEQ AETSSIHLPS
DIMEDDSSRP AAAGVEEGQV VESATAPQQE KINPQKTVRR QRAIIDPVTE LSSKQMKKQL ADTSSITSPL CLNTSSIVFN
ATVNFTRNGK FNTSIFSSNL NPKVNELLQA DFKQAILRKR KNESPEEVEP AKHQRTDTST ENQETAEVLD PEEIAAAELA
NITEAAIATL PQETVVQPEG EAPELGSPMG FPVTALESAD DSLFDAPPVM LDEADLLGSE RLDSSVSEAL PSSQTAKDSL
RNKWDPYTEG EKVSFQTLSA GCNREEAVQL FFDVLVLATK DVISVKQDVA IQNEITLTAK RGMLLSSL

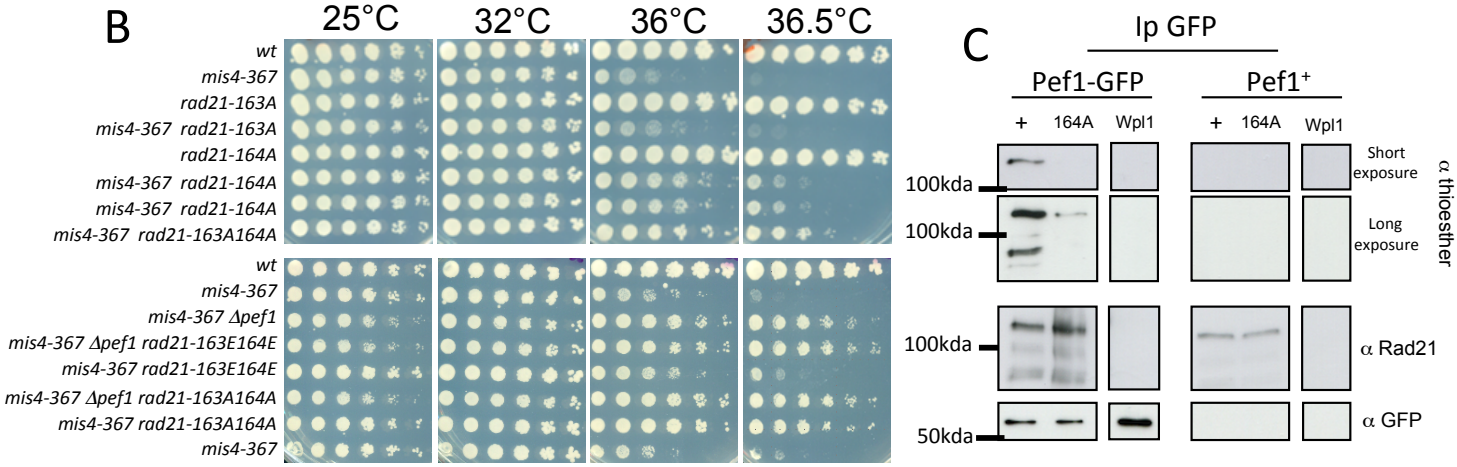


**Figure 22 : Pef1 may phosphorylate Rad21 S164**. **A.** Phosphorylated residues identified in Rad21-PK purified from wild-type cells. The frame shows the position of serine 163 and 164. **B.** Serial dilutions of cells were spotted on YES medium and incubated at the indicated temperatures. **C.** *In vitro* phosphorylation assay was made by mixing Rad21 produced *in vitro* with anti-GFP immunoprecipitates from *pef1-GFP* or *pef1*$^{+}$ cycling cells. Proteins were analysed by Western blotting using anti-GFP, anti-Rad21 and anti-thioesther antibodies. (+) = wt Rad21 (164A) = Rad21-S164A.

incubated with protein extracts made from either a *pef1-F78A* strain or a wild type strain, in the presence of N6-ATP-y-S with or without 1-NA-PP1 for 1 hour. N6-ATP-y-S was used as a phosphate donor to generate thiophosphorylated substrates. N6-ATP-y-S has been described as specific for analogue sensitive kinases, presumably because of its large size (Allen and al. 2007). At the end of the phosphorylation assay, p-nitrobenzyl mesylate (PNBM) was added to react with the thiophosphorylated residues to form a thiophosphate-ester that is detected with a specific antibody (Material and methods). Unfortunately, an aspecific thiophosphorylated signal was detected in all samples, independently of Pef1-F78A and its inhibition suggesting that the ATP analogue was used by other kinases in this assay (Figure 21D). However, a specific thiophosphorylated signal was detected at a molecular weight that may correspond to Rad21-FLAG. This signal was only detected in Pef1-F78A and abrogated if the reaction was performed with 1-NA-PP1, suggesting it may indeed correspond to Pef1-directed protein phosphorylation.

To test whether Rad21 was directly phosphorylated by Pef1 CDK we performed another *in vitro* kinase assay in which Rad21 was produced *in vitro* by using *E.coli* extracts. Pef1-GFP was immunoprecipitated from *S. pombe* extracts and incubated with the *in vitro*-produced Rad21 and ATP-y-S for 1 hour. Rad21 was found thio-phosphorylated after incubation with Pef1-GFP immunoprecipitates indicating that Pef1 directly phosphorylates Rad21 *in vitro* (figure 21E).

In an attempt to identify Rad21 residue(s) that is (are) phosphorylated *in vitro*, Rad21 was analysed by tandem mass spectrometry (MS/MS). The poor sequence coverage did not allow for the detection of phosphorylated residues (not shown). To overcome this problem, we switched to a candidate approach. In a distinct study (cf page 129) we mapped 15 phosphorylation sites by MS/MS analysis of Rad21 purified from wild-type cycling cells. Interestingly, we identified a specific zone within Rad21 containing a CDK consensus site and phosphorylated Serine residues at position 163 and 164 (Figure 22A). We decided to investigate whether the phosphorylation status of these sites might be relevant to Pef1 function. We reasoned that if these serine residues are Pef1 targets that must be un-phosphorylated to allow *mis4-367* suppression, then substitution of these serine residues by an alanine that mimics the non-phosphorylated state should be sufficient to suppress *mis4-367* thermosensitivity. Indeed, as shown in figure 22B, *rad21-164A* reduced the thermosensitive growth defect of *mis4-367*. An additional level of suppression was observed when S163 was also substituted to alanine (*rad21-163A164A*). Interestingly, *rad21-163A164A* gave a

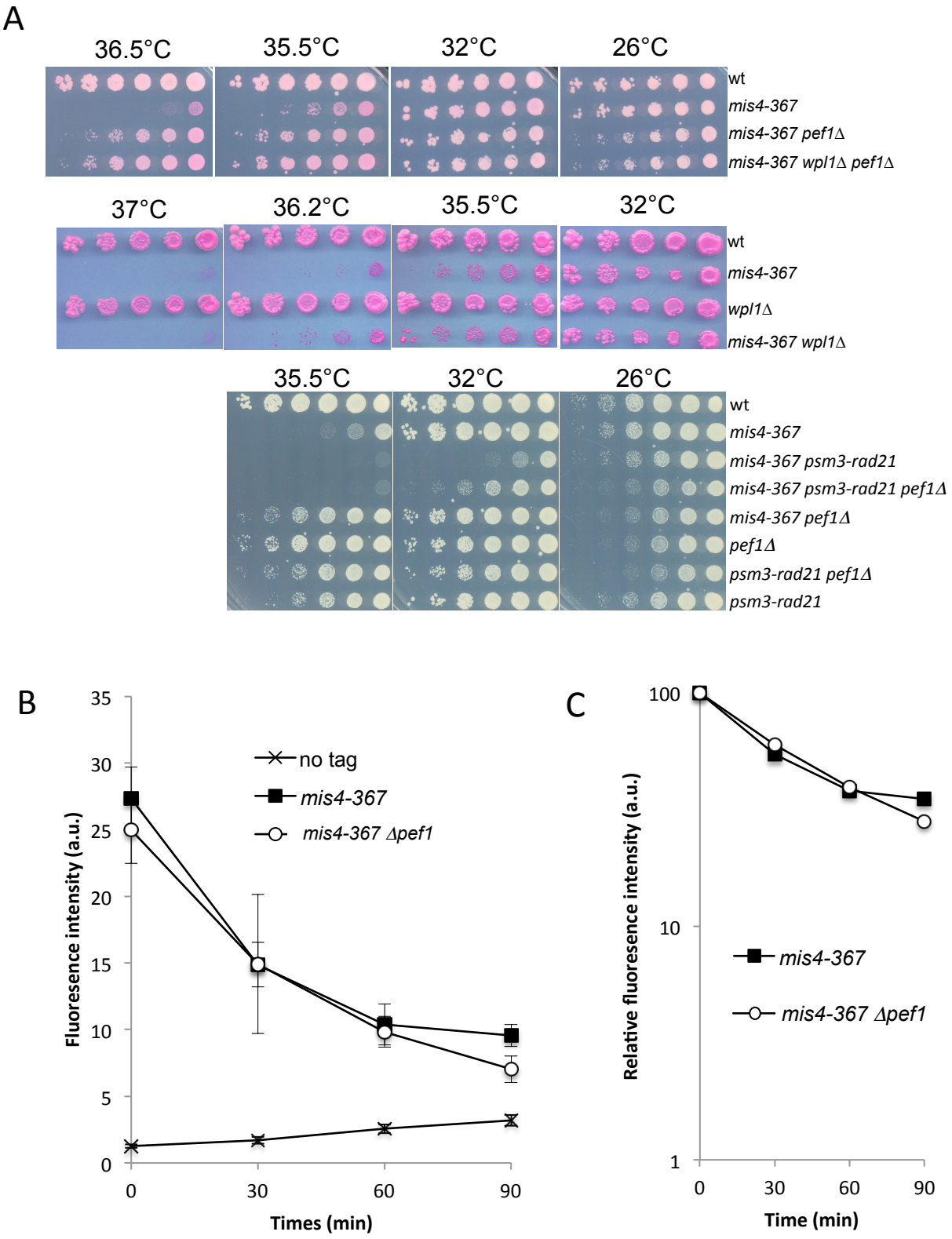


**Figure 23 : Pef1 deletion does not affect cohesin release from DNA . A.** Serial dilutions of cells were spotted on YES medium and incubated at the indicated temperatures. **B.** Kinetics of Rad21 removal from G1 chromatin. Cells bearing the *mis4-367* mutation were arrested in G1 at 25°C by overexpression of C-ter-Res1 and then shifted to 36.5°C. Rad21-PK fluorescence per nucleus was measured from nuclear spreads at the indicated time-points (50-100 nuclei per sample). Error bar = 95% confidence interval of the mean with $\alpha$=0.05. **C.** Normalisation of kinetics obtain in (B). Data were normalized to value at time 0 fixed to 100.

suppression level similar to *pef1Δ* and no additive effect was observed for the double mutant, consistent with Pef1 acting through these two Rad21 residues. Reciprocally, the substitution of these residues with glutamic acid that is thought to mimic the phosphorylated state should abrogate *mis4-367* suppression by *pef1* deletion. However, *rad21-163E164E* was essentially neutral when combined with *mis4-367* and did not abolish the suppressor effect of *pef1Δ* (Figure 22B). This suggested that Pef1 might phosphorylate other residues within Rad21 (see discussion).

The above genetic analysis suggested that Rad21 S164 might be a Pef1 target. If this was true, Rad21-164A should not be phosphorylated in our *in vitro* Pef1 kinase assay. As shown in Figure 22C, Rad21 thiophosphorylation by Pef1 kinase was largely abrogated with the Rad21-164A mutant protein, suggesting that Ser164 is a Pef1 phosphorylation site. However, a slight thiophosphorylation signal was detected after longer exposure times suggesting that S164 may not be the sole potential Pef1 phosphorylation site (see discussion).

## *V. Pef1 deletion does not affect cohesin release from DNA in G1*

Our data so far indicate that Pef1 kinase inhibition suppresses *mis4-367* sister-chromatid cohesion and chromosome segregation defects. In a previous study, it was shown that when the cohesin loading machinery is inactivated in G1-arrested cells, cohesin that was bound to chromosomes dissociated to completion in a reaction stimulated by Wpl1 (Bernard and al., 2008). Pef1 kinase inhibition may stimulate the residual loading activity of Mis4-367 or may restrain the unloading reaction. The Wpl1 protein stimulates cohesin unloading from chromosome and is supposed to act by disrupting the Smc3-Rad21 interface. If Pef1 ablation rescues *mis4-367* cohesion defects by reducing Wpl1-dependent cohesin unloading then the deletion of the *wpl1* gene should behave similarly. However, as shown in figure 23A, *wpl1* deletion does not suppress the thermosensitive phenotype of *mis4-367* and does not increase suppression by *pef1*Δ. In the same vein, the covalent linkage between Smc3 and Rad21 (a Smc3-Rad21 fusion protein) was shown to abolish Wpl1-dependent cohesin release from DNA (Chan and al. 2012). The cell growth assay (Figure 23A) shows that the fusion protein

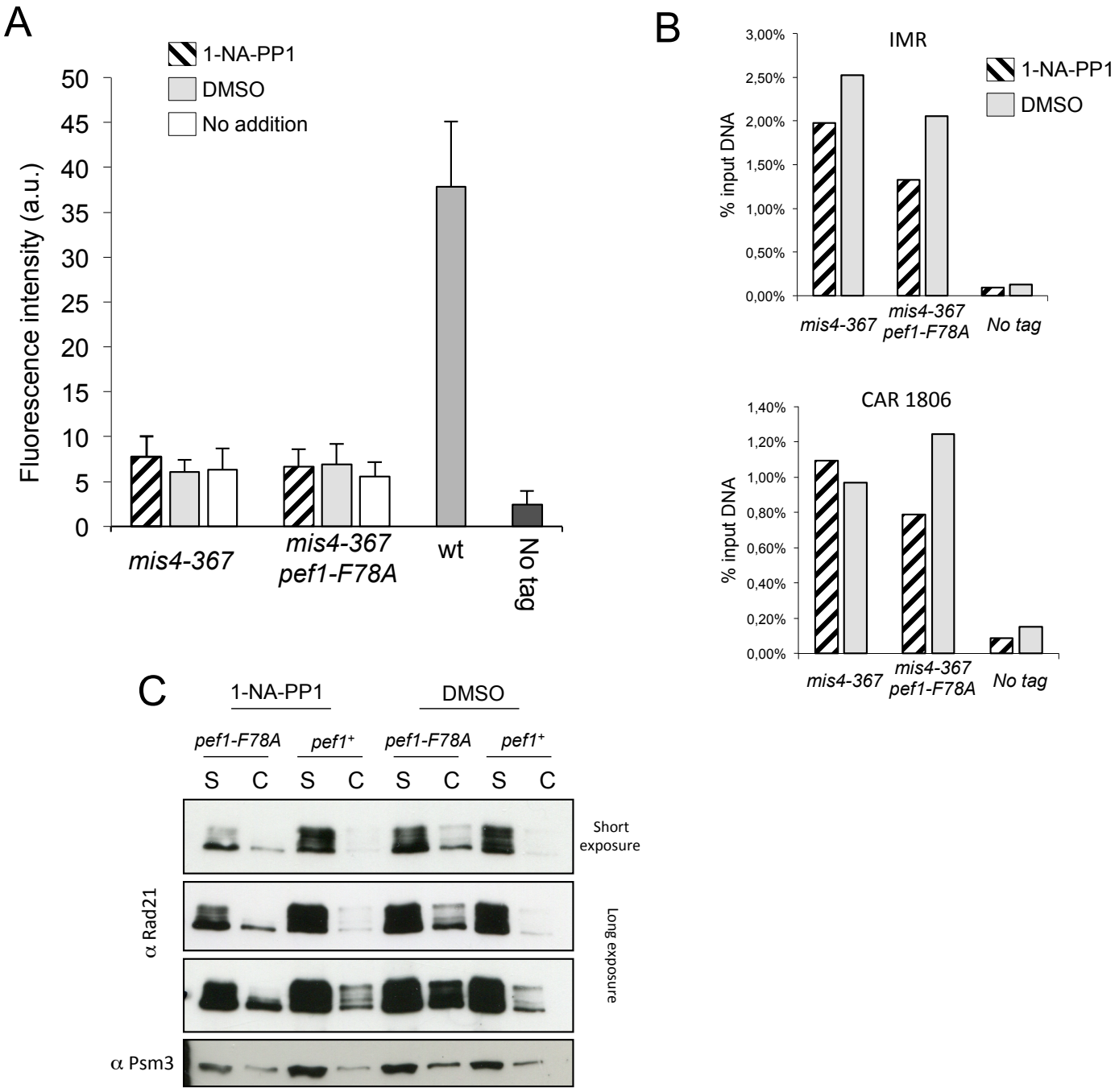


**Figure 24. Pef1 kinase inhibition does not increase the amount of chromatin-bound Rad21 in *mis4-367* G1 arrested cells but affects its phosphorylation status**. *mis4-367 cdc10-129 pef1-F78A rad21-FLAG* cells were grown at 25°C and shifted to 36.5°C for 5 hours at which time 1-NA-PP1, DMSO or nothing were added. At time 5h30, cells were collected to analyse Rad21-FLAG binding to chromatin by three different assays. **A.** Quantification of Rad21-FLAG bound to chromosomes by nuclear spreads. Fluorescence intensity was measured for 50-100 nuclei per sample. Error bar=95% confidence interval of the mean with α=0.05. **B.** ChiP assay showing the amount of Rad21-FLAG bound at the indicated loci. **C.** Cellular fractionation. Soluble (S) and chromatin (C) fractions were probed with anti-Rad21 and anti-Psm3 antibodies.

does not rescue *mis4-367* although *pef1*Δ still shows a suppressing effect in this background. These genetic data suggest that Pef1 does not act through Wpl1-mediated cohesin release.

Next we looked at the kinetics of Rad21 dissociation from G1 chromatin in *mis4-367* and *mis4-367 pef1*Δ cells. Cells were arrested in late G1 by titrating out the Cdc10 transcription factor by overexpression of a C-terminal fragment of its binding partner Res1 (Bernard and al. 2008). Once arrested in G1 at permissive temperature, cells were shifted to 36.5°C while remaining arrested in G1. Cohesin association to chromatin was assessed by chromosome spreads before and after the shift every thirty minutes. As shown in figure 23B-C, the kinetics of Rad21 removal from DNA was very similar, suggesting that Pef1 ablation does not affect the equilibrium between loading and unloading reactions.

## *VI. Pef1 kinase inhibition modifies the phosphorylation status but not the steady-state amount of chromatin-bound Rad21 in G1 cells*

The above experiment indicates that Pef1 kinase inhibition does not modify the kinetics of cohesin removal from DNA. We next asked whether CDK inhibition would stimulate cohesin binding to chromatin. To address this question, the amount of chromatin-bound Rad21 was measured on nuclear spreads in *cdc10-129* arrested cells in which Pef1 kinase was inactivated or not. As expected, cohesin loader inactivation resulted in a strong decrease of chromatin bound Rad21 when compared to wild-type cells. However, the amount was unchanged whether Pef1 kinase activity was inhibited or not (Figure 24A). The same conclusion was reached when Rad21 binding was monitored at centromeres and at a Cohesin Associated Region using a chromatin immunoprecipitation assay (Figure 24B). We conclude that Pef1 inhibition does not increase the amount of DNA-bound Rad21 in *mis4-367* G1-arrested cells.

The above data prompted us to ask whether Pef1 kinase inhibition may modify the phosphorylation pattern of residual chromatin-bound Rad21. The chromatin fraction was prepared from *cdc10-129* arrested cells in which the Pef1 kinase was inhibited or not, and

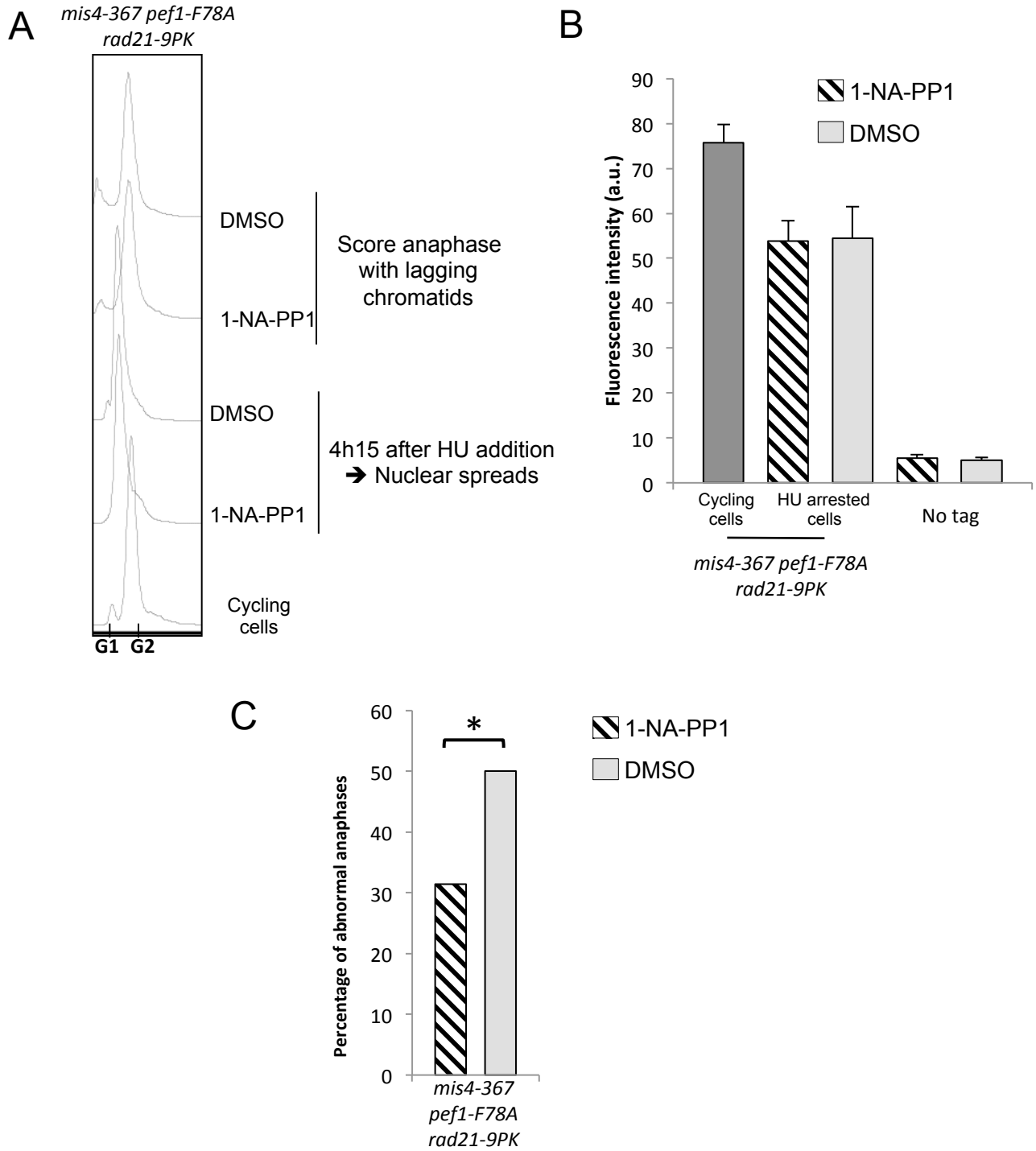


**Figure 25 : Pef1 kinase inhibition does not increase the steady state amount of chromatin-bound Rad21 in HU-arrested cells**. Exponentially growing cells (*mis4-367 pef1-F78A rad21-9PK*) at 25°C were shifted to 35.5°C and HU, DMSO or 1-NA-PP1 were added. **A.** DNA content analysis was monitored by flow cytometry. After 4h15 cells were arrested in early S phase as seen by a 1C DNA content. Cells were synchronously release at 36.5°C and 1h45 after abnormal anaphases were scored **B.** Quantification of Rad21-9PK bound to chromosomes in HU arrested cells. Fluorescence intensity was measured for 50–100 nuclei per sample. Error bar=95% confidence interval of the mean with $\alpha$=0.05. **C.** The frequency of abnormal anaphases was determined from the examination of 50–100 anaphases per sample. Abnormal anaphases were defined as cells with a spindle length >3µm displaying DAPI-stained material that had not reached the spindle poles (* $p<0.05$, $\chi^2$ test).

Rad21 analysed by Western blotting. As shown in Figure 24C, we observed a residual Rad21 binding to chromatin in *mis4-367* in agreement with nuclear spreads experiments.

Interestingly, chromatin-bound Rad21 appeared as several isoforms in *pef1-F78A* in the presence of DMSO while only the faster migrating species was detected in the presence of 1-NA-PP1.

From the above experiment it appears that the inhibition of Pef1 kinase activity does not increase the amount of chromatin-bound cohesin in *mis4-367* G1-arrested cells. However, the residual amount of chromatin-bound Rad21 appears dephosphorylated when the CDK is inactivated.

## *VII. Pef1 kinase inhibition does not modify the amount of chromatin-bound Rad21 in hydroxyurea arrested mis4-367 cells*

We found that Pef1 kinase inactivation during the pre-replicative stage was sufficient to suppress *mis4-367* chromosome segregation defects without increasing Rad21 binding to chromatin. Next we asked whether inactivation of the CDK might increase the amount of chromatin-bound Rad21 in early S phase. To test this, *mis4-367 pef1-F78A* cycling cells were shifted to the restrictive temperature. At the same time, 1-NA-PP1 was added or not, and cells were arrested in early S phase by hydroxyurea (HU). DNA content analysis showed that cells had a 1C DNA content 4h15 after the temperature shift, as expected for HU-arrested cells (Figure 25A). At that time, Rad21 binding to chromatin was assessed by nuclear spreads. Cells were then released from the HU arrest and collected to score anaphase cells with lagging chromosomes (Figure 25C). As shown in figure 25B, Pef1 kinase inhibition did not modify the amount of Rad21 bound to spread nuclei. Cycling cells (*i.e.* cells grown at 25°C) were included in the experiment. It can be noticed that the amount of Rad21 per nuclei is not dramatically reduced in HU-treated samples although these *mis4-367* cells had experienced G2-M-G1 and early S phase at the restrictive temperature. A wild-type control is missing to further analyse this “side observation”. The poor effect of cohesin loader inactivation may be explained by HU treatment in which cohesin is stabilized on chromatin independently of

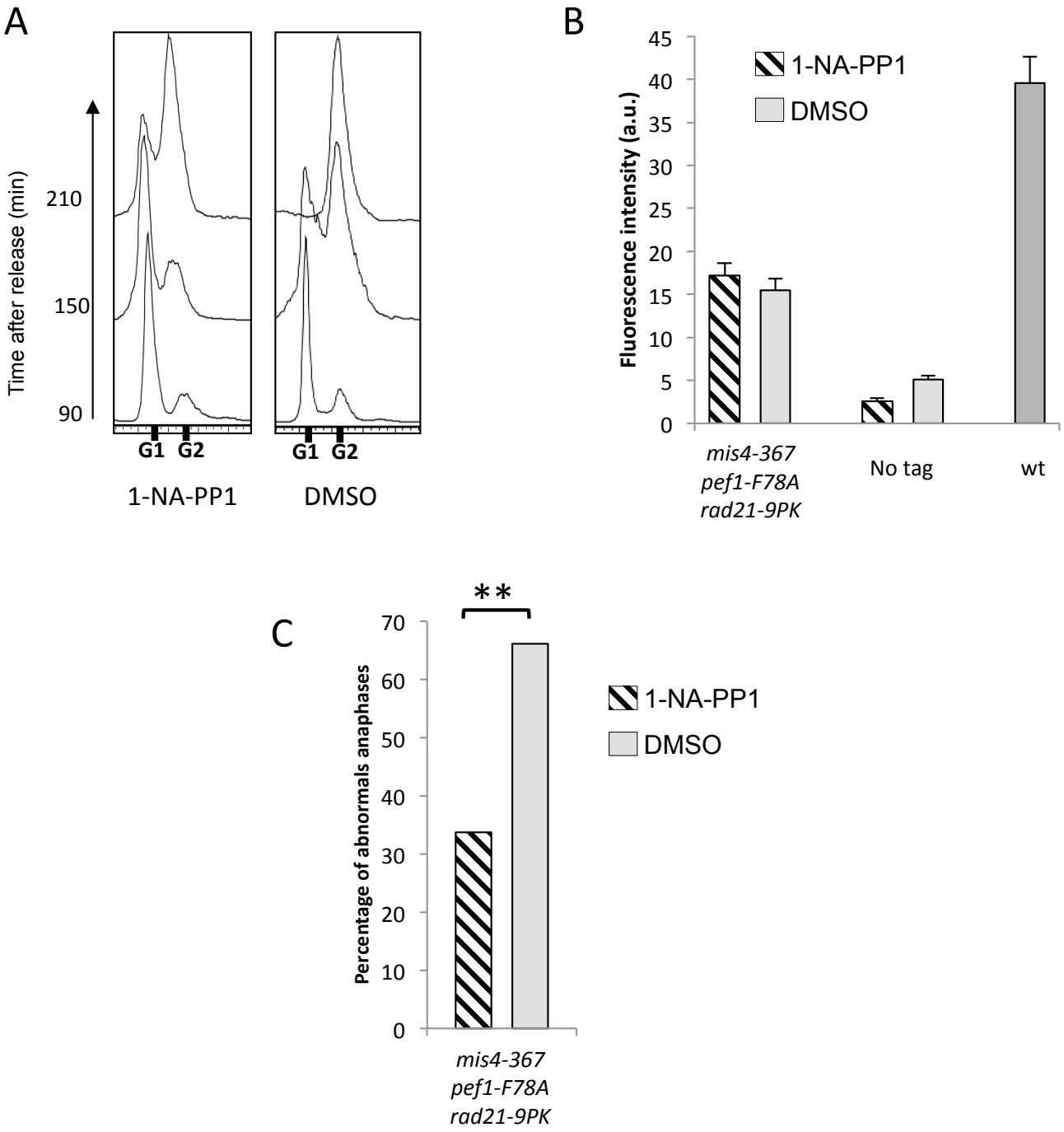


**Figure 26 : Pef1 kinase inhibition does not modify the steady state amount of chromatin-bound Rad21 in *mis4-367* cells.** Nitrogen starved cells from *mis4-367 pef1-F78A rad21-9PK* were released at 35.5°C with DMSO or 1-Na-PP1. **A.** DNA content analysis was monitored by flow cytometry. **B.** Quantification of DNA-bound Rad21 per nucleus. Rad21-9PK bound to chromosomes was detected by nuclear spreads at time 210 min after release. Fluorescence intensity was measured for 50–100 nuclei per sample. Error bar=95% confidence interval of the mean with α=0.05. **C.** The frequency of abnormal anaphases was determined from the examination of 50–100 anaphases per sample. Abnormal anaphases were defined as cells with a spindle length >3µm displaying DAPI-stained material that had not reached the spindle poles (** $p<0.01$, $\chi^2$ test).

DNA replication (Bernard and al. 2008). From this set of experiments, we conclude that the inhibition of the Pef1 kinase does not increase the amount of chromatin-bound Rad21.

## *VIII. Pef1 kinase inhibition does not modify the steady state amount of chromatin-bound Rad21 in post-replicative mis4-367 cells*

We previously failed to observe a cohesin binding stimulation in G1 or S phase arrested cells. We asked now if Pef1 kinase inhibition could induce an increase of cohesin binding to DNA in a post replicative stage, *i.e.* after sister chromatid cohesion establishment. We synchronized *mis4-367 pef1-F78A rad21-9PK* cells in G1 by nitrogen starvation and released the cells into the cell cycle at the restrictive temperature with or without 1-NA-PP-1. The amount of chromatin-bound Rad21-9PK per nucleus was measured by nuclear spreads. Because spheroplasts were difficult to obtain after release of nitrogen-starved cells, we analysed Rad21-9PK binding to chromatin at time 3h30 after release. Suppression of the *mis4-367* phenotype was checked by measuring the frequency of anaphases with lagging chromatids during the following mitosis. As expected, the amount of DNA-bound Rad21 was reduced in *mis4-367* as compared to wild-type (Figure 26B). Still, we observed residual Rad21 binding to chromatin by this assay, and importantly we didn't observe any change upon Pef1-F78A kinase inhibition although the frequency of anaphases with lagging chromatids was lowered (Figure 26C). This experiment supports the idea that Pef1-F78A kinase inhibition apparently does not increase cohesin binding to chromatin in the *mis4* mutant. There are however some concerns with this conclusion. A single time point was analysed and FACs analysis revealed that 1-NA-PP1 treated cells showed a delay in cell cycle progression. Therefore the two samples were not matched.

To see whether the cell cycle delay was induced by Pef1 kinase inhibition, we compared the cell cycle progression of wild type, *mis4-367*, *pef1-F78A* and *mis4-367 pef1-F78A* cells in a similar block and release experiment (Figure 27). Interestingly, we observed a delay in S phase entry when Pef1-F78A kinase was inhibited while the duration of S phase appeared unaffected.

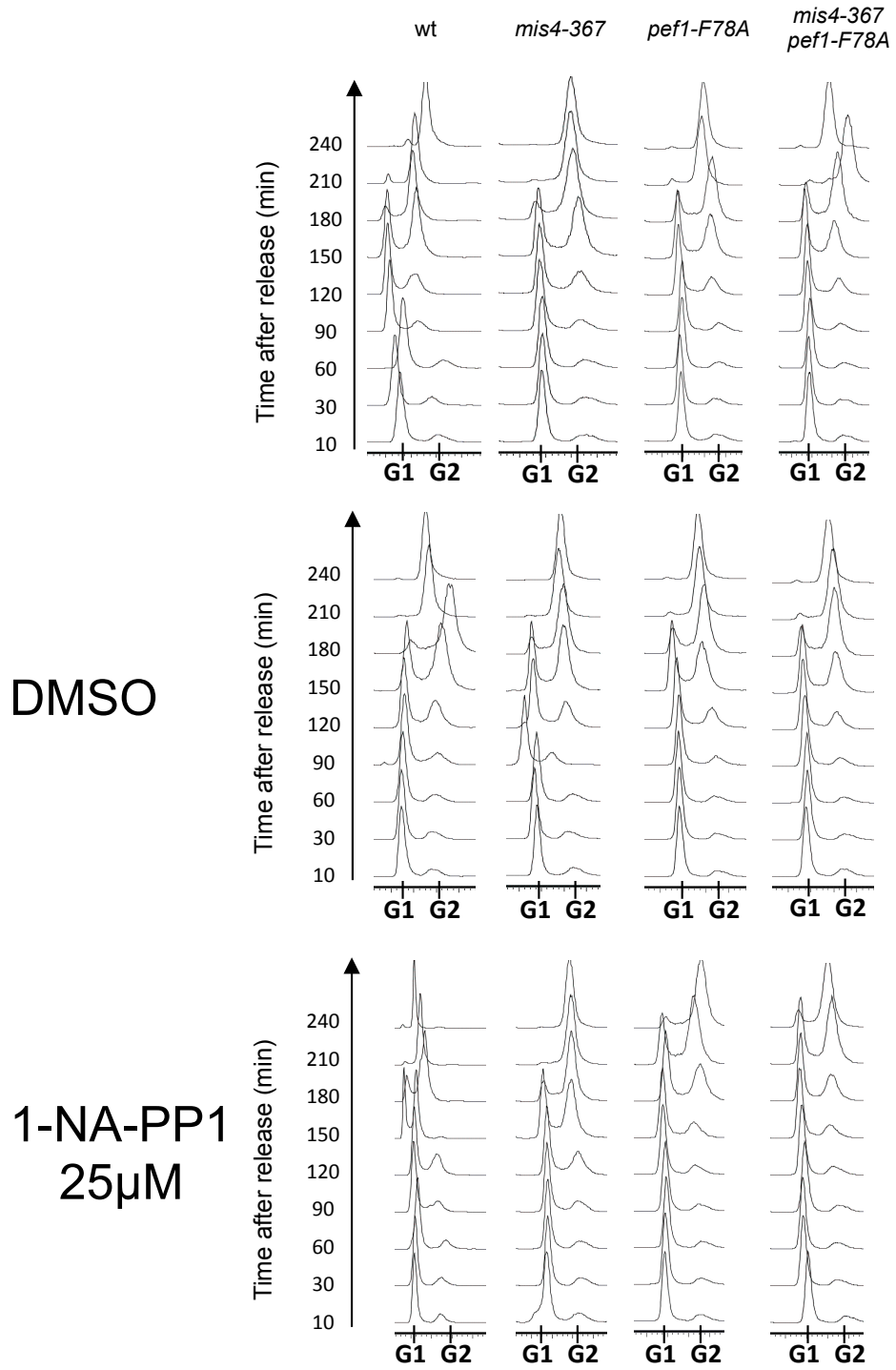


**Figure 27. Pef1 kinase inhibition delays S phase entry**. Nitrogen starved cells were released into the cell cycle at 36.5°C in the presence of DMSO or 1-NA-PP1. The top panel is a control without addition of DMSO or 1-NA-PP1. Every 30min DNA content was monitored by flow cytometry.

# *IX. Pef1 kinase inhibition in mis4-367 G1 cells stimulated chromatin binding of ectopically expressed Rad21*

The previous data failed to reveal a cohesin binding stimulation in *mis4-367* cells when Pef1-F78A kinase was inhibited. However, we observed a change in the phosphorylation status of chromatin bound Rad21 in G1-arrested cells. In fission yeast, only a fraction of cohesin is cleaved by Separase at anaphase, the other fraction remaining apparently bound to chromosomes (Tomonaga and al. 2000; Schmidt, Brookes, and Uhlmann 2009). In our experiments, we do not know whether chromatin-bound Rad21 observed in G1 cells originated from the previous cell cycle or was loaded *de novo* in G1 or both. The sole examination of chromatin bound Rad21 does not tell us when it was actually loaded.

To circumvent this problem, we developed an *in vivo* cohesin loading assay that uses the inducible expression of an ectopic copy of FLAG-tagged *rad21*. The construct was integrated within a gene free region on chromosome 3 (Fennessy and al. 2014). The *rad21* ORF is driven by a tetracycline regulable promoter and expression is induced by tetracycline addition in the culture medium (Zilio, Wehrkamp-Richter, and Boddy 2013). The growth assays in Figure 28 show that ectopically expressed Rad21-FLAG is able to compensate for the deletion of the endogenous *rad21* gene. Importantly, *pef1Δ* still behaves as a *mis4-367* suppressor in this genetic set-up. We therefore assumed that ectopically expressed Rad21-FLAG is functional.

Next, we asked whether Pef1-F78A kinase inhibition would stimulate ectopic Rad21 binding to chromatin in *mis4-367* G1-arrested cells. Cycling cells were shifted to the restrictive temperature for *cdc10-129* and *mis4-367*. Cell cycle arrest was confirmed by FACS analysis of cellular DNA content. At time 4h30, when cells were arrested in G1, ectopic-Rad21-FLAG was induced by tetracycline addition. Thirty minutes later, 1-NA-PP1 was added to inhibit Pef1-F78A during 30min. First, we monitored ectopic-Rad21-FLAG binding to chromatin by nuclear spreads. As shown in figure 29C-D the amount of chromatin-bound ectopic-Rad21-FLAG was strongly increased when Pef1 kinase was inhibited. A slight increase was also observed in the *pef1*$^{+}$ strain, suggesting an off-target effect of 1-NA-PP1. The increase was however within the error bars of the quantification. Next, we separated cell extracts into soluble and chromatin-bound fractions. As shown in figure 29E, ectopic-Rad21-

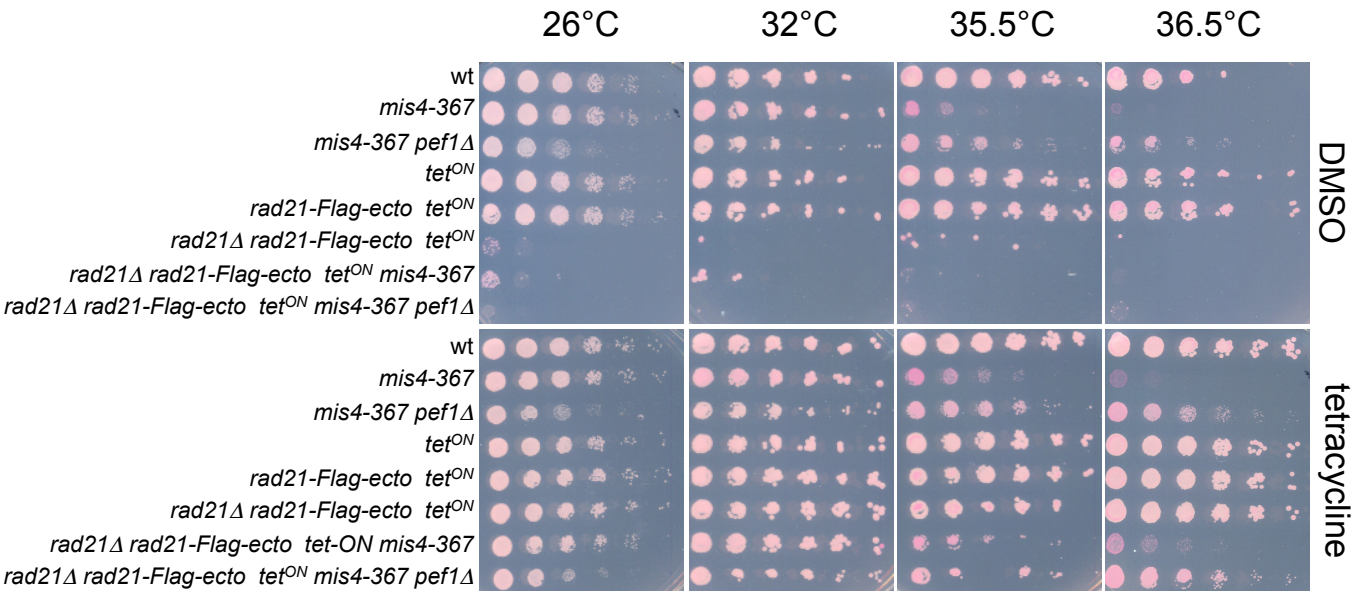


**Figure 28 : Ectopically expressed Rad21-FLAG is functional.** Serial dilutions of cells were spotted on YES medium supplemented with tetracycline or DMSO and incubated at the indicated temperatures.

FLAG was enriched in the chromatin-bound fraction when Pef1-F78A kinase was inhibited and chromatin-bound Rad21-FLAG appeared mostly hypo-phosphorylated.

To further characterize the pattern of ectopically expressed Rad21 binding along chromosomes, we used a chromatin immunoprecipitation assay (Figure 29F). Ectopic-Rad21 binding was assayed within peri-centromeric domains and at two cohesin-associated regions (CARs) on chromosome 2. These CARs were chosen because they were among those with the largest amounts of Rad21 based on published genome wide data (Schmidt, Brookes, and Uhlmann 2009). In a *pef1*$^{+}$ background, the enrichment was similar whether 1-NA-PP1 was added or not and whatever the site examined, suggesting no or little off target effect of the drug. In a *pef1-F87A* background, the results are somewhat difficult to interpret. Addition of 1-NA-PP1 resulted in an increase of DNA-bound Rad21 at all three sites when compared to the matched DMSO control. However, the percentage of immunoprecipitated DNA was lower in *pef1-F87A* DMSO than in the *pef1*$^{+}$ DMSO control, indicating that *pef1-F87A* does not behave as a *pef1*$^{+}$ allele in the absence of 1-NA-PP1. The reason for this is unknown. The alternative was to compare *pef1-F87A* 1-NA-PP1 with *pef1*$^{+}$ 1-NA-PP1. By using these criteria, inhibition of Pef1 kinase activity seemed to enhance Rad21-FLAG binding at peri-centromeres and CAR82 but would be without effect at CAR2898. This may additionally suggest that Pef1 kinase inhibition would stimulate Rad21 binding to a subset of CARs within the genome.

## *X. Pef1 kinase inhibition stimulates ectopically expressed Rad21 binding to chromatin in G1 mis4*$^{+}$ *cells*

The above experiments indicate that Pef1 acts as a negative regulator of cohesin binding to chromatin in a *mis4-367* background. This suggests that Pef1 may act similarly in wild-type *mis4*$^{+}$ cells.

To address this question we asked whether Pef1 kinase inhibition in *mis4*$^{+}$ cells would increase cohesin binding to chromatin. As before, ectopic Rad21-FLAG was induced in *cdc10-129* arrested cells, Pef1-F78A kinase activity was inhibited or not and the amount of chromatin-bound Rad21-FLAG was analysed by nuclear spreads and ChiP at known cohesin

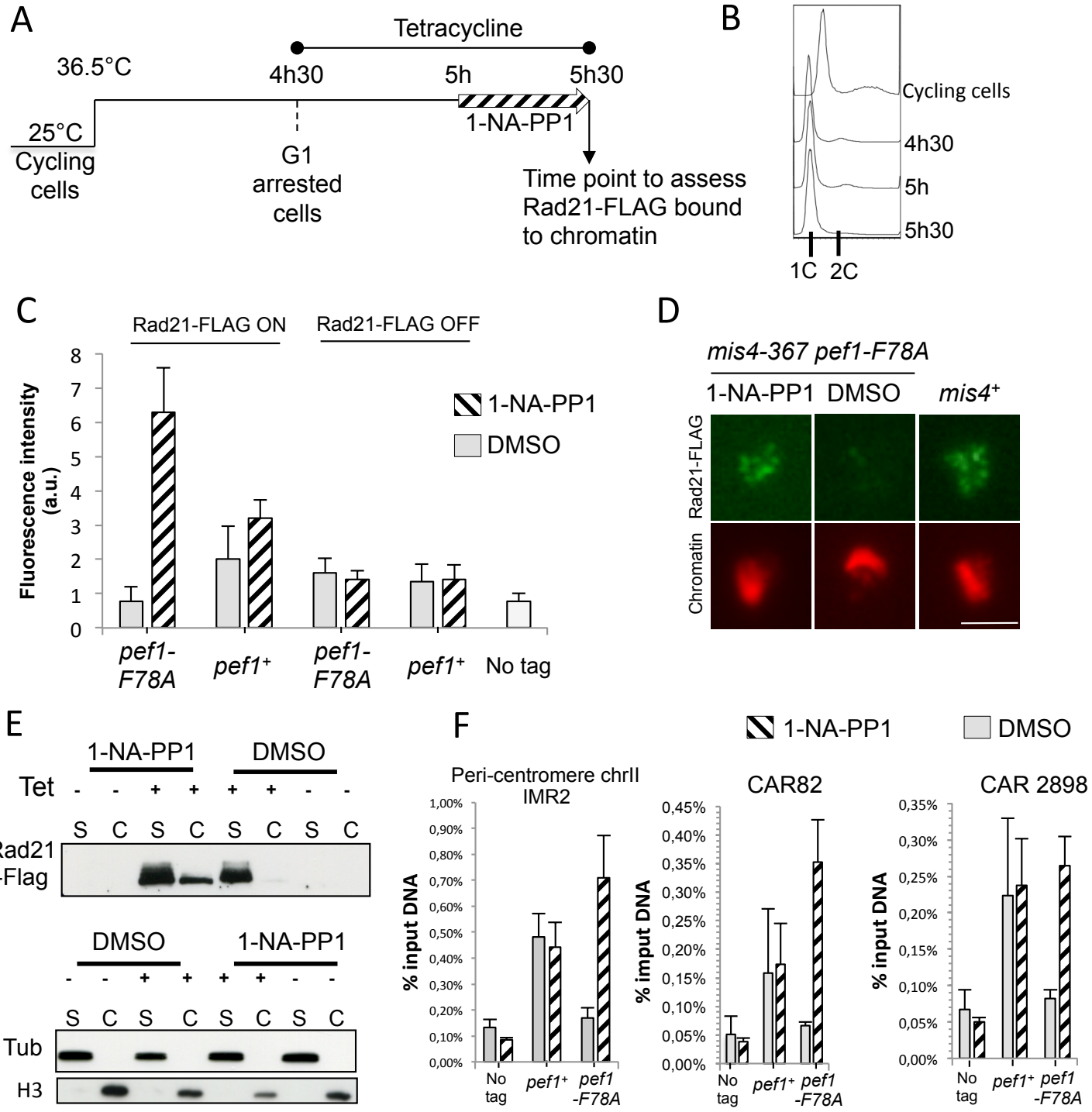


**Figure 29. Pef1 kinase inhibition induces ectopic Rad21–FLAG binding to chromatin in G1-arrested *mis4-367* cells**. **A.** Exponentially growing cells (*mis4-367 cdc10-129 pef1-F78A ectopic-rad21-FLAG*) at 25°C were shifted to 36.5°C. 4h30 after temperature shift when cells were arrested in G1, tetracycline was added to allow Rad21-FLAG production. Thirty minutes later, 1-NA-PP1 was added to inhibit Pef1-F78A kinase. At time 5h30, cells were collected to analyse Rad21-FLAG binding to chromatin by three different assays. **B.** DNA content analysis by flow cytometry. **C.** Quantification of ectopic-Rad21-FLAG bound to chromosomes. Fluorescence intensity was measured for 50–100 nuclei per sample. Error bar=95% confidence interval of the mean with α=0.05. **D.** Images of Rad21-FLAG immunofluorescence on nuclear spreads. Chromatin was counterstained with DAPI (red, pseudo-colour). Bar=2 μm. **E.** Cellular fractionation analysis. Soluble (S) and chromatin (C) fractions were probed with FLAG antibodies to detect ectopic Rad21-FLAG. Anti-histone H3 and anti-tubulin were used as fractionation controls. **F.** ChiP assay showing the amount of ectopic-Rad21-FLAG bound at the indicated loci. Error bar=s.d. from three ChiPs.

binding sites (Figure 30). A *pef1*$^{+}$ strain was included as to detect and measure a potential off-target effect of 1-NA-PP1. Indeed, a small increase in chromatin bound Rad21 was observed upon 1-NA-PP1 addition in *pef1*$^{+}$ cells, indicating a potential off-target effect. However, a much higher increase was observed with *pef1-F78A*, arguing that inhibition of the Pef1 kinase activity stimulates Rad21 binding to chromatin in G1-arrested cells.

Altogether, the data gathered in *mis4-367* and *mis4*$^{+}$ cells indicate that Pef1 kinase activity negatively regulates cohesin binding to chromatin during the pre-replicative stage of the cell cycle.

# *XI. Genome-wide analysis of ectopically expressed Rad21 distribution on chromosomes*

The above analyses indicated that inhibition of Pef1 kinase activity in G1 stimulates DNA binding of ectopically expressed Rad21. To further investigate this effect, we turned to a genome-wide analysis using ChIP-sequencing. I spent 3 months in Karl Ekwall's laboratory (Karolinska Institutet, Department of Biosciences and Nutrition, Epigenetics, chromatin remodelling and cancer group) learning the technique and doing the experiments.

The experiments are depicted in Figure 31. The first two strains (Figure 31A) were used to generate a standard reference cohesin map. The third strain was to assess the binding profile of ectopically produced Rad21-FLAG. Strains 3 to 6 were designed to map ectopically produced Rad21-FLAG bound to chromosomes upon inhibition of the Pef1 kinase in *mis4-367* and *mis4*$^{+}$ background. The ChIP experiments were done in duplicate. DNA sequences alignments were performed with Bowtie2 and peak calling was calculated with SeqMonk (Materials and Methods).

Results obtained by ChIP-seq experiments require an in-depth investigation. To date, only a preliminary analysis has been achieved and is presented in the following sections.

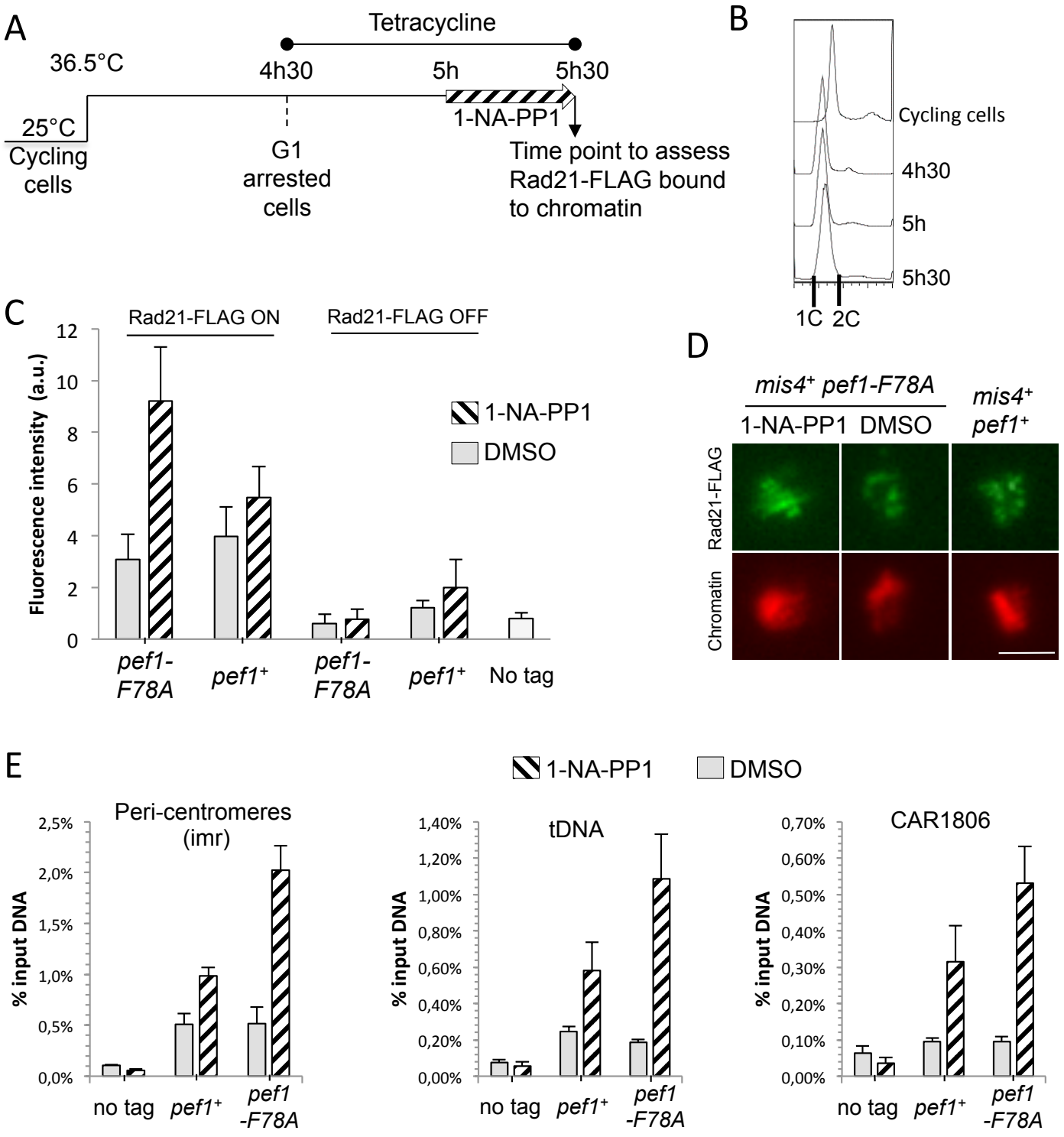


**Figure 30: Pef1 kinase inhibition stimulates ectopic Rad21–FLAG binding to chromatin in G1-arrested *mis4*⁺ cells. A.** Exponentially growing cells at 25°C (*cdc10-129 pef1-F78A ectopic-rad21-FLAG*) were shifted to 36.5°C. At time 4h30 after the temperature shift, when cells were G1-arrested, tetracycline was added to allow Rad21-FLAG production. Thirty minutes later, 1-NA-PP1 was added to inhibit Pef1-F78A kinase. At time 5h30, cells were collected to analyse Rad21-FLAG binding to chromatin by two different assays. **B.** DNA content analysis by flow cytometry of cells at the indicated time points. **C.** Quantification of ectopic Rad21-FLAG bound to chromosomes by nuclear spreads. Fluorescence intensity was measured for 50–100 nuclei per sample. Error bar=95% confidence interval of the mean with α=0.05. A *pef1*⁺ strain was included to measure a potential off-target effect of 1-NA-PP1. **D.** Images of Rad21-FLAG immunofluorescence on nuclear spreads. Chromatin was counterstained with DAPI. Bar=2µm. **E.** ChiP assay showing the amount of ectopic Rad21-FLAG bound at the indicated loci. Error bar=s.d. from four ChiPs. (1-NA-PP1 and tetracycline were added at time 4h30 for ChIP experiments).

## A. Generation of a reference cohesin map

The first aim was to validate the procedure by generating a Rad21-FLAG cohesin map and see how it fitted with available published data. A *cdc10-129 rad21-FLAG* and its matched untagged control were used for this first experiment (strains 1 and 2 in Figure 31A). A Rad21-FLAG binding map was generated for the DMSO and 1-NA-PP1 conditions. The Venn diagrams in Figure 32A show that a number of peaks are specific to the DMSO or 1-NA-PP1 conditions and 651 peaks were common to 1-NA-PP1 and DMSO conditions. The scatter plots (Fig. 32B-C) show a good correlation between the two experimental conditions as well as for the duplicates. For chromosome 2, 229 peaks were common to 1-NA-PP1 and DMSO conditions (Fig. 32B). Those 229 peaks included 80% of the 228 peaks found in *cdc25-22* arrested cells (Schmidt, Brookes, and Uhlmann 2009).

The 651 peaks common to DMSO and 1-NA-PP1 were used as the reference list for further analyses.

## B. Genome-wide distribution of ectopically expressed Rad21 in G1 *mis4*$^{+}$ cells

Using the same procedure, we asked whether ectopic-Rad21-FLAG in a *mis4*$^{+}$ background would bind chromatin at endogenous Rad21-FLAG binding sites. DMSO and 1-NA-PP1 conditions were pooled together to generate an ectopic-Rad21-FLAG binding map and compared with our reference list of the 651 peaks determined in the previous section (Figure 33). We observed 417 common peaks with endogenous Rad21-FLAG (with an overlap windows of 2000pb, Figure 33A). The non-overlapping peaks were not further analysed. We assumed that most originated from the difference between DMSO and 1-NA-PP1 conditions, as in Fig. 32A.

A

*1: h⁻ cdc10-129 mis4⁺* (no tag)
*2: h⁻ cdc10-129 mis4⁺ rad21-FLAG*
*3: h⁻ cdc10-129 mis4⁺ rad21-FLAG-ectopic pef1⁺*
*4: h⁻ cdc10-129 mis4⁺ rad21-FLAG-ectopic pef1-F78A*
*5: h⁻ cdc10-129 mis4-367 rad21-FLAG-ectopic pef1⁺*
*6: h⁻ cdc10-129 mis4-367 rad21-FLAG-ectopic pef1-F78A*

B

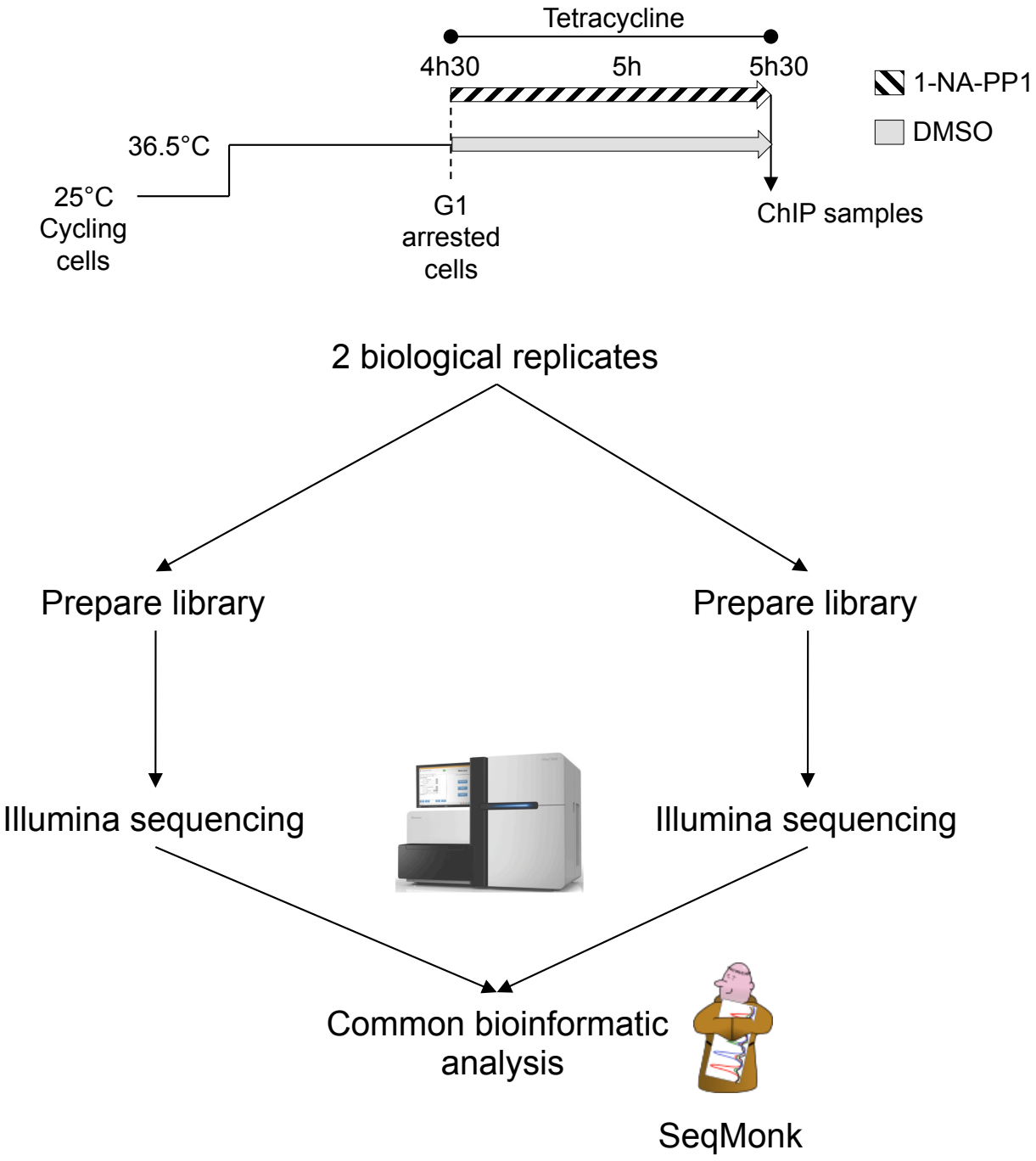


**Figure 31: A.** Genotype of strains for ChIP sequencing experiments. **B.** Workflow of Chip-sequencing experiments. Exponentially growing cells at 25°C were shifted to 36.5°C. At time 4h30 after the temperature shift, when cells were G1-arrested, tetracycline and 1-NA-PP1 or DMSO were added. At time 5h30, cells were collected to analyse Rad21-FLAG binding to chromatin by ChIP-sequencing. The above experiment was performed twice (biological replicates). Two independent DNA libraries were prepared and sequenced. Sequence data were pooled for the bioinformatics analysis using SeqMonk.

## C. Genome-wide distribution of ectopically expressed Rad21 in G1 *mis4-367* cells

We next focused on the *mis4-367* mutant, asking the effect of Pef1 kinase inhibition on the pattern of ectopically expressed Rad21 binding to chromosomes.

**➔ 127 Rad21 peaks were increased in intensity upon inhibition of the CDK.**

First, we analysed ectopically expressed Rad21-FLAG binding to chromatin to ask whether and how newly synthetised Rad21-FLAG actually binds chromatin in the *mis4-367 pef1*$^{+}$ background. As shown in Figure 34, Rad21-FLAG binding to chromatin was observed in *mis4-367* mutant suggesting a residual activity of the loader. However, when compared to *mis4*$^{+}$, a global decrease in peaks intensity was observed in *mis4-367* mutant and particularly at known strong cohesin binding sites such as centromeres and sub-telomeric regions (Figure 34).

To ask whether some Rad21 peaks would be increased in intensity in *mis4-367 pef1*-F78A upon kinase inhibition, we made a quantitative analysis of ChIP-seq data by determining an enrichment ratio (R). It was calculated by dividing the log2 score enrichment for each 1-NA-PP1 peak with the log2 score enrichment of each DMSO peak. R calculation in the *pef1*$^{+}$ background identified peaks whose intensity changed (at least two fold) between DMSO and 1-NA-PP1 conditions ("off target peaks"). These were eliminated from the analysis. 495 peaks common to both DMSO and 1-NA-PP1 conditions and found in our reference cohesin map did not show any change in peak intensity (fold<2). Those 495 peaks were next examined in the *pef1-F78A* samples. Of these 495 peaks, 344 sites were also found in the *pef1-F78A* samples (DMSO or 1-NA-PP1). Finally, of these 344, 127 showed an R score >2. An example is shown in Figure 35 as well as their distribution across the genome. Preliminary observations did not reveal any special feature associated with these peaks but in depth examination will be necessary.

**➔ 94 neo-peaks are formed in response to Pef1 kinase inhibition.**

Next, we investigated the possibility that Pef1 inhibition may provoke the generation of new Rad21 binding sites ("neo-peaks"). To address this question, the peak list from *mis4-367 pef1-F78A* in 1-NA-PP1 was made. Then the following peak lists were subtracted: *mis4-367 pef1-F78A* DMSO; *mis4-367 pef1*$^{+}$ DMSO *and mis4-367 pef1*$^{+}$ 1-NA-

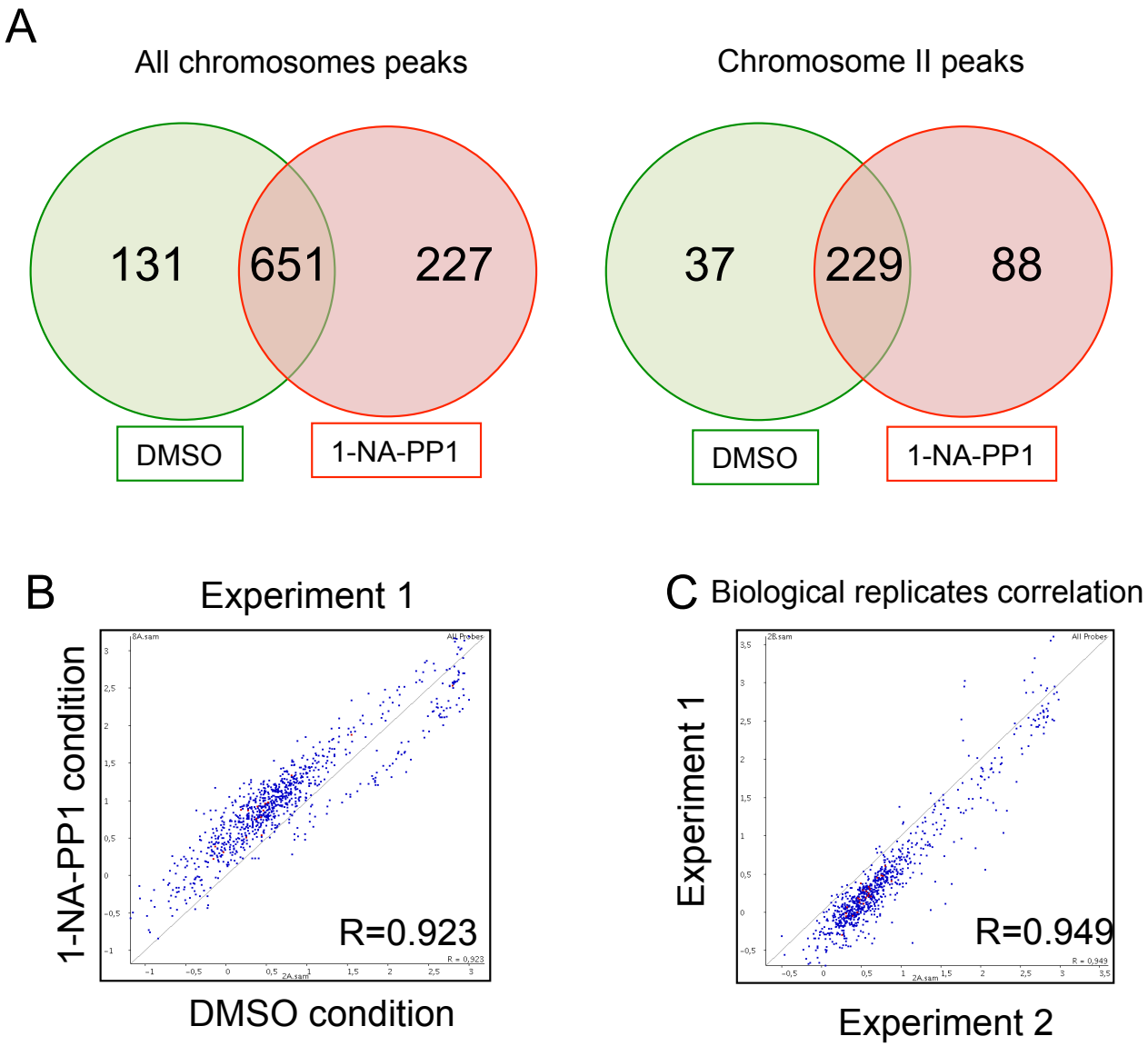


**Figure 32: A.** Venn diagrams showing endogenous Rad21-FLAG peaks in 1-NA-PP1 or DMSO conditions. Peaks are considered as common when they fall in the same 2000bp window. **B.** The scatter plot allows to look at the correlation between the two growth conditions (1-NA-PP1 and DMSO) for the endogenous Rad21-FLAG peaks. One point represent one peak. **C.** Scatter plot illustrating strong positive correlation between the two biological replicates (endogenous Rad21-FLAG peaks for DMSO conditions is shown).

PP1. This yielded a total of 160 peaks of which 94 were assigned as “neo-peaks” from their absence in our reference cohesin binding map. An example is shown in Figure 36. Regular cohesin binding sites are preferentially located within intergenic regions with a strong bias towards convergent transcription units (Lengronne and al. 2004; Schmidt, Brookes, and Uhlmann 2009). By contrast, the neo peaks found here did not follow this rule as from 94 “neo peaks” one half is located on core genes and the other half within intergenic regions. Interestingly, only 9% of the intergenic peaks map to convergent transcription units and 50% are located between divergent genes.

These analyses reveal two aspects. First, inhibition of the kinase does not result in a global, uniform stimulation of Rad21 binding at known cohesin binding sites. Rather, only a subset of these appeared influenced. Secondly, Rad21 peaks appeared at unconventional locations in the genome. These “neo-peaks” are preferentially located within divergent transcription units. Therefore, Pef1 appears as a local regulator of cohesin binding to chromosomes.

# *Discussion*

In this study, we have identified the CDK Pef1 in a genetic screen for *mis4-367* suppressors. We demonstrated that Pef1 kinase inhibition before S-phase reduced *mis4-367* sister-chromatid cohesion and chromosome segregation defects. By using an inducible ectopic *rad21-FLAG* gene, we observed that Pef1 kinase inhibition restored cohesin association with chromatin in G1-arrested *mis4-367* mutant cells and stimulated cohesin binding to chromatin in G1-arrested wild type cells. Genome wide analyses suggested that the Pef1 kinase may regulate Rad21 binding to a subset of known Rad21 binding sites and may prevent Rad21 binding to other loci. The Rad21 cohesin subunit may be a key Pef1 target. A *rad21-163A164A* allele behaved as a *mis4-367* suppressor, phenocopied the effect of a *pef1* null allele and the combination of both did not show any additive effect. Pef1 phosphorylated Rad21 *in vitro* and the reaction was largely abolished when Rad21-164A was used as a substrate. Based on these results, it is tempting to discuss the proposal that Pef1 negatively

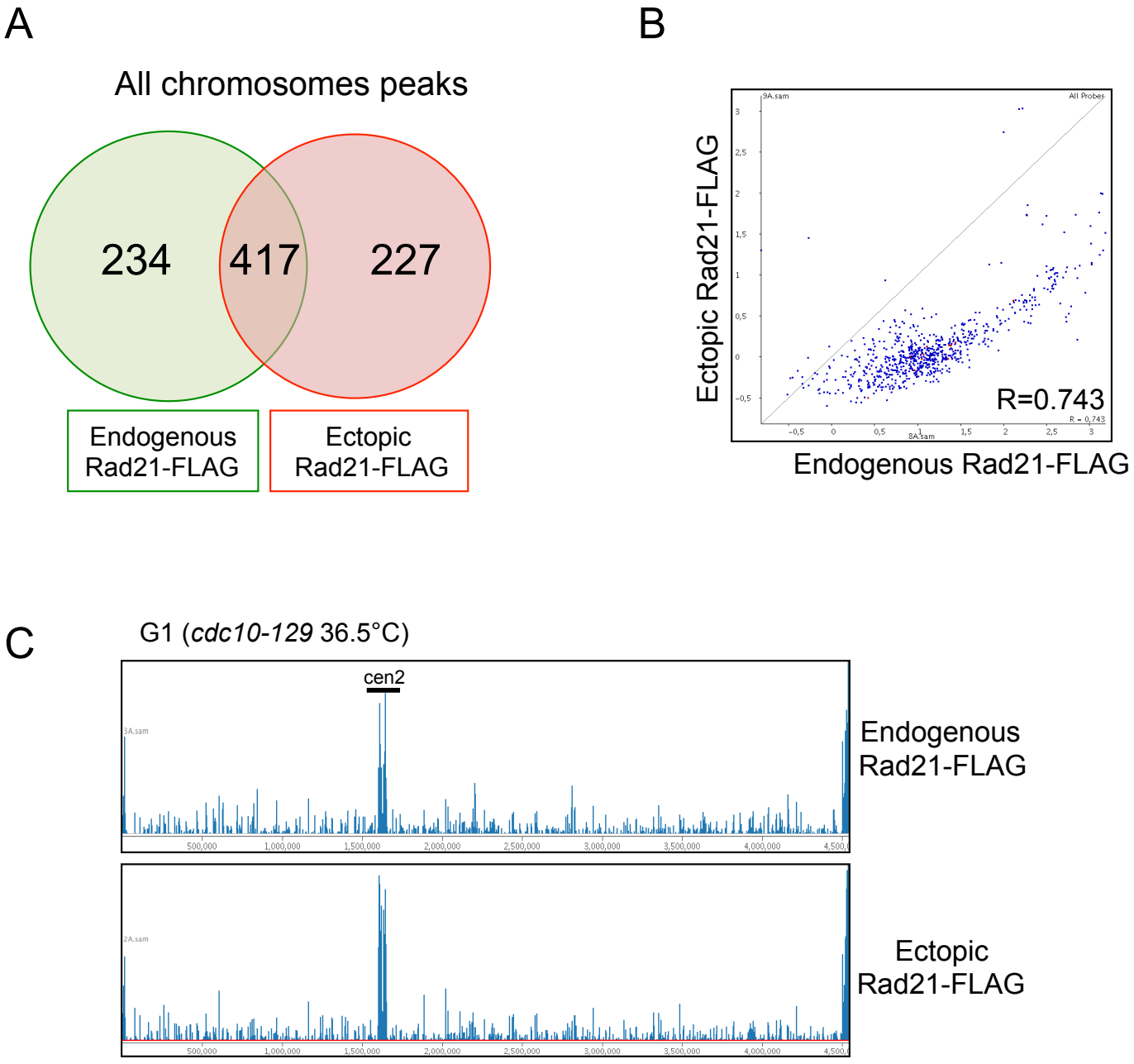


**Figure 33: A.** Venn diagram showing the overlap between peaks from ectopically expressed Rad21-FLAG and the 651 endogenous Rad21-FLAG binding sites. **B.** Scatter plot illustrating moderate positive correlation between endogenous and ectopic Rad21-FLAG peaks. **C.** Visualisation of Rad21-FLAG (endogenous and ectopic) enrichment along chromosome II.

regulates cohesin binding to chromatin, possibly through the phosphorylation of the Rad21 kleisin subunit on residues Ser163-Ser164.

## A. How does Pef1 kinase inhibition suppress *mis4-367*?

### *1) Stimulation of cohesin binding to chromatin*

The Mis4-Ssl3 complex is described as a cohesin loader whose essential function is during G1-early S phase. We expected a suppressor to act by stimulating the residual loading activity of *mis4-367* at the restrictive temperature but we failed to detect any effect on endogenous cohesin. We may have missed the relevant time window during the cell cycle. Recent findings in budding yeast reported a transient increase of cohesin binding to chromatin at the beginning of S phase dependent on the Chl1 replisome component (Rudra and Skibbens 2013; Samora and al. 2016). Chl1 promotes association of the cohesin loader Scc2 onto DNA such that both Scc2 and cohesin enrichment to chromatin are defective in *chl1* mutant cells. The level of acetylated Smc3 is reduced which would be responsible for the cohesion defect observed in the *chl1* mutant. It was proposed that Chl1 helps cohesin acetylation by increasing the amount of cohesin available for Eco1 at the replication fork and accordingly, overexpression of Scc1 increased the amount of acetylated Smc3 and reduced the cohesion defect of *chl1* mutant cells (Samora et al. 2016). Whether this phenomenon is also taking place in fission yeast is unknown and should be addressed. If it were conserved, it would be important to see whether Pef1 is involved in this transient loading. As a preliminary experiment, we should ask whether Pef1-as inhibition in *mis4-367* cells translates into an increased level of acetylated Psm3.

However, we did detect a stimulation of Rad21 binding to chromatin using ectopically expressed Rad21 in *cdc10-129* arrested *mis4-367* G1 cells whereas we did not detect such a stimulation for endogenous Rad21. The reason for this is not understood. There are differences between endogenous and ectopically expressed Rad21. The promoter and 3'UTR regions are different, and the ectopic copy is FLAG-tagged. However, fractionation experiments showed that both are present in the soluble fraction and therefore both are available for loading.

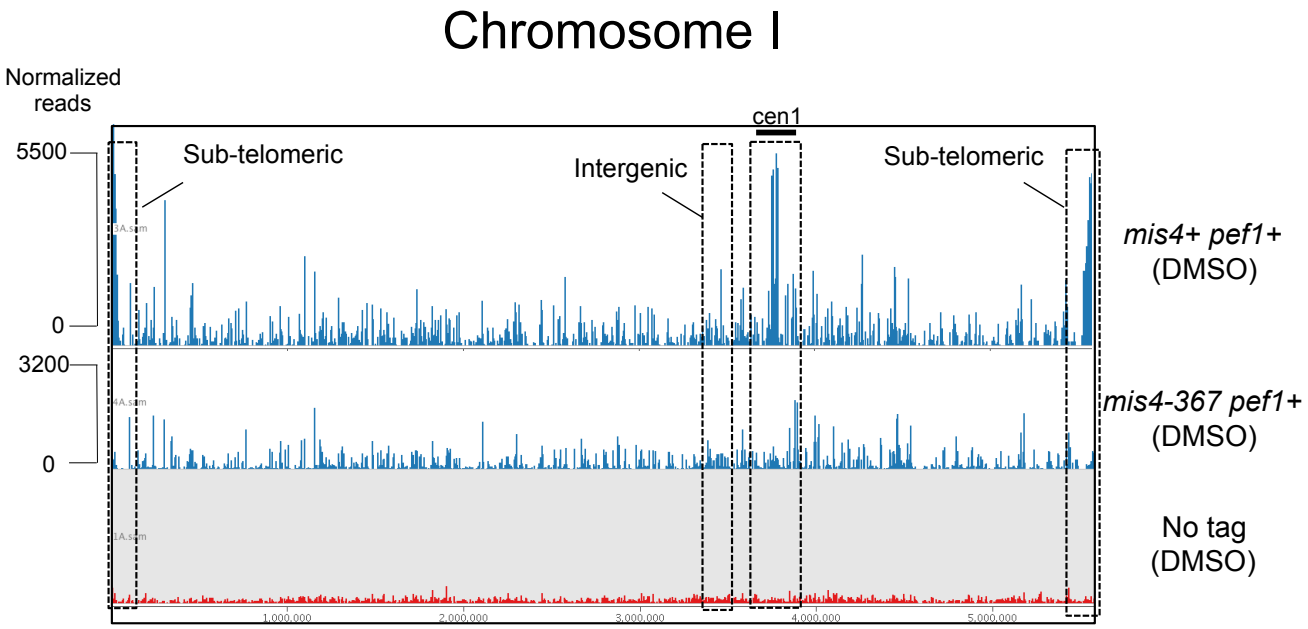


**Figure 34 :** Ectopic Rad21-FLAG binding profile along chromosome I in wt and *mis4-367* samples.

One possible explanation would be an artefact in these experiments. During the course of this work, we noticed some differences in the amount of Rad21-FLAG produced from the ectopic locus. For instance in Figure 29E, there is more Rad21-FLAG in the soluble fraction in the 1-NA-PP1 sample when compared to its matched DMSO control, leaving the possibility that this may be sufficient to account for the difference seen in the chromatin fraction. To investigate this possibility we repeated the experiments and made total protein extracts to assess the amount of ectopically produced Rad21-FLAG. As shown in Figure 37, there is indeed more Rad21-FLAG in the 1-NA-PP1 samples than in the DMSO controls. The reason is unknown. We therefore cannot rule out the possibility that the apparent stimulation of Rad21 binding to DNA was due to increased Rad21 availability in the 1-NA-PP1 samples. A strain carrying *rad21-FLAG* at the endogenous locus was included in these experiments to estimate the amount of ectopically Rad21-FLAG relative to endogenous Rad21-FLAG. As shown in Figure 37, ectopically Rad21-FLAG is less abundant than endogenous Rad21-FLAG, ruling out possible artefacts due to massive over-expression. A low expression level is even preferred for the ectopic Rad21-FLAG to ensure it behaves as a tracer for the kinetics of endogenous Rad21. Originally, we thought that this system would be ideally suited to unambiguously detect cohesin loading in G1 as opposed to reduced unloading, or increased persistence of cohesin from the previous cell cycle. The experiments have revealed that ectopically expressed Rad21 does bind upon inhibition of the kinase whereas the steady state amount of endogenous Rad21 does not increase. This is apparently contradictory. However, it must be noted that these two measurements are not in the same range and they have not been made in the same strain but rather in independent experiments. In other words, the detection of a cohesin loading activity using ectopically expressed Rad21 might be a sensitive assay revealing that indeed inhibition of the CDK stimulates cohesion loading. This wouldn't translate into an increased steady state amount of endogenous Rad21 because the equilibrium between loading and unloading might not change or the change is not big enough to result in a measurable difference in steady state amounts. In conclusion, there is some concern about the interpretation of the experiments conducted with the ectopically expressed Rad21. Experiments should be repeated along with accurate quantification of protein levels.

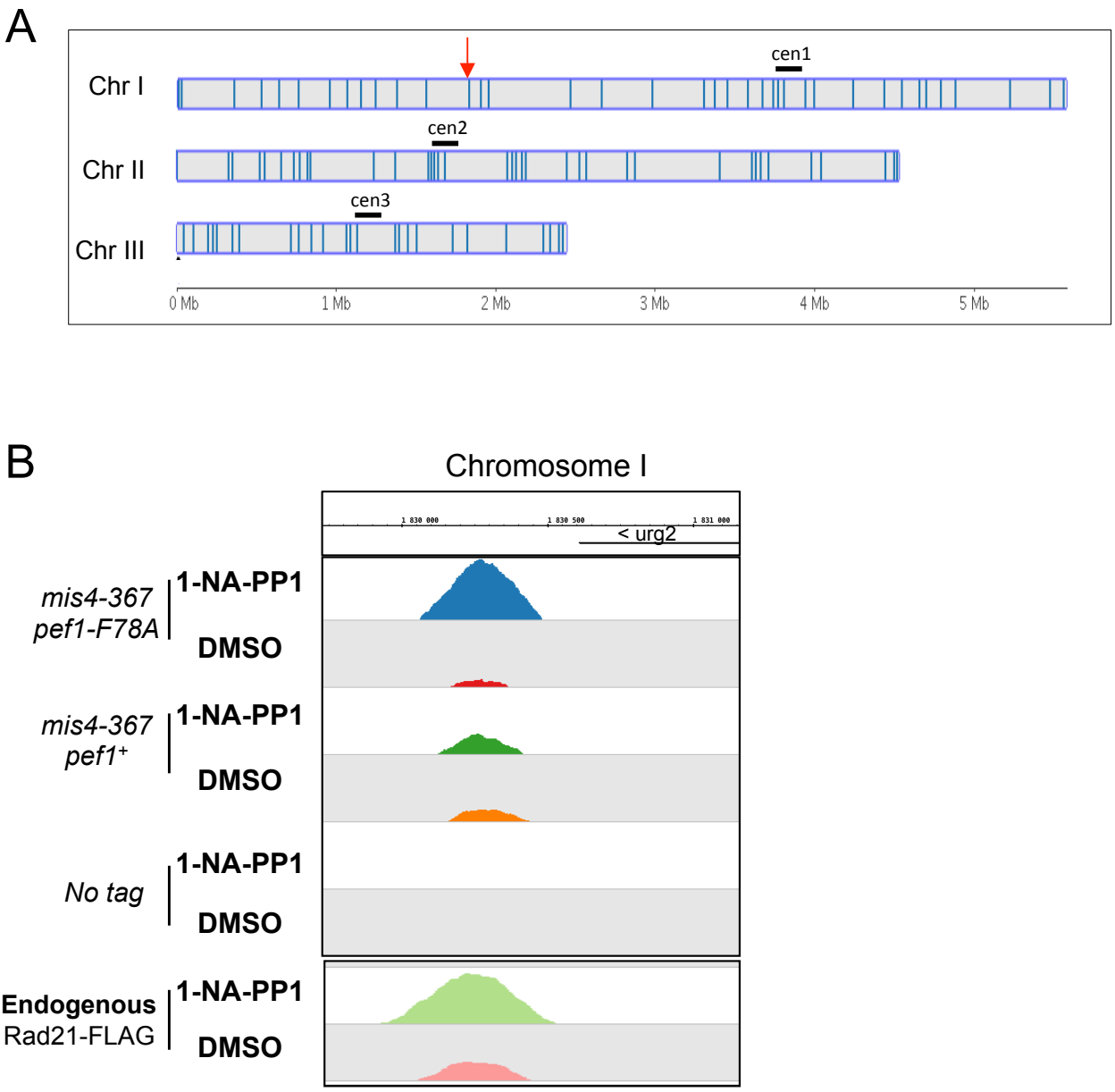


**Figure 35 : Loci showing an increase of ectopically expressed Rad21-FLAG binding upon Pef1-F78A inhibition in *mis4-367* cells. A.** Distribution view across the genome of 128 enhanced binding sites of Rad21-FLAG. Red arrow indicates chosen peaks enlarged in B. **B.** Detailed view of one stimulated Rad21-FLAG binding site.

### *2) The suppression may not arise from increased cohesin binding to chromatin*

Models of cohesion establishment propose that cohesin loading must occur before the passage of the replication fork, meaning that the only function of the cohesin loader would be to provide cohesin loading to un-replicated DNA. This is not entirely clear however. Only one study addressed this question (Lengronne and al. 2006). Cells from *scc2-4* (thermosensitive) were arrested in early S phase by HU treatment at 25°C and then released into the cell cycle at 36°C to inactivate the cohesin loader. Cell viability remains relatively high but still dropped progressively after release. Since cells remained "globally" viable it was concluded that cohesin loaded at 25°C (*i.e.* until early S phase) was sufficient to generate sister-chromatid cohesion. However, this experiment can be interpreted in the opposite direction. Early replication origins fired in HU-arrested cells meaning that cohesion may have been established at the permissive temperature. In addition, the continuous drop in cell viability after release suggests that replication of the bulk of the genome may have failed to generate proper sister-chromatid cohesion. We think that this question remains open. Recent *in vitro* experiments have shown that cohesin can slide along DNA but is arrested by small obstacles (~20nm), which is much smaller than the expected size of a replicating fork (Stigler and al. 2016). It seems therefore unlikely that the replisome is able to pass through intact cohesin rings. The loading complex may help by remodelling cohesin or by providing cohesin loading in the wake of the fork. Following this idea, the suppression by Pef1 inhibition may be through cohesion establishment rather than "loading" *per se*. As mentioned earlier, it will be important to see whether Pef1 kinase inhibition may increase Smc3 acetylation in *mis4-367* cells. An increased ratio (Acetylated Psm3/Total Psm3) would argue for an improved cohesion establishment reaction.

## B. What is (are) the relevant Pef1 substrate(s)?

### *1) Rad21*

We report here genetics and biochemical evidences arguing that Rad21 may be a relevant Pef1 substrate. We observed that the double alanine mutant of Rad21 at position 163 and 164 restores *mis4-367* viability at the restrictive temperature in a manner very similar to *pef1* deletion. Moreover, there is no additive effect when both are combined together,

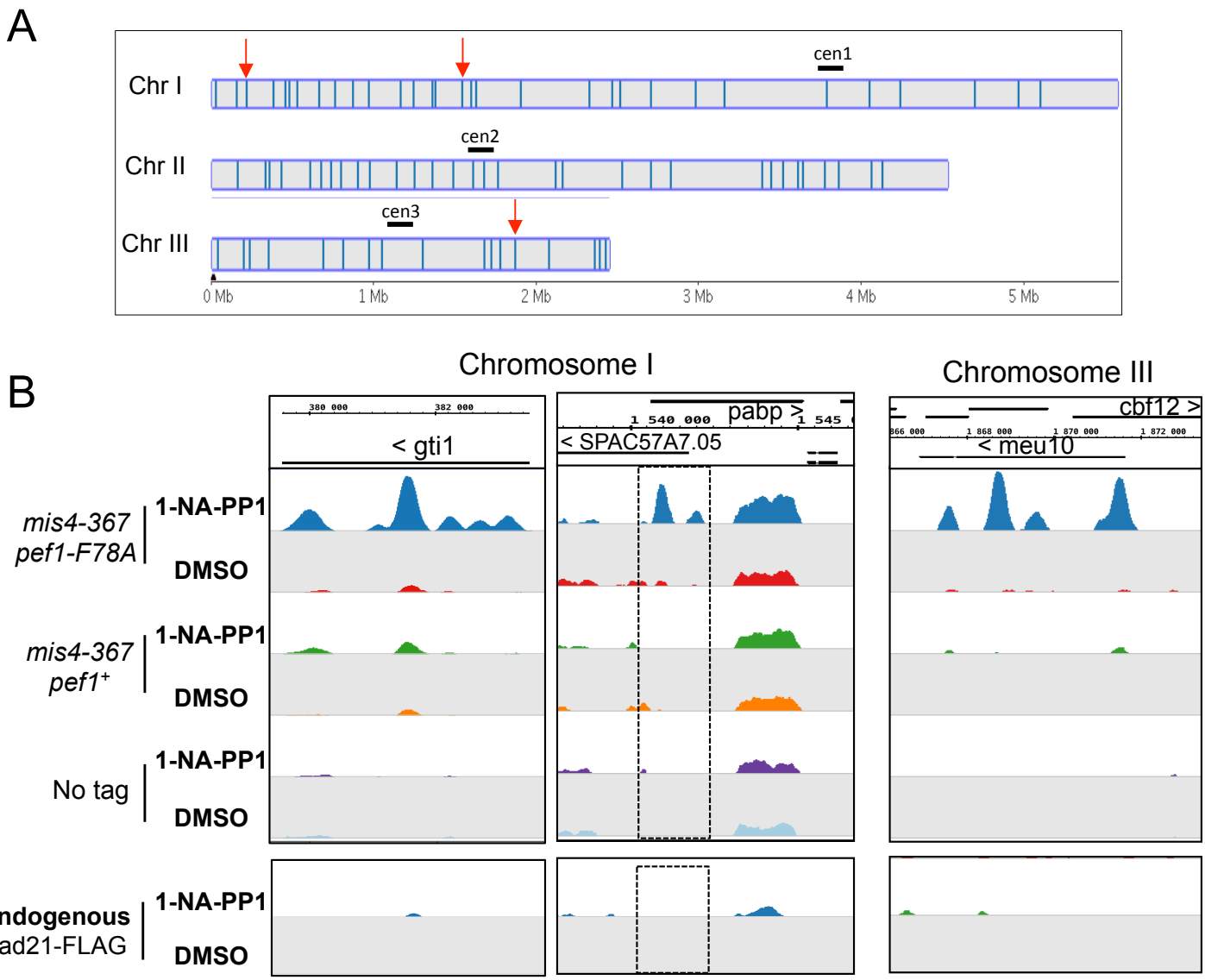


**Figure 36 : Neo binding sites of ectopically expressed Rad21-FLAG upon Pef1-F78A inhibition in *mis4-367* cells. A.** Distribution view across the genome of 94 neo binding sites of Rad21-FLAG. Red arrows indicate chosen peaks enlarged in B. **B.** Detailed view of three neo Rad21-FLAG binding sites.

consistent with the two mutations acting in the same pathway. Pef1 phosphorylated Rad21 in an *in vitro* assay and this was largely abrogated when Rad21-164A was used as a substrate. These data argue for a negative control of cohesin loading through Pef1 mediated phosphorylation of Rad21 Ser163 and Ser164. There are however a number of observations that do not fit well with this conclusion.

The CDK consensus site predicts that serine 165 would be the phosphorylated residue. However, a *rad21-165A* was neutral for *mis4-367* whereas S163A S164A produced the suppressor effect. It remains possible that Pef1 does not comply with the CDK rule and may phosphorylate other residues.

More surprising was the finding that the *rad21-163E164E* phospho-mimicking allele was essentially neutral for *mis4-367* and did not prevent suppression by *pef1Δ*. One possibility would be that the S to E substitutions failed to mimic the phosphorylated state. However, the very same mutations did produce a phospho-mimic phenotype (see next chapter).

One possibility would be that serine 163 and 164 govern Pef1 binding to Rad21 (Figure 38). The un-phosphorylated state would bind the CDK with low affinity while the phosphorylated state would create a high affinity Pef1 CDK binding site. The actual relevant Pef1 target would be at another (unknown) location within Rad21. This possibility was appealing because we found that Rad21-164A did reduce but did not abolish Rad21 phosphorylation *in vitro*, suggesting the existence of another target residue within Rad21. The prediction of this model would be that Rad21-163E164E should not abolish (or even enhance) Rad21 phosphorylation *in vitro*. The other prediction is that the CDK should interact better with Rad21-163E164E. However Pef1 immunoprecipitated Rad21-163E164E from total cycling cell extracts as efficiently as wild type or Rad21-163A164A did (not shown). *In vitro* experiments may be helpful to understand the mechanism by which the CDK docks onto Rad21.

### *Possible mechanisms by which Rad21 phosphorylation would negatively regulate cohesin binding to DNA*

Cohesin shows two types of chromatin association in G1: a transient association in the range of tens of seconds that does not depend on cohesin ATPase activity, and a more long-

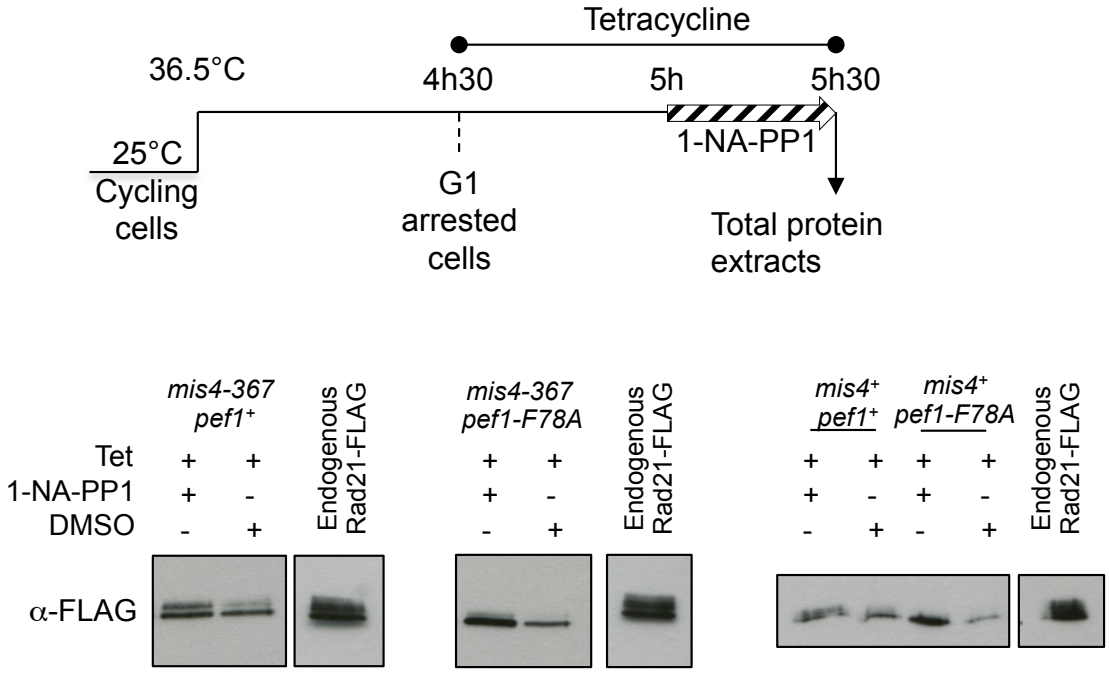


**Figure 37: Ectopically expressed-Rad21-FLAG is differentially detected in G1 arrested cells.**
Exponentially growing cells at 25°C were shifted to 36.5°C. Tetracycline was added 4h30 and 1-NA-PP1 30 min later. Cells were collected at time 5h30. Total protein extract were made and probed with anti-FLAG antibodies.

lasting “dynamic” type of chromatin interaction that depends on cohesin ability to hydrolyse ATP. Pef1 may regulate one or both of this association:

**➔ Control of the initial stage of cohesin loading reaction**

Rad21 may act as a DNA sensor in its un-phosphorylated state. Thus phosphorylated Rad21 would negatively regulate the transient association of cohesin with DNA. Conversely, the un-phosphorylated state would create a more advantageous electrostatic context. In cohesin loader mutants, increased cohesin contact with DNA in time or in frequency would ensure a minimum threshold of cohesin binding to DNA, which, together with residual Mis4 activity, would be sufficient to rescue viability.

**➔ Control of cohesin interaction with the cohesin loader**

Cohesin and cohesin loading machinery interaction is required for cohesin association with DNA. Rad21 phosphorylation may negatively regulate cohesin interaction with its loader. In a recent study, two specific zones within Rad21 were identified as cohesin loader binding sites. Interestingly, one of them includes the PIS$^{163}$S$^{164}$S region of Rad21. Moreover, the region includes threonine 147 with lies within a predicted CDK consensus site. Threonine 147 phosphorylation is detected at the G1-S transition after release from nitrogen starvation (Adachi and al. 2008) and corresponds to the cell cycle window in which Pef1 kinase inhibition is required to correct *mis4-367* thermosensitive phenotypes. It will be interesting to see whether a *rad21-147A* mutant would behave as a *mis4-367* suppressor.

### *2) Mis4*

We have focussed our attention on Rad21 but Pef1 may phosphorylate other relevant proteins. Cohesin loader Mis4 is one of those. Indeed, we found that Mis4 co-immunoprecipitated with Pef1 (figure 21B). However, we did not detect any change in Mis4 or Ssl3 protein mobility by PAGE in *pef1*$^{+}$ versus *pef1Δ* extract(Figure 39A). This however does not exclude the possibility that Pef1 may phosphorylate these proteins.

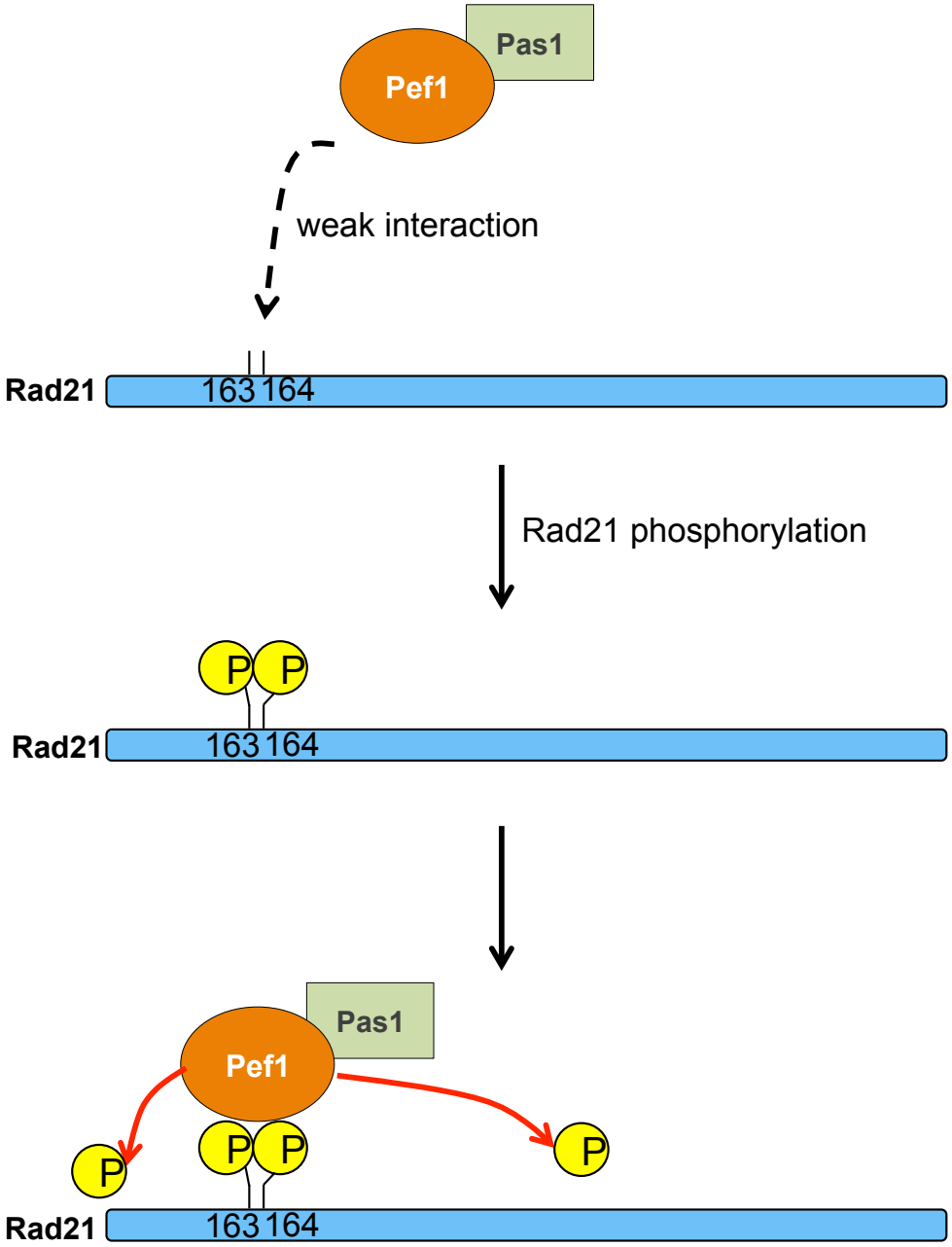


**Figure 38 : Model of Pef1-mediated phosphorylation of Rad21.** Un-phosphorylated Rad21 at serine 163 and 164 has a low affinity for Pef1. Rad21 phosphorylation at serine 163 and/or 164 would enhance Pef1/ Rad21 interaction allowing Pef1 to phosphorylate Rad21 at other(s) site(s). The non-phosphorylatable Rad21-163A164A would suppress *mis4-367* by preventing Rad21 phosphorylation. The phospho-mimicking form Rad21-163E164E would not be phosphorylatable on Ser163 and Ser164 but would not prevent Rad21 phosphorylation at other locations.

***Possible mechanisms by which Mis4 phosphorylation would negatively regulate cohesin binding to DNA***

**➔ Mis4 targeting to chromatin**

In fission yeast, little is known about Mis4 phosphorylation as opposed to budding yeast in which Scc2 is highly phosphorylated (Woodman and al. 2014). A Scc2-8E mutant modestly reduced Scc2 binding to chromatin while Scc2-8A was neutral, suggesting that Scc2 function is modulated by its phosphorylation status (Woodman and al. 2015). Structure analysis of the cohesin loader Scc2-Scc4 revealed a complex arrangement of these proteins (Chao and al. 2015). Interestingly, the head domain contains several CDK consensus sites. This domain corresponds to the NScc2-Scc4 contact and is dispensable for *in vitro* loading of cohesin on DNA (Murayama and Uhlmann 2014). It was suggested that this domain might be involved in addressing the loader to chromatin. The phosphorylation status would regulate the flexibility of the Scc2-Scc4 complex and thereby its interaction with chromatin.

In *S. pombe* phosphorylation sites within Mis4 were identified by global mass spectrometry analysis. All phosphorylated residues mapped at the transition between the head and the body domains. Among these, three sites (S183, S204 and S208) are found within CDK consensus sites (Carpy and al. 2014; Koch and al. 2011). It is therefore possible that phosphorylation by Pef1 CDK may modify the ability of the cohesin loader to interact with chromatin.

**➔ Mis4 interaction with Cohesin**

As mentioned in the previous section, Mis4/Ssl3 binds two domains of Rad21 *in vitro*. The regions by which Mis4/Ssl3 contacts Rad21 are not known. It remains possible that Mis4 phosphorylation may modulate its ability to bind cohesin.

**➔ Mis4 nuclear localisation**

A NLS is found within the N-terminal domain of Mis4 overlapping with the CDK consensus sites described above, opening the possibility of a nuclear import / export regulated by a CDK.

At the present time, the mechanism by which Pef1 negatively regulates cohesin binding to chromosomes remains unclear. If indeed Rad21 phosphorylation is causative the

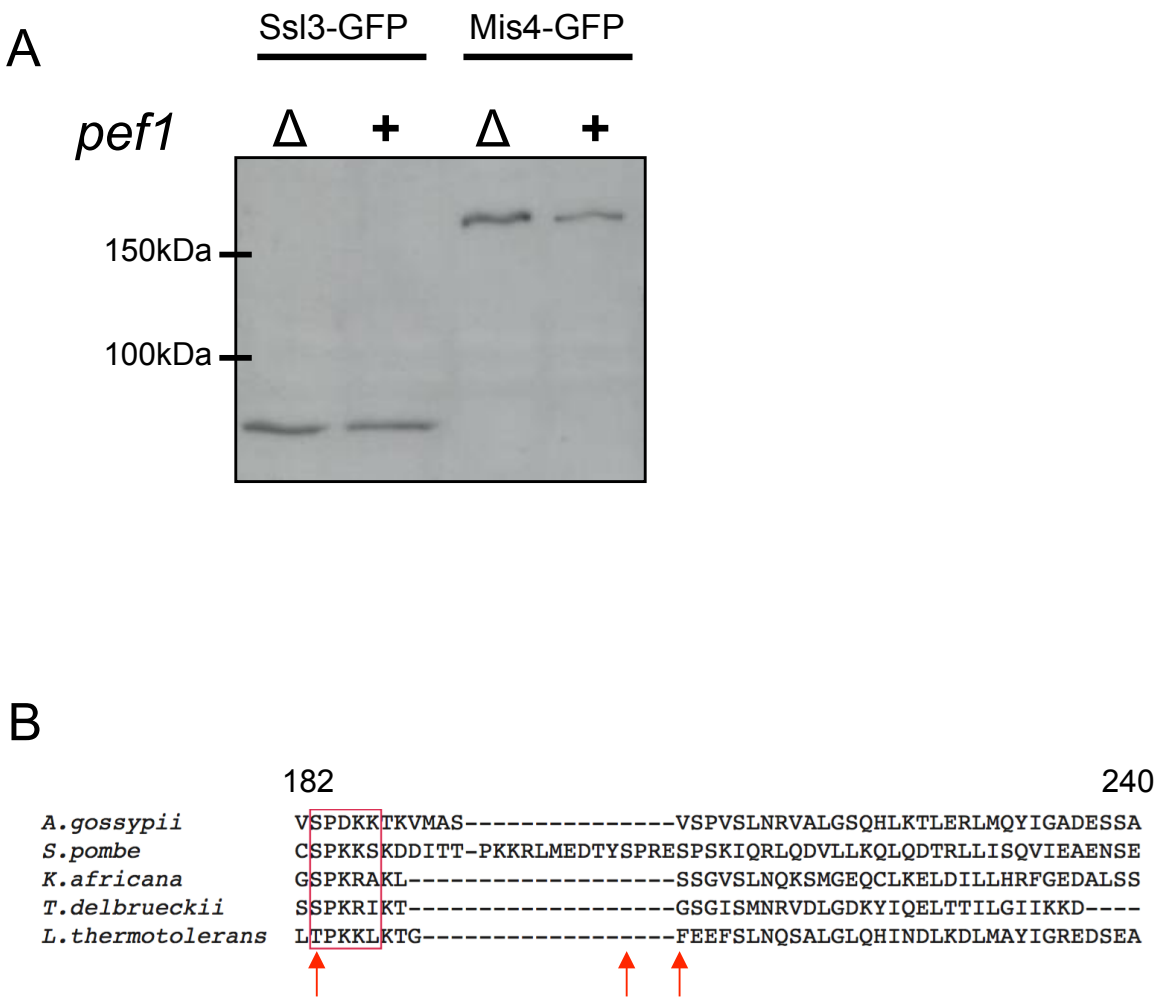


**Figure 39 : A.** Exponential growing cells from *pef1*$^{+}$ or *pef1Δ* strains were lysed and total protein extracts were probed with anti-GFP antibodies (Amelie Feytout). **B.** Mis4 sequence alignment of chosen species (adapted form Chao, 2015). Framed box indicates a conserved CDK consensus site. Arrows indicate known Mis4 phosphorylation sites.

next step will be to understand how / by which molecular mechanism. The central region of Rad21 is described as unstructured and is poorly conserved between species. It is however similarly phosphorylated in Human, suggesting a conserved role for the phosphorylated state. *In vitro* cohesin loading experiments may help answering this question.

The following chapter is presented in the form of a manuscript that is currently submitted for publication describing a distinct study to which I participated. Strangely enough, the very same Rad21 phosphorylation sites are shown to play an essential role, although in an apparent distinct pathway

# Chapter III. Wpl1 anti-cohesion function requires de-phosphorylation of cohesin by Protein Phosphatase 4

Sabine Vaur[1], Karen Eguienta[1], Adrien Birot[1], Stéphanie Vazquez[1], Stéphane Claverol[2], Marc Bonneu[2], Karl Ekwall[3] and Jean-Paul Javerzat[1*]

[1]Institut de Biochimie et Génétique Cellulaires, UMR 5095 CNRS - Université de Bordeaux, 1 rue Camille Saint Saëns, 33077 Bordeaux, France

[2]UMR 5248 CNRS-Université, Bordeaux-IPB, 146 rue Léo Saignat, 33076 Bordeaux Cedex, France

[3]Department of Biosciences and Nutrition, Karolinska Institutet, Huddinge, Sweden

*Correspondence to: JPaul.Javerzat@ibgc.cnrs.fr

# *SUMMARY*

Sister chromatid cohesion is mediated by cohesin, a ring shaped protein complex essential for chromosome segregation and repair. Sister chromatid cohesion requires a cohesin acetyl-transferase counteracting Wpl1, an anti-cohesion factor promoting cohesin release from DNA. We show that Wpl1 is coupled with Protein Phosphatase 4 (PP4). Both are required for de-phosphorylating key residues within the central region of Rad21, the kleisin subunit of cohesin. PP4 ablation or Rad21 phospho-mimicking forms dampened Wpl1 anti-cohesion activity showing that Wpl1 function requires PP4-mediated de-phosphorylation of Rad21. Wpl1 induction experiments in post-replicative cells lacking the acetyl-transferase revealed two cohesin populations. Type 1 is released from DNA in a PP4-independent manner. Type 2 cohesin is not removed from DNA but loss of its cohesiveness is dependent on Rad21 de-phosphorylation by PP4. Wpl1 is therefore equipped with PP4 activity towards the cohesin kleisin subunit for disrupting an alternative mode of sister-chromatid cohesion.

**One Sentence Summary:** Phosphorylation of Rad21 shelters cohesin from Wpl1 anti-cohesion activity and is reversed by Protein Phosphatase 4.

# *INTRODUCTION*

To ensure proper chromosome segregation in mitosis and meiosis, sister-chromatids are held together from S-phase and until nuclear division by cohesin, a protein complex also required for chromosome organization, gene expression and DNA repair (*1-3*). Defects in cohesin functions in human can lead to severe pathologies such as Down syndrome, developmental defects and cancer (*4*). The ring shape of cohesin is formed by two coiled-coil SMC proteins (Structural Maintenance of Chromosomes, Psm1 and Psm3 in fission yeast) that dimerize through their hinge domain at one end. At the other end, the SMCs fold into head domains which bind together in an ATP-dependent manner. A third protein, the kleisin Rad21/Scc1/Mcd1, bridges the two SMCs heads. Pds5, Wpl1 and Psc3 are conserved additional subunits that bind to Rad21 (*1-3*).

How cohesin ensures sister-chromatid cohesion is still controversial. Cohesin is able to concatenate sister DNA molecules (*5*) leading to a model in which a single cohesin ring encircles sister-chromatids. Alternative models propose that cohesin may function as dimers, each ring encircling a single chromatid or even as interacting oligomers (*6-9*). Although it is clear that cohesin function involves DNA capture, the conformation of cohesive cohesin remains elusive and may not be unique. DNA capture by cohesin requires ATP hydrolysis by the SMCs and a loading complex called Mis4/Ssl3 in fission yeast. Conversely, DNA escape from cohesin is thought to involve DNA passage through two interfaces. ATP hydrolysis by the SMCs would disengage the SMC's heads while Wpl1 would disrupt the Psm3-Rad21 interface in a reaction that involves Pds5, Psc3 and Psm3 head domain (*2, 10-14*).

Sister-chromatid cohesion is essential for chromosome segregation implying that cohesion must be stable enough to last from S-phase and until nuclear division, a time frame ranging from hours in vegetative cells to decades in human oocytes. Concomitantly with the establishment of sister-chromatid cohesion in S-phase, a sub-population of cohesin becomes stably bound to DNA and mediates sister-chromatid cohesion (*10, 15-18*). This requires a conserved acetyl-transferase (Eso1 in fission yeast) that acetylates two conserved lysine residues within Smc3 globular head domain (*2*). Recent evidence indicates that Smc3 acetylation would prevent DNA release from cohesin by preventing ATP hydrolysis by the SMCs (*11, 14, 19*).

In mammals the cohesin acetyl-transferases down-regulate Wpl1 anti-cohesion function by promoting Sororin mediated eviction of Wpl1 from cohesin (*20*). Sororin is not conserved through evolution and is apparently lacking in fungi, raising the possibility that Wpl1 might be regulated by an ancient, yet to be discovered, ubiquitous pathway.

In fission yeast, the *eso1* gene is essential for sister-chromatid cohesion and cell viability but dispensable when the *wpl1* gene is deleted (*16, 21*). The thermosensitive *eso1-H17* mutant is deficient for $Psm3^{K106}$ acetylation even at the permissive temperature, indicating that Eso1 may counteract Wpl1 through another function besides Psm3 acetylation (*16, 22*).

To search for novel components of the pathway we made a genetic screen for mutants able to bypass Eso1 function and uncovered *pph3*, encoding the catalytic subunit of PP4. PP4 is a member of the PP2A family of Ser/Thr phosphoprotein phosphatases conserved from yeast to human. The common form of PP4 comprises a catalytic and two regulatory subunits and is involved in a variety of cellular processes, including chromosome biology and cell cycle progression (*23*). Here, we present evidence that PP4 is integral to Wpl1 function and identified Rad21 as a relevant PP4 substrate. We identified key residues within Rad21 that must be de-phosphorylated to authorize Wpl1-dependent loss of sister-chromatid cohesion. Surprisingly, PP4 is not required for Wpl1 mediated cohesin release from DNA. Rather, our data reveal the existence of a sub-population of cohesin whose cohesiveness is abolished by the combined action of Wpl1 and PP4-mediated de-phosphorylation of Rad21 without apparent cohesin removal from DNA.

# *RESULTS*

## PP4 is required for Wpl1 anti-cohesion function

Through a genetic screen for suppressors of the thermosensitive phenotype of eso1-H17 we recovered mutations in Psm3, Wpl1, Pds5 and Psc3 that is in all known components of the Wpl1-Eso1 pathway (Fig. S1). A mutation within a fifth gene, pph3, encoding the catalytic subunit of PP4 was also recovered. Deletion of the genes encoding pph3 or its regulatory subunit psy2 suppressed the thermosensitive growth defect of eso1-H17 (Fig. 1A)

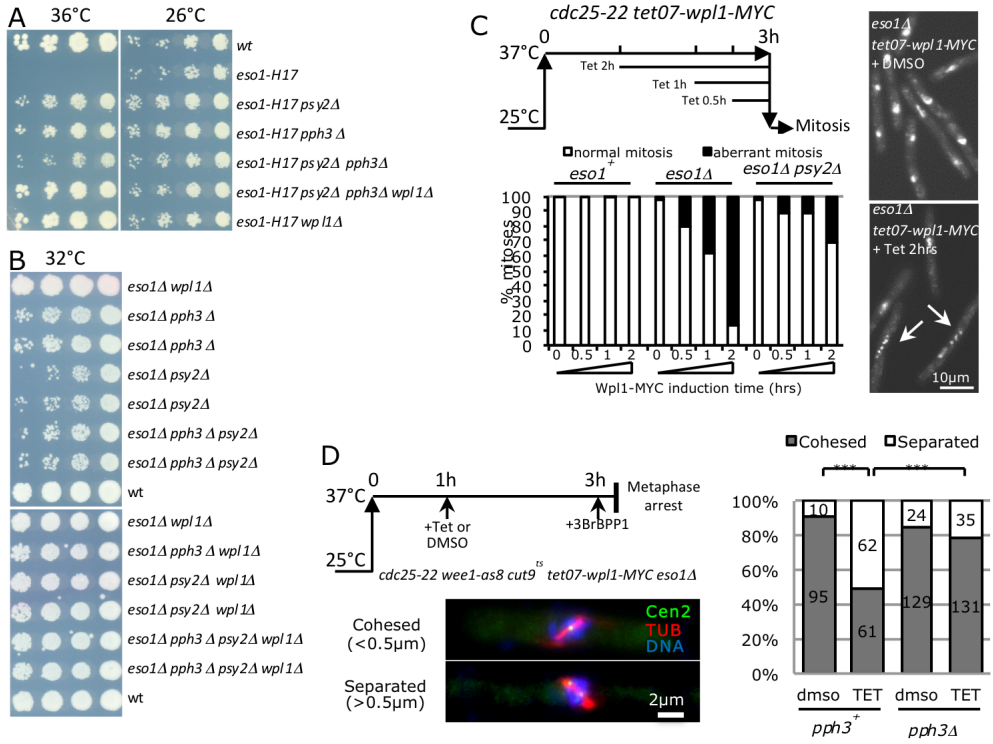


**Fig. 1. Wpl1 anti-cohesion function requires PP4**. (**A-B**) Cell growth assays showing that *pph3* or *psy2* deletion (encoding PP4 catalytic and regulatory subunits, respectively) suppresses the thermosensitive growth phenotype of *eso1-H17* (A) and allows cell growth in the absence of the otherwise essential eso1 gene (B). The deletion of *wpl1* bypasses *eso1* requirement more efficiently and is epistatic on PP4 deletion mutants. (C-D) Wpl1 induction in *eso1Δ* G2 cells induces loss of sister-chromatid cohesion and aberrant mitosis in a PP4-dependent manner. (**C**) Cycling *cdc25-22* cells (~80% G2 cells) were shifted to 37°C to prevent mitotic entry and Wpl1-MYC was induced at the indicated time-points. Cells were released into mitosis by shifting the temperature back to 25°C, DNA was stained with DAPI and aberrant mitoses (arrows) were scored. (D) Wpl1-MYC was induced for 2 hours after which time Wee1-as8 was inhibited with 3-BrB-PP1 to override the *cdc25-22* arrest (30). Cells progressed into M phase at 37°C and were arrested at metaphase by the thermosensitive APC mutation cut9ts (30, 31). Cells were fixed; tubulin stained to visualize the mitotic spindle and sister-chromatid cohesion was monitored by FISH using a probe proximal to the centromere of chromosome 2. *** $p < 0.0001$ Two-sided Fisher's exact test with $\alpha < 0.05$

and remarkably, allowed cell survival in the complete absence of the otherwise essential eso1 gene (Fig. 1B). The cell growth assays indicated that Eso1 bypass by PP4 mutants was incomplete but the additional deletion of wpl1 restored wild-type growth. This suggested the possibility that PP4 may be contributing to Wpl1 function. To test this idea, we set up an in vivo assay for Wpl1 anti-cohesion activity. In budding yeast, Wpl1 induction after S-phase in an eco1-1 mutant destroyed sister-chromatid cohesion (10). We constructed a strain in which Wpl1 expression is induced by tetracycline (tet07-wpl1-MYC). As expected, Wpl1 induction in G2 cells did not affect chromosome segregation during the ensuing mitosis when the experiment was made in an *eso1*$^{+}$ background (Fig. 1C). By contrast in an *eso1Δ* strain, ~90% of mitotic cells showed a severe chromosome segregation defect. Importantly, this phenotype was attenuated when PP4 was ablated (33% aberrant mitoses, Fig. 1C). To directly assess the status of sister-chromatid cohesion, cells were arrested at metaphase and cohesion monitored by FISH using a probe proximal to the centromere of chromosome 2 (cen2FISH). Wpl1 induction provoked a pronounced cohesion defect which was significantly attenuated by *pph3* deletion (Fig. 1D). Hence, PP4 is required for Wpl1 anti-cohesion function.

## Wpl1 triggers Rad21 de-phosphorylation in a PP4-dependent manner

Co-immunoprecipitation experiments from total protein extracts showed that Psy2-FLAG pulled down Wpl1 and all three core cohesin components suggesting that cohesin and/or associated factors might be PP4 substrates (Fig. 2AB). Consistently, Rad21 electrophoretic mobility was modified in PP4 mutants. In wild-type cycling cells (which are mainly in the G2 phase of the cell cycle (*24*)) Rad21 is present as several phospho-isoforms (Fig. 2C and (*25, 26*)). By contrast, the slowest-migrating Rad21 species accumulated in *pph3Δ* cells (Fig. 2C). The mobility shift was due to phosphorylation since it was abrogated by phosphatase treatment (Fig. 2D). Importantly, Rad21 showed a similar pattern in *wpl1Δ* and *pds5Δ* cells (Fig. 2C), suggesting that Rad21 de-phosphorylation is integral to the Wpl1 pathway. Consistently, the Wpl1 induction experiments showed that the bulk of Rad21 is de-phosphorylated in a Wpl1 and PP4-dependent manner (Fig. 2E). Wpl1 activity is therefore coupled with PP4-dependent Rad21 de-phosphorylation.

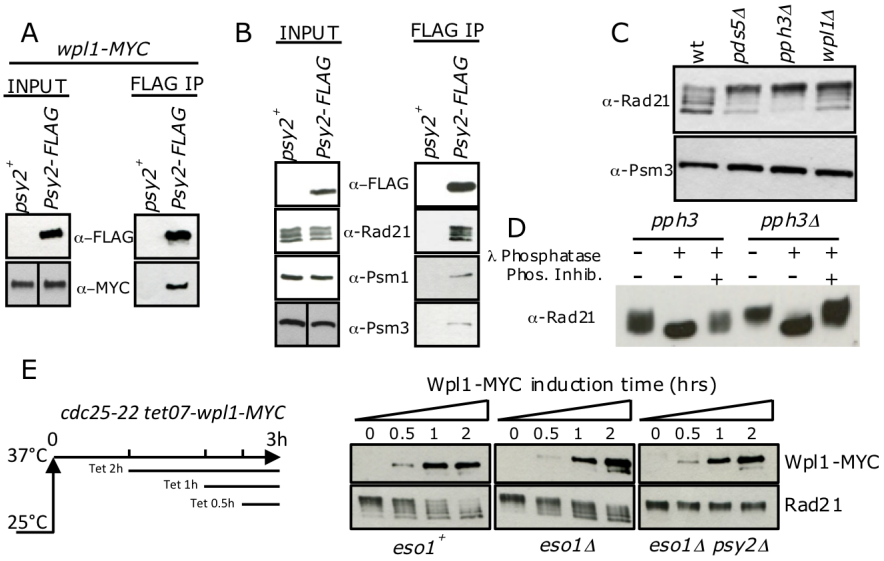


**Fig. 2. Wpl1 activity is coupled with PP4-dependent de-phosphorylation of Rad21.** (**A-B**) The regulatory PP4 subunit Psy2 co-immunoprecipitates Wpl1 (A) and all three core cohesin components (B) from total protein extracts. (**C-D**) Rad21 is hyper-phosphorylated in *pph3*, *pds5* and *wpl1* deletion mutants. In vitro treatment with l phosphatase shows that Rad21 mobility shift is due to phosphorylation (D). (**E**) Western blot analysis of total protein extracts shows that Wpl1 induction in G2 cells triggers PP4-dependent Rad21 de-phosphorylation.

## Identification of key phosphorylated residues within Rad21

To identify the relevant residues, Rad21 was purified from wild-type and *pph3Δ* and analyzed by mass spectrometry. A total of 15 phosphorylated residues were identified with high confidence (Fig. S2 and Table S2). We did not find residues specifically phosphorylated in the absence of Pph3, suggesting that the same set of residues are phosphorylated in wt and *pph3Δ* cells but phosphorylated forms accumulate in the mutant. Quantitative analysis indicated that two serine-rich regions from the central domain of Rad21 were more frequently phosphorylated in *pph3Δ* (Fig. S3 and Table S2). If some of these residues hinder Wpl1 anti-cohesion function when phosphorylated, phospho-mimicking *rad21* alleles may behave similarly and act as *eso1* suppressors. A genetic screen was designed to identify those residues. A combinatorial *rad21* DNA library was synthesized that incorporates either an alanine (non phosphorylatable), a glutamic acid (phospho-mimicking) or a wild-type serine codon for each of the 12 chosen sites (Fig. S4). The library was cloned into an episomal expression vector, transformed into *eso1-H17* and suppressor clones were selected. Individual plasmids were recovered and the *rad21* mutant sequences were inserted at the endogenous *rad21* locus to create *rad21* phospho-mutants. Seven *rad21* alleles were found to suppress the thermosensitive phenotype of *eso1-H17* (Fig.S5). Sequence analysis revealed that all encoded a glutamic acid at position 163 with several suppressors having an additional phospho-mimicking residue at positions 164 or/and 165. To confirm this assumption new *rad21* alleles were generated. A single S to E change at position 163 was sufficient to reduce the thermosensitive phenotype of *eso1-H17*. A better suppression was observed with an additional phospho-mimicking residue at position 164 or 165 and no further suppression was observed with the triple substituted allele *rad21-163E164E165E* (Fig. S5). We therefore focused on the *rad21-S163S164* substitution mutants.

It should be noted at this stage that *pph3Δ* is a better *eso1-H17* suppressor than *rad21-163E164E* (Fig. 3A) indicating that PP4 must have other relevant substrates. The alanine substituted allele *rad21-163A164A* exacerbated the thermosensitive phenotype of *eso1-H17* and partially compromised the suppression by *pph3Δ*, arguing that persistent phosphorylation of Rad21-S163S164 is part of the mechanism by which *pph3Δ* suppresses *eso1-H17*. Finally, *wpl1Δ* was epistatic on *rad21-163A164A* and *rad21-163E164E* for *eso1-H17* suppression

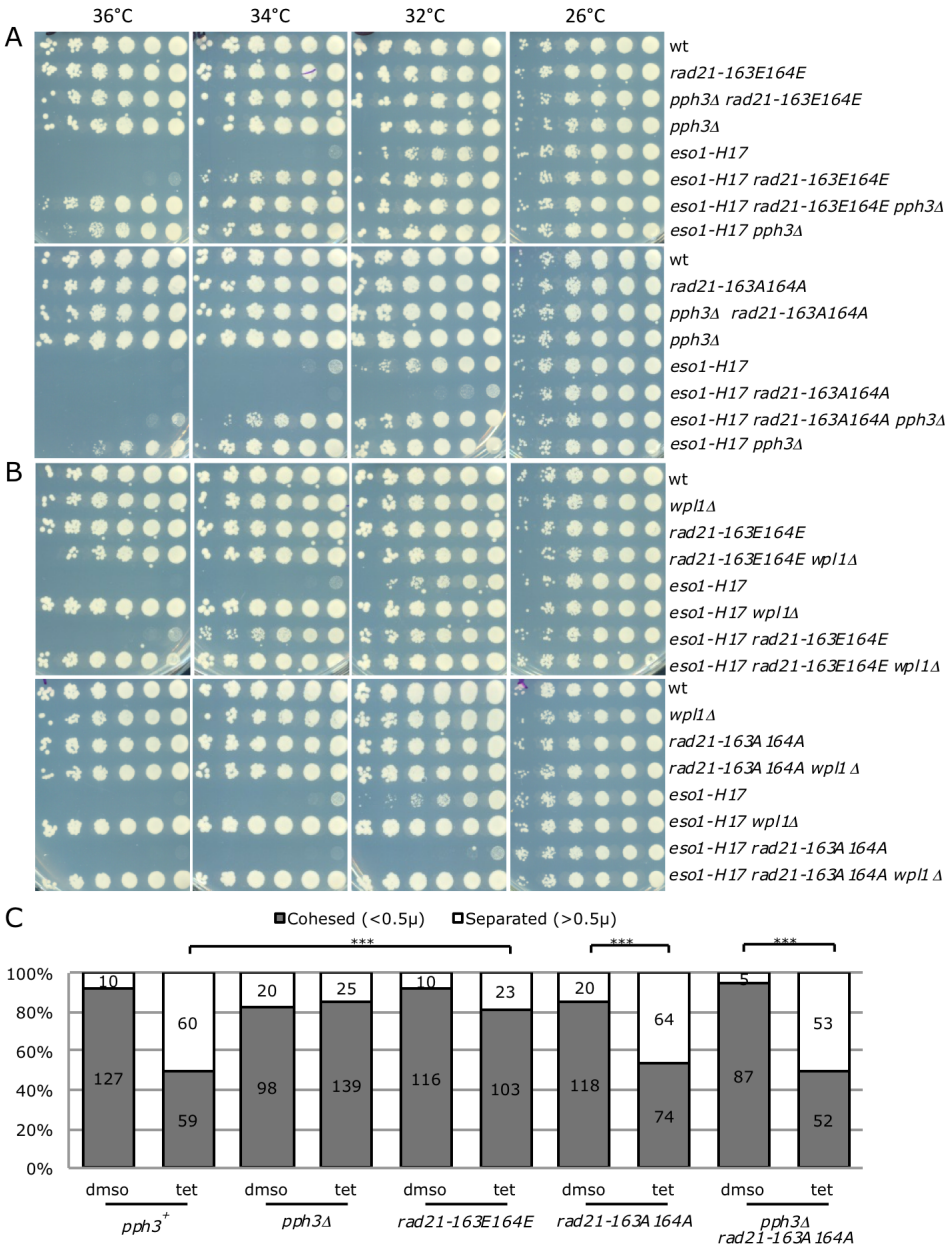


**Fig. 3. The phosphorylation status of Rad21 S163 S164 regulates Wpl1 anti-cohesion function.** (**A-B**) Cell growth assays showing that *rad21-S163E164E* and *rad21-S163A164A* are *eso1-H17* suppressor and enhancer, respectively. (A) Deletion of the *pph3* gene is epistatic *on rad21-163E164E* and conversely, the suppression by *pph3D* is reduced by *rad21-S163AS164A*. (B) *wpl1D* is epistatic on *rad21* phospho-alleles for *eso1-H17* suppression. (**C**) Cen2FISH on metaphase cells. Wpl1-MYC was induced in *cdc25-22 wee1-as8 cut9$^{ts}$ eso1D* cells and sister-chromatid cohesion monitored at metaphase by cen2FISH as in Fig.1. The number of metaphase cells examined is indicated. *** p< 0.0001 Two-sided Fisher's exact test with $\alpha$<0.05.

(Fig. 3B), consistent with the notion that the phosphorylation status of Rad21 modulates Wpl1 function.

To assess the effect of Rad21 phosphorylation on Wpl1 activity, we used the *in vivo* Wpl1 anti-cohesion assay. As before, Wpl1 was induced in *eso1Δ* G2 cells and sister-chromatid cohesion was assayed by cen2FISH at metaphase (Fig. 3C). Wpl1 anti-cohesion activity was reduced in *rad21-163E164E*, largely mimicking the effect of *pph3Δ* while *rad21-163A164A* was essentially neutral. This indicates that Rad21 phosphorylation *per se* is dispensable for sister-chromatid cohesion but protects sister-chromatid cohesion from Wpl1 when de-phosphorylation is prevented. Importantly *pph3Δ* suppression was compromised in a *rad21-163A164A* background, consistent with PP4 acting through the de-phosphorylation of these two residues. Collectively, these data argue that Wpl1 is coupled with PP4-dependent de-phosphorylation of serine residues within the PISSS motif of Rad21 and this event is required for Wpl1 anti-cohesion function.

## Wpl1 induction experiments in *eso1*-deleted cells uncover two cohesin populations

Wpl1 is known to promote cohesin release from DNA, a straightforward mechanism for disrupting sister-chromatid cohesion (*10, 14, 15, 27, 28*). We therefore asked whether the loss of sister-chromatid cohesion in *eso1Δ* cells upon Wpl1 induction was correlated with cohesin release. Wpl1 was induced (TET) or not (DMSO) for two hours in G2 cells in which the cohesin loader Mis4 was inactivated to prevent further cohesin deposition (cohesin loaded in G2 does not form functional cohesion and is prevented here to focus on stably bound cohesin (*15, 16, 18, 29*)). Cells were released into mitosis and arrested at metaphase (Fig. 4A). The status of sister-chromatid cohesion was monitored by cen2FISH (Fig. 4B) and DNA-bound cohesin was measured by Rad21-9PK ChIP at cohesin associated regions (CARs) at and around the region covered by the cen2FISH probe (Fig. 4C). The ratio ChIP TET/ChIP DMSO (Fig. 4D) illustrates the efficiency of Wpl1-dependent cohesin release from DNA (the ratio would be equal to 0 if cohesin was fully dissociated by Wpl1, raw ChIP data are shown in Fig. S6). As expected, Wpl1 induction had little effect in an *eso1*$^{+}$ background. In *eso1Δ* it was expected that Wpl1 would release cohesin from DNA. However, the reaction was far from complete. The efficiency of Wpl1-dependent cohesin release was variable among CARs

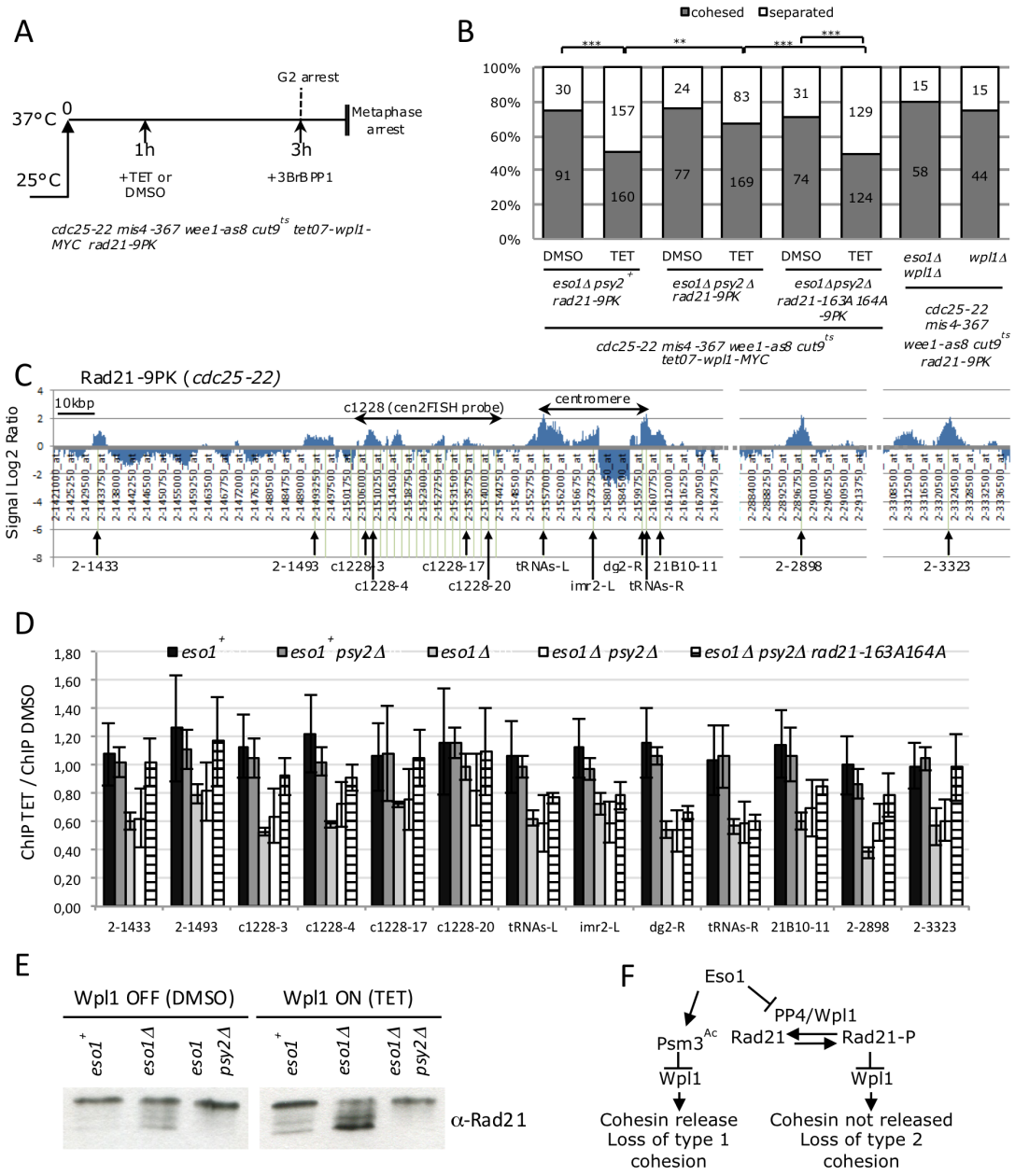


**Fig. 4. Analysis of chromatin-bound Rad21 after Wpl1 induction.** (**A**) Wpl1-MYC was induced as in Fig. 1. The *mis4-367* mutation prevents further cohesin loading at 37°C. (**B**) cen2FISH on metaphase cells. *** p< 0.0001 Two-sided Fisher's exact test with $\alpha$<0.05. (**C**) Cohesin (Rad21-9PK) map at and around the centromere of chromosome 2 in *cdc25-22* arrested cells (32) was used to design primer pairs for chromatin immunoprecipitation (ChIP). (**D**) % of DNA-bound Rad21-9PK left at metaphase after Wpl1-MYC induction in G2. The ratio ChIP TET / ChIP DMSO was calculated from 4 ChIPs pairs (mean +/- SD). (**E**) Western blot analysis of chromatin-bound Rad21 in G2 cells two hours after Wpl1 induction. (**F**) Proposed pathway downstream the Eso1 acetyl-transferase. See text for details.

and a fraction of Rad21 remained bound to DNA at all sites examined. This indicates that DNA-bound cohesin is made of two sub-populations. One is released from DNA in a Wpl1-dependent manner (type 1 cohesin) while the other is not and remains stably bound to DNA although in a non-cohesive state (type 2 cohesin).

## Wpl1 requires PP4 mediated Rad21 de-phosphorylation to abolish type 2 cohesion

In *eso1Δ psy2Δ*, the efficiency of Rad21 release was not significantly affected as compared to *eso1Δ* cells (Fig. 4D) arguing that PP4 is dispensable for Wpl1-dependent cohesin removal (type 1 cohesin). However, sister-chromatid cohesion was significantly improved (Fig. 4B) implying that the fraction of cohesin that remained DNA-bound (type 2 cohesin) was cohesive in *psy2Δ* but not in *psy2*$^{+}$ cells. Importantly, the rescue of sister-chromatid cohesion by *psy2Δ* was abrogated in a *rad21-163A164A* background (Fig. 4BD). This confirms that Rad21-S163S164 is a critical PP4 target and reinforces the notion that type 2 cohesion is sensitive to Wpl1 but in a manner dependent on Rad21-S163S164 de-phosphorylation by PP4. It can be noted that although sister-chromatid cohesion was compromised in a *rad21-163A164A* background, cohesion loss was not correlated with an increase in Wpl1-dependent cohesin release, arguing that cohesion is lost by a mechanism distinct from cohesin removal from DNA.

If this were correct we would expect Rad21 to become de-phosphorylated while remaining chromatin-bound in the above Wpl1 induction experiments. Cell fractionation confirmed that a fraction of Rad21 remained chromatin-bound after Wpl1 induction and further showed that chromatin-bound Rad21 remained phosphorylated when Wpl1 was induced in an *eso1*$^{+}$ background whereas it became de-phosphorylated in a PP4-dependent manner when *eso1* was deleted (Fig. 4E and Fig. S7 for fractionation controls). Hence, Wpl1 triggers PP4-dependent Rad21 de-phosphorylation on chromatin without cohesin release. Chromatin-bound Rad21 remains phosphorylated when Eso1 is functional, consistent with Eso1 acting at the top of the pathway.

# *DISCUSSION*

Collectively, these data suggest the existence of two modes by which cohesin ensures sister-chromatid cohesion (Fig. 4F). In type 1 cohesion, sister-chromatids would be trapped within cohesin and Wpl1 would disrupt cohesion by opening the Psm3-Rad21 interface resulting in cohesin release from DNA and cohesion loss. This type of cohesion is not regulated by PP4. In type 2 cohesion, Wpl1 does not provoke cohesin release but cohesion is nevertheless lost in a Wpl1-dependent manner. Rad21 phosphorylation is an obstacle to this reaction but is erased by PP4 whose activity is coupled with Wpl1. Eso1 acts at the top of the pathway through Psm3 acetylation which would prevent cohesin release (type 1 cohesion) and by protecting Rad21 de-phosphorylation (type 2 cohesion). The mechanism by which Eso1 may shelter Rad21 from PP4 is unknown. Psm3 acetylation does not seem involved as we observed that Rad21 is not hyper-phosphorylated in *psm3-K105NK106N*, a *psm3* allele mimicking the acetylated state ((*16*), data not shown).

The conformation of type 2 cohesin is unknown. To keep on with current models, only one sister chromatid might be released by Wpl1 in a PP4-dependent manner or alternatively, cohesiveness may stem from cohesin-cohesin interactions regulated by Wpl1 and Rad21 phosphorylation. It is worth mentioning that type 2 cohesin may exist in budding yeast since a pool of cohesin remained stably bound to DNA upon inactivation of Eco1 (10) and mutations within the kleisin central region impaired sister-chromatid cohesion while preserving a stable cohesin-DNA interaction (*29*).

We have shown here that the status of Rad21 phosphorylation modulates cohesin susceptibility to Wpl1 with the important implication that sister-chromatid cohesion and possibly the other functions of cohesin may be fine-tuned in space and time by altering the balance between kinase and phosphatase activities. The central region of Rad21 is poorly conserved but numerous phosphorylation sites map to the equivalent region within human Rad21 (*30*). Given the conservation of PP4 and cohesin, a similar mechanism may operate across species, including humans.

# *REFERENCES AND NOTES:*


1. K. Nasmyth, C. H. Haering, Cohesin: its roles and mechanisms. *Annu Rev Genet* **43**, 525 (2009).
2. J. M. Peters, T. Nishiyama, Sister chromatid cohesion. *Cold Spring Harbor perspectives in biology* **4**, (Nov, 2012).
3. S. Remeseiro, A. Losada, Cohesin, a chromatin engagement ring. *Curr Opin Cell Biol* **25**, 63 (Feb).
4. E. Watrin, F. J. Kaiser, K. S. Wendt, Gene regulation and chromatin organization: relevance of cohesin mutations to human disease. *Curr Opin Genet Dev* **37**, 59 (Apr, 2016).
5. C. H. Haering, A. M. Farcas, P. Arumugam, J. Metson, K. Nasmyth, The cohesin ring concatenates sister DNA molecules. *Nature* **454**, 297 (Jul 17, 2008).
6. N. Zhang *et al.*, A handcuff model for the cohesin complex. *J Cell Biol* **183**, 1019 (Dec 15, 2008).
7. C. E. Huang, M. Milutinovich, D. Koshland, Rings, bracelet or snaps: fashionable alternatives for Smc complexes. *Philos Trans R Soc Lond B Biol Sci* **360**, 537 (Mar 29, 2005).
8. T. Eng, V. Guacci, D. Koshland, Interallelic complementation provides functional evidence for cohesin-cohesin interactions on DNA. *Mol Biol Cell* **26**, 4224 (Nov 15, 2015).
9. A. Surcel, D. Koshland, H. Ma, R. T. Simpson, Cohesin interaction with centromeric minichromosomes shows a multi-complex rod-shaped structure. *PLoS One* **3**, e2453 (2008).
10. K. L. Chan *et al.*, Cohesin's DNA exit gate is distinct from its entrance gate and is regulated by acetylation. *Cell* **150**, 961 (Aug 31, 2012).
11. F. Beckouet *et al.*, Releasing Activity Disengages Cohesin's Smc3/Scc1 Interface in a Process Blocked by Acetylation. *Mol Cell* **61**, 563 (Feb 18, 2016).
12. T. G. Gligoris *et al.*, Closing the cohesin ring: structure and function of its Smc3-kleisin interface. *Science* **346**, 963 (Nov 21, 2014).
13. P. J. Huis in 't Veld *et al.*, Characterization of a DNA exit gate in the human cohesin ring. *Science* **346**, 968 (Nov 21, 2014).
14. Y. Murayama, F. Uhlmann, DNA Entry into and Exit out of the Cohesin Ring by an Interlocking Gate Mechanism. *Cell* **163**, 1628 (Dec 17, 2015).
15. P. Bernard *et al.*, Cell-cycle regulation of cohesin stability along fission yeast chromosomes. *EMBO J* **27**, 111 (Jan 9, 2008).
16. A. Feytout, S. Vaur, S. Genier, S. Vazquez, J. P. Javerzat, Psm3 acetylation on conserved lysine residues is dispensable for viability in fission yeast but contributes to Eso1-mediated sister chromatid cohesion by antagonizing Wpl1. *Mol Cell Biol* **31**, 1771 (Apr, 2011).
17. D. Gerlich, B. Koch, F. Dupeux, J. M. Peters, J. Ellenberg, Live-cell imaging reveals a stable cohesin-chromatin interaction after but not before DNA replication. *Curr Biol* **16**, 1571 (Aug 8, 2006).
18. S. Vaur, A. Feytout, S. Vazquez, J. P. Javerzat, Pds5 promotes cohesin acetylation and stable cohesin-chromosome interaction. *EMBO Rep* **13**, 645 (Jul, 2012).
19. A. M. Elbatsh *et al.*, Cohesin Releases DNA through Asymmetric ATPase-Driven Ring Opening. *Mol Cell* **61**, 575 (Feb 18, 2016).
20. T. Nishiyama *et al.*, Sororin mediates sister chromatid cohesion by antagonizing Wapl. *Cell* **143**, 737 (Nov 24, 2010).
21. K. Tanaka *et al.*, Fission yeast Eso1p is required for establishing sister chromatid cohesion during S phase. *Mol. Cell. Biol.* **20**, 3459 (2000).
22. A. Kagami *et al.*, Acetylation regulates monopolar attachment at multiple levels during meiosis I in fission yeast. *EMBO Rep* **12**, 1189 (Nov, 2011).
23. P. T. Cohen, A. Philp, C. Vazquez-Martin, Protein phosphatase 4--from obscurity to vital functions. *FEBS Lett* **579**, 3278 (Jun 13, 2005).

24. C. R. Carlson, B. Grallert, T. Stokke, E. Boye, Regulation of the start of DNA replication in Schizosaccharomyces pombe. *J Cell Sci* **112 ( Pt 6)**, 939 (Mar, 1999).

25. R. P. Birkenbihl, S. Subramani, The rad21 gene product of Schizosaccharomyces pombe is a nuclear, cell cycle-regulated phosphoprotein. *J Biol Chem* **270**, 7703 (Mar 31, 1995).

26. Y. Adachi, A. Kokubu, M. Ebe, K. Nagao, M. Yanagida, Cut1/separase-dependent roles of multiple phosphorylation of fission yeast cohesion subunit Rad21 in post-replicative damage repair and mitosis. *Cell Cycle* **7**, 765 (Mar 15, 2008).

27. R. Gandhi, P. J. Gillespie, T. Hirano, Human Wapl is a cohesin-binding protein that promotes sister-chromatid resolution in mitotic prophase. *Curr Biol* **16**, 2406 (Dec 19, 2006).

28. S. Kueng *et al.*, Wapl controls the dynamic association of cohesin with chromatin. *Cell* **127**, 955 (Dec 1, 2006).

29. T. Eng, V. Guacci, D. Koshland, ROCC, a conserved region in cohesin's Mcd1 subunit, is essential for the proper regulation of the maintenance of cohesion and establishment of condensation. *Mol Biol Cell* **25**, 2351 (Aug 15, 2014).

30. http://www.phosphosite.org/.

31. Y. D. Tay, A. Patel, D. F. Kaemena, I. M. Hagan, Mutation of a conserved residue enhances the sensitivity of analogue-sensitised kinases to generate a novel approach to the study of mitosis in fission yeast. *J Cell Sci* **126**, 5052 (Nov 1, 2013).

32. H. Yamada, K. Kumada, M. Yanagida, Distinct subunit functions and cell cycle regulated phosphorylation of 20S APC/cyclosome required for anaphase in fission yeast. *J Cell Sci* **110 ( Pt 15)**, 1793 (Aug, 1997).

33. C. K. Schmidt, N. Brookes, F. Uhlmann, Conserved features of cohesin binding along fission yeast chromosomes. *Genome Biol* **10**, R52 (2009).

34. S. Moreno, A. Klar, P. Nurse, Molecular genetic analysis of fission yeast Schizosaccharomyces pombe. *Methods Enzymol.* **194**, 795 (1991).

35. J. Bahler *et al.*, Heterologous modules for efficient and versatile PCR-based gene targeting in Schizosaccharomyces pombe. *Yeast* **14**, 943 (Jul, 1998).

36. N. Zilio, S. Wehrkamp-Richter, M. N. Boddy, A new versatile system for rapid control of gene expression in the fission yeast Schizosaccharomyces pombe. *Yeast* **29**, 425 (Oct, 2012).

37. G. Basi, E. Schmid, K. Maundrell, TATA box mutations in the *Schizosaccharomyces pombe nmt1* promoter affect transcription efficiency but not the transcription start point or thiamine repressibility. *Gene* **123**, 131 (1993).

38. A. Woods *et al.*, Definition of individual components within the cytoskeleton of Trypanosoma brucei by a library of monoclonal antibodies. *J. Cell Sci.* **93**, 491 (1989).

39. B. Steglich *et al.*, The Fun30 chromatin remodeler Fft3 controls nuclear organization and chromatin structure of insulators and subtelomeres in fission yeast. *PLoS Genet* **11**, e1005101 (Mar, 2015).

40. T. Mizukami *et al.*, A 13 kb resolution cosmid map of the 14 Mb fission yeast genome by nonrandom sequence-tagged site mapping. *Cell* **73**, 121 (Apr 9, 1993).

41. L. Kall, J. D. Canterbury, J. Weston, W. S. Noble, M. J. MacCoss, Semi-supervised learning for peptide identification from shotgun proteomics datasets. *Nature methods* **4**, 923 (Nov, 2007).

42. T. Taus *et al.*, Universal and confident phosphorylation site localization using phosphoRS. *J Proteome Res* **10**, 5354 (Dec 2, 2011).

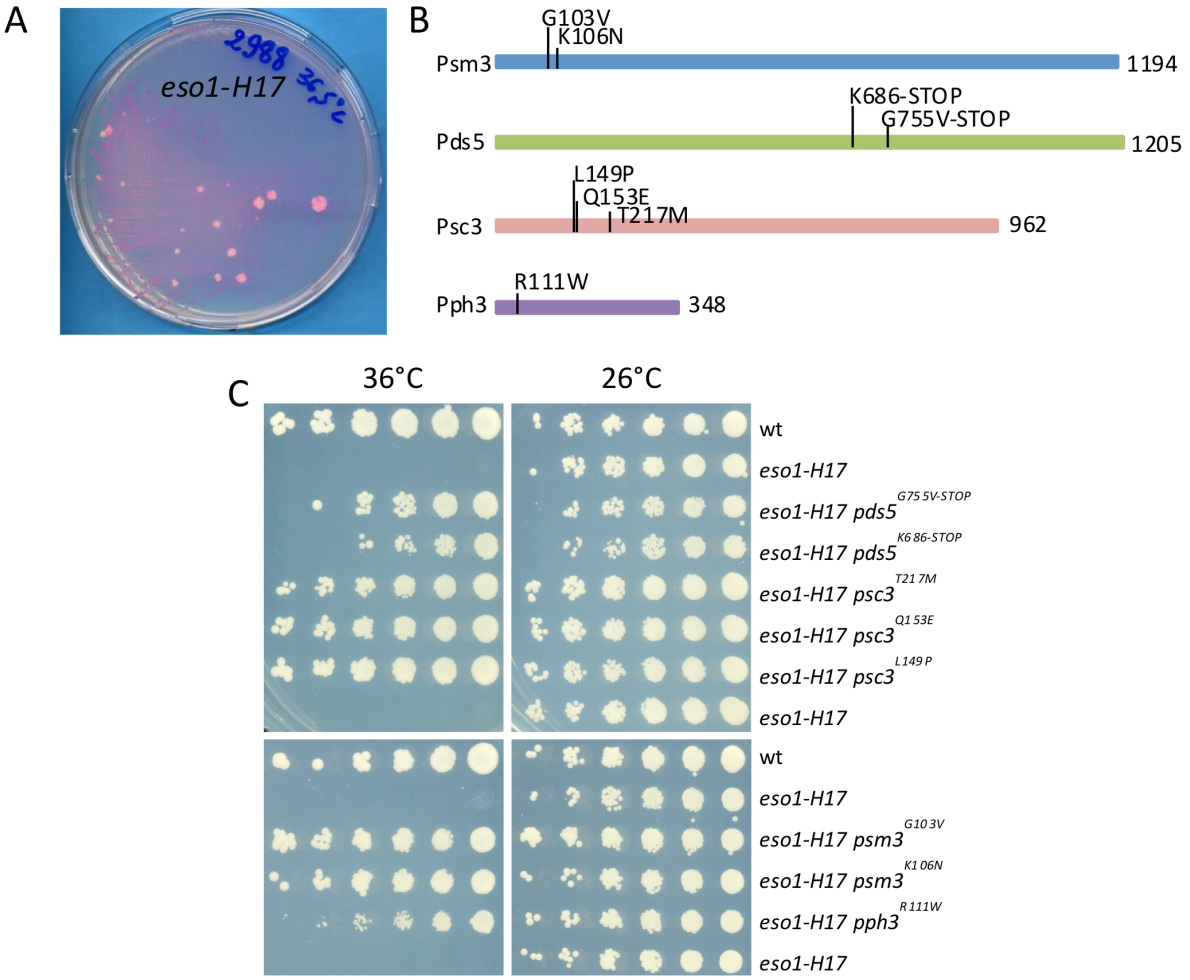


**Fig. S1. Genetic screen for *eso1-H17* suppressors.** (**A**) The *eso1-H17* mutant is thermosensitive for growth (*21*). After 3 days at 36.5°C, spontaneous suppressors emerged as white colonies on an otherwise background of dead cells (colored dark red by the vital dye phloxine B). (**B**) 59 suppressors were isolated. Most (51) were allelic to *wpl1* or *eso1*. Two mapped to *pds5*, three to *psc3* and two to *psm3*. The last mutation was genetically linked to *eso1* (20% recombinants) on the right arm of chromosome 2. The mutation was mapped within the SPBC26H8.05c open reading frame (*pph3*) by tilling array hybridization and sequencing. The mutation (R111W) is located near to the annotated active site (H114) of the phosphatase. (**C**) Cell growth assay showing that all mutants are *eso1-H17* suppressors at 36°C.

**Acknowledgments:** We thank our colleagues Iain Hagan and Nicolas Zilio for the kind gift of reagents and strains. This work was supported by the Centre National de la Recherche Scientifique, l'Université de Bordeaux, la Région Aquitaine, l'Association pour la Recherche sur le Cancer (PJA 2013 1200 205) and l'Agence Nationale de la Recherche (ANR-14-CE10-0020-01). Karen Eguienta was supported by a fellowship from the Ministère de l'Enseignement Supérieur et de la Recherche. Adrien Birot was supported by a fellowship from the Agence Nationale de la Recherche Investissements d'Avenir ANR-10-IDEX-03-02. Karl Ekwall was supported by grants from the Swedish Research Council and Cancer Society.

3789 (*pph3*$^{+}$) Total aa: 628 Covered: 569 Coverage 90.6% P Phospho (S,T) probability 95-100%

MFYSEAILSKKGPLAKVWLAAHWEKKLSKVQTLHTSIEQSVHAIVTEETAPMALRLSGQLMLGVVRIYSR
KARYLLEDCTEALMRLKMSFQPGQVDMIEPATALQSLKGKDAVTQSANLTLPETITEFDLLVPDSTFDFQ
WSQLLRTPSRSSNTLELHSLPI**SSS**PSFPSSQL**S**IEAGRNAQVESGFSLGESFAHVGNDMQFHLPISN**S**G
AATPR**S**VH**S**DNQSQI**S**IEVGRDAPAAAATDLSGIIGPQMTKSPASSVTHFSTPSMLPIGGTSLDDELLAP
VDDLNLDLGLDDLLGDEQGANAPAIEADEQAETSSIHLPSDIMEDDSSRPAAAGVEEGQVVESATAPQQE
KINPQKTVRRQRAIIDPVTELSSKQMKKQLADTSSITSPLCLNTSSIVFNATVNFTRNGKFNTSIFSSNL
NPKVNELLQADFKQAILRKRKNE**S**PEEVEPAKHQRTDTSTENQETAEVLDPEEIAAAELANITEAAIATL
PQETVVQPEGEAPELG**S**PMGFPVTALESADDSLFDAPPVMLDEADLLGSERLD**SS**VSEALPS**S**QTAKDSL
RNKWDPYTEGEKVSFQTLSAGCNREEAVQLFFDVLVLATKDVISVKQDVAIQNEITLTAKRGMLLSSL

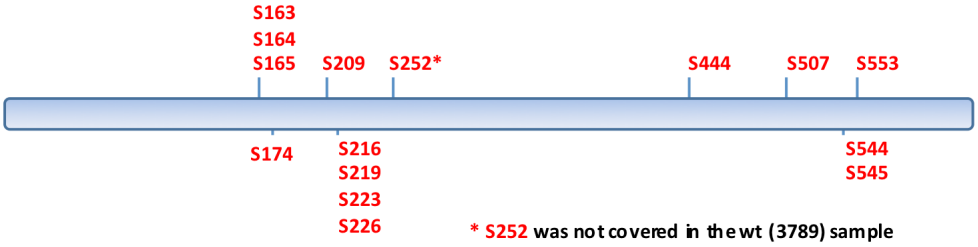


6284 (*pph3Δ*) Total aa: 628 Covered: 554 Coverage 88.2% P Phospho (S,T) probability 95-100%

MFYSEAILSKKGPLAKVWLAAHWEKKLSKVQTLHTSIEQSVHAIVTEETAPMALRLSGQLMLGVVRIYSR
KARYLLEDCTEALMRLKMSFQPGQVDMIEPATALQSLKGKDAVTQSANLTLPETITEFDLLVPDSTFDFQ
WSQLLRTPSRSSNTLELHSLPI**SSS**PSFPSSQL**S**IEAGRNAQVESGFSLGESFAHVGNDMQFHLPISN**S**G
AATPR**S**VH**S**DNQ**S**QI**S**IEVGRDAPAAAATDLSGIIGPQMTK**S**PASSVTHFSTPSMLPIGGTSLDDELLAP
VDDLNLDLGLDDLLGDEQGANAPAIEADEQAETSSIHLPSDIMEDDSSRPAAAGVEEGQVVESATAPQQE
KINPQKTVRRQRAIIDPVTELSSKQMKKQLADTSSITSPLCLNTSSIVFNATVNFTRNGKFNTSIFSSNL
NPKVNELLQADFKQAILRKRKNE**S**PEEVEPAKHQRTDTSTENQETAEVLDPEEIAAAELANITEAAIATL
PQETVVQPEGEAPELG**S**PMGFPVTALESADDSLFDAPPVMLDEADLLGSERLD**SS**VSEALPS**S**QTAKDSL
RNKWDPYTEGEKVSFQTLSAGCNREEAVQLFFDVLVLATKDVISVKQDVAIQNEITLTAKRGMLLSSL

**Fig. S2. Phosphorylated residues identified in Rad21-9PK purified from *pph3*$^{+}$ and *pph3D*.**

# *SUPPLEMENTARY MATERIALS:*

## Materials and Methods

*S. pombe* strains and genetics

General *S. pombe* methods, reagents and media are described in (*33*). All strains are listed in Table S1. Experiments were carried out using YES medium unless otherwise stated. Gene deletions and epitope tagging were performed by gene targeting using polymerase chain reaction (PCR) products (*34*). The *tetO7-wpl1-MYC* allele was constructed as follows. A DNA fragment carrying hphMX-tetO7-Pcyc1 was amplified by PCR using pFA6a-hphMX-tetO-Pcyc1-3xFLAG (*35*) as template and oligonucleotides tet07-wpl1_fw (CATTGTGAGTTGGTACGACCGTGTTCCTCCATTTTTGTAAAGAATCGATGTCAAG CCAGGCGGATTGAAGAAACCTTGAAGAATTCGAGCTCGTTTAAAC) and tet07-wpl1_rev (ACGTCTAAAAAGTTCCAAACTTCCGATTCCGAAGAAATTCTCTTCAAACCATTAT CTTTTTCCTTACATTTTCCTCTTTTCATATTAATTAACCTCCAGG). The tetracycline sensitive repressor was introduced by crossing with *ura4*$^{+}$*-tet*$^{ON}$ (*TetR-tup11D70* integrated at the *ura4* locus (*35*)).

Genetic screen for *eso1-H17* suppressors

Cells from strain 4042 (*h*$^{+}$ *eso1-H17 wpl1*$^{+}$*-hygR*) were plated on YES medium, incubated at 25°C until colony formation and then replica plated at 36°C onto YES plates containing the vital dye phloxine B. After 24h incubation, the replicated colonies stained dark red with phloxine B, insuring that colonies were built from a thermosensitive cell founder. After two to four days at 36°C, white growing sectors (suppressors) appeared and were recovered. To screen out mutations within *wpl1* and *eso1-H17*, the suppressors were crossed with 4043 (*h*$^{-}$ *natR-eso1-H17 Δwpl1::kanR*) and the segregation of the thermosensitive phenotype (Ts) was analyzed within the NatR HygR progeny. Suppressors arising from *eso1-H17* reversion were expected to yield 100% Ts whereas those arising from *wpl1* mutation should be 100% non Ts. Similar crosses with appropriate marked strains were made to identify suppressors linked to the *psm3*, *psc3* and *pds5* loci. Mutations were identified by PCR amplification of the relevant genes and DNA sequencing. One suppressor called *sup111* segregated against all the above loci and mapped ~20cM away from the *eso1* locus on chromosome 2. The mutation was identified by Comparative Genome Sequencing (CGH). Genomic DNA was extracted from the suppressor strain and the wild-type *S. pombe* reference strain, SP972 (strain 2 in Table S1) and co-hybridized to a CGH tiling array (29-32 mer probes with 7 or 8 base spacing from the start of one probe to the start of the next, Roche Nimblegen). The array spanned most of the right arm of chromosome 2, from coordinate 3220000 to coordinate 4720000 (NC_003423, Genbank version NC_003423.3 GI:162312348). DNA regions carrying candidate Single Nucleotide Polymorphisms (SNPs) were used to design a high resolution tiling array (29-30 mer probes tiled such as each candidate SNP is analyzed by 8 probes, 4 on each DNA strand). A single G to A SNP (R111W) was found at position 395548 within SPBC26H8.05c (*pph3*). The mutation was confirmed by PCR and DNA sequencing from two independent *sup111* and wt strains. The *pph3* gene was deleted and genetic analyses showed that *pph3Δ* was allelic to *sup111* and suppressed the Ts phenotype of *eso1-H17*.

Phospho-Quant 140604

| Sequence | Phosphorylated residue | Ratio *pph3Δ / pph3⁺* |
|---|---|---|
| SVHSDNQSQISIEVGR | S216 S219 S226 | 4,43 |
| SVHSDNQSQISIEVGR | S219 S226 | 3,27 |
| SVHSDNQSQISIEVGR | S216 S219 S226 | 3,04 |
| SVHSDNQSQISIEVGR | S216 S219 | 1,91 |
| SVHSDNQSQISIEVGR | S216 S219 | 1,74 |
| LDSSVSEALPSSQTAK | S553 | 1,68 |
| SVHSDNQSQISIEVGR | S219 | 1,63 |
| SSNTLELHSLPISSSPSFPSSQLSIEAGR | S164 S165 | 1,60 |

Phospho-Quant 140630

| Sequence | Phosphorylated residue | Ratio *pph3Δ / pph3⁺* |
|---|---|---|
| SSNTLELHSLPISSSPSFPSSQLSIEAGR | S165 | 123,15 |
| HSLPISSSPSFPSSQL | S165 | 6,89 |
| SVHSDNQSQISIEVGR | S216 | 6,24 |

Phospho-Quant 131008

| Sequence | Phosphorylated residue | Ratio *pph3Δ / pph3⁺* |
|---|---|---|
| SSNTLELHSLPISSSPSFPSSQLSIEAGR | (S164 OR S165) S174 | 84,77 |
| LDSSVSEALPSSQTAK | S545 | 54,23 |
| SVHSDNQSQISIEVGR | S216 | 42,43 |
| SSNTLELHSLPISSSPSFPSSQLSIEAGR | S164 S165 | 7,38 |
| SSNTLELHSLPISSSPSFPSSQLSIEAGR | S165 | 4,04 |
| SVHSDNQSQISIEVGR | S219 | 1,68 |
| SVHSDNQSQISIEVGR | S226 | 1,50 |

**Fig. S3. Two clusters of serine residues (PISS$^{164}$S$^{165}$) and (S$^{216}$VHS$^{219}$DNQSQIS$^{226}$) within Rad21 central region are more frequently phosphorylated in the absence of Pph3.** Phospho-quant analysis was performed from three independent experiments.

Screening of a *rad21* phosphomutant library and creation of *rad21* phosphomutants.

The library of *rad21* phospho-alleles was synthesized and cloned by ThermoFisher Scientific. The entire *rad21* open reading frame was synthesized with randomized codons Ser (33.3%), Ala (33.3%), Glu (33.3%) at each of the 12 chosen positions (163, 164, 165, 167, 170, 171, 216, 219, 223, 226, 314, 315) and the library cloned as NdeI / XmaI fragments into pREP41(*36*).

The library was transformed into strain 2960 (*eso1-H17 leu1-32*) and cells plated on PMG to select for $Leu^+$ transformants. After 24h at 25°C, plates were transferred to 32°C (a restrictive temperature for *eso1-H17* on miminal medium) to select for clones able to rescue the thermosensitive phenotype of *eso1-H17*. Plasmid DNA was recovered by transformation of *E. coli* and transformed back into 2960 to verify that plasmid DNA suppressed the Ts phenotype of *eso1-H17*.

The *rad21* mutant alleles were created by two step gene replacement. As *rad21* is essential for cell survival the constructions were made in a *psm3-rad21* gene fusion background which renders the endogenous *rad21* gene dispensable (*10*). A portion of the *rad21* ORF (from nucleotide 486 to 945) was replaced with the $ura4^+$ gene by one step gene replacement using a PCR fragment generated with primers rad21d(486-945)ura4-fw CATTTGATTTTCAATGGTCTCAACTTCTTCGTACACCCTCTCGTTCTTCGAACACTC TTGAACTACATTCTTTACCAATATAGCTACAAATCCCACTGGC and rad21d(486-945)ura4-rev TCAACAACCTGACCTTCCTCTACTCCTGCTGCTGCAGGACGAGATGAATCATCTTC CATAATGTCAGAAGGGAGATGAATTGTGGTAATGTTGTAGGAGC and the $ura4^+$ gene as a template. The $ura4^+$ sequence was then replaced by homologous recombination with a 1325 bp DNA fragment amplified from the pREPrad21 plasmids carrying the *rad21* alleles of interest using primers rad21+45_FW (AAGGTATGGTTGGCAGCTCAC) and rad21+1369_rev (TCAGTACGTTGGTGCTTGGC). $Ura^-$ clones were selected on 5-fluoroorotic acid containing plates. Correct gene replacement was confirmed by PCR and DNA sequencing of the entire *rad21* gene and the strains backcrossed to eliminate the *psm3-rad21* gene fusion and auxotrophic markers. Twenty *rad21* mutants were generated and placed into an *eso1-H17* background to select for those able to suppress the thermosensitive phenotype.

Wpl1-MYC induction experiments.

All strains carried the thermosensitive *cdc25-22* mutation that prevents entry into mitosis at 37°C. Cells were grown to early log phase at 25°C and shifted to 37°C. In a typical experiment, Wpl1-MYC was induced after 1 hour at 37°C by the addition of 5µg/ml tetracycline (anydrotetracycline hydrochloride SIGMA, stock solution 10mg/ml in DMSO) or DMSO alone for the uninduced condition and the cells kept at 37°C for an additional 2 hours. To assess chromosome segregation during the following mitosis, the cultures were shifted back to 25°C. Cells entered mitosis synchronously and were fixed with 70% ethanol 80 min after transfer to 25°C at which time anaphase cells were the most abundant. Fixed cells were re-hydrated in PBS, stained with DAPI and observed by fluorescence microscopy. Aberrant mitoses were defined by the presence of DAPI-stained material lagging along the cell axis. For FISH and ChIP experiments, cells were released from the *cdc25-22* arrest by the inhibition of Wee1-as8 with 30µM 3-BrB-PP1 (Toronto Research Chemicals Inc., stock solution 50mM in methanol) and arrested at metaphase by the thermosensitive $cut9^{ts}$ mutation as described (*30*). Cells were collected 30 minutes after 3-BrB-PP1 addition, at which time the cell population was mainly composed of metaphase cells (~90% cells with condensed

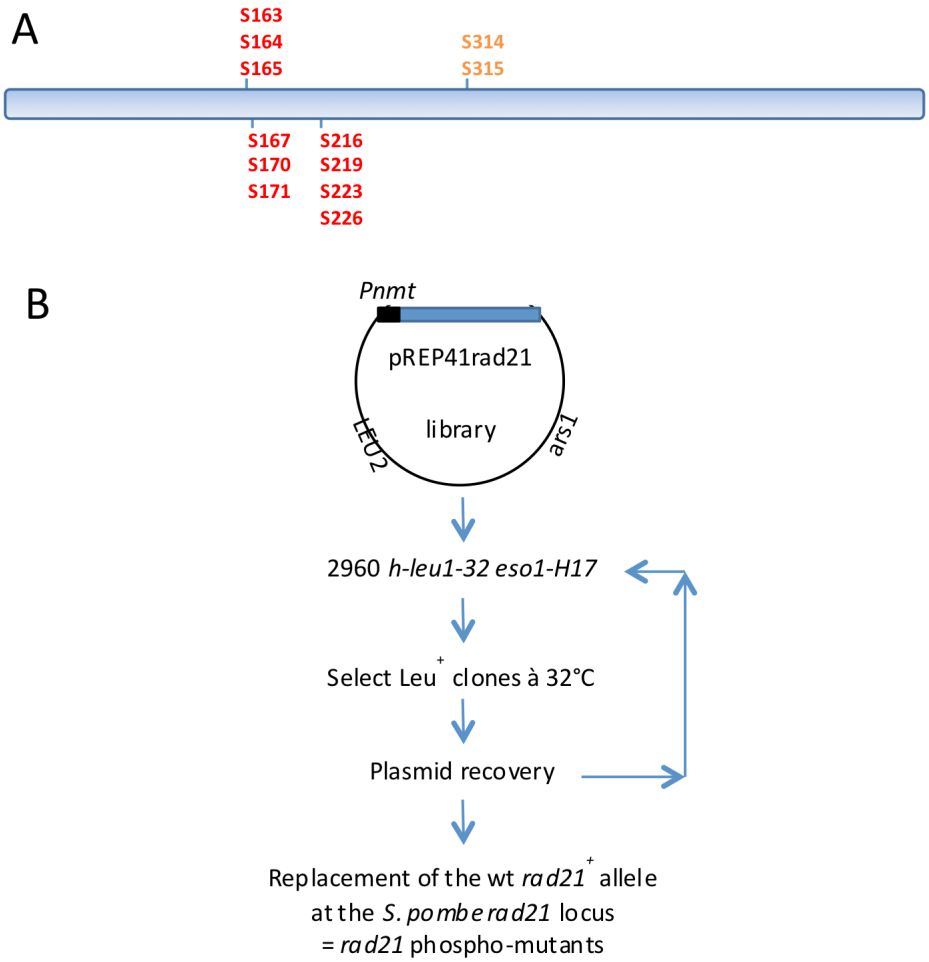


**Fig. S4. Screen for *rad21* phospho-mutants suppressors of *eso1-H17*.** (**A**) A combinatorial *rad21* DNA library was synthesized that incorporates either an alanine (non phosphorylatable), a glutamic acid (phospho-mimicking) or a serine codon for each of the 12 sites shown in the diagram. These include serine residues more frequently phosphorylated in the absence of Pph3 (S164 S165, S216 S219 S226, see Fig. S3 and Table S2) and their neighboring serine residues. We included S314 and S315 as they were detected as phosphorylated only in the absence of Pph3 although with low confidence (only in one experiment and two peptides with an ambiguity on the position of the phosphorylated residue, Table S2). (**B**) Workflow of the selection procedure. The *rad21* DNA library was cloned in the pREP41 vector carrying the down-regulated version of the *nmt* promoter and the *LEU2* selection marker. The library was transformed into a *leu1-32 eso1-H17* recipient strain. Transformants were allowed to grow for 24h at 25°C and then shifted to 32°C (a restrictive temperature for *eso1-H17* on minimal medium). Plasmid DNA was recovered from individual clones and transformed again into strain 2960 to ensure that suppression was conferred by plasmid DNA. The region surrounding the variable codons was used to replace the wild-type *rad21*$^+$ allele to generate *rad21* phospho-mutants. The complexity of the library is $3^{12}$ (~$5x10^5$). About 4-$5x10^5$ transformants were screened, yielding 109 clones able to grow at 32°C. Of these, 36 plasmids were recovered that conferred growth at 32°C when introduced back into strain 2960. Finally, 20 *rad21* phospho-mutants were generated.

chromosomes and loss of the interphase array of microtubule and 70-80% with a metaphase spindle, as seen by DAPI and tubulin staining).

Fluorescence In Situ Hybridization (FISH). Cells were fixed by the addition of paraformaldehyde to a final concentration of 1.8% in 1.2M sorbitol. The flasks were removed from 37°C, incubated at 21°C for 45 min and processed for tubulin staining using TAT1 antibodies (*37*). Cells were refixed and processed for FISH as described (*38*) using the centromere linked c1228 cosmid as a probe (*39*). Metaphase cells were imaged using a Leica DMRXA microscope and a 100X objective. Distances between FISH signals were measured from maximum projections of images created from z series of eight 0.4-μm steps using MetaMorph software.

Chromatin Immunoprecipitation (ChIP). The procedure was as described (*16*) with the following modifications. Cells were fixed for 15 min at 37°C with 2.54% formaldehyde (SIGMA). Fixation was stopped by the addition of 0.125M glycine and samples transferred on ice for 5 min. DNA was recovered using ChIP DNA Clean & Concentrator columns (Zymo Research). ChIP enrichments were calculated as % DNA immunoprecipitated at the locus of interest relative to the input sample. The ratio ChIP TET / ChIP DMSO was calculated from 4 ChIP TET and 4 ChIP DMSO with errors bars representing standard deviation.

General protein methods. Antibodies, protein extracts, immunoprecipitation (IP), Western blotting and cell fractionation were as described (*16, 32*). Lambda phosphatase treatment of Rad21 was performed on Rad21-9PK immunoprecipitated from total cell extracts. Rad21-9PK bound to magnetic beads was washed twice in phosphatase buffer (50 mM HEPES ; 100 mM NaCl; 2 mM DTT; 0.01% Brij 35 pH 7.5) and beads dispensed into three 50μL aliquots (without phosphatase, 400 units phosphatase (New England Biolabs), 400 units phosphatase and 50mM Na-vanadate and 10mM β-glycerophosphate). MnCl2 was added to 1 mM and reactions were carried out for 40 min at 30°C, stopped by addition of Laemmli buffer and heating for 10 min at 95°C.

Mass spectrometry. Rad21 analysis was conducted from five individual mass spectrometry experiments. Rad21-9PK was immunopurified from strains 3789 (wt) and 6284 (*pph3Δ*) using $10^{10}$ cells grown to late log phase at 25°C. Rad21-9PK was eluted in 50μL of Laemmli buffer and the sample loaded onto a preparative 8% PAGE. After a short electrophoresis, the gel was stained with Colloidal Blue and the protein containing band was excised. Gel pieces were destained in 25 mM ammonium bicarbonate 50% ACN, rinsed twice in ultrapure water and shrunk in ACN for 10 min. The proteases used were Trypsin (Proteomic Grade from Sigma), GluC, Chymotrypsin, Thermolysine or Elastase (Sequencing Grade from Promega).

After ACN removal, gel pieces were dried at room temperature, covered with the enzyme solution (10 ng/μL in 40 mM NH4HCO3 and 10% ACN for trypsin; 10 ng/μL in 25 mM NH4HCO3 and 4% CAN pH 4 for GluC), rehydrated at 4°C for 10 min, and finally incubated overnight at 37°C for trypsin or 25°C for GluC. When GluC and trypsin were used in combination, GluC digestion was performed prior to trypsinolysis. Chymotrypsin digestion was conducted overnight at 25°C in Tris-HCl 100 mM,10 mM CaCl2 pH 8. Thermolysine digestion was conducted overnight at 70°C in 50mM Tris-HCl 0.5mM CaCl2 pH 7.8 and Elastase digestion overnight at 37°C in Tris-HCl 50mM pH9.

After proteolysis, supernatants were collected, and an H2O/ACN/HCOOH (47.5:47.5:5) extraction solution was added onto gel pieces for 15 min. The extraction step was repeated twice. Supernatants were pooled and concentrated down to 40 μl before addition of formic acid (0.1% final concentration). Samples were stored at -20°C.

A

| *rad21* allele | Genetic interaction with *eso1-H17* | S163 | S164 | S165 | S167 | S170 | S171 | S216 | S219 | S223 | S226 | S314 | S315 |
|---|---|---|---|---|---|---|---|---|---|---|---|---|---|
| RV38S | Enhancer | A | A | A | A | S | E | A | A | A | S | S | E |
| RV79W1 | Enhancer | A | A | A | A | A | S | S | S | E | E | S | A |
| RV100S1 | Neutral | A | A | E | A | A | E | A | A | A | S | E | S |
| RV53B1 | Neutral | A | E | A | E | E | A | A | E | S | E | S | A |
| RV46I | Neutral | S | A | S | A | S | A | A | S | A | A | A | E |
| RV52L | Neutral | S | A | S | A | S | A | S | S | A | E | E | A |
| RV45T | Neutral | S | A | S | E | A | A | S | A | S | S | E | A |
| RV79K1 | Neutral | S | E | E | S | E | A | A | E | A | A | E | S |
| RV79L1 | Neutral | S | E | E | S | E | A | S | S | E | E | S | A |
| RV18N | Neutral | S | S | E | A | E | E | A | A | A | A | A | S |
| RV37F2 | Neutral | S | A | S | A | A | S | A | A | A | A | S | S |
| RV37G2 | Neutral | S | A | S | A | A | S | A | A | A | A | A | E |
| RV87Y1 | Neutral | A | S | S | A | S | E | A | S | A | A | A | E |
| RV20B | suppressor | E | A | S | A | S | E | A | A | A | A | A | A |
| RV38R | suppressor | E | E | A | A | S | A | A | S | A | A | A | A |
| RV43D | suppressor | E | E | E | A | S | S | S | A | A | A | A | S |
| RV63G1 | suppressor | E | E | S | E | S | E | S | E | A | E | S | E |
| RV25E1 | suppressor | E | E | A | A | A | A | A | S | A | A | E | A |
| RV33C2 | suppressor | E | A | S | A | A | A | S | E | A | E | E | E |
| RV43C | suppressor | E | S | S | A | E | S | S | A | A | A | A | S |

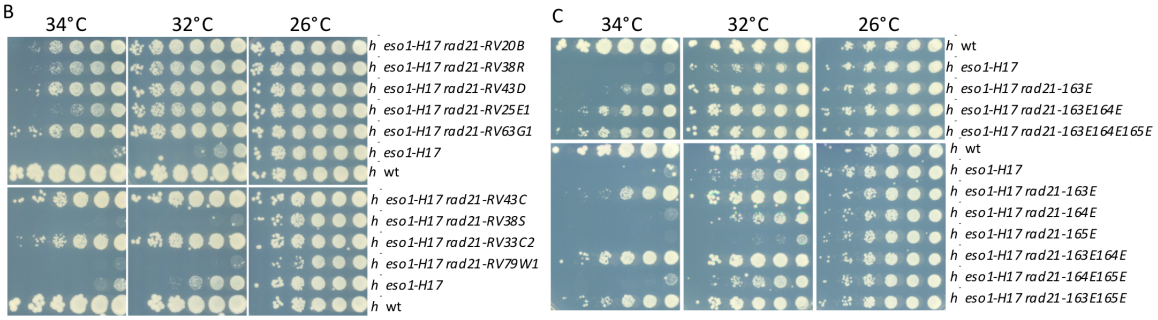


**Fig. S5. *rad21* phosphomutants genetically interact with *eso1-H17*.** (**A**) Primary amino-acid sequence at each of the 12 variable positions encoded by the 20 *rad21* phospho-alleles. All mutants were tested for a genetic interaction with *eso1-H17*. Eleven alleles did not modify the restrictive temperature of *eso1-H17*. Two mutants enhanced the thermosensitive phenotype (enhancer) and 7 behaved as *eso1-H17* suppressors as shown by the cell growth assay (**B**). All suppressors had a phospho-mimetic residue at position 163 (163E) and most had also a glutamic acid at position 164. Conversely, the two enhancers had a non phosphorylatable residue (Alanine) at position 163 and 164 suggesting that the phosphorylation status of S163 and S164 modulates the thermosensitive phenotype of *eso1-H17*. To confirm this assumption, new *rad21* alleles were generated. Cell growth assays (**C**) show that a single phospho-mimicking residue at position 163 (S163E) is sufficient to partially suppress the thermosensitive phenotype of *eso1-H17* and the level of suppression is increased with an additional phospho-mimicking residue at position 164 and/or 165.

The peptide mixtures were analyzed on an Ultimate 3000 nanoLC system (Dionex) coupled to a nanospray LTQ-Orbitrap XL mass spectrometer (ThermoFinnigan, San Jose, CA) or an Electrospray Q-Exactive quadrupole Orbitrap benchtop mass spectrometer (Thermo Fisher Scientific, San Jose, CA).

nLC-MS/MS analysis with LTQ-Orbitrap XL was done as follows. Ten microliters of peptide digests were loaded onto a 300-µm-inner diameter x 5-mm C18 PepMapTM trap column (LC Packings) at a flow rate of 30 µL/min. The peptides were eluted from the trap column onto an analytical 75-mm id x 15-cm C18 Pep-Map column (LC Packings) with a 5–40% linear gradient of solvent B in 95 min (solvent A was 0.1% formic acid in 5% ACN, and solvent B was 0.1% formic acid in 80% ACN). The separation flow rate was set at 200 nL/min. The mass spectrometer operated in positive ion mode at a 1.8-kV needle voltage and a 41-V capillary voltage. Data were acquired in a data-dependent mode, alternating an FTMS scan survey over the range m/z 300–1700 and six ion trap MS/MS scans with CID (Collision Induced Dissociation) as activation mode. MS/MS spectra were acquired using a 3-m/z unit ion isolation window and normalized collision energy of 35. Mono-charged ions and unassigned charge-state ions were rejected from fragmentation. Dynamic exclusion duration was set to 30s.

nLC-MS/MS analysis QX was done by loading ten microliters of peptide digests onto a 300-µm-inner diameter x 5-mm C18 PepMapTM trap column (LC Packings) at a flow rate of 30 µL/min. The peptides were eluted from the trap column onto an analytical 75-mm id x 15-cm C18 Pep-Map column (LC Packings) with a 4–40% linear gradient of solvent B in 108 min (solvent A was 0.1% formic acid in 5% ACN, and solvent B was 0.1% formic acid in 80% ACN). The separation flow rate was set at 300 nL/min. The mass spectrometer operated in positive ion mode at a 1.8-kV needle voltage. Data were acquired using Xcalibur 2.2 software in a data-dependent mode. MS scans (m/z 300-2000) were recorded at a resolution of R = 70000 (@ m/z 200) and an AGC target of 1 x 106 ions collected within 100 ms. Dynamic exclusion was et to 30 s and top 15 ions were selected from fragmentation in HCD mode. MS/MS scans with a target value of 1 x 105 ions were collected with a maximum fill time of 120 ms and a resolution of R = 35000. Additionally, only +2 and +3 charged ions were selected for fragmentation. Other settings were as follows: no sheath nor auxiliary gas flow, heated capillary temperature, 200°C; normalized HCD collision energy of 25% and an isolation width of 3 m/z.

Data were searched by SEQUEST through Proteome Discoverer 1.4 (ThermoFisher Scientific Inc.) against the Rad21-9PK sequence embedded in the *Schizosaccharomyces pombe* Reference Proteome Set (Uniprot version 2014-06; 5092 entries). Spectra from peptides higher than 5000 Da or lower than 350 Da were rejected. The search parameters were as follows: precursor tolerance was set to 10 ppm and fragment tolerance was set at 0.02 Da for FTMS MS/MS data or 0.6 Da for In Trap MS/MS data. Only b- and y-ions were considered for mass calculation. Oxidation of methionine (+16 Da), phosphorylation (+80 Da) were considered as variable modifications and carbamidomethylation of cysteines (+57 Da) was considered as fixed modification. Two missed trypsin cleavages were allowed. Peptide validation was performed using Percolator algorithm (*40*) and only "high confidence" peptides were retained corresponding to a 1% False Positive Rate at peptide level.

Phosphorylation Site Localization and quantitative analysis. To ascertain phosphorylation sites localization PhosphoRS 3.1 (*41*) implemented in Proteome Discoverer was used and a cutoff of 95% for the site probability was applied. MS/MS spectra were visually inspected.

Phosphopeptide abundance was determined from Mass Spectrometry scan survey: Area Under the Curve was determined using Progenesis QI 2.0 (Nonlinear Dynamics Ltd, Newcastle, UK) after alignment of the peptide across compared samples. Alignment quality

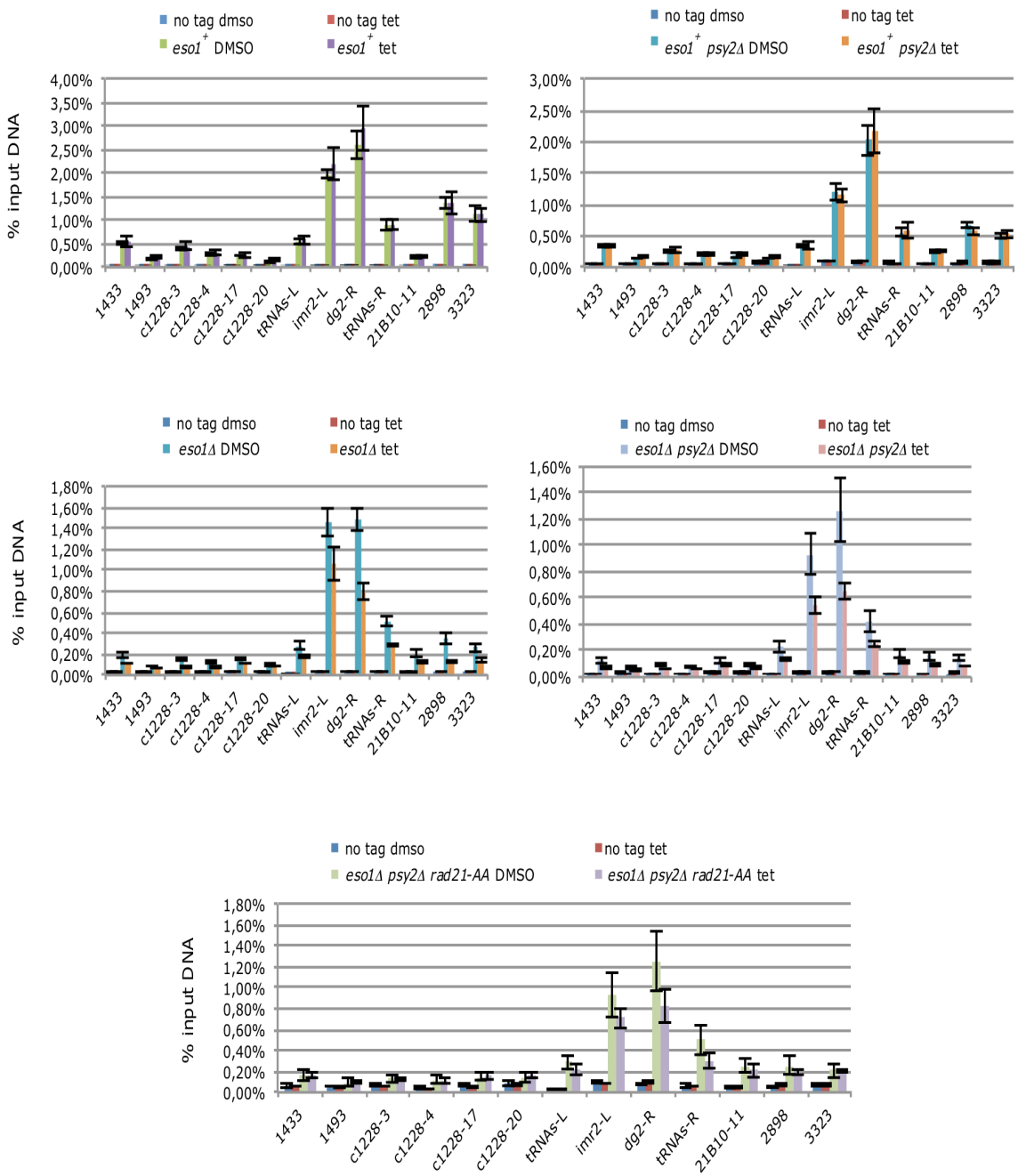


**Fig. S6. Raw ChIP data related to Fig. 4.** The values are the mean +/- SD from 4 ChIPs.

was also manually inspected. Finally, ratios were normalized based on the ratio median of unmodified peptides.

All conducted experiments are listed in Table S2 (Sheet “Experiments”). Database search results are grouped according to strain (3789 vs 6284) and instruments (LTQ-Orbitrap vs Q-Exactive) see sheets “3789-QX”, “6284-QX”, “3789-Orbi” and “6284-Orbi”).

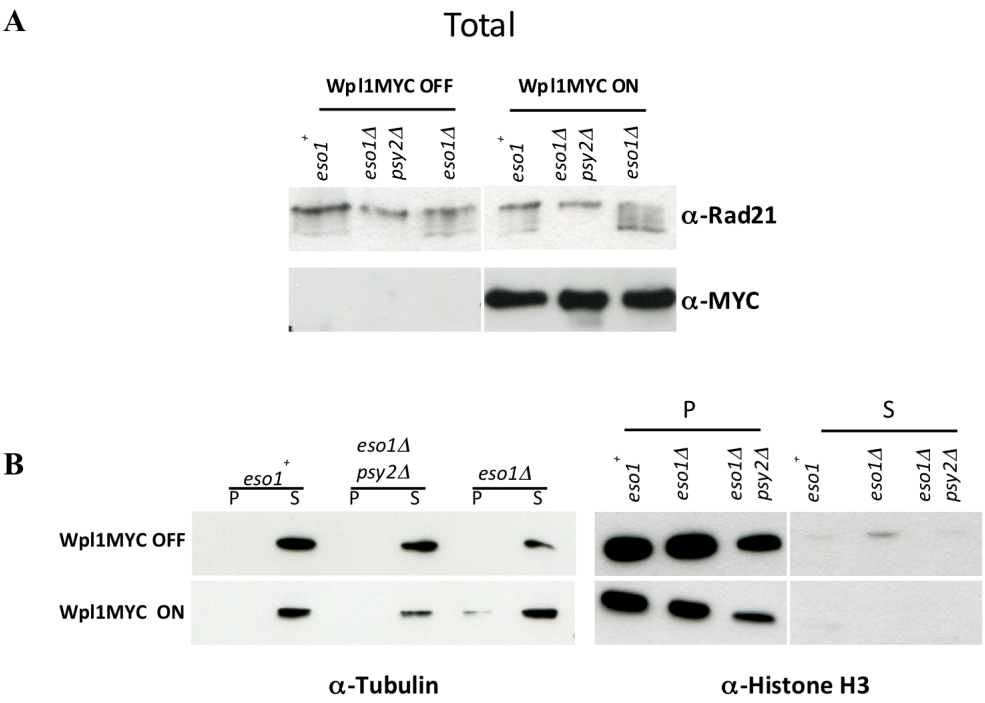


**Fig. S7. Fractionation controls, related to Fig.4.** (**A**) Total protein extracts were analyzed by Western blotting with the indicated antibodies. (**B**) Fractionation was controlled by probing with anti-tubulin antibodies as a marker for soluble proteins (S) and with anti-histone H3 for the chromatin fraction (P).

# Concluding remarks

Cohesin has probably evolved from an ABC type transporter, in which the energy of ATP hydrolysis is converted into a mechanical force driving conformational changes and transportation of small molecules. Cohesin (and Condensin) have an additional subunit, the kleisin that may act as a gate. *In vitro* cohesin loading experiments showed that DNA can enter or exit the cohesin ring at the Smc3-Rad21 interface depending on the ionic strength, suggesting that there is no intrinsic directionality (Murayama and Uhlmann 2015). Rather, the direction would be driven by conformational changes as suggested by the influence of salt. *In vivo*, we assume the directionality to be extremely important: when cohesin must be loaded directionality must be biased towards DNA entry and conversely, a bias towards DNA exit should take place to remove cohesin from DNA. Whereas salt conditions may give directionality *in vitro*, the directionality may be given *in vivo* by interacting proteins or protein modifications.

It is striking to see that a mutation that suppresses cohesin loader deficiency (*pef1Δ*) enhances the defect of a cohesion establishment mutant (*eso1-H17*). Conversely, ablation of PP4 suppresses Eso1 deficiency. Moreover, the two pathways appear to converge on Rad21 and its modification by phosphorylation, suggesting that the directionality of cohesin may be driven by the phosphorylation status of its kleisin. The un-phosphorylated state may favour cohesin loading (DNA entry would be easier) and conversely, the phosphorylated state would act the opposite way. However, this does not fit with the fact that *rad21-163E164E* does not affect *mis4-367* (DNA entry would be less favourable). However, we have to consider DNA exit at the same time. The un-phosphorylated state may increase DNA exit and conversely, the phosphorylated state may reduce it. In other words, the dynamics of cohesin binding to DNA may be increased by un-phosphorylated Rad21 and reduced when the kleisin is phosphorylated. It will be interesting to address this important question *in vivo* using FRAP experiments and *in vitro* using phospho-mimicking Rad21 forms.

A control of cohesin dynamics through the phosphorylation status of its kleisin is appealing as it provides a mean to fine-tune cohesin function in space and time by altering the balance between kinase and phosphatase activities. Along the cell cycle by the rise and fall of CDK activities and locally, through the regulated activity of kinases and phosphatases.

In this study, we focussed on the chromosome segregation function of cohesin. Rad21 modifications may well impinge on the other functions of cohesin. It is of note that *rad21-45* deficient for DSB repair is hypo-phosphorylated (Birkenbihl and Subramani 1995). For what concerns the control of gene expression by cohesin, several *rad21* mutations were found in Cornelia de Lange patients ( Deardorff, Bando, and al. 2012; Deardorff, Wilde, and al. 2012; Minor and al. 2014). More recently, several studies point towards Rad21 mutations as causative for myeloid leukaemia (Fisher and al. 2016). Here Rad21 is thought to act as a negative regulator of hematopoietic self-renewal through repression of Hox genes.

Given the conservation of cohesin across species, the findings reported here may be of general relevance to all eukaryotes, including humans.

# Bibliography


Adachi, Yoh, Aya Kokubu, Masahiro Ebe, Koji Nagao, et Mitsuhiro Yanagida. 2008. « Cut1/Separase-Dependent Roles of Multiple Phosphorylation of Fission Yeast Cohesion Subunit Rad21 in Post-Replicative Damage Repair and Mitosis ». *Cell Cycle (Georgetown, Tex.)* 7 (6): 765‑76. doi:10.4161/cc.7.6.5530.

Allen, Jasmina J., Manqing Li, Craig S. Brinkworth, Jennifer L. Paulson, Dan Wang, Anette Hübner, Wen-Hai Chou, et al. 2007. « A Semisynthetic Epitope for Kinase Substrates ». *Nature Methods* 4 (6): 511‑16. doi:10.1038/nmeth1048.

Anderson, David E., Ana Losada, Harold P. Erickson, et Tatsuya Hirano. 2002. « Condensin and Cohesin Display Different Arm Conformations with Characteristic Hinge Angles ». *The Journal of Cell Biology* 156 (3): 419‑24. doi:10.1083/jcb.200111002.

Andrade, Miguel A, Carlo Petosa, Sean I O'Donoghue, Christoph W Müller, et Peer Bork. 2001. « Comparison of ARM and HEAT protein repeats1 ». *Journal of Molecular Biology* 309 (1): 1‑18. doi:10.1006/jmbi.2001.4624.

Arumugam, Prakash, Stephan Gruber, Koichi Tanaka, Christian H. Haering, Karl Mechtler, et Kim Nasmyth. 2003. « ATP Hydrolysis Is Required for Cohesin's Association with Chromosomes ». *Current Biology: CB* 13 (22): 1941‑53.

Arumugam, Prakash, Tatsuya Nishino, Christian H. Haering, Stephan Gruber, et Kim Nasmyth. 2006. « Cohesin's ATPase Activity Is Stimulated by the C-Terminal Winged-Helix Domain of Its Kleisin Subunit ». *Current Biology: CB* 16 (20): 1998‑2008. doi:10.1016/j.cub.2006.09.002.

Ayté, José, Colleen Schweitzer, Patrick Zarzov, Paul Nurse, et James A. DeCaprio. 2001. « Feedback Regulation of the MBF Transcription Factor by Cyclin Cig2 ». *Nature Cell Biology* 3 (12): 1043‑50. doi:10.1038/ncb1201-1043.

Beckouët, Frederic, Madhusudhan Srinivasan, Maurici Brunet Roig, Kok-Lung Chan, Johanna C. Scheinost, Paul Batty, Bin Hu, et al. 2016. « Releasing Activity Disengages Cohesin's Smc3/Scc1 Interface in a Process Blocked by Acetylation ». *Molecular Cell* 61 (4): 563‑74. doi:10.1016/j.molcel.2016.01.026.

Bellows, Aaron M., Margaret A. Kenna, Lynne Cassimeris, et Robert V. Skibbens. 2003. « Human EFO1p Exhibits Acetyltransferase Activity and Is a Unique Combination of Linker Histone and Ctf7p/Eco1p Chromatid Cohesion Establishment Domains ». *Nucleic Acids Research* 31 (21): 6334‑43.

Bernard, P., J. F. Maure, J. F. Partridge, S. Genier, J. P. Javerzat, et R. C. Allshire. 2001. « Requirement of Heterochromatin for Cohesion at Centromeres ». *Science (New York, N.Y.)* 294 (5551): 2539‑42. doi:10.1126/science.1064027.

Bernard, Pascal, Julie Drogat, Jean-François Maure, Sonia Dheur, Sabine Vaur, Sylvie Genier, et Jean-Paul Javerzat. 2006. « A Screen for Cohesion Mutants Uncovers Ssl3, the Fission Yeast Counterpart of the Cohesin Loading Factor Scc4 ». *Current Biology: CB* 16 (9): 875‑81. doi:10.1016/j.cub.2006.03.037.

Bernard, Pascal, Christine Katrin Schmidt, Sabine Vaur, Sonia Dheur, Julie Drogat, Sylvie Genier, Karl Ekwall, Frank Uhlmann, et Jean-Paul Javerzat. 2008. « Cell-cycle regulation of cohesin stability along fission yeast chromosomes ». *The EMBO journal* 27 (1): 111–121.

Birkenbihl, Rainer P., et Suresh Subramani. 1995. « The rad21 Gene Product of Schizosaccharomyces Pombe Is a Nuclear, Cell Cycle-Regulated Phosphoprotein ». *Journal of Biological Chemistry* 270 (13): 7703‑11. doi:10.1074/jbc.270.13.7703.

Blat, Y., et N. Kleckner. 1999. « Cohesins Bind to Preferential Sites along Yeast Chromosome III, with Differential Regulation along Arms versus the Centric Region ». *Cell* 98 (2): 249‑59.

Carpy, Alejandro, Karsten Krug, Sabine Graf, André Koch, Sasa Popic, Silke Hauf, et Boris Macek. 2014. « Absolute Proteome and Phosphoproteome Dynamics during the Cell Cycle of Schizosaccharomyces Pombe (Fission Yeast) ». *Molecular & Cellular Proteomics: MCP* 13 (8): 1925‑36. doi:10.1074/mcp.M113.035824.

Carretero, María, Miguel Ruiz-Torres, Miriam Rodríguez-Corsino, Isabel Barthelemy, et Ana Losada. 2013. « Pds5B Is Required for Cohesion Establishment and Aurora B Accumulation at Centromeres ». *The EMBO Journal* 32 (22): 2938‑49. doi:10.1038/emboj.2013.230.

Chan, Kok-Lung, Thomas Gligoris, William Upcher, Yuki Kato, Katsuhiko Shirahige, Kim Nasmyth, et Frédéric Beckouët. 2013. « Pds5 Promotes and Protects Cohesin Acetylation ». *Proceedings of the National Academy of Sciences* 110 (32): 13020‑25. doi:10.1073/pnas.1306900110.

Chan, Kok-Lung, Maurici B. Roig, Bin Hu, Frédéric Beckouët, Jean Metson, et Kim Nasmyth. 2012. « Cohesin's DNA Exit Gate Is Distinct from Its Entrance Gate and Is Regulated by Acetylation ». *Cell* 150 (5): 961‑74. doi:10.1016/j.cell.2012.07.028.

Chao, William C. H., Yasuto Murayama, Sofía Muñoz, Alessandro Costa, Frank Uhlmann, et Martin R. Singleton. 2015. « Structural Studies Reveal the Functional Modularity of the Scc2-Scc4 Cohesin Loader ». *Cell Reports* 12 (5): 719‑25. doi:10.1016/j.celrep.2015.06.071.

Chen, Bo-Ruei, Yanhui Li, Jessica R. Eisenstatt, et Kurt W. Runge. 2013. « Identification of a Lifespan Extending Mutation in the Schizosaccharomyces pombe Cyclin Gene clg1 + by Direct Selection of Long-Lived Mutants ». *PLOS ONE* 8 (7): e69084. doi:10.1371/journal.pone.0069084.

Ciosk, R., M. Shirayama, A. Shevchenko, T. Tanaka, A. Toth, A. Shevchenko, et K. Nasmyth. 2000. « Cohesin's Binding to Chromosomes Depends on a Separate Complex Consisting of Scc2 and Scc4 Proteins ». *Molecular Cell* 5 (2): 243‑54.

Coleman, Thomas R., Zhaohua Tang, et William G. Dunphy. 1993. « Negative regulation of the weel protein kinase by direct action of the nim1/cdr1 mitotic inducer ». *Cell* 72 (6): 919‑29. doi:10.1016/0092-8674(93)90580-J.

Connolly, T., M. Caligiuri, et D. Beach. 1997. « The Cdc2 Protein Kinase Controls Cdc10/Sct1 Complex Formation. » *Molecular Biology of the Cell* 8 (6): 1105‑15. doi:10.1091/mbc.8.6.1105.

Coudreuse, Damien, et Paul Nurse. 2010. « Driving the Cell Cycle with a Minimal CDK Control Network ». *Nature* 468 (7327): 1074‑79. doi:10.1038/nature09543.

Deardorff, Matthew A., Masashige Bando, Ryuichiro Nakato, Erwan Watrin, Takehiko Itoh, Masashi Minamino, Katsuya Saitoh, et al. 2012. « HDAC8 Mutations in Cornelia de Lange Syndrome Affect the Cohesin Acetylation Cycle ». *Nature* 489 (7415): 313‑17. doi:10.1038/nature11316.

Deardorff, Matthew A., Jonathan J. Wilde, Melanie Albrecht, Emma Dickinson, Stephanie Tennstedt, Diana Braunholz, Maren Mönnich, et al. 2012. « RAD21 Mutations Cause a Human Cohesinopathy ». *The American Journal of Human Genetics* 90 (6): 1014‑27. doi:10.1016/j.ajhg.2012.04.019.

Edgar, Bruce A., Norman Zielke, et Crisanto Gutierrez. 2014. « Endocycles: A Recurrent Evolutionary Innovation for Post-Mitotic Cell Growth ». Nature Reviews Molecular Cell Biology 15 (3): 197‑210. doi:10.1038/nrm3756.

Eichinger, Christian S., Alexander Kurze, Raquel A. Oliveira, et Kim Nasmyth. 2013. « Disengaging the Smc3/Kleisin Interface Releases Cohesin from Drosophila Chromosomes during Interphase and Mitosis ». *The EMBO Journal* 32 (5): 656‑65. doi:10.1038/emboj.2012.346.

Eng, Thomas, Vincent Guacci, et Douglas Koshland. 2016. « Interallelic Complementation Provides Functional Evidence for Cohesin–cohesin Interactions on DNA ». Consulté le août 22. http://www.molbiolcell.org.

Feeney, Ann J., et Jiyoti Verma-Gaur. 2012. « CTCF-Cohesin Complex: Architect of Chromatin Structure Regulates V(D)J Rearrangement ». *Cell Research* 22 (2): 280‑82. doi:10.1038/cr.2011.188.

Fennessy, Dorota, Agnes Grallert, Andrea Krapp, Adisa Cokoja, Alan J. Bridge, Janni Petersen, Avinash Patel, et al. 2014. « Extending the Schizosaccharomyces pombe Molecular Genetic Toolbox ». *PLOS ONE* 9 (5): e97683. doi:10.1371/journal.pone.0097683.

Fernius, Josefin, et Adele L. Marston. 2009. « Establishment of Cohesion at the Pericentromere by the Ctf19

Kinetochore Subcomplex and the Replication Fork-Associated Factor, Csm3 ». *PLOS Genet* 5 (9): e1000629. doi:10.1371/journal.pgen.1000629.

Fernius, Josefin, Olga O. Nerusheva, Stefan Galander, Flavia de Lima Alves, Juri Rappsilber, et Adele L. Marston. 2013. « Cohesin-Dependent Association of Scc2/4 with the Centromere Initiates Pericentromeric Cohesion Establishment ». *Current Biology* 23 (7): 599‑606. doi:10.1016/j.cub.2013.02.022.

Feytout, Amélie. 2010. *Régulation dynamique de l'association des cohésines aux chromosomes, établissement et maintien de la cohésion des chromatides sœurs*. Bordeaux 2. http://www.theses.fr/2010BOR21773.

Feytout, Amélie, Sabine Vaur, Sylvie Genier, Stéphanie Vazquez, et Jean-Paul Javerzat. 2011. « Psm3 Acetylation on Conserved Lysine Residues Is Dispensable for Viability in Fission Yeast but Contributes to Eso1-

Mediated Sister Chromatid Cohesion by Antagonizing Wpl1 ». *Molecular and Cellular Biology* 31 (8): 1771‑86. doi:10.1128/MCB.01284-10.

Fisher, J. B., J. Peterson, M. Reimer, C. Stelloh, K. Pulakanti, Z. J. Gerbec, A. M. Abel, et al. 2016. « The Cohesin Subunit Rad21 Is a Negative Regulator of Hematopoietic Self-Renewal through Epigenetic Repression of Hoxa7 and Hoxa9 ». *Leukemia*, septembre. doi:10.1038/leu.2016.240.

Fragkos, Michalis, Olivier Ganier, Philippe Coulombe, et Marcel Méchali. 2015. « DNA replication origin activation in space and time ». *Nature Reviews Molecular Cell Biology* 16 (6): 360‑74. doi:10.1038/nrm4002.

Furuya, K., K. Takahashi, et M. Yanagida. 1998. « Faithful Anaphase Is Ensured by Mis4, a Sister Chromatid Cohesion Molecule Required in S Phase and Not Destroyed in G1 Phase ». *Genes & Development* 12 (21): 3408‑18.

Gandhi, Rita, Peter J. Gillespie, et Tatsuya Hirano. 2006. « Human Wapl Is a Cohesin-Binding Protein That Promotes Sister-Chromatid Resolution in Mitotic Prophase ». *Current Biology: CB* 16 (24): 2406‑17. doi:10.1016/j.cub.2006.10.061.

Gerlich, Daniel, Birgit Koch, Florine Dupeux, Jan-Michael Peters, et Jan Ellenberg. 2006. « Live-Cell Imaging Reveals a Stable Cohesin-Chromatin Interaction after but Not before DNA Replication ». *Current Biology* 16 (15): 1571‑78. doi:10.1016/j.cub.2006.06.068.

Gligoris, Thomas G., Johanna C. Scheinost, Frank Bürmann, Naomi Petela, Kok-Lung Chan, Pelin Uluocak, Frédéric Beckouët, Stephan Gruber, Kim Nasmyth, et Jan Löwe. 2014. « Closing the cohesin ring: structure and function of its Smc3-kleisin interface ». *Science (New York, N.Y.)* 346 (6212): 963‑67. doi:10.1126/science.1256917.

Glynn, Earl F., Paul C. Megee, Hong-Guo Yu, Cathy Mistrot, Elcin Unal, Douglas E. Koshland, Joseph L. DeRisi, et Jennifer L. Gerton. 2004. « Genome-Wide Mapping of the Cohesin Complex in the Yeast Saccharomyces cerevisiae ». *PLOS Biol* 2 (9): e259. doi:10.1371/journal.pbio.0020259.

Gregan, Juraj, Chao Zhang, Cornelia Rumpf, Lubos Cipak, Zhang Li, Pelin Uluocak, Kim Nasmyth, et Kevan M. Shokat. 2007. « Construction of Conditional Analog-Sensitive Kinase Alleles in the Fission Yeast Schizosaccharomyces Pombe ». *Nature Protocols* 2 (11): 2996‑3000. doi:10.1038/nprot.2007.447.

Gregan, Juraj, Silvia Polakova, Lijuan Zhang, Iva M. Tolić-Nørrelykke, et Daniela Cimini. 2011. « Merotelic Kinetochore Attachment: Causes and Effects ». Trends in Cell Biology 21 (6): 374‑81. doi:10.1016/j.tcb.2011.01.003.

Gruber, Stephan, Prakash Arumugam, Yuki Katou, Daria Kuglitsch, Wolfgang Helmhart, Katsuhiko Shirahige, et Kim Nasmyth. 2006. « Evidence That Loading of Cohesin onto Chromosomes Involves Opening of Its SMC Hinge ». *Cell* 127 (3): 523‑37. doi:10.1016/j.cell.2006.08.048.

Gruber, Stephan, Christian H Haering, et Kim Nasmyth. 2003. « Chromosomal Cohesin Forms a Ring ». *Cell* 112 (6): 765‑77. doi:10.1016/S0092-8674(03)00162-4.

Guillou, Emmanuelle, Arkaitz Ibarra, Vincent Coulon, Juan Casado-Vela, Daniel Rico, Ignacio Casal, Etienne Schwob, Ana Losada, et Juan Méndez. 2010. « Cohesin Organizes Chromatin Loops at DNA Replication Factories ». *Genes & Development* 24 (24): 2812‑22. doi:10.1101/gad.608210.

Gullerova, Monika, et Nick J. Proudfoot. 2008. « Cohesin Complex Promotes Transcriptional Termination between Convergent Genes in S. pombe ». *Cell* 132 (6): 983‑95. doi:10.1016/j.cell.2008.02.040.

Guse, Annika, Christopher W. Carroll, Ben Moree, Colin J. Fuller, et Aaron F. Straight. 2011. « In vitro centromere and kinetochore assembly on defined chromatin templates ». *Nature* 477 (7364): 354‑58. doi:10.1038/nature10379.

Haering, Christian H., Ana-Maria Farcas, Prakash Arumugam, Jean Metson, et Kim Nasmyth. 2008. « The Cohesin Ring Concatenates Sister DNA Molecules ». *Nature* 454 (7202): 297‑301. doi:10.1038/nature07098.

Haering, Christian H., Jan Löwe, Andreas Hochwagen, et Kim Nasmyth. 2002. « Molecular Architecture of SMC Proteins and the Yeast Cohesin Complex ». *Molecular Cell* 9 (4): 773‑88. doi:10.1016/S1097-2765(02)00515-4.

Haering, Christian H., Doris Schoffnegger, Tatsuya Nishino, Wolfgang Helmhart, Kim Nasmyth, et Jan Löwe. 2004. « Structure and Stability of Cohesin's Smc1-Kleisin Interaction ». *Molecular Cell* 15 (6): 951‑64. doi:10.1016/j.molcel.2004.08.030.

Hartwell, Leland H., Joseph Culotti, et Brian Reid. 1970. « Genetic Control of the Cell-Division Cycle in Yeast, I. Detection of Mutants ». *Proceedings of the National Academy of Sciences of the United States of America* 66 (2): 352‑59.

Heidinger-Pauli, Jill M., Elçin Ünal, et Douglas Koshland. 2009. « Distinct Targets of the Eco1 Acetyltransferase Modulate Cohesion in S Phase and in Response to DNA Damage ». *Molecular Cell* 34 (3): 311‑21. doi:10.1016/j.molcel.2009.04.008.

Higashi, Torahiko L., Megumi Ikeda, Hiroshi Tanaka, Takuro Nakagawa, Masashige Bando, Katsuhiko Shirahige, Yumiko Kubota, Haruhiko Takisawa, Hisao Masukata, et Tatsuro S. Takahashi. 2012. « The Prereplication Complex Recruits XEco2 to Chromatin to Promote Cohesin Acetylation in Xenopus Egg Extracts ». *Current Biology: CB* 22 (11): 977‑88. doi:10.1016/j.cub.2012.04.013.

Hinshaw, Stephen M., Vasso Makrantoni, Alastair Kerr, Adèle L. Marston, et Stephen C. Harrison. 2015. « Structural Evidence for Scc4-Dependent Localization of Cohesin Loading ». *eLife* 4 (juin): e06057. doi:10.7554/eLife.06057.

Holzmann, Johann, Johannes Fuchs, Peter Pichler, Jan-Michael Peters, et Karl Mechtler. 2011. « Lesson from the Stoichiometry Determination of the Cohesin Complex: A Short Protease Mediated Elution Increases the Recovery from Cross-Linked Antibody-Conjugated Beads ». *Journal of Proteome Research* 10 (2): 780‑89. doi:10.1021/pr100927x.

Hou, Fajian, et Hui Zou. 2005. « Two Human Orthologues of Eco1/Ctf7 Acetyltransferases Are Both Required

for Proper Sister-Chromatid Cohesion ». *Molecular Biology of the Cell* 16 (8): 3908‑18. doi:10.1091/mbc.E04-12-1063.

Hu, Bin, Takehiko Itoh, Ajay Mishra, Yuki Katoh, Kok-Lung Chan, William Upcher, Camilla Godlee, Maurici B. Roig, Katsuhiko Shirahige, et Kim Nasmyth. 2011. « ATP Hydrolysis Is Required for Relocating Cohesin from Sites Occupied by Its Scc2/4 Loading Complex ». *Current Biology* 21 (1): 12‑24. doi:10.1016/j.cub.2010.12.004.

Huang, Dongqing, Helena Friesen, et Brenda Andrews. 2007. « Pho85, a Multifunctional Cyclin-Dependent Protein Kinase in Budding Yeast ». *Molecular Microbiology* 66 (2): 303‑14. doi:10.1111/j.1365-2958.2007.05914.x.

Huis in 't Veld, Pim J., Franz Herzog, Rene Ladurner, Iain F. Davidson, Sabina Piric, Emanuel Kreidl, Venugopal Bhaskara, Ruedi Aebersold, et Jan-Michael Peters. 2014. « Characterization of a DNA Exit Gate in the Human Cohesin Ring ». *Science (New York, N.Y.)* 346 (6212): 968‑72. doi:10.1126/science.1256904.

Intyre, John Mc, Eric GD Muller, Stefan Weitzer, Brian E. Snydsman, Trisha N. Davis, et Frank Uhlmann. 2007. « In Vivo Analysis of Cohesin Architecture Using FRET in the Budding Yeast Saccharomyces Cerevisiae ». *The EMBO Journal* 26 (16): 3783‑93. doi:10.1038/sj.emboj.7601793.

Ivanov, Dmitri, et Kim Nasmyth. 2005. « A Topological Interaction between Cohesin Rings and a Circular Minichromosome ». *Cell* 122 (6): 849‑60. doi:10.1016/j.cell.2005.07.018.

Ivanov, Dmitri. 2007. « A Physical Assay for Sister Chromatid Cohesion In Vitro ». *Molecular Cell* 27 (2): 300‑310. doi:10.1016/j.molcel.2007.07.002.

Ivanov, Dmitri, Alexander Schleiffer, Frank Eisenhaber, Karl Mechtler, Christian H. Haering, et Kim Nasmyth. 2002. « Eco1 Is a Novel Acetyltransferase That Can Acetylate Proteins Involved in Cohesion ». *Current Biology: CB* 12 (4): 323‑28.

Khodjakov, Alexey, et Jonathon Pines. 2010. « Centromere Tension: A Divisive Issue ». *Nature Cell Biology* 12 (10): 919‑23. doi:10.1038/ncb1010-919.

Kitajima, Tomoya S., Yousuke Miyazaki, Masayuki Yamamoto, et Yoshinori Watanabe. 2003. « Rec8 Cleavage by Separase Is Required for Meiotic Nuclear Divisions in Fission Yeast ». *The EMBO Journal* 22 (20): 5643‑53. doi:10.1093/emboj/cdg527.

Koch, André, Karsten Krug, Stuart Pengelley, Boris Macek, et Silke Hauf. 2011. « Mitotic Substrates of the Kinase Aurora with Roles in Chromatin Regulation Identified through Quantitative Phosphoproteomics of Fission Yeast ». *Science Signaling* 4 (179): rs6. doi:10.1126/scisignal.2001588.

Kõivomägi, Mardo, Ervin Valk, Rainis Venta, Anna Iofik, Martin Lepiku, David O. Morgan, et Mart Loog. 2011. « Dynamics of Cdk1 Substrate Specificity during the Cell Cycle ». *Molecular Cell* 42 (5): 610‑23. doi:10.1016/j.molcel.2011.05.016.

Kueng, Stephanie, Björn Hegemann, Beate H. Peters, Jesse J. Lipp, Alexander Schleiffer, Karl Mechtler, et Jan-Michael Peters. 2006. « Wapl Controls the Dynamic Association of Cohesin with Chromatin ». *Cell* 127 (5): 955‑67. doi:10.1016/j.cell.2006.09.040.

Kurze, Alexander, Katharine A. Michie, Sarah E. Dixon, Ajay Mishra, Takehiko Itoh, Syma Khalid, Lana Strmecki, et al. 2011. « A Positively Charged Channel within the Smc1/Smc3 Hinge Required for Sister Chromatid Cohesion ». *The EMBO Journal* 30 (2): 364‑78. doi:10.1038/emboj.2010.315.

Ladurner, Rene, Venugopal Bhaskara, Pim J. Huis in 't Veld, Iain F. Davidson, Emanuel Kreidl, Georg Petzold, et Jan-Michael Peters. 2014. « Cohesin's ATPase Activity Couples Cohesin Loading onto DNA with Smc3 Acetylation ». *Current Biology* 24 (19): 2228‑37. doi:10.1016/j.cub.2014.08.011.

Lafont, Andrea L., Jianhua Song, et Susannah Rankin. 2010. « Sororin Cooperates with the Acetyltransferase Eco2 to Ensure DNA Replication-Dependent Sister Chromatid Cohesion ». *Proceedings of the National Academy of Sciences* 107 (47): 20364‑69. doi:10.1073/pnas.1011069107.

Lee, Byung-Gil, Maurici B. Roig, Marijke Jansma, Naomi Petela, Jean Metson, Kim Nasmyth, et Jan Löwe. 2016a. « Crystal Structure of the Cohesin Gatekeeper Pds5 and in Complex with Kleisin Scc1 ». *Cell Reports* 14 (9): 2108‑15. doi:10.1016/j.celrep.2016.02.020.

Lee, Byung-Gil, Maurici B. Roig, Marijke Jansma, Naomi Petela, Jean Metson, Kim Nasmyth, et Jan Löwe. 2016b. « Crystal Structure of the Cohesin Gatekeeper Pds5 and in Complex with Kleisin Scc1 ». *Cell Reports* 14 (9): 2108‑15. doi:10.1016/j.celrep.2016.02.020.

Lengronne, Armelle, Yuki Katou, Saori Mori, Shihori Yokobayashi, Gavin P. Kelly, Takehiko Itoh, Yoshinori Watanabe, Katsuhiko Shirahige, et Frank Uhlmann. 2004. « Cohesin Relocation from Sites of Chromosomal Loading to Places of Convergent Transcription ». *Nature* 430 (6999): 573‑78. doi:10.1038/nature02742.

Lengronne, Armelle, John McIntyre, Yuki Katou, Yutaka Kanoh, Karl-Peter Hopfner, Katsuhiko Shirahige, et Frank Uhlmann. 2006. « Establishment of Sister Chromatid Cohesion at the S. Cerevisiae Replication Fork ». *Molecular Cell* 23 (6): 787‑99. doi:10.1016/j.molcel.2006.08.018.

Liu, F., J. J. Stanton, Z. Wu, et H. Piwnica-Worms. 1997. « The Human Myt1 Kinase Preferentially Phosphorylates Cdc2 on Threonine 14 and Localizes to the Endoplasmic Reticulum and Golgi Complex ». *Molecular and Cellular Biology* 17 (2): 571‑83.

Loog, Mart, et David O. Morgan. 2005. « Cyclin Specificity in the Phosphorylation of Cyclin-Dependent Kinase Substrates ». *Nature* 434 (7029): 104‑8. doi:10.1038/nature03329.

Lopez-Serra, Lidia, Gavin Kelly, Harshil Patel, Aengus Stewart, et Frank Uhlmann. 2014a. « The Scc2-Scc4 Complex Acts in Sister Chromatid Cohesion and Transcriptional Regulation by Maintaining Nucleosome-Free Regions ». *Nature Genetics* 46 (10): 1147‑51. doi:10.1038/ng.3080.

Lopez-Serra, Lidia. 2014b. « The Scc2-Scc4 Complex Acts in Sister Chromatid Cohesion and Transcriptional Regulation by Maintaining Nucleosome-Free Regions ». *Nature Genetics* 46 (10): 1147‑51. doi:10.1038/ng.3080.

Lopez-Serra, Lidia, Armelle Lengronne, Vanessa Borges, Gavin Kelly, et Frank Uhlmann. 2013. « Budding Yeast Wapl Controls Sister Chromatid Cohesion Maintenance and Chromosome Condensation ». *Current Biology* 23 (1): 64‑69. doi:10.1016/j.cub.2012.11.030.

Maradeo, Marie E., et Robert V. Skibbens. 2009. « The Elg1-RFC Clamp-Loading Complex Performs a Role in Sister Chromatid Cohesion ». *PloS One* 4 (3): e4707. doi:10.1371/journal.pone.0004707.

Maresca, Thomas J., et E. D. Salmon. 2010. « Welcome to a New Kind of Tension: Translating Kinetochore Mechanics into a Wait-Anaphase Signal ». *J Cell Sci* 123 (6): 825‑35. doi:10.1242/jcs.064790.

Mayer, M. L., S. P. Gygi, R. Aebersold, et P. Hieter. 2001. « Identification of RFC(Ctf18p, Ctf8p, Dcc1p): An Alternative RFC Complex Required for Sister Chromatid Cohesion in S. Cerevisiae ». *Molecular Cell* 7 (5): 959‑70.

Megee, P. C., C. Mistrot, V. Guacci, et D. Koshland. 1999. « The Centromeric Sister Chromatid Cohesion Site Directs Mcd1p Binding to Adjacent Sequences ». *Molecular Cell* 4 (3): 445‑50.

Mehta, Gunjan D., Ravinder Kumar, Sanjeeva Srivastava, et Santanu Kumar Ghosh. 2013. « Cohesin: Functions beyond Sister Chromatid Cohesion ». *FEBS Letters* 587 (15): 2299‑2312. doi:10.1016/j.febslet.2013.06.035.

Merkenschlager, Matthias, et Elphège P. Nora. 2016. « CTCF and Cohesin in Genome Folding and Transcriptional Gene Regulation ». *Annual Review of Genomics and Human Genetics* 17 (1): 17‑43. doi:10.1146/annurev-genom-083115-022339.

Minor, Agata, Marwan Shinawi, Jacob S. Hogue, Marisa Vineyard, Damara R. Hamlin, Christopher Tan, Kirsten Donato, et al. 2014. « Two novel RAD21 mutations in patients with mild Cornelia de Lange syndrome-like presentation and report of the first familial case ». *Gene* 537 (2): 279‑84. doi:10.1016/j.gene.2013.12.045.

Mizukami, Toru, William I. Chang, Igor Garkavtsev, Nancy Kaplan, Diane Lombardi, Tomohiro Matsumoto, Osami Niwa, et al. 1993. « A 13 kb resolution cosmid map of the 14 Mb fission yeast genome by nonrandom sequence-tagged site mapping ». *Cell* 73 (1): 121‑32. doi:10.1016/0092-8674(93)90165-M.

Moser, Bettina A, et Paul Russell. 2000. « Cell cycle regulation in Schizosaccharomyces pombe ». Current Opinion in Microbiology 3 (6): 631‑36. doi:10.1016/S1369-5274(00)00152-1.

Muir, Kyle W., Marc Kschonsak, Yan Li, Jutta Metz, Christian H. Haering, et Daniel Panne. 2016. « Structure of the Pds5-Scc1 Complex and Implications for Cohesin Function ». *Cell Reports* 14 (9): 2116‑26. doi:10.1016/j.celrep.2016.01.078.

Murayama, Yasuto, et Frank Uhlmann. 2014. « Biochemical Reconstitution of Topological DNA Binding by the Cohesin Ring ». *Nature* 505 (7483): 367‑71. doi:10.1038/nature12867.

Murayama, Yasuto, et Frank Uhlmann. 2015. « DNA Entry into and Exit out of the Cohesin Ring by an Interlocking Gate Mechanism ». *Cell* 163 (7): 1628‑40. doi:10.1016/j.cell.2015.11.030.

Muzi Falconi, M., G. W. Brown, et T. J. Kelly. 1996. « cdc18+ Regulates Initiation of DNA Replication in Schizosaccharomyces Pombe ». *Proceedings of the National Academy of Sciences of the United States of America* 93 (4): 1566‑70.

Nagy, Gergely, Erik Czipa, László Steiner, Tibor Nagy, Sándor Pongor, László Nagy, et Endre Barta. 2016. « Motif Oriented High-Resolution Analysis of ChIP-Seq Data Reveals the Topological Order of CTCF and Cohesin Proteins on DNA ». *BMC Genomics* 17 (1). doi:10.1186/s12864-016-2940-7.

Natsume, Toyoaki, Carolin A. Müller, Yuki Katou, Renata Retkute, Marek Gierliński, Hiroyuki Araki, J. Julian Blow, Katsuhiko Shirahige, Conrad A. Nieduszynski, et Tomoyuki U. Tanaka. 2013. « Kinetochores Coordinate Pericentromeric Cohesion and Early DNA Replication by Cdc7-Dbf4 Kinase Recruitment ». *Molecular Cell* 50 (5): 661‑74. doi:10.1016/j.molcel.2013.05.011.

Nishiyama, Tomoko, Rene Ladurner, Julia Schmitz, Emanuel Kreidl, Alexander Schleiffer, Venugopal Bhaskara, Masashige Bando, et al. 2010. « Sororin Mediates Sister Chromatid Cohesion by Antagonizing Wapl ». *Cell* 143 (5): 737‑49. doi:10.1016/j.cell.2010.10.031.

Nonaka, Nobuhiro, Tomoya Kitajima, Shihori Yokobayashi, Guoping Xiao, Masayuki Yamamoto, Shiv I. S. Grewal, et Yoshinori Watanabe. 2002. « Recruitment of Cohesin to Heterochromatic Regions by Swi6/HP1 in Fission Yeast ». *Nature Cell Biology* 4 (1): 89‑93. doi:10.1038/ncb739.

Ocampo-Hafalla, Maria, Sofía Muñoz, Catarina P. Samora, et Frank Uhlmann. 2016. « Evidence for Cohesin Sliding along Budding Yeast Chromosomes ». *Open Biology* 6 (6): 150178. doi:10.1098/rsob.150178.

Pauli, Andrea, Friederike Althoff, Raquel A. Oliveira, Stefan Heidmann, Oren Schuldiner, Christian F. Lehner, Barry J. Dickson, et Kim Nasmyth. 2008. « Cell-Type-Specific TEV Protease Cleavage Reveals Cohesin Functions in Drosophila Neurons ». *Developmental Cell* 14 (2): 239‑51. doi:10.1016/j.devcel.2007.12.009.

Remeseiro, Silvia, Ana Cuadrado, et Ana Losada. 2013. « Cohesin in Development and Disease ». *Development* 140 (18): 3715‑18. doi:10.1242/dev.090605.

Remeseiro, Silvia, et Ana Losada. 2013. « Cohesin, a chromatin engagement ring ». *Current Opinion in Cell Biology*, Cell architecture, 25 (1): 63‑71. doi:10.1016/j.ceb.2012.10.013.

Rieder, C. L., R. W. Cole, A. Khodjakov, et G. Sluder. 1995. « The Checkpoint Delaying Anaphase in Response to Chromosome Monoorientation Is Mediated by an Inhibitory Signal Produced by Unattached Kinetochores. » *The Journal of Cell Biology* 130 (4): 941‑48. doi:10.1083/jcb.130.4.941.

Rolef Ben-Shahar, Tom, Sebastian Heeger, Chris Lehane, Philip East, Helen Flynn, Mark Skehel, et Frank Uhlmann. 2008. « Eco1-Dependent Cohesin Acetylation during Establishment of Sister Chromatid Cohesion ». *Science (New York, N.Y.)* 321 (5888): 563‑66. doi:10.1126/science.1157774.

Rudra, Soumya, et Robert V. Skibbens. 2013. « Chl1 DNA Helicase Regulates Scc2 Deposition Specifically during DNA-Replication in Saccharomyces Cerevisiae ». *PloS One* 8 (9): e75435. doi:10.1371/journal.pone.0075435.

Russo, A. A., P. D. Jeffrey, et N. P. Pavletich. 1996. « Structural Basis of Cyclin-Dependent Kinase Activation by Phosphorylation ». *Nature Structural Biology* 3 (8): 696‑700.

Sakuno, Takeshi, Kenji Tada, et Yoshinori Watanabe. 2009. « Kinetochore Geometry Defined by Cohesion within the Centromere ». *Nature* 458 (7240): 852‑58. doi:10.1038/nature07876.

Samora, Catarina P., Julie Saksouk, Panchali Goswami, Ben O. Wade, Martin R. Singleton, Paul A. Bates, Armelle Lengronne, Alessandro Costa, et Frank Uhlmann. 2016. « Ctf4 Links DNA Replication with Sister Chromatid Cohesion Establishment by Recruiting the Chl1 Helicase to the Replisome ». *Molecular Cell* 63 (3): 371‑84. doi:10.1016/j.molcel.2016.05.036.

Schmidt, Christine K., Neil Brookes, et Frank Uhlmann. 2009. « Conserved Features of Cohesin Binding along Fission Yeast Chromosomes ». *Genome Biology* 10 (5): R52. doi:10.1186/gb-2009-10-5-r52.

Schulman, Brenda A., Derek L. Lindstrom, et Ed Harlow. 1998. « Substrate Recruitment to Cyclin-Dependent Kinase 2 by a Multipurpose Docking Site on Cyclin A ». *Proceedings of the National Academy of Sciences* 95 (18): 10453‑58.

Sclafani, R. A., et T. M. Holzen. 2007. « Cell Cycle Regulation of DNA Replication ». *Annual Review of Genetics* 41 (1): 237‑80. doi:10.1146/annurev.genet.41.110306.130308.

Simchen, G. 1978. « Cell Cycle Mutants ». *Annual Review of Genetics* 12 (1): 161‑91. doi:10.1146/annurev.ge.12.120178.001113.

Sjögren, Camilla, et Kim Nasmyth. 2001. « Sister chromatid cohesion is required for postreplicative double-strand break repair in Saccharomyces cerevisiae ». *Current Biology* 11 (12): 991–995.

Sjögren, Camilla, et Lena Ström. 2010. « S-Phase and DNA Damage Activated Establishment of Sister Chromatid Cohesion--Importance for DNA Repair ». *Experimental Cell Research* 316 (9): 1445‑53. doi:10.1016/j.yexcr.2009.12.018.

Skibbens, Robert V., Laura B. Corson, Doug Koshland, et Philip Hieter. 1999. « Ctf7p Is Essential for Sister Chromatid Cohesion and Links Mitotic Chromosome Structure to the DNA Replication Machinery ». *Genes & Development* 13 (3): 307‑19.

Steever, Alexander B., Achim Wach, PETER PHILIPPSEN, et John R. Pringle. 1998. « Heterologous modules for efficient and versatile PCR-based gene targeting in Schizosaccharomyces pombe ». *Yeast* 14: 943–951.

Steglich, Babett, Annelie Strålfors, Olga Khorosjutina, Jenna Persson, Agata Smialowska, Jean-Paul Javerzat, et Karl Ekwall. 2015. « The Fun30 Chromatin Remodeler Fft3 Controls Nuclear Organization and Chromatin Structure of Insulators and Subtelomeres in Fission Yeast ». *PLOS Genet* 11 (3): e1005101. doi:10.1371/journal.pgen.1005101.

Stigler, Johannes, Gamze Ö. Çamdere, Douglas E. Koshland, et Eric C. Greene. 2016. « Single-Molecule Imaging Reveals a Collapsed Conformational State for DNA-Bound Cohesin ». *Cell Reports* 15 (5): 988‑98. doi:10.1016/j.celrep.2016.04.003.

Ström, Lena, Hanna Betts Lindroos, Katsuhiko Shirahige, et Camilla Sjögren. 2004. « Postreplicative Recruitment of Cohesin to Double-Strand Breaks Is Required for DNA Repair ». *Molecular Cell* 16 (6): 1003‑15. doi:10.1016/j.molcel.2004.11.026.

Takagi, Masatoshi, Keigo Bunai, Ken-ichiro Yanagi, et Naoko Imamoto. 2008. « Cloning of Xenopus Orthologs of Ctf7/Eco1 Acetyltransferase and Initial Characterization of XEco2 ». *The FEBS Journal* 275 (24): 6109‑22. doi:10.1111/j.1742-4658.2008.06736.x.

Takahashi, Tatsuro S., Pannyun Yiu, Michael F. Chou, Steven Gygi, et Johannes C. Walter. 2004. « Recruitment of Xenopus Scc2 and Cohesin to Chromatin Requires the Pre-Replication Complex ». *Nature Cell Biology* 6 (10): 991‑96. doi:10.1038/ncb1177.

Tanaka, K., et H. Okayama. 2000. « A Pcl-like Cyclin Activates the Res2p-Cdc10p Cell Cycle “start” transcriptional Factor Complex in Fission Yeast ». *Molecular Biology of the Cell* 11 (9): 2845‑62.

Tanaka, K., T. Yonekawa, Y. Kawasaki, M. Kai, K. Furuya, M. Iwasaki, H. Murakami, M. Yanagida, et H. Okayama. 2000. « Fission Yeast Eso1p Is Required for Establishing Sister Chromatid Cohesion during S Phase ». *Molecular and Cellular Biology* 20 (10): 3459‑69.

Tanaka, T., M. P. Cosma, K. Wirth, et K. Nasmyth. 1999. « Identification of Cohesin Association Sites at Centromeres and along Chromosome Arms ». *Cell* 98 (6): 847‑58.

Tedeschi, Antonio, Gordana Wutz, Sébastien Huet, Markus Jaritz, Annelie Wuensche, Erika Schirghuber, Iain Finley Davidson, et al. 2013. « Wapl is an essential regulator of chromatin structure and chromosome segregation ». *Nature* 501 (7468): 564‑68. doi:10.1038/nature12471.

Terret, Marie-Emilie, Rebecca Sherwood, Sadia Rahman, Jun Qin, et Prasad V. Jallepalli. 2009. « Cohesin Acetylation Speeds the Replication Fork ». *Nature* 462 (7270): 231‑34. doi:10.1038/nature08550.

Tomonaga, Takeshi, Koji Nagao, Yosuke Kawasaki, Kanji Furuya, Akiko Murakami, Jun Morishita, Tatsuro Yuasa, et al. 2000. « Characterization of Fission Yeast Cohesin: Essential Anaphase Proteolysis of Rad21 Phosphorylated in the S Phase ». *Genes & Development* 14 (21): 2757‑70. doi:10.1101/gad.832000.

Toselli-Mollereau, Esther, Xavier Robellet, Lydia Fauque, Sébastien Lemaire, Christoph Schiklenk, Carlo Klein, Clémence Hocquet, et al. 2016. « Nucleosome Eviction in Mitosis Assists Condensin Loading and Chromosome Condensation ». *The EMBO Journal* 35 (14): 1565‑81. doi:10.15252/embj.201592849.

Tóth, Attila, Rafal Ciosk, Frank Uhlmann, Marta Galova, Alexander Schleiffer, et Kim Nasmyth. 1999. « Yeast Cohesin Complex Requires a Conserved Protein, Eco1p(Ctf7), to Establish Cohesion between Sister Chromatids during DNA Replication ». *Genes & Development* 13 (3): 320‑33.

Toyoda, Yusuke, Kanji Furuya, Gohta Goshima, Koji Nagao, Kohta Takahashi, et Mitsuhiro Yanagida. 2002. « Requirement of Chromatid Cohesion Proteins rad21/scc1 and mis4/scc2 for Normal Spindle-Kinetochore Interaction in Fission Yeast ». *Current Biology: CB* 12 (5): 347‑58.

Uhlmann, F., F. Lottspeich, et K. Nasmyth. 1999. « Sister-Chromatid Separation at Anaphase Onset Is Promoted by Cleavage of the Cohesin Subunit Scc1 ». *Nature* 400 (6739): 37‑42. doi:10.1038/21831.

Uhlmann, F., D. Wernic, M. A. Poupart, E. V. Koonin, et K. Nasmyth. 2000. « Cleavage of Cohesin by the CD Clan Protease Separin Triggers Anaphase in Yeast ». *Cell* 103 (3): 375‑86.

Vaur, Sabine, Amélie Feytout, Stéphanie Vazquez, et Jean-Paul Javerzat. 2012. « Pds5 Promotes Cohesin Acetylation and Stable Cohesin–chromosome Interaction ». *EMBO Reports* 13 (7): 645‑52. doi:10.1038/embor.2012.72.

Vega, Hugo, Quinten Waisfisz, Miriam Gordillo, Norio Sakai, Itaru Yanagihara, Minoru Yamada, Djoke van Gosliga, et al. 2005. « Roberts Syndrome Is Caused by Mutations in ESCO2, a Human Homolog of Yeast ECO1 That Is Essential for the Establishment of Sister Chromatid Cohesion ». *Nature Genetics* 37 (5): 468‑70. doi:10.1038/ng1548.

Waizenegger, Irene C, Silke Hauf, Andreas Meinke, et Jan-Michael Peters. 2000. « Two Distinct Pathways Remove Mammalian Cohesin from Chromosome Arms in Prophase and from Centromeres in Anaphase ». *Cell* 103 (3): 399‑410. doi:10.1016/S0092-8674(00)00132-X.

Walczak, Claire E., Shang Cai, et Alexey Khodjakov. 2010. « Mechanisms of Chromosome Behaviour during Mitosis ». *Nature Reviews Molecular Cell Biology* 11 (2): 91‑102. doi:10.1038/nrm2832.

Watanabe, Yoshinori. 2004. « Modifying Sister Chromatid Cohesion for Meiosis ». *Journal of Cell Science* 117 (18): 4017‑23. doi:10.1242/jcs.01352.

Watrin, Erwan, Alexander Schleiffer, Koichi Tanaka, Frank Eisenhaber, Kim Nasmyth, et Jan-Michael Peters. 2006. « Human Scc4 Is Required for Cohesin Binding to Chromatin, Sister-Chromatid Cohesion, and Mitotic Progression ». *Current Biology* 16 (9): 863‑74. doi:10.1016/j.cub.2006.03.049.

Weitzer, Stefan, Chris Lehane, et Frank Uhlmann. 2003. « A Model for ATP Hydrolysis-Dependent Binding of Cohesin to DNA ». *Current Biology* 13 (22): 1930‑40. doi:10.1016/j.cub.2003.10.030.

Wendt, Kerstin S., Keisuke Yoshida, Takehiko Itoh, Masashige Bando, Birgit Koch, Erika Schirghuber, Shuichi Tsutsumi, et al. 2008. « Cohesin Mediates Transcriptional Insulation by CCCTC-Binding Factor ». *Nature* 451 (7180): 796‑801. doi:10.1038/nature06634.

Williams, Byron C., Carrie M. Garrett-Engele, Zexiao Li, Erika V. Williams, Elizabeth D. Rosenman, et Michael L. Goldberg. 2003. « Two Putative Acetyltransferases, San and Deco, Are Required for Establishing Sister Chromatid Cohesion in Drosophila ». *Current Biology* 13 (23): 2025‑36. doi:10.1016/j.cub.2003.11.018.

Woodman, Julie, Tyler Fara, Monika Dzieciatkowska, Michael Trejo, Nancy Luong, Kirk C. Hansen, et Paul C. Megee. 2014. « Cell Cycle-Specific Cleavage of Scc2 Regulates Its Cohesin Deposition Activity ». *Proceedings of the National Academy of Sciences of the United States of America* 111 (19): 7060‑65. doi:10.1073/pnas.1321722111.

Woodman, Julie, Matthew Hoffman, Monika Dzieciatkowska, Kirk C. Hansen, et Paul C. Megee. 2015. « Phosphorylation of the Scc2 Cohesin Deposition Complex Subunit Regulates Chromosome Condensation through Cohesin Integrity ». *Molecular Biology of the Cell* 26 (21): 3754‑67. doi:10.1091/mbc.E15-03-0165.

Woods, A., T. Sherwin, R. Sasse, T. H. MacRae, A. J. Baines, et K. Gull. 1989. « Definition of Individual Components within the Cytoskeleton of Trypanosoma Brucei by a Library of Monoclonal Antibodies ». *Journal of Cell Science* 93 (3): 491‑500.

Xiao, Tiaojiang, Julie Wallace, et Gary Felsenfeld. 2011. « Specific Sites in the C Terminus of CTCF Interact with the SA2 Subunit of the Cohesin Complex and Are Required for Cohesin-Dependent Insulation Activity ». *Molecular and Cellular Biology* 31 (11): 2174‑83. doi:10.1128/MCB.05093-11.

Zhang, Jinglan, Xiaomin Shi, Yehua Li, Beom-Jun Kim, Junling Jia, Zhiwei Huang, Tao Yang, et al. 2008. « Acetylation of Smc3 by Eco1 Is Required for S Phase Sister Chromatid Cohesion in Both Human and Yeast ». *Molecular Cell* 31 (1): 143‑51. doi:10.1016/j.molcel.2008.06.006.

Zhang, Nenggang, Sergey G. Kuznetsov, Shyam K. Sharan, Kaiyi Li, Pulivarthi H. Rao, et Debananda Pati. 2008. « A handcuff model for the cohesin complex ». *The Journal of Cell Biology* 183 (6): 1019‑31. doi:10.1083/jcb.200801157.

Zilio, Nicola, Sophie Wehrkamp-Richter, et Michael Nicholas Boddy. 2013. « A New Versatile System for Rapid Control of Gene Expression in the Fission Yeast Schizosaccharomyces Pombe ». *Yeast* 30 (7): 291‑291. doi:10.1002/yea.2963.

## Régulation des cohésines chez *Schizosaccharomyces pombe* par la Kinase Cycline Dépendante Pef1

Le complexe cohésine est un complexe protéique en forme d'anneau composé de quatre sous-unités essentielles très conservées: Smc1, Smc3, Rad21 et Scc3. Par sa capacité à encercler les molécules d'ADN, les cohésines participent à de nombreux processus cellulaires tels que la ségrégation des chromosomes, la signalisation et la réparation des dommages à l'ADN, la régulation de la transcription et l'organisation du génome.

Pour assurer ces différentes fonctions biologiques les cohésines doivent être finement régulées à la fois dans le temps et l'espace. Ces régulations reposent en partie sur le contrôle de leur association à la chromatine (capture de l'ADN). Cela nécessite l'action d'un «facteur de chargement » composé de deux protéines conservées et essentielles, Mis4 et Ssl3 chez la levure *S. pombe*. Comment ce complexe régule la capture de l'ADN par l'anneau de cohésine dans l'espace et le temps demeure à ce jour très mal compris.

Afin d'identifier des régulateurs de l'association des cohésines à la chromatine, nous avons réalisé un crible génétique visant à rechercher des suppresseurs de la mutation thermosensible *mis4-367*. Ce crible a conduit à l'identification de la Cyclin-Dependent Kinase Pef1 qui agit comme un régulateur négatif de la cohésion des chromatides sœurs en contrôlant vraisemblablement négativement l'association des cohésines à la chromatine. De forts arguments expérimentaux indiquent que Pef1 exerce sa fonction en régulant directement la phosphorylation de la sous-unité Rad21 du complexe cohésine. De façon intéressante, via un autre crible génétique, nous avons identifié la phosphatase Pph3/Psy2 qui joue un rôle dans l'établissement de la cohésion des chromatides sœurs en contrôlant la déphosphorylation de Rad21. Ensemble, ces données suggèrent que le contrôle de l'état de phosphorylation de la sous-unité Rad21 du complexe cohésine joue un rôle central dans le processus de cohésion chez la levure *S. Pombe*.

**Mots clés :** Cohésine, cycle cellulaire, CDK

## Regulation of fission yeast cohesin by the Cyclin Dependent Kinase Pef1

Cohesin is a highly conserved ring-shaped protein complex made of four essential subunits: Psm1, Psm3, Rad21 and Psc3. By its ability to capture DNA molecules within its ring-like structure, cohesin plays a key role in many cellular processes such as chromosome segregation, DNA damage signalling and repair, transcriptional gene regulation and nuclear organization.

To ensure all of its biological functions, cohesin must be tightly regulated in space and time. This regulation relies in part on the control of cohesin binding to chromatin (DNA capture). Cohesin recruitment to chromatin requires the action of a "loading complex" made of two conserved and essential proteins named Mis4 and Ssl3 in the fission yeast. How this complex regulates where and when DNA capture by the cohesin ring must occur remains poorly understood.

To identify regulators of cohesin binding to chromatin we have performed a genetic screen for suppressors of the thermosensitive mutation *mis4-367*. This genetic screen has led to the identification of the cyclin-dependent-kinase Pef1 that acts as a negative regulator of sister chromatids cohesion may be by negatively controlling cohesin binding to chromatin. Strong experimental evidences indicate that Pef1 exerts its function at least in part by directly phosphorylating the Rad21 subunit of the cohesin complex. Interestingly, a genetic screen made in parallel identified the Pph3/Psy2 phosphatase as implicated in the establishment of sister chromatid cohesion by regulating Rad21 dephosphorylation. Strikingly, the control of Rad21 phosphorylation status appears central to the cohesion process in the fission yeast *S. pombe*.

**Keywords :** Cohesin, cell cyle, CDK, phosphorylation